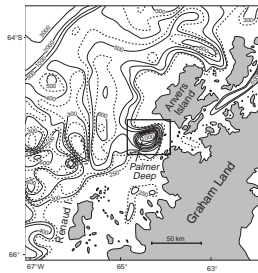


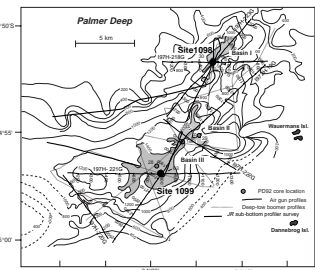
F1. Location of Palmer Deep (Sites 1098 and 1099), [p. 28](#).



7. PALMER DEEP (SITES 1098 AND 1099)¹

Shipboard Scientific Party²

F2. Bathymetry and location of site-survey seismic reflection profiles on Palmer Deep, [p. 29](#).



BACKGROUND AND SCIENTIFIC OBJECTIVES

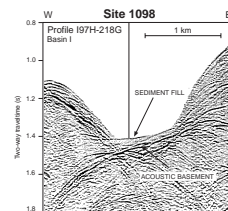
Sites 1098 and 1099 are located in Palmer Deep (Fig. F1; Leventer et al., 1996), a glacially overdeepened basin on the inner shelf of the Pacific margin of the Antarctic Peninsula, southwest of Anvers Island.

Site 1098 lies at a water depth of 1012 m in Basin I (Kirby, 1993), the shallowest of the three ponded sub-basins aligned in an approximately southwest-northeast direction that comprise Palmer Deep (Fig. F2). The basin floor is ~4 km long and 1 km wide and is surrounded by steep slopes (16° to 26°). High-resolution acoustic surveys of the basins suggested that a sediment fill ~50 m thick rests on a highly reflective, probably hard-rock basement (Rebesco et al., 1998; Fig. F3; also see “Appendix,” p. 24, and Fig. AF1, p. 59, both in the “Leg 178 Summary” chapter). Piston cores collected from this basin (Leventer et al., 1996) indicate that laminated sediments composed of alternations of biogenic siliceous and hemipelagic muds have accumulated at extremely high rates (260–390 cm/k.y.). This means that an ultrahigh-resolution Holocene sedimentary record is preserved, possibly extending back to the Last Glacial Maximum (LGM).

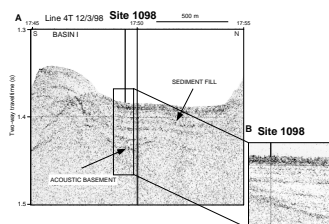
Site 1098 is located at the southwest end of Basin I, where the sediment fill is draped, contrasting with the overall ponded geometry of the rest of the basin. In this location, Core PD92-30 (Leventer et al., 1996) indicates only minor turbiditic deposition in the upper 9 m and a linear trend of radiocarbon ages.

Site 1099 lies in 1400 m of water in Basin III, the largest and deepest of the three sub-basins comprising Palmer Deep (Fig. F2). Basin III is more than 6 km long, 3–4 km wide, and elongated markedly northeast-southwest. It has a thicker sediment fill than Basin I; in the center of the basin, it reaches 260 m (310 ms two-way traveltime [TWT] [Figs. F4, F5; also see “Appendix,” p. 24, and Fig. AF1, p. 59, both in the “Leg 178 Summary” chapter]). Normal faulting is suggested by stratigraphic

F3. East-west air gun single-channel seismic reflection profile crossing Basin I, Site 1098, [p. 30](#).



F4. 3.5-kHz sub-bottom profile at ~5 kt across Site 1098, Basin I, [p. 31](#).



¹Examples of how to reference the whole or part of this volume.

²Shipboard Scientific Party addresses.

growth in the sediment fill on the northwest side of the basin, implying that overdeepening of the basin may be related not only to glacial erosion but also to neotectonic subsidence. Of the three major acoustic units present in Basin III, the uppermost (97 ms TWT, equivalent to ~70 m) shows character similar to the fill of Basin I: low reflectivity at the seafloor and acoustic transparency. In Basin III, a continuous reflector (mid-basin reflector [MBR]) within the uppermost transparent unit was considered to be a mass-flow deposit. The two underlying units are highly reflective, with subparallel reflectors showing a moderately divergent pattern suggestive of turbiditic deposition from the east or northeast.

Sedimentation in Basin III was recognized as more affected by mass flow than in Basin I. Additional stratigraphic data derived from piston cores, including radiocarbon dating from the upper unit in Basin III (Kirby et al., 1998), suggest that the base of the unit, as well as the deeper units, may predate the most recent glaciation on the shelf (LGM). The seismic units below the MBR were therefore considered to be older than the basin-fill unit of Basin I.

Because Basin III is sufficiently wide, Site 1099, selected originally at the crossing of two site-survey seismic profiles ~275 m from Core PD92-63 in the center of the basin floor, could be occupied using predetermined Global Positioning System (GPS) coordinates without the aid of an additional survey (Fig. F6).

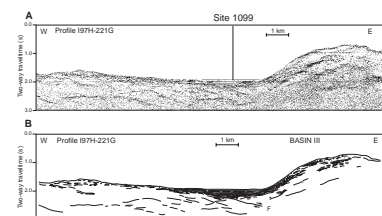
The aim of drilling in Palmer Deep (Sites 1098 and 1099) was to reconstruct the most recent glacial history of the Antarctic Peninsula, through recovery of a Holocene, and possibly latest Pleistocene, paleoproductivity record representative of regional climate at a decadal and millennial scale. Such a record might be compared with those of low-latitude regions and with that recorded in ice cores. In addition, Site 1099 would provide a potential test of the hypothesis that Palmer Deep was a subglacial lake during the most recent episode of ice grounding on the Antarctic Peninsula continental shelf.

OPERATIONS

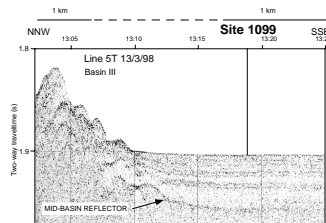
The 192-nmi transit to Site 1098 (scientific prospectus site APSHE-13A) was accomplished at an average speed of 10.5 kt. During the voyage, a total of 52 icebergs appeared on the 24-nmi range of the radar, and the vessel had to alter course to avoid one large iceberg. Because the target was narrow, the site was approached slowly (2 kt), using the GPS to follow the south-to-north track of a site-survey deep-tow boomer profile that intersected the location of Core PD92-30 (Fig. F2). The final site location was chosen by comparison of basin-floor morphology with 3.5-kHz and narrow-beam echosounder records. Drilling operations began at 1530 hr on 12 March with the deployment of a beacon.

During operations at this site, Eugene Domack joined the vessel for less than 1 day from the *Laurence M. Gould* (*LMG*) to observe procedures. Domack was the lead proponent of the proposal for drilling the Palmer Deep sites. Shortly before the *LMG* arrived, the *Polar Duke* came alongside Crane 3 to off-load a logging tool and acetone, which had been shipped to Punta Arenas but failed to arrive in time at the port call. These supplies had been delivered to the American base at Palmer Station a few miles away by the *LMG* for pickup by the *Polar Duke*.

F5. East-west air gun single-channel seismic reflection profile and line drawing, Basin III, Site 1099, p. 32.



F6. 3.5-kHz sub-bottom profile at ~5 kt across Site 1099, Basin III, p. 33.



Site 1098

The initial core of Hole 1098A recovered 1.9 m and established seafloor depth at 1012 m (1022.6 meters below rig floor [mbrf]). Advanced hydraulic piston corer (APC) work then continued through Core 178-1098A-7H, where contact with glacial till or hard basement concluded coring in the hole at 45.9 meters below seafloor (mbsf) (Table T1). Calm conditions permitted very good core recovery. The drill string was raised above the seafloor and the ship offset 10 m north to begin Hole 1098B.

To achieve stratigraphic overlap, Hole 1098B was spudded with the pipe 3.5 m lower than for the first core of Hole 1098A. Core recovery indicated a seafloor depth ~1.4 m shallower than at Hole 1098A. APC coring advanced to 43.0 mbsf (Core 178-1098B-5H). Adara tool temperature measurements were obtained with Cores 178-1098B-4H (34.5 mbsf) and 5H (43.0 mbsf). The drill string was raised above the seafloor at 0355 hr and the vessel offset 10 m north to begin Hole 1098C.

The pipe was set 3 m lower than at Hole 1098B for the first APC core at Hole 1098C. Coring began at 0430 hr 13 March with an Adara tool deployment just above the bottom before spudding in the first core. Five APC cores were collected, and coring operations ended at 0630 hr. Core recovery for the site averaged 101.6%. The drill string was recovered, the beacon was successfully retrieved, and the vessel was under way at 0930 hr 13 March for a 6-nmi transit to Site 1099.

Site 1099

Site 1099 (scientific prospectus site APSHE-15A) was located using GPS coordinates, and a beacon was launched at 1030 hr 13 March. APC coring at Hole 1099A began at 1445 hr on 13 March with a 5.3-m core that established the seafloor depth at 1399.9 m (1411.2 mbrf). Continuous cores were taken to 62.3 mbsf (102% recovery [Table T1]) with Adara tool temperature measurements at Cores 178-1099A-5H (43.3 mbsf) and 7H (62.3 mbsf). An additional Adara tool was deployed with the initial core barrel before spudding the hole to measure the bottom-water temperature. A change of wind then moved several icebergs toward the vessel. The bit was pulled above the seafloor at 1900 hr, and the vessel was offset away from the icebergs.

At 2145 hr, after the icebergs had moved past, Hole 1099B was spudded and the bit washed down to 60 mbsf, where APC coring resumed. Core recovery averaged 102% while advancing to 107.5 mbsf, which was considered the depth objective for the hole (Table T1). The drill string was retrieved and the beacon recovered before the vessel departed at 0445 hr on 14 March. For a summary of drilling at Sites 1098 and 1099 in Palmer Deep, see Table T1, p. 54, in the “Leg Summary” chapter.

T1. Coring summary for Sites 1098 and 1099, [p. 79](#).

LITHOSTRATIGRAPHY

Site 1098

Sediments recovered at Site 1098 consist of alternating massive muddy diatom oozes, laminated mud-bearing diatom oozes, and diatom-bearing silty clays and clayey silts with a generally low sand content. Sediment color varies between olive (5Y 4/3), olive gray (5Y 4/2),

and dark olive gray (5Y 3/2) in the diatomaceous muds and between orange brown (10YR 5/6), dark brown (10YR 4/3 and 3/3), dark grayish brown (2.5Y 4/2), and dark gray (5Y 4/1) in the laminated oozes. Different degrees of bioturbation are present; burrows are mainly bedding-parallel (*Planolites* type), although a few long, open vertical burrows were observed. Diatom preservation is generally good. Diatom species composition varies between laminated and bioturbated intervals, and also from top to base of the hole. Graded sands and silts associated with structureless intervals above and slumped material below are interpreted as turbidites. Most of the sequence at Site 1098 is horizontally bedded, but slump features and inclined bedding were observed at the base of Holes 1098B and 1098C. Ice-raftered pebbles increase in number downhole. At the base of Holes 1098A and 1098C, a further increase in coarse clastic material and pebbles is observed. Depositional processes included (1) pelagic/hemipelagic settling and (2) sediment gravity flows from the steep sides of the Palmer Deep basin. Sponge debris was found in Section 178-1098C-5H-2 at 98 cm, and fish debris (vertebrae and teeth) at 105 cm. We describe the entire section as one lithostratigraphic unit divided into Subunits IA and IB (Table T2).

Unit I

Subunit IA

Intervals: Core 178-1098A-1H through Section 6H-3, 60 cm; Core 178-1098B-1H through Section 5H-CC; Core 178-1098C-1H through Section 5H-4, 50 cm

Depth: 0–43.5 (mbsf) in Hole 1098A; 0–43.0 mbsf in Hole 1098B; 0–42.2 mbsf in Hole 1098C

Age: Holocene

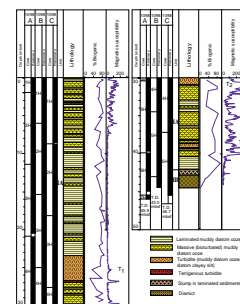
Description. Lithostratigraphic Subunit IA consists mainly of alternations of massive, bioturbated, muddy diatom ooze with laminated, mud-bearing diatom ooze (Figs. F7, F8). Diatoms, including resting spores, form 45%–80% of the sediment (estimated from smear slides), with sponge spicules averaging 5% in the three holes. Minor amounts (<4%) of silicoflagellates, radiolarians, and benthic foraminifers are present in certain intervals.

Massive, muddy diatom ooze ranges from olive (5Y 4/3) to olive gray (5Y 4/2) and dark olive gray (5Y 3/2) in color. Although no primary structures are preserved, faint burrow mottling is visible as slightly grayer burrow fills. Burrows are mainly bedding-parallel (*Planolites* type), although a few long, open, vertical burrows 3–6 mm wide were observed (e.g., intervals 178-1098B-1H-2, 13–65 cm, and 1H-3, 110–142 cm, and Sections 3H-2 and 3H-3). Diatom preservation is good at the top of the hole and moderate in the lower part (below ~25 mbsf), and the assemblage is diverse.

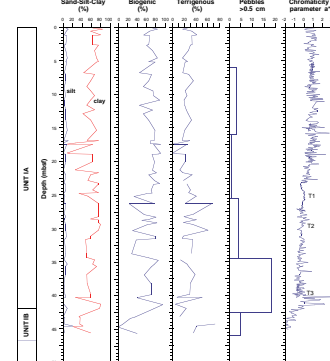
Laminated muddy and mud-bearing diatom oozes are quite variable in color and species composition. Colors include olive (5Y 4/3, 5Y 5/3), olive gray (5Y 4/2), dark olive gray (5Y 3/2) orange brown (10YR 5/6), dark brown (10YR 4/3, 10YR 3/3), dark grayish brown (2.5Y 4/2), and dark gray (5Y 4/1). In the upper part of the hole, the laminae are 5–20 mm thick and have diffuse tops and bases, locally with minor bioturbation (Fig. F9). No consistent color sequence was observed within laminated units. In the lower part of the hole (below 40 mbsf), the laminae are sharply defined, 3–40 mm thick, are not bioturbated, and may show

T2. Lithostratigraphic Unit I of Site 1098, [p. 80](#).

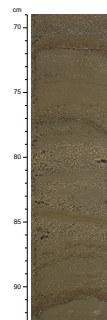
F7. Lithostratigraphic column for Site 1098, [p. 34](#).



F8. Sand:silt:clay ratio, percent biogenic and terrigenous, pebble occurrence, and chromaticity parameter a^* for Site 1098, [p. 35](#).



F9. Laminated diatom ooze, interval 178-1098B-1H-3, 69–93 cm, [p. 36](#).



weak grading. Individual laminae are each composed of a very restricted diatom assemblage. They are dominated by *Chaetoceros* spp. resting spores (the most common, particularly toward the base of the hole; orange brown, dark brown, and dark gray laminae); *Corethron criophilum* (the lighter olive laminae, most common near the top of the hole); and *Eucampia antarctica* (dark gray laminae). Diatom preservation in the laminae is excellent, with some samples resembling fresh plankton hauls.

The downhole occurrence of massive (bioturbated) and laminated sediments is shown in the lithology column in Figure F7. Laminated sediments predominate from 8 to 23 mbsf.

Sand-size particles are present throughout the sequence in low amounts (<10%; Fig. F8). Moderate to intense bioturbation is common in the massive muddy diatom oozes and seems to be more distinct in the upper part of the holes (Cores 178-1098A-1H through 3H; 1098B-1H through 3H; 1098C-1H through 3H).

Subunit IB

Intervals: Sections 178-1098A-6H-3, 60 cm, through 7H-CC; Sections 178-1098C-5H-4, 50 cm, through 5H-CC

Depth: 43.5–45.9 mbsf in Hole 1098A; 42.2–46.7 mbsf in Hole 1098C

Age: Holocene

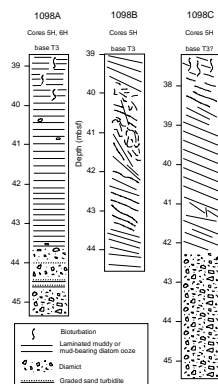
Description. Lithostratigraphic Subunit IB is characterized by dark gray (5Y 4/1) silty clays, an increase in coarse clastic material, and a high abundance of pebbles at the base of Holes 1098A and 1098C (Fig. F7).

Turbidites and Mass Flows

The lithostratigraphy at Site 1098 shows intervals of graded silt or sand to mud. Three prominent intervals occur within the sequence between ~23 and 40 mbsf. Each appears entirely homogeneous, with no bioturbation except at the very top, and all three have low and uniform values of chromaticity parameter a^* (Fig. F8). The uppermost is nearly 4 m thick (Sections 178-1098A-4H-2, 79 cm, through 4H-5, 27 cm; 178-1098B-3H-6, 40 cm, through 4H-2, 45 cm; 178-1098C-3H, 5–7 cm, to the base of Core 3H; not seen at the top of Core 178-1098C-4H). This bed shows a well-developed normal grading from diatom-bearing sandy muds to ooze and corresponds to a high in magnetic susceptibility (Fig. F7). The second is 1.2 m thick (Sections 178-1098B-4H-4, 30 cm, through 4H-5, 4 cm; 178-1098C-4H-2, 90 cm, through 4H-1, 60 cm; poorly recovered between Cores 178-1098A-3H and 4H), including 10–25 cm of graded medium to coarse sand at its base. In Section 178-1098B-4H-4, the sand contains mollusk fragments with one small articulated bivalve. The third was noted as a graded fine sand lamina just below 39 mbsf (Sections 178-1098A-5H-6, 81 cm, and 178-1098B-5H-4, 25 cm), with very high magnetic susceptibility (Fig. F7). These three graded layers are interpreted as turbidites and are numbered T1, T2, and T3 from the top down (Figs. F7, F8).

Most of the sequence at Site 1098 is horizontally bedded, but slump features and inclined bedding were observed at the base of Holes 1098B and 1098C (Fig. F10). Below a conspicuously laminated, nonbioturbated interval of mud-bearing diatom ooze, the lowest intact sediments at Hole 1098A (interval 178-1098A-6H-3, 130 cm, to the base of the

F10. Deformation style in lowest sediments recovered in Holes 1098A, 1098B, and 1098C, **p. 37.**



core) consist of 1.8 m of sandy, pebbly, gray mud (diamict; 5Y 5/1) with thin, graded, fine sand-silt beds. Bedding is horizontal, except for moderate coring disturbance. Hole 1098B terminated within the laminated ooze interval without recovering the graded sands; the upper part of the laminated interval dips at 60° beneath a meter-thick slumped bed. In Hole 1098C, the entire section below the uppermost turbidite dips at ~20°. Beneath the laminated ooze interval is 3.3 m of massive diatom-bearing diamict.

Pebbles

Pebbles >0.5 cm in diameter occur throughout the sequence except in the upper 6 m (Fig. F8; Table T3); abundance ranges from two to four pebbles in Cores 178-1098A-2H through 5H, 178-1098B-2H and 4H, and 178-1098C-2H through 4H. As many as 18 pebbles were identified in Cores 178-1098B-5H and 6H and in Core 178-1098C-5H, which indicates an increase in coarse clast material downhole.

Site 1099

Sediments recovered at Site 1099 consist of alternating massive muddy diatom oozes, laminated mud-bearing diatom oozes, and diatom-bearing silty clays and clayey silts with a generally low sand content. Hole 1099A sediments vary in color between olive (5Y 4/3) and dark olive gray (5Y 3/2) in the diatomaceous muds; colors are orange brown (10YR 5/6), dark brown (10YR 4/3 and 3/3), dark grayish brown (2.5Y 4/2), and dark gray (5Y 4/1) in the laminated oozes. Hole 1099B sediment color varies from dark greenish gray (5Y 4/1) to very dark gray (5BG 4/1), which may indicate a decrease in oxygen after deposition because of the decay of organic matter. Site 1099 sediments show varying intensities of bioturbation. Graded sands and silts associated with structureless intervals above and slumped material below are interpreted as turbidites. They commonly show pervasive bioturbation of bed tops by small *Phycosiphon* burrows. Steep burrows (*Fugichnia*) were made following deposition of thin (1 cm) laminations and record the upward escape of burrowing organisms. Diatom preservation is generally good. Diatom species composition varies between laminated and bioturbated intervals, and also from top to base of the hole. Ice-raftered pebbles show two maxima (in Cores 178-1099A-4H and 1099B-3H). Depositional processes included (1) pelagic/hemipelagic settling and (2) sediment gravity flows from the sides of the Palmer Deep Basin III. We describe the entire section as one lithostratigraphic unit.

Unit I

Intervals: Core 178-1099A-1H through Section 7H-CC; Core 178-1099B-1H through Section 5H-CC

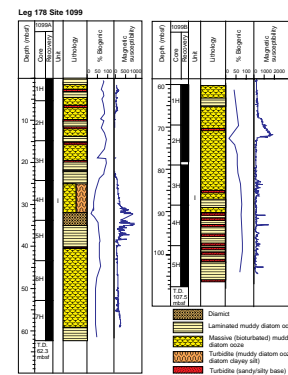
Depth: 0.0–62.3 mbsf in Hole 1099A; 60.0–107.5 mbsf in Hole 1099B

Age: Holocene

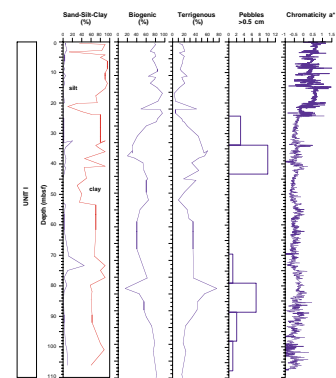
Description. Lithostratigraphic Unit I consists dominantly of alternations of massive, bioturbated, muddy diatom ooze with laminated mud-bearing diatom ooze and very fine-grained graded beds interpreted as turbidites (Figs. F11, F12). Diatoms, including resting spores, form 35%–80% of the sediment (estimated from smear slides), with sponge spicules

T3. Occurrence of pebbles >0.5 cm at Sites 1098 and 1099, [p. 81](#).

F11. Lithostratigraphic column for Site 1099, [p. 38](#).



F12. Sand:silt:clay ratio, percent biogenic and terrigenous, pebble occurrence, and chromaticity parameter a^* for Site 1099, [p. 39](#).



averaging 5% throughout the two holes. Diatom preservation is good at the top of the section and moderate in the lower part (below ~25 mbsf), and the assemblage is diverse. In Cores 178-1099A-4H and 178-1099B-3H, two minima of biogenic abundance (~20%) are revealed. Minor amounts (<4%) of silicoflagellates, radiolarians, and benthic foraminifers are present in certain intervals.

The color of the massive, muddy diatom ooze varies between olive (5Y 4/4, 4/3, 3/2), olive gray (5Y 4/2), and dark olive gray (5Y 3/2) at Hole 1099A (Fig. F13A). Colors of the massive, muddy diatom oozes at Hole 1099B are significantly darker (dark gray, 5Y 3/1, to very dark gray, 5BG 4/1) and may show faint color banding. The thickness of the massive diatom ooze layers varies downhole. From Core 178-1099A-1H through 3H, thickness averages 40 cm, whereas the thickness increases to as much as 19 m in Cores 178-1099A-5H through 7H (Fig. F11). This lithology is intensely bioturbated, and burrows of *Planolites* type, as well as longer vertical open burrows of *Phycosiphon* type, were observed.

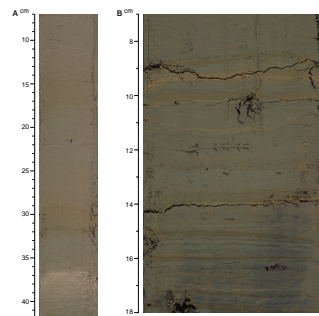
The laminated mud-bearing diatom oozes and diatom-bearing clayey silts and silty clays vary between orange brown (10YR 5/6), dark brown (10YR 4/3 and 3/3), dark grayish brown (2.5Y 4/2), and dark gray (5Y 4/1) at Hole 1099A. They are generally darker, varying from dark greenish gray (5Y 4/1) to very dark gray (5BG 4/1), at Hole 1099B. In the upper part of Hole 1099A, the laminae are typically 5–20 mm thick and have diffuse tops and bases. Downhole, the thickness of laminae ranges between 1 and 10 mm (Fig. F13B). Individual laminae are each composed of a nearly monospecific diatom assemblage. They are dominated by *Chaetoceros* spp. resting spores (the most common, particularly toward the base of the hole; orange brown, dark brown, and dark gray laminae); *Corethron criophilum* (the lighter olive laminae, most common near the top of the hole); and *Eucampia antarctica* (dark gray laminae). Diatom preservation in the laminae is excellent, with some samples resembling fresh plankton hauls. Bioturbation of the laminated lithology is minor and involved trace fossils similar to those mentioned above. In the interval 178-1099B-4H-3, 103–104 cm, a calcium carbonate concretion was found in the laminated mud-bearing diatom ooze. The concretion is bedded in millimeter-thick planktonic foraminifer ooze.

The darker colors found in both lithologies of Hole 1099B correspond to a pronounced increase in pyrite to as much as 8% estimated from smear slides in Cores 178-1099B-2H through 5H. This may indicate a decrease in oxygen during or after deposition because of the decay of organic matter (see “**Inorganic Geochemistry**,” p. 13). Color started to change to olive gray (5Y 4/2) immediately after the core was split and exposed to laboratory conditions.

Turbidites

Sediment sequences of graded fine sand and silt, millimeters to centimeters thick, occur throughout Cores 178-1099A-1H through 4H and 178-1099B-1H through 5H in both the massive and the laminated lithologies (Fig. F11). The graded turbidite beds (Fig. F13C, F13D) commonly show pervasive bioturbation of bed tops by small *Phycosiphon* burrows. *Phycosiphon* is a very common trace fossil in successions deposited in such environments (Wetzel, 1984).

F13. Massive mud-bearing diatom ooze, laminated diatom ooze, diatom-bearing silty mud base of a turbidite, and turbidite bed, **p. 40**.



Diamict and Pebbles

A clast-poor olive (5Y 4/3) to gray (5Y 4/1) diamict layer with a diatom clayey silt matrix (Fig. F11) was recovered in the interval from Sections 178-1099A-4H-6, 115 cm, through 5H-2, 20 cm. This diamict layer coincides with a maximum occurrence of 10 pebbles (as much as 2 cm), mainly basalts, observed in Core 178-1099A-4H (Fig. F12; Table T3). A second concentration of pebbles (as many as eight pebbles) occurs in Core 178-1099B-3H. Fewer pebbles are recorded in Cores 178-1099A-3H and 178-1099B-2H, 4H, and 5H.

Interpretation of Sites 1098 and 1099

Site 1098 is located within Basin I of Palmer Deep; the water depth is 1040 m and the width of the basin floor only ~1 km, with the site near one edge (Fig. F3). The basin sides slope at 16°–26° from the inner shelf, which is ~200 m deep off Anvers Island (Rebesco et al., 1998). Site 1099 is located within Basin III of Palmer Deep; the water depth is 1430 m. In comparison to Basin I, Basin III may be more open to water-mass exchange to the west. However, the basins act as a sediment trap, both for biogenic material sinking from the surface waters and for near-bottom suspended sediment transported by turbidites or mass flows derived from surrounding shallow water. The area is sea-ice free for at least 4 months/yr; surface waters are strongly affected by winter cooling, and diatom productivity is therefore very seasonal. Water masses below the 200-m sill depth in Palmer Deep may be influenced by periodic influx of the warm Circumpolar Deep Water (CDW) of adjacent oceanic regions.

Palmer Deep sediments are ponded in Basins II and III, but the fill of Basin I (Site 1098) is draped (Rebesco et al., 1998). Likely depositional processes include pelagic/hemipelagic settling and sediment gravity flows. The basin is considered to be bounded by active faults (Rebesco et al., 1998), and the presence of turbidite beds may reflect this setting.

The sequences interpreted as turbidites at Sites 1098 and 1099 are coarse- to fine-grained graded sand and silt. Graded turbidite beds commonly show pervasive bioturbation of bed tops by small *Phycosiphon* burrows and an increase of burrow size upward over a few centimeters. *Phycosiphon* is a very common trace fossil in turbidite successions and is a shallow burrower normally restricted to depths <10 cm from bed tops (Wetzel, 1984). At Site 1099, this trace fossil occurs in the upper laminated divisions of turbidites (e.g., Fig. F13C), which indicates the ability of the trace maker to keep pace with the high deposition rates suggested during phases of multiple turbidite events.

The style of lamination in the upper part of the section (indistinct, diffuse laminae showing minor bioturbation, alternating with strongly bioturbated intervals) is consistent with pelagic settling into a deep basin that was oxygenated enough to support a benthic fauna. Leventer et al. (1996) studied a 9-m piston core taken at Site 1098. They suggested that the laminated mud-bearing diatom oozes indicate very rapid biosiliceous sedimentation with strong seasonal fluctuation in diatom abundance and species composition, whereas the bioturbated muddy diatom oozes record a lower biosiliceous sedimentation rate. According to Leventer et al. (1996), the inferred fluctuations in productivity of biosiliceous material (200-yr periodicity in the upper 9 m of sediment) may be related to global climate fluctuations. We agree with this interpretation and suggest that similarly alternating environmental

conditions prevailed during the time represented by the upper 23 m of the sequence above T1. Good preservation of the delicate frustules of *Corethron criophilum* implies rapid burial after sinking of each diatom bloom. During deposition of the lower part of the sequence, in addition to pelagic settling, gravity flows were important. In addition to turbidites T1, T2, and T3, which are clearly graded with coarse material at the base, many of the sharp-based, nonbioturbated laminae in the lower part of the hole may have originated as small downslope flows. An additional explanation for the lack of bioturbation may be that the bottom water was low in oxygen.

Leventer et al. (1996) measured a sedimentation rate of 260 cm/k.y. by radiocarbon dating (Basin I). If this sedimentation rate has been constant at Site 1098, then the base of the lowest laminated sediments would be at ~16 ka, earlier than the ~11 ka onset of marine conditions determined by Pudsey et al. (1994) on the outer shelf west of Anvers Island. However, the sedimentation rate at Site 1098 remains to be determined by ^{14}C measurements postcruise.

The diamicts at the base of Site 1098 and from Hole 1099A in the interval 178-1099A-4H-6, 115 cm, through 5H-2, 20 cm, are thought to be of glacial origin, but their age is unknown. The lateral variation at the base of Holes 1098A, 1098B, and 1098C may result from downslope movement on irregular basin-floor topography (seismic Unit 4b of Rebisco et al., 1998).

Preliminary investigations of diatom species assemblages recovered from Sites 1098 and 1099 help explain environmental variation in the basins. In the upper 9 m of a piston core recovered at the Site 1098 location, Leventer et al. (1996) noted that laminated sediments (low magnetic susceptibility) and massive, bioturbated sediments (high magnetic susceptibility) were characterized by different diatom assemblages. Laminated layers included variable species composition, but massive layers were more uniform, at least in the top 9 m. At Sites 1098 and 1099, the diatom assemblages in both major lithologies (massive sediments and the most common types of laminae) were examined to determine long-term trends downcore. Selected species known as environmental indicators (Table T4) were recorded as abundant, common, or rare. These data were then assigned values based on their abundance (i.e., abundant = 50, common = 30, rare = 10). A plot of indicator species was generated by summing all the species data to 100% for each sample (Fig. F14). Note that several species are not included in the plot (e.g., *Rhizosolenia*, *Thalassiosira lentiginosa*, and *Thalassiosira gracilis*).

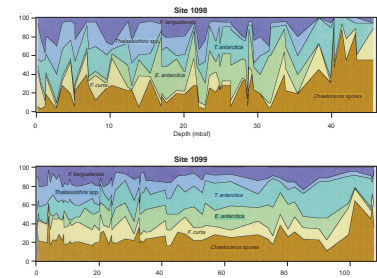
Results of relative species abundance in the major lithologies are shown in Figure F14. At both sites, the abundance of the open-ocean species *Fragilariopsis kerguelensis* and *Thalassiothrix* spp. decreases downward, and that of *Thalassiosira antarctica* remains roughly constant. *Eucampia antarctica* is rare near the surface and common below 15 mbsf, down to near the base of the sequence at each site. *Fragilariopsis curta* is present throughout, but more consistently at Site 1099. *Chaetoceros* spp. spores show a marked increase toward the base of the sequence at both sites.

The data suggest decreasing open-ocean influence and restriction of the basin downward at both sites. The higher variability in species composition at Site 1098 is attributed to the more laminated, thin-bedded style of sedimentation. Many of the samples at Site 1099 come from the thick turbidites where the record may be averaged.

Many of the distinctive colored laminae are composed of nearly monospecific assemblages of *Chaetoceros* spp. spores, *Corethron criophili-*

T4. Environmental indicative species used at Sites 1098 and 1099, [p. 82](#).

F14. Relative diatom species abundance of *F. kerguelensis*, *Thalassiothrix* spp., *T. antarctica*, *E. antarctica*, *F. curta*, and *Chaetoceros* spp. spores, [p. 42](#).



lum, *T. antarctica*, or *Rhizosolenia*. *Fragilaropsis curta* is a common minor species, but the open-ocean forms *F. kerguelensis* and *Thalassiothrix* spp. are not common in any laminae. The presence of these laminae throughout the cored sequences indicates that unusual productivity events (diatom blooms), followed by rapid sedimentation, occurred repeatedly during the time represented. Variation in diatom production is most likely related to change in shallow water–mass properties (a result of regional climate change) through the Holocene.

BIOSTRATIGRAPHY

The Palmer Deep Sites recovered a continuous, high-resolution section of Holocene sediments. Two nearshore basins were cored: Basin I (Site 1098), a shallow inner basin with little evidence of turbidites in previously collected piston cores; and Basin III (Site 1099), a deeper basin with significant terrigenous deposits reported. Approximately half of the section at Site 1099 is in fact composed of debris flows and turbidites (see “[Lithostratigraphy](#),” p. 3). The preservation of microfossils in Palmer Deep is generally good. The paleoenvironmental evolution of Palmer Deep as recorded by diatoms, radiolarians, and foraminifers suggests a low-salinity, restricted marine environment with a strong glacial influence in the oldest sediments. There is also a gradual transition to open-marine conditions and periodic CDW influx.

Diatoms

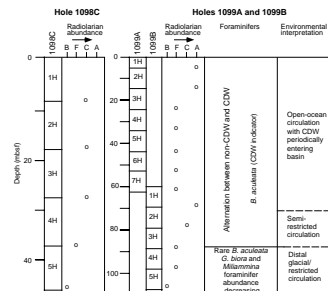
Samples from Holes 1098C, 1099A, and 1099B core catchers and toothpick samples (from characteristic lithologies, including laminae) were analyzed. Diatom assemblages are excellently preserved and very diverse except in the lower portion of Core 178-1098C-5H, which was barren of diatoms. Many fine laminae were observed at both sites, each having a distinct assemblage, often different from the others. Most diatomaceous laminae are olive green to olive brown and composed of a nearly monospecific assemblage of *Chaetoceros* spp. spores. Light gray “fluffy” laminae that are dominantly *Corethron criophilum* occur sporadically. The overall background assemblage at both sites is dominated by several species of diatoms: *Chaetoceros* spp. spores, *Eucampia antarctica*, *Fragilaropsis curta*, *Fragilaropsis kerguelensis*, *Fragilaropsis ritscherii*, *Odontella* spp., *Rhizosolenia* spp., *Thalassiosira antarctica*, *Thalassiosira lentiginosa*, and *Thalassiothrix* spp. Only one biostratigraphic zone is represented at these two sites, the *Thalassiosira lentiginosa* Zone. Changes in assemblage were observed downhole, with more open-marine species abundant in the upper parts at the two sites. Species living in more restricted environments increase downhole (see “[Lithostratigraphy](#),” p. 3).

Radiolarians

At Site 1098, radiolarians are common and well preserved in the upper 28 mbsf with relatively diverse assemblages (Fig. F15). Diversity and abundance gradually decrease to zero at the bottom of the hole (47 mbsf). This pattern is interpreted as a transition from restricted circulation at the bottom of the core to open-marine conditions at the top.

Radiolarians at Site 1099 exhibit a pattern of decreasing abundance and diversity downcore similar to that at Site 1098. This pattern, how-

F15. Radiolarian abundance, foraminiferal assemblage zones, and depositional environments for Holes 1098C, 1099A, and 1099B, p. 43.



ever, occurs over 108 m, in contrast to 47 m at Site 1098. The interval from 24 to 62 mbsf is diluted by large amounts of terrigenous material, which diminishes radiolarian abundance. The radiolarians at Sites 1098 and 1099 appear to record the same events; the section at Site 1099 is thicker because of increased terrigenous supply.

Foraminifers

Because of reduced shipboard sampling, no material from Site 1098 was available for analysis of foraminifers. At Site 1099, 12 core-catcher samples of $\sim 10 \text{ cm}^3$ were processed for foraminifers. An additional 13 samples of $\sim 2 \text{ cm}^3$ were processed from material scraped from the core surface. Benthic foraminifers are abundant and well preserved in the upper 87 mbsf; they decrease below that depth to a rare and poorly preserved assemblage in the lowest samples (Fig. F15). The planktonic foraminifer *Neogloboquadrina pachyderma* sinistral is rare throughout Holes 1099A and 1099B.

Preliminary analysis indicates that the benthic foraminifers in the upper 87 mbsf of Hole 1099A are similar to previously reported benthic foraminiferal fauna of the Bellingshausen Sea (Ishman and Domack, 1994). Ishman and Domack (1994) report two benthic foraminiferal assemblages: the *Bulimina aculeata* assemblage, related to CDW; and the *Fursenkoina* assemblage, related to shelf water. Fluctuations between these two assemblages have been recognized in piston cores from Palmer Deep and tied to 200-yr productivity cycles (Leventer et al., 1996).

Beneath 87 mbsf in Hole 1099B (depth of the highest black interval), however, *B. aculeata* is rare; *Globocassidulina biora* and the agglutinated genus *Miliammina* become more common. *Miliammina* spp. is linked to CDW by Ishman and Domack (1994), but *G. biora* is not closely related to either end-member. Both *G. biora* and *Miliammina* were found to be related to ice-front conditions in the Ross Sea (Osterman and Kellogg, 1979). In addition, the numbers of both foraminifers and diatoms observed in the sieved sediments decrease downcore in this lower interval. Sample 178-1099B-5H-CC (108.15 mbsf) at the bottom of the hole contains a large amount of pyrite as well as a decreased number of foraminifers, suggesting restricted basin circulation (Fig. F15).

PALEOMAGNETISM

Split-Core Measurements

Archive halves of all cores recovered from Sites 1098 and 1099 were measured at 5-cm intervals (Tables T5, T6, T7, T8, T9, T10, T11, T12, T13, T14, T15, T16, T17, T18, T19, T20, T21, T22, T23, T24, all also in ASCII format in the TABLES directory). Alternating field (AF) demagnetization of the natural remanent magnetization (NRM) was performed at 10 and 20 mT. The low peak demagnetization level was chosen to preserve the remanence for future U-channel studies. Holes 1098A, 1098B, and 1098C have similar inclination profiles (Fig. F16). Inclinations at both sites are steeply negative, except within lithologies that have been interpreted as turbidites and diamicts (see “**Lithostratigraphy**,” p. 3). The intensity of remanence is generally correlated with magnetic susceptibility (Fig. F17), which indicates that the intensity is

T5. Split-core paleomagnetic measurements for Hole 1098A before demagnetization, [p. 83](#).

T6. Split-core paleomagnetic measurements for Hole 1098A after 10-mT demagnetization, [p. 84](#).

T7. Split-core paleomagnetic measurements for Hole 1098A after 20-mT demagnetization, [p. 85](#).

T8. Split-core paleomagnetic measurements for Hole 1098A, results from 20-mT demagnetization, [p. 86](#).

T9. Split-core paleomagnetic measurements for Hole 1098B before demagnetization, [p. 87](#).

T10. Split-core paleomagnetic measurements for Hole 1098B after 10-mT demagnetization, [p. 88](#).

T11. Split-core paleomagnetic measurements for Hole 1098B after 20-mT demagnetization, [p. 89](#).

T12. Split-core paleomagnetic measurements for Hole 1098B, results from 20-mT demagnetization, [p. 90](#).

T13. Split-core paleomagnetic measurements for Hole 1098C before demagnetization, [p. 91](#).

T14. Split-core paleomagnetic measurements for Hole 1098C after 10-mT demagnetization, [p. 92](#).

T15. Split-core paleomagnetic measurements for Hole 1098C after 20-mT demagnetization, [p. 93](#).

T16. Split-core paleomagnetic measurements for Hole 1098C, results from 20-mT demagnetization, [p. 94](#).

partly dependent upon the composition and concentration of the magnetic mineral assemblage.

Discrete Samples

Discrete samples were collected from the working half of Hole 1098C. There is good agreement between the discrete samples and split-core measurements (Fig. F18). The steeply inclined drill-string overprint was removed at the 10-mT demagnetization step, and the characteristic remanent magnetization direction of most samples was stable up to the 50-mT demagnetization step (Fig. F19; Table T25, also in ASCII format in the TABLES directory). Of the 25 samples measured, 20 had a maximum angular deviation angle $<5^\circ$, and the remaining samples had maximum angular deviation angles $<11^\circ$ (Table T26, also in ASCII format in the TABLES directory). Samples that had a weak intensity of remanence and low susceptibility generally had a higher maximum angular deviation angle (Fig. F20).

Holocene Chronology

The 50- and 107-m sedimentary sections recovered at Basins I (Site 1098) and III (Site 1099), respectively, are assumed to be Holocene in age, on the basis of radiocarbon dates and sedimentation rates published by Leventer et al. (1996). The intensity of remanence was normalized by magnetic susceptibility to examine the relative paleointensity of the geomagnetic field and thus derive an approximate chronology by correlation with the well-dated Holocene geomagnetic paleointensity record for the Northern Hemisphere. Normalization at this site was complicated by the long interval of extremely low susceptibility occurring between ~8 and 24 mbsf in both Basins I and III, and by the high susceptibility values within turbidites. Although normalization using susceptibility yields similar profiles in Holes 1098A, 1098B, and 1098C (Fig. F21), the resulting normalized intensity record cannot, at this time, be confidently matched with the Northern Hemisphere record. More work is planned to investigate the magnetic mineralogy and alternate methods of relative paleointensity normalization.

ORGANIC GEOCHEMISTRY

Routine monitoring of hydrocarbon gases was performed for Holes 1098A, 1099A, and 1099B (Table T27). The organic geochemistry analyses performed at Sites 1098 and 1099 included measurements of inorganic carbon and elemental analyses of carbon, sulfur, and nitrogen for Holes 1098C, 1099A, and 1099B (Table T28). Samples for inorganic carbon and elemental analyses were taken from each section, using care to avoid monospecific diatom oozes.

Volatile Hydrocarbons

At Site 1098, headspace gas measurements give background levels of methane (<200 ppm) in the upper 25 mbsf and substantially higher values ($>15,000$ ppm) at greater depths (Table T27). At Site 1099, methane concentrations exceed background levels at all depths and reach a maximum ($>100,000$ ppm) at ~ 50 mbsf. No other hydrocarbon gases were detected at either site.

T17. Split-core paleomagnetic measurements for Hole 1099A before demagnetization, [p. 95](#).

T18. Split-core paleomagnetic measurements for Hole 1099A after 10-mT demagnetization, [p. 96](#).

T19. Split-core paleomagnetic measurements for Hole 1099A after 20-mT demagnetization, [p. 97](#).

T20. Split-core paleomagnetic measurements for Hole 1099A, results from 20-mT demagnetization, [p. 98](#).

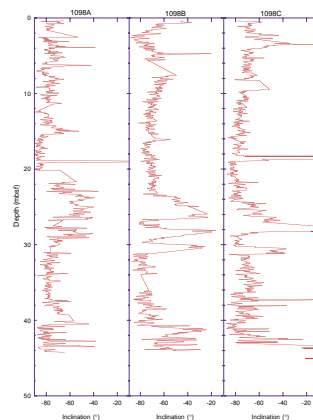
T21. Split-core paleomagnetic measurements for Hole 1099B before demagnetization, [p. 99](#).

T22. Split-core paleomagnetic measurements for Hole 1099B after 10-mT demagnetization, [p. 100](#).

T23. Split-core paleomagnetic measurements for Hole 1099B after 20-mT demagnetization, [p. 101](#).

T24. Split-core paleomagnetic measurements for Hole 1099B, results from 20-mT demagnetization, [p. 102](#).

F16. Inclination records from Basin I vs. depth, [p. 44](#).



Inorganic and Total Organic Carbon

Sediment from Sites 1098 and 1099 contains uniformly low amounts (≤ 0.3 wt%) of inorganic carbon, except for slightly higher values at the base of Hole 1098C (Figs. F22, F23). The low values are comparable to those measured at other sites investigated during Leg 178. Total organic carbon concentrations are relatively high (≥ 1 wt%) in the uppermost 20–25 mbsf at Sites 1098 and 1099 and reflect the locally high primary productivity of diatoms. At both sites, total organic carbon decreases with depth as contents of terrigenous sediment increase (see “**Lithostratigraphy**,” p. 3). Organic carbon decreases to zero in the carbonate-rich clay at the base of Hole 1098C. (This clay is not present in Holes 1098A and 1098B.) A negative covariance of total organic carbon and terrigenous sediment input suggests a dilution of organic carbon instead of a decrease in primary (diatom) productivity.

Elemental Analyses

Sulfur is present throughout Holes 1098C and 1099A. The variations in concentration of sulfur generally follow the total organic carbon profiles. Nitrogen concentrations are near the lower detection limits of the CNS analyzer.

INORGANIC GEOCHEMISTRY

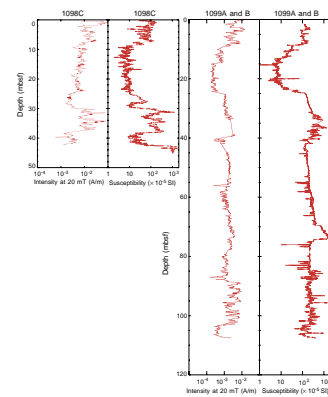
Interstitial Water Chemistry (Site 1098)

At the request of shore-based participants, we sampled interstitial water at Site 1098 with unusually high resolution, squeezing a total of 30 whole-round core samples, one per core section, from Hole 1098C (Table T29). The resulting profiles of interstitial water chemistry (Fig. F24) illustrate a sharply stratified diagenetic environment, influenced at least partly by variations in sediment lithology. Chloride concentrations remain constant through the upper 20 mbsf and decrease slightly by 2% from 20 to 40 mbsf, then remain constant at greater depths. Any stronger trends seen in profiles of other dissolved constituents should reflect chemical reaction processes.

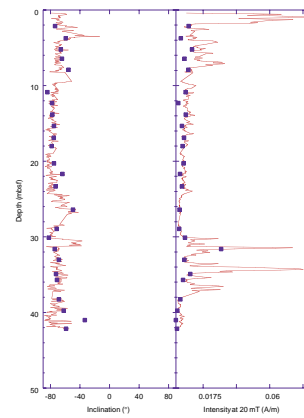
Organic-Matter Degradation

Sulfate concentrations decrease linearly from a seawater value (28 mM) to zero in the interval from 20 to 30 mbsf (Fig. F24), and this gradient delineates the sulfate reduction zone at Site 1098. In addition, acidified aliquots of interstitial water from between 13 and 25 mbsf emitted a noticeable odor of hydrogen sulfide, a direct product of sulfate reduction. The presence of hydrogen sulfide within this depth range indicates an absence of dissolved oxygen and nitrate, as well as a lack of enough reduced iron and manganese to precipitate all of the reduced sulfur as sulfide minerals. Iron and manganese concentrations lie close to detection limits (≤ 2 μ M) in the upper 30 mbsf (Fig. F24), except for a few random samples with higher iron concentrations (4–17 μ M). Curiously, iron and manganese increase to maximum values (10 μ M and 7 μ M, respectively) below the sulfate reduction zone at ~36 mbsf, then decrease at greater depths. Normally during early diagenesis, the highest concentrations of dissolved iron and manganese occur near

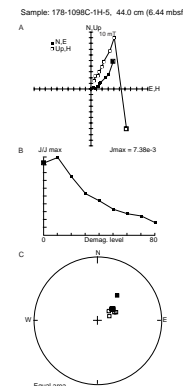
F17. Intensity of remanence and magnetic susceptibility in Holes 1098C, 1099A, and 1099B vs. depth, [p. 45](#).



F18. Split-core and discrete sample measurements from Hole 1098C vs. depth, [p. 46](#).



F19. AF demagnetization of a typical discrete sample (178-1098C-1H-5, 44 cm), [p. 47](#).



T25. Discrete sample NRM and AF demagnetization results for Hole 1098C, [p. 103](#).

the top of the sulfate reduction zone (Froelich et al., 1979), as observed at Sites 1095, 1096, and 1101. The highly variable iron concentrations measured at Site 1098 could represent an artifact caused by partial oxidation of the sediment before squeezing, incomplete filtration of colloidal particles during and after squeezing, or contamination.

Organic-matter decay has surprisingly little effect on the interstitial water chemistry above the sulfate reduction zone at Site 1098, despite the relatively high organic carbon content (1.0–1.2 wt%; see “[Organic Geochemistry](#),” p. 12) and rapid sedimentation rate (300 cm/k.y.; Leventer et al., 1996). For example, direct byproducts of organic-matter decay, such as alkalinity, ammonium, and phosphate, increase only slightly with depth in the upper 20 mbsf (Fig. F24) and yield weak concentration gradients similar to those observed in the less organic-rich, much more slowly deposited sediment at the rise sites. Within the sulfate reduction zone, however, alkalinity, ammonium, and phosphate increase sharply and approach maximum concentrations (40 mM, 6 mM, and 175 µM, respectively) at slightly greater depths, between 30 and 45 mbsf. Below 40 mbsf, phosphate decreases sharply to a low concentration (28 µM) in the deepest sample. Fluoride decreases slightly with depth in the upper 20 mbsf (to 54 µM), then much more sharply with depth to a minimum concentration (10 µM) at 27 mbsf (Fig. F24), slightly above the base of the sulfate reduction zone and directly within a 3-m interval identified as a turbidite (see “[Lithostratigraphy](#),” p. 3). As noted at other sites in this region, substantial uptake of fluoride represents a sign of authigenic apatite precipitation (Jahnke et al., 1983; Schuffert et al., 1994). A qualitative comparison of the shapes of the alkalinity, ammonium, and phosphate profiles suggests that phosphate uptake may also occur in the turbidite layer, in support of apatite authigenesis.

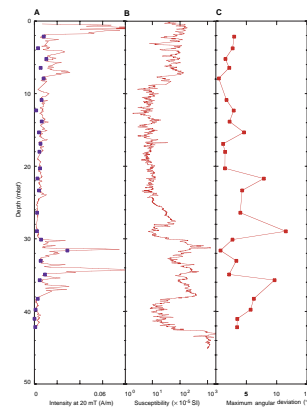
We do not entirely understand the apparently low intensity of organic-matter decay in the upper 20 m of the sediment column at Site 1098. Radiocarbon ages from a nearby gravity core indicate that these relatively organic-rich deposits have accumulated rapidly during the last ~6 k.y. (Leventer et al., 1996), thus organic diagenesis by now should have established strong chemical gradients within the interstitial water. The occurrence of well-laminated intervals between 8 and 23 mbsf and the presence of H₂S below 13 mbsf preclude the rather unlikely possibility that extremely vigorous bioturbation or other mixing has maintained a well-irrigated environment to such depths. We note that many of the laminae in the upper 20 mbsf consist of a nearly monospecific assemblage of the resting spores of *Chaetoceros* diatoms (see “[Lithostratigraphy](#),” p. 3). These tightly encased siliceous spores protect the internal biomass, perhaps rendering it unavailable for bacterial consumption until dissolution breaches the external casing. Other more readily degradable organic matter must exist, however, in the upper 20 mbsf. Also, this scenario conflicts with the occurrence of a shallow sulfate reduction zone in nearby Site 1099 (see “[Organic-Matter Degradation](#),” p. 15), where the sediment also contains an abundance of *Chaetoceros* spores. Finally, we wonder whether the position of the aforementioned turbidite layer precisely within the zone of steepest chemical gradients represents more than a coincidence.

Silica and Carbonate Diagenesis

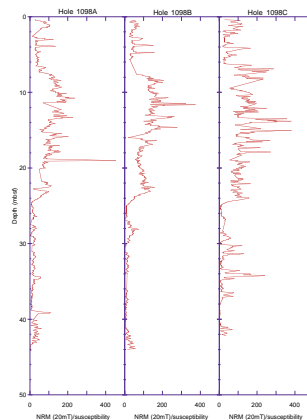
Other inorganic processes, such as dissolution of biogenic silica and precipitation of authigenic carbonate phases, influence the chemical

T26. Results from the PCA of discrete paleomagnetic samples, [p. 104](#).

F20. Intensity of remanence after AF demagnetization at 20 mT for split-core and discrete samples vs. depth, [p. 48](#).



F21. Relative paleointensity at Site 1098, [p. 49](#).



T27. Headspace methane concentrations at Sites 1098 and 1099, [p. 105](#).

T28. Inorganic carbon and elemental analyses for Holes 1098C, 1099A, and 1099B, [p. 106](#).

composition of interstitial water at Site 1098 (Fig. F24). Dissolved silica reaches a high concentration (>0.8 mM) at only 1.5 mbsf, increases slightly (to 0.9 mM) with depth in the upper 42 mbsf, then decreases sharply to a low concentration (0.4 µM) in the deepest sample, at 45 mbsf. The silica profile reflects a state of near saturation with respect to biogenic opal in the predominantly diatomaceous ooze that lies above 42 mbsf in Hole 1098C (Kastner et al., 1977) and undersaturation in the calcareous mud encountered below 42 mbsf (see “[Lithostratigraphy](#),” p. 3).

Dissolved calcium and magnesium concentrations do not change significantly from their seawater values above 20 mbsf, but they decrease sharply by equivalent amounts (~10 mM) between 20 and 30 mbsf and remain essentially constant at greater depths. The coincident uptake of calcium and magnesium in a 1:1 ratio at the base of the sulfate reduction zone strongly suggests the possibility of dolomite formation (Baker and Kastner, 1981), presumably promoted by the high alkalinity produced in the sulfate reduction zone. Although examination of smear slides confirms the presence of authigenic carbonate mineral grains in this depth range and below, we did not find any dolomite. A negligible amount of calcium may also precipitate as authigenic apatite, as discussed above. Dissolved strontium remains constant at its seawater concentration (90 µM) in the upper 20 mbsf at Site 1098, decreases slightly with depth to a minimum concentration (72 µM) at 27 mbsf, and then increases sharply to a high concentration (240 µM) in the deepest sample. Either the calcareous mud encountered at the bottom of the hole or some underlying lithology must act as a strong source of strontium to the interstitial water. Potassium remains essentially constant at its seawater concentration throughout the hole and thus does not participate extensively in clay mineral reactions within the shallow sediment section recovered at this site.

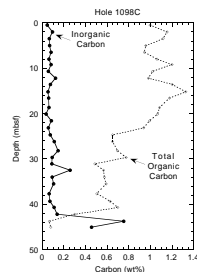
Interstitial Water Chemistry (Site 1099)

We squeezed 12 whole-round core samples for interstitial water at Site 1099 (Table T29). One sample was taken from each core in Holes 1099A and 1099B. Chloride concentrations remain constant with depth (Fig. F25) and indicate an unmodified seawater source for the interstitial water throughout the cored interval.

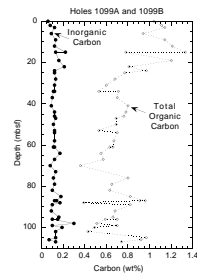
Organic-Matter Degradation

The interstitial water chemistry profiles at Site 1099 (Fig. F25) reflect conditions of rapid burial and intense decay of organic matter. Dissolved sulfate decreases to <50% of its normal seawater value (28 mM) in the upper 3 mbsf and approaches zero by 10 mbsf, and detectable concentrations of methane are present in all samples from below 3 mbsf (Table T27). The sulfate reduction zone thus extends from near the seafloor to <10 mbsf, much shallower than at Site 1098. Dissolved manganese concentrations remain low (<7 µM) in all samples and show no consistent trend with depth. Dissolved iron concentrations remain near zero in the upper 10 mbsf but increase significantly at greater depths and reach a maximum (30 µM) near 50 mbsf. Unless these iron data represent an artifact of contamination or sample processing, the presence of soluble ferrous iron below the sulfate reduction zone implies that either a ferric iron phase persists to such depths before it reduces or iron sulfide minerals have begun to dissolve. Considering

F22. Inorganic carbon and total organic carbon from Hole 1098C, p. 50.

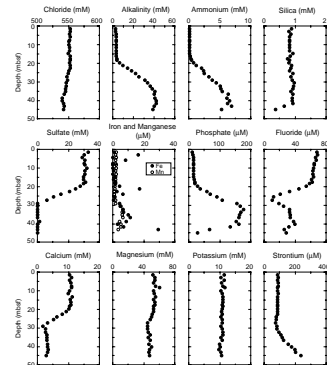


F23. Inorganic carbon and total organic carbon from Holes 1099A and 1099B, p. 51.



T29. Interstitial water analyses for Holes 1098C, 1099A, and 1099B, p. 108.

F24. Profiles of interstitial water chemistry in Hole 1098C, p. 52.



that the sediment at Site 1099 commonly contains as much as 5% pyrite, particularly below 50 mbsf (see “[Site 1098 Smear Slides](#),” p. 18, and “[Site 1099 Smear Slides](#),” p. 13), significant redistribution of iron must occur after deposition.

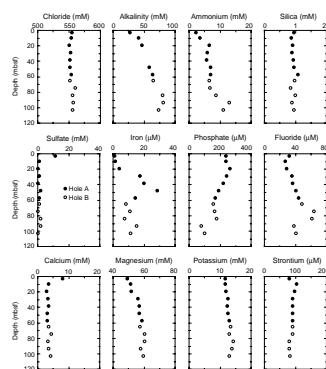
Other direct byproducts of organic-matter decay, such as alkalinity, ammonium, and phosphate, reach extremely high concentrations at Site 1099, even in the upper 3 mbsf (Fig. F25). Alkalinity and ammonium increase steadily with depth to maximum concentrations (80 mM and 13 mM, respectively) at 90 mbsf, whereas phosphate reaches a maximum concentration (260 μ M) at only 20 mbsf, then decreases with depth to lower concentrations (80–100 μ M) below 90 mbsf. Furthermore, the high phosphate concentrations could promote precipitation of authigenic apatite (Jahnke et al., 1983; Schuffert et al., 1994) and account for the low fluoride concentrations (<30 μ M) observed in the upper 20 mbsf. Overall, these results illustrate an order of magnitude increase in the effects of organic-matter decay at Site 1099 compared to Sites 1095, 1096, and 1101 on the continental rise. We attribute this large difference to the higher organic carbon concentrations (0.4–1.2 wt%; Table T28) and much faster sedimentation rate in Palmer Deep. As discussed above, however, the upper portion of the sediment column at Site 1098, located only 6 km away, seems anomalous within this context.

Silica and Carbonate Diagenesis

Inorganic processes, such as dissolution of biogenic silica, precipitation of authigenic carbonate phases, and perhaps diagenesis of clay minerals, may all influence the chemical composition of interstitial water at Site 1099 (Fig. F25). Dissolved silica remains essentially constant (0.9 to 1.0 mM) and nearly saturated with respect to opal-A (Kastner et al., 1977) over the entire depth range, as expected in these diatomaceous sediments (see “[Lithostratigraphy](#),” p. 3). Calcium concentrations decrease sharply in the upper 10 mbsf and remain constant at greater depths, most probably because of authigenic calcite precipitation induced by high alkalinity.

The magnesium and potassium profiles show remarkably similar trends with depth, first increasing by ~20% between 3 and 80 mbsf, then decreasing by a few percent in the lower 20 m of Hole 1099B. This represents the only one of our sites where either of these constituents increases above its seawater concentration. Although these changes could relate to diagenetic reactions in the sediment or interaction with basement rocks, this seems unlikely because the Mg/K value does not vary significantly downcore. Chloride concentrations also do not vary significantly downcore; thus, we exclude the possibility that these data reflect mixing with more-saline water, trapped in the restricted basin at Palmer Deep. Alternatively, the magnesium and potassium data could simply reflect a drift in the performance of the ion chromatograph used in their measurement. Strontium remains within ~10% of its seawater concentration (90 μ M) but decreases slightly (to 80 μ M) below 80 mbsf.

F25. Profiles of interstitial water chemistry in Holes 1099A and 1099B, [p. 53](#).



PHYSICAL PROPERTIES

Whole-Core Measurements

Multisensor Track (MST)

Natural gamma-ray activity, magnetic susceptibility, gamma-ray attenuation porosity evaluator (GRAPE) density, and *P*-wave velocity were measured on whole-round core sections (see “Physical Properties,” p. 20, in the “Explanatory Notes” chapter). All measurements were made to the base of the cores in Holes 1098A, 1098B, and 1098C to depths of 44.98 mbsf (Core 178-1098A-6H), 44.1 mbsf (Core 178-1098B-5H), and 45.17 mbsf (Core 178-1098C-5H), respectively. At Site 1099, GRAPE density, susceptibility, and natural gamma radiation (NGR) measurements were made to the base of Holes 1099A and 1099B at depths of 62.38 mbsf (Core 178-1099A-7H) and 107.62 mbsf (Core 178-1099B-5H), respectively. *P*-wave velocity was measured to the base of Hole 1099A at 62 mbsf and to 69.0 mbsf in Hole 1099B (Core 178-1099B-1H).

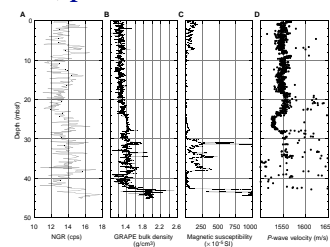
Magnetic Susceptibility

Whole-core magnetic susceptibility was measured at 2-cm intervals (averaged over 2 s). The raw data are provided [on CD-ROM and the World Wide Web](#) for Sites 1098 and 1099. The raw data from Hole 1098C, which was the most continuous of the three holes and apparently covered the greatest stratigraphic range, and the record for Site 1099 are presented in Figures F26 and F27.

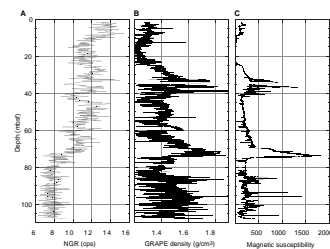
The susceptibility record shows broad intervals of alternating high and low susceptibility (Site 1098 highs are at 0–8 and 30–38 mbsf, and Site 1099 highs are at 0–8, 24–40, and 70–75 mbsf). The low values in the upper 8 m of Hole 1098C coincide with laminated (nonbioturbated) layers. Only one obvious magnetic susceptibility low (at ~4 mbsf) does not correlate with a nonbioturbated region; there is no visible lamination on the split-core surface. The GRAPE density correlates strongly with the magnetic susceptibility (Fig. F28; correlation coefficients of 0.81 and 0.72 for the records are shown in Figures F26 and F27, using programs from Paillard et al., 1996). Within this upper record are variations that have been correlated with climatic cycles of ~2500 and 200 yr by Leventer et al. (1996).

The variability in magnetic susceptibility seen in Core 178-1098C-1H disappears downcore at 9 mbsf, with values dropping steadily to 9×10^{-5} SI (Fig. F28). These lows in susceptibility and GRAPE density are again associated with the laminated (nonbioturbated) diatomaceous ooze. The diatom-rich laminae contain better preserved diatom chains and spines than the bioturbated units (see “[Biostratigraphy](#),” p. 10). It is therefore likely that the low values of density and susceptibility reflect a semi-interlocked skeleton of biosiliceous material. In such a material, porosity is not linearly related to overburden stress, and consolidation does not occur until the overburden stress reaches the yield strength of the diatom chain-links and spines that support the skeleton. The homogeneity of the diatom species and limited size range (see “[Biostratigraphy](#),” p. 10) in these layers also allow a more porous structure to develop in the same manner as a well-sorted granular sediment. The high water content resulting from these processes reduces the bulk density and magnetic susceptibility. More importantly, susceptibility and magnetic

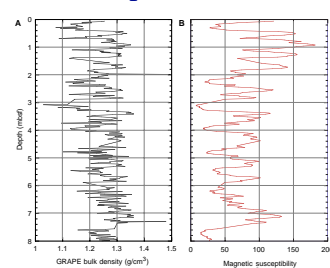
F26. Raw data for NGR, GRAPE density, magnetic susceptibility, and *P*-wave velocity from Hole 1098C, [p. 54](#).



F27. Amalgamated raw data for NGR, GRAPE density, and magnetic susceptibility from Holes 1099A and 1099B, [p. 55](#).



F28. GRAPE bulk density and magnetic susceptibility vs. depth for Hole 1098C, [p. 56](#).



intensity are influenced by the change in the composition of magnetic minerals (see “[Paleomagnetism](#),” p. 11).

GRAPE Bulk Density

Density was measured by gamma-ray attenuation (referred to as GRAPE density) at 2-cm intervals (averaged over 2 s at each point). The raw data are provided [on CD-ROM and the World Wide Web](#) for Sites 1098 and 1099. Hole 1098C and Site 1099 data are shown in Figures [F26](#) and [F27](#), respectively.

The density increases down through the sediments at both sites and further increases steeply below 42 mbsf in Hole 1098C, where the lithology of the sediments changes (see “[Lithostratigraphy](#),” p. 3). Superimposed on this broad trend in Hole 1098C are a decrease in density variability and an increase in density and susceptibility between 24.4 and 28 mbsf, which correspond to a turbidite. However, the higher variability in GRAPE density below 30 mbsf at both sites may be an artifact of gas expansion in the sediments in the laboratory.

P-wave Velocities

The raw data are given [on CD-ROM and the World Wide Web](#). Hole 1098C data are presented in Figure [F26](#). The P-wave velocities are low, as is typical of diatomaceous sediments with a high water content. Velocity decreases between 24.4 and 28 mbsf in Hole 1098C, coincident with increased GRAPE density and the greater sorting and dilution of diatomaceous material within a turbidite (see “[Lithostratigraphy](#),” p. 3). The P-wave data from Hole 1099A are of poor quality because of the extensive presence of gas in cores and show an increase of P-wave velocities only from 1540 to 1570 m/s between 2 and 20 mbsf.

NGR Emissions

Whole-core natural gamma-ray emissions (averaged over 15 s) were counted at 15-cm intervals. The raw data are provided [on CD-ROM and the World Wide Web](#). Hole 1098C and Site 1099 data are given in Figures [F26](#) and [F27](#), respectively.

The NGR record is roughly constant (at 12–16 cps) in Hole 1098C, with an increase below 42 mbsf where the lithology changes significantly (see “[Lithostratigraphy](#),” p. 3). Site 1099 shows a broad trend of decreasing NGR emissions down to 73 mbsf, after which the emissions remain at ~7 cps. The variation may reflect charging of the sediments with radioisotopes as the basins became increasingly influenced by open-marine conditions at the seafloor with time (see “[Biostratigraphy](#),” p. 10). Alternatively, the variation may reflect a lithologic change in the composition of the terrigenous fraction or a diagenetic alteration of clays.

The NGR record shows little correlation with either GRAPE density (correlation coefficients of 0.52 and -0.29 for Hole 1098C and Site 1099, respectively) or magnetic susceptibility (0.48 and -0.16), although any strong correlation would be masked by the lower NGR sampling frequency.

Split-Core Measurements

Index Properties

Gravimetric and volumetric determinations of index properties were made for 17 samples in Hole 1098C, 20 samples in Holes 1099A, and 15 samples in Hole 1099B. Three to four samples were taken per core where appropriate.

Wet mass, dry mass, and dry volume were measured, and from these measurements percentage water weight, porosity, dry density, bulk density, and grain density were calculated (see “Physical Properties,” p. 20, in the “Explanatory Notes” chapter; raw data [on CD-ROM and the World Wide Web](#)). The results for bulk density, grain density, and porosity are given in Figures F29 and F30.

Bulk density from the GRAPE and the index properties bulk density (Figs. F29A, F30A) correlate strongly for both sites. The porosity remains constant in the upper 20 mbsf at Holes 1098C and 1099A, which may reflect the large, well-preserved biogenic component. Below this depth, porosity decreases. In Hole 1098C, grain density increases steadily below 20 mbsf, which suggests a lithologic change that may be reflected in the porosity (for example, a reduction in biogenic material). The relationship is less apparent at Site 1099.

Discrete P-wave Velocities

Discrete P-wave velocity measurements were performed on all cores from Hole 1098C using the Hamilton Frame (PWS3) transducers of the velocity-strength system. The raw data set is provided [on CD-ROM and the World Wide Web](#) and displayed in Figure F31A. The average spatial resolution of the measurements is 1.5 m. In general, the velocities are low (~1560 m/s) with no velocity contrasts in the upper two-thirds of the hole. The increase and stronger contrast in P-wave velocity in the lower part of Hole 1098C coincide with silty and sandy turbidite layers.

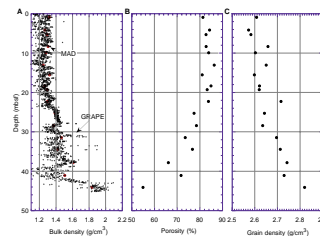
Discrete P-wave measurements were also made on Cores 178-1099A-1H through 7H and on Cores 178-1099B-1H and 2H. This data set is provided [on CD-ROM and the World Wide Web](#) and displayed in Figure F31B. The average spatial resolution of the measurements is 1.4 m. The velocities in the upper part of Hole 1099A (0–20 mbsf) are low (below 1560 m/s) with only small variations. The increase in variability between 20 and 30 mbsf is related to interbedded thin graded silts (see “[Lithostratigraphy](#),” p. 3). The velocity peak between 37 and 40 mbsf is derived from measurements in thin (<4 mm) gray diatom laminae, suggesting a species- or concentration-dependent velocity response in the biogenic material as compared with the MST data. A “low velocity” zone between 42 and 55 mbsf correlates with more bioturbated sections in Cores 178-1099A-5H through 7H (see “[Lithostratigraphy](#),” p. 3).

The exsolution of gas and consequent expansion of cores from below 70 mbsf caused a complete attenuation of the acoustic signal. This zone appeared to be one of slightly larger grain size.

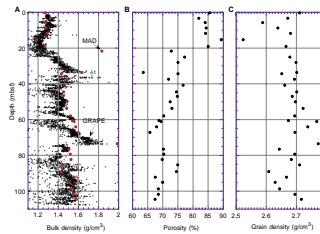
Thermal Conductivity

Thermal conductivity was measured once per core, on average, for almost all holes at Sites 1098 and 1099, usually in the middle of Section 3 and always by the needle-probe method (see “[Physical Properties](#),” p. 20, in the “Explanatory Notes” chapter). Thermal conductivity was

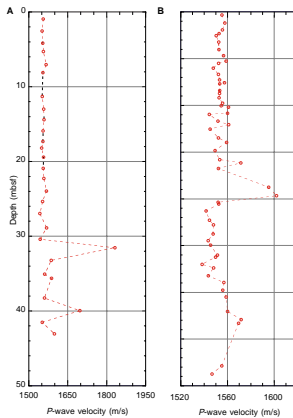
F29. MAD bulk density from index properties and raw GRAPE density, porosity, and grain density for Hole 1098C, [p. 57](#).



F30. MAD bulk density from index properties and raw GRAPE density, porosity, and grain density for Holes 1099A and 1099B, [p. 58](#).



F31. Raw PWS3 data from Sites 1098 and 1099, [p. 59](#).



used at these sites, in combination with downhole temperature measurements, to estimate heat flow and the temperature at the bottom of the hole.

Measured thermal conductivity values at both sites are extremely low. Porosities at these sites are very high (see “[Split-Core Measurements](#),” p. 19; Figs. [F29](#), [F30](#)), ~85% in the upper 20 m at both sites, so that low values of thermal conductivity, approaching that of salt water, are reasonable. However, values from cores in Hole 1099B, below 60 mbsf where porosities are ~70% (above), are among the lowest measured; it is therefore not clear whether all of these measurements are valid. From core images it is evident that free gas was present in these cores in the laboratory, which may have reduced thermal conductivity (see also “[GRAPE Bulk Density](#),” p. 18, and “[P-wave Velocities](#),” p. 18). At this preliminary stage, bearing in mind the few temperature measurements made (below), an average value of thermal conductivity for each hole of 0.71 W/(m·K) has been assumed, which is reasonably compatible with the data (Figs. [F32](#), [F33](#)).

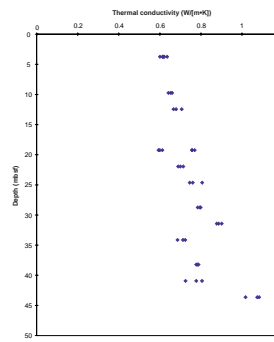
Downhole Temperature Measurements and Geothermal Heat Flow

Temperature measurements were made by the Adara temperature tool at the mudline of both sites, and at two other depths in Hole 1098B and one in Hole 1099A. The temperature gradients (assumed constant at both sites) are 0.103°C/m at Site 1098 and 0.064°C/m at Site 1099. With so few measurements of temperature and uncertainty in the thermal conductivity measurements, only approximate determinations of heat flow are possible. Nevertheless, they are clearly different: heat flow at Site 1098 is about 73 mW/m², whereas at Site 1099 it is 45 mW/m².

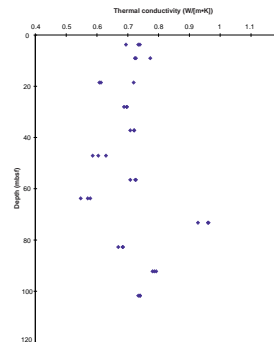
COMPOSITE DEPTHS

Two composite depth scales were developed for Sites 1098 and 1099 based on correlation between spectral reflectance, GRAPE density, natural gamma ray, magnetic susceptibility, and P-wave velocity data (see “[Physical Properties](#),” p. 17, and “[Lithostratigraphy](#),” p. 3; “[Composite Depths](#),” p. 23, in the “Explanatory Notes” chapter). The correlated section lies mainly within the Holocene, with recovery of ~100% for all holes. All parameters (except for P-wave data in Hole 1099B) were measured to 44.98, 44.10, and 45.12 mbsf in Holes 1098A, 1098B, and 1098C, respectively, and as much as 62.38 and 107.62 mbsf in Holes 1099A and 1099B. One composite section for each site was developed, which must be considered preliminary (see also “[Composite Depths](#),” p. 23, in the “Explanatory Notes” chapter). The base of the Site 1098 composite section is at 46.94 meters composite depth (mcd), and the base of the Site 1099 composite section is at 107.94 mcd. The depth offsets that were used to calculate the composite depth sections are given in Table [T30](#). Recovery at Site 1098 was remarkably continuous except for gaps between 1.67 and 1.96, 20.22 and 20.98, and 38.82 and 39.98 mbsf in Hole 1098A; between 5.76 and 6.10, and 34.02 and 34.58 mbsf in Hole 1098B; and between 8.34 and 8.76 mbsf in Hole 1098C. Similar continuity was found at Site 1099 except for three gaps between depths 33.95 and 35.38 mbsf in Hole 1099A and between 77.82 and 79.12, and 97.57 and 98.08 mbsf in Hole 1099B. It was therefore possible to obtain

F32. Thermal conductivity measurements at Site 1098, [p. 60](#).



F33. Thermal conductivity measurements at Site 1099, [p. 61](#).



T30. Depth offsets of Sites 1098 and 1099 mcd scale relative to mbsf depth, [p. 109](#).

a continuous sedimentary sequence for Site 1098 using the data from the three holes. At Site 1099, however, the overlap between Holes 1099A and 1099B was only 2.22 m, so the successive cores in 1099B, below the overlap, were placed at their original depth (mbsf) corrected by addition of the accumulated offset from the upper part of the section.

Chromaticity parameters a^* and b^* were measured at intervals of 1 cm in Hole 1098A, 2 cm in Holes 1098B and 1098C and in the first 27 mbsf of Hole 1099A, and at intervals of 5 cm in the remaining part of Holes 1099A and 1099B. These data were used at both sites as primary correlation parameters (see “[Composite Depths](#),” p. 23, in the “Explanatory Notes” chapter); GRAPE density and magnetic susceptibility were the other primary parameters used for correlation at Sites 1098 and 1099, respectively.

Magnetic susceptibility was not employed as a primary parameter at Site 1098 because the data show broad scale changes. This effect probably resulted from lithologic and diagenetic changes (see “[Physical Properties](#),” p. 17), which made splicer correlation with other parameters uncertain. Natural gamma ray and P -wave measurements provided supplementary verification of core overlap and depth offset.

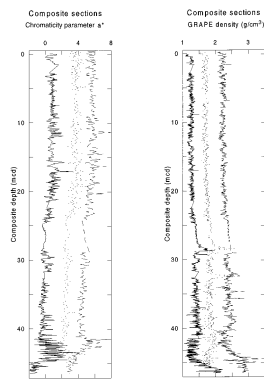
The two principal parameters of the MST records that were useful in correlation are displayed on the composite depth scales in Figures [F34](#) and [F35](#). No smoothing or culling was applied to the data (except for GRAPE density at values lower than one). The correlations between GRAPE density, color reflectance (chromaticity parameter a^*), natural gamma ray, and magnetic susceptibility for Sites 1098 and 1099 are shown in Figures [F36](#) and [F37](#). At Site 1098, we found that all data were well correlated in the first 6.5 mcd, revealing a cyclic pattern with a wavelength of ~60 cm. Color reflectance and GRAPE data were correlated down to 12.5 mcd. Below this depth, the data seem not to correlate except for three intervals: from 25 to 30 mcd (color reflectance and GRAPE density), from ~32 to 34 mcd (magnetic susceptibility, GRAPE density, and natural gamma ray data), and from ~41.5 to 43.5 mcd (inverse correlation between magnetic susceptibility and color reflectance).

At Site 1099, the upper 15 mcd seem to show a cyclic pattern with a wavelength of 2.5 m. Below this depth down to 60 mcd, mostly inverse or no correlation was observed between magnetic susceptibility, color reflectance (chromaticity parameter a^*), and natural gamma ray. Between ~60 and 85 mcd, the data seem to show no correlation except for a 62–72 mcd interval, in which GRAPE density and magnetic susceptibility correlate quite well. GRAPE density, magnetic susceptibility, and spectral reflectance appear to be directly correlated between 85 mcd and the base of the section.

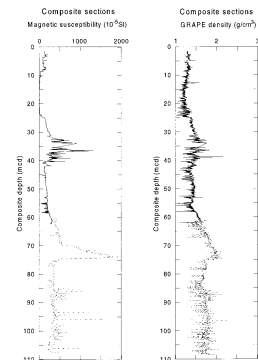
Depth offset typically increases with depth, reflecting the fact that cumulative depth corrections are determined for each core. At Sites 1098 and 1099, the “growth” of the mcd scale with respect to the mbsf scale is of 6% and 1%, respectively (Figs. [F38](#), [F39](#)).

Following construction of the composite depth section for Sites 1098 and 1099, two single-spliced records were built, avoiding where possible intervals with significant disturbance or distortion. They consist of Cores 178-1098C-1H, 178-1098A-2H, 178-1098C-2H, 178-1098A-3H, 178-1098B-3H, 178-1098A-4H, 178-1098B-4H, 178-1098A-5H, and 178-1098C-5H for Site 1098 and of all cores with the exception of the first 2.2 m in Core 178-1099B-1H for Site 1099 (Figs. [F40](#), [F41](#)). The tie points for the splices are given in Table [T31](#).

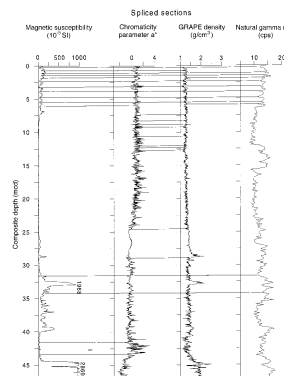
F34. Color reflectance and GRAPE density data from Site 1098 on the mcd scale, [p. 62](#).



F35. Magnetic susceptibility and GRAPE density data from Site 1099 on the mcd scale, [p. 63](#).



F36. Magnetic susceptibility, color reflectance, GRAPE density, and natural gamma ray data with correlations, [p. 64](#).



SEISMIC STRATIGRAPHY

Previous geophysical surveys in the Palmer Deep area comprise the 1992 cruise of the *Polar Duke* (U.S. Antarctic Program) and the 1997 survey of the *OGS-Explora* (Programma Nazionale di Ricerche in Antartide) (see “**Seismic Stratigraphy**,” p. 22, in the “Explanatory Notes” chapter, and “**Appendix**,” p. 24, and Fig. AF1, p. 59, both in the “Leg 178 Summary” chapter). During these surveys, very high-resolution (i.e., decimeter scale) Huntec deep-tow boomer (DTB) and lower resolution, single-channel air gun seismic profiles, respectively, were collected (see “**Background and Scientific Objectives**,” p. 1). Seismic stratigraphic interpretations of these profiles were made by Kirby (1993) and Rebisco et al. (1998). Both data sets have been used at Sites 1098 and 1099 to establish the acoustic stratigraphy described below. Physical properties of cores are used to correlate the cored section with seismic units and assign true depths to reflectors.

Seismic Models and Correlations

Density/Velocity Models

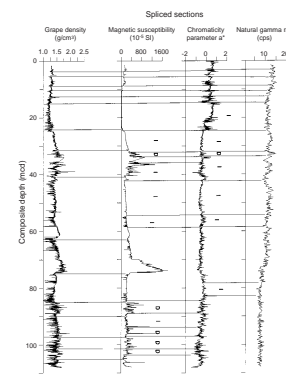
Bulk densities for the formation have been derived from MST (GRAPE) measurements (2-cm spatial resolution) and index property measurements (3.1-m spatial resolution, Site 1098; 3.5-m spatial resolution, Site 1099 [see “**Physical Properties**,” p. 17]). Both sections were cored using an APC, which provides undisturbed sediment that yields a high-quality MST (GRAPE) density record. Low GRAPE density values resulting from gas expansion gaps in the core from the lower part of Site 1099 have been removed using methods described in “**Seismic Stratigraphy**,” p. 29, in the “Explanatory Notes” chapter. Spliced density and velocity data (see “**Composite Depths**,” p. 20) have been used for acoustic models at both sites (Figs. F42, F43).

Two differently derived velocities are available. The MST logger provided continuous data (4-cm spatial resolution) for all cores of Site 1098 and the upper 70 mbsf of Site 1099. Additionally, discrete PWS3 Hamilton Frame measurements with a lower spatial resolution (1.4–1.5 m; see “**Physical Properties**,” p. 17) are available. The model for Site 1098 uses MST velocities, and PWS3 velocities are used for the Site 1099 model. High MST *P*-wave velocities below 35 mbsf at Site 1098 are possibly an artifact (they show no correlation with the density) and should be re-evaluated (Fig. F42 [note that not all of the scatter is displayed in Fig. F26]). The lack of *P*-wave data below 77.5 mbsf at Site 1099, resulting from core disturbance by gas exsolution, has been compensated for by extrapolation, using a third-order polynomial (Fig. F43).

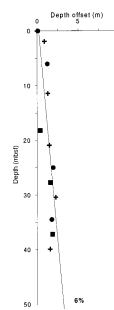
Source Signals

Three different source signals are used for the seismic models at Sites 1098 and 1099: the far-field and seafloor signatures of the Generator Injector (GI) gun (as described in “**Seismic Stratigraphy**,” p. 33, in the “Site 1095” chapter) and a high-resolution digital recording of a Huntec far-field signal (P. Simptkan, pers. comm., 1997). The very short Huntec signal with a length of 0.25 ms and a continuous energy spectrum up to 10,000 Hz is displayed in Figure F44. With a vertical resolution of 0.2 m (under optimal circumstances), the DTB system is capable of producing ultrahigh-resolution records of non-indurated sediments.

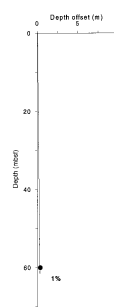
F37. GRAPE density, magnetic susceptibility, color reflectance, and natural gamma ray data with correlations, p. 65.



F38. Depth offsets of Site 1098 mcd scale relative to mbsf depth, p. 66.



F39. Depth offsets of Site 1099 mcd scale relative to mbsf depth, p. 67.



Time-Depth Models

Depth/traveltime curves have been calculated using the available velocity data (Fig. F45). At both sites, the traveltime/depth relationship is close to linear. The steepening of the Site 1098 curve in the lower part is possibly the result of incautious use of MST P -wave data (velocities increase in the lower part [see PWS3 data, in “Physical Properties,” p. 17]).

Synthetic Seismograms

The spliced and corrected velocity and density data were resampled at 0.2-m (Site 1098) and 0.15-m (Site 1099) resolution. The reflectivity series of Site 1098 was convolved only with the Huntec signal because no profile taken over Basin I with any other acoustic source (air gun and GI gun) showed comparable detail within the shallow basin fill. The velocity/density data, the impedance curve, reflectivity coefficients, and an unfiltered synthetic trace are displayed in Figure F42.

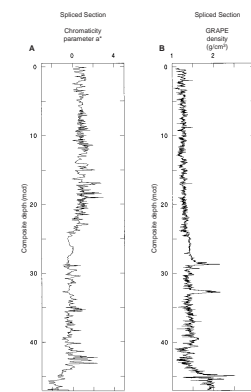
For Site 1099, the acoustic impedance model was convolved with the GI gun far-field and seafloor, and with Huntec signals (Fig. F43). A depth axis is displayed next to the time scale to allow convenient travelttime/depth conversion for both sites. Extreme frequency and resolution differences are obvious within the synthetic traces derived from the three different source signals at Site 1099. The time delay between an impedance contrast (e.g., at 0.043 s) and the corresponding reflection within the synthetic trace increases dramatically with the wavelength of the different signals. The response of the Huntec trace is “instant.” The GI far-field response occurs at 0.048 s, and the GI seafloor trace of 40 ms shows a response at 0.055. To eliminate these effects, reflector depths must be measured with respect to the onset of the seafloor reflection.

Comparison of Synthetic Seismograms and the Seismic Reflection Profiles

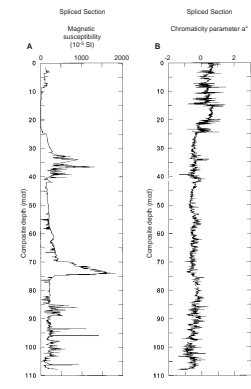
The Huntec traces for Sites 1098 and 1099 were resampled at 20,000 Hz and subsequently filtered using a zero-phase equi-ripple band-pass filter (pass band = 800–4500 Hz; attenuation = 40 dB; and filter order = 40 [Fig. F44]) to match their frequency content to a commonly used frequency range for the DTB-record display (Fig. F46). Most of the prominent reflectors are represented within the synthetic traces for Site 1098 (see “Seismic Units,” p. 24). At Site 1099, the upper 40 ms reveal all the important reflectors of the DTB profile (Fig. F47). For a detailed discussion and description of the seismic section, see “Seismic Units,” p. 24.

Additionally, the GI gun seafloor synthetic trace (based on the same impedance model) has been filtered using a zero-phase equi-ripple band-pass filter (pass band = 30–110 Hz; attenuation = 35 dB; and filter order = 70) and processed to meet the processing specifications of seismic line I97H-219G crossing Basin III (zero-phase Butterworth band-pass filter [pass band = 30–110 Hz], automatic-gain recovery window of 100 ms, static shift and cutting, and interpolation to 0.5-ms resolution). The only feature that can be identified with some confidence is a broad reflector at 50 ms TWT (Fig. F48).

F40. Spliced records for Site 1098: color reflectance and GRAPE density data, p. 68.

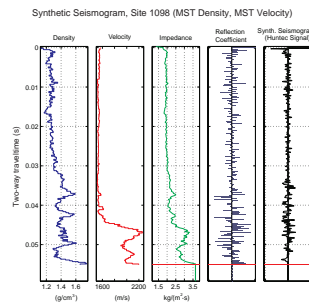


F41. Spliced records for Site 1099: magnetic susceptibility and color reflectance data, p. 69.



T31. Spliced cores for Holes 1098A, 1098B, 1098C, 1099A, and 1099B, p. 110.

F42. Synthetic seismogram and acoustic properties of Site 1098 using Huntec signal, p. 70.



Seismic Stratigraphy: Site 1098

Seismic Units

At Site 1098, we sampled sediments within a narrow basin, Basin I of Kirby (1993) and Rebescu et al. (1998) in Palmer Deep, to a depth of 46.7 mbsf, reaching acoustic basement. In the single-channel air gun seismic profile I97H-218G, we identified one seismic unit above acoustic basement (Fig. F49).

Seismic Unit I (0–46.7 mbsf) is acoustically semitransparent with some low-amplitude reflectors toward the base of the unit that onlap the irregularities of acoustic basement (Fig. F49). High-resolution DTB seismic profiles penetrate to ~43 mbsf and allow division of seismic Unit I into three subunits (Fig. F46): (1) Subunit Ia (0–7 mbsf) is characterized by stratified continuous reflectors with a high-amplitude reflector at its base, (2) Subunit Ib (7–23 mbsf) consists of parallel reflectors at the top but becomes more transparent toward the bottom, and (3) Subunit Ic (23–43 mbsf) is mainly acoustically transparent but with high-amplitude reflectors at 30, 33, and 38 mbsf (T1, T2, and T3 in Fig. F46). The synthetic seismogram clearly reveals the high-amplitude reflections that occur at the base of Subunit Ia and at the T1, T2, and T3 reflectors in Subunit Ic. Higher and lower amplitude reflection patterns in the synthetic traces can be correlated with acoustically stratified and semitransparent acoustic facies, respectively, in the DTB seismic profile (Fig. F46). Seismic Unit I has a drape geometry, indicated by uniform thickness of the unit in the central part of the basin and a bottom morphology that follows the irregularities of acoustic basement (Fig. F46).

Interpretation

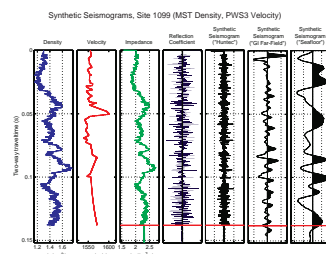
Parallel reflectors and sheet drape geometries in both air gun and DTB seismic profiles are compatible with sedimentation dominated by hemipelagic/pelagic settling and low-density gravity flows. High-resolution DTB profiles allow direct correlation between acoustic character, synthetic traces, and lithology (Fig. F46). The reflector marking the base of seismic Subunit Ia corresponds roughly to the base of a massive, bioturbated muddy diatom ooze (see “[Lithostratigraphy](#),” p. 3). This reflector is located ~2.5 m below the base of Subunit Ia of Rebescu et al. (1998). Semitransparent and stratified reflectors of seismic Subunit Ib correspond to a 15-m interval where laminated sediments predominate. The base of Subunit Ib coincides with the base of Unit Ib of Rebescu et al. (1998) (Fig. F46) (see “[Lithostratigraphy](#),” p. 3). High-amplitude reflections in the synthetic traces of seismic Subunit Ic correspond to an acoustically semitransparent subunit in the DTB profiles. This suggests that the acoustic character of this unit is the result of limitations in the penetration of the DTB system and is not a real consequence of the stratigraphic and lithologic character of Subunit Ic. Three turbidite layers, T1 through T3, are correlated with high-amplitude reflectors at 30, 33, and 38 mbsf (see “[Lithostratigraphy](#),” p. 3).

Seismic Stratigraphy: Site 1099

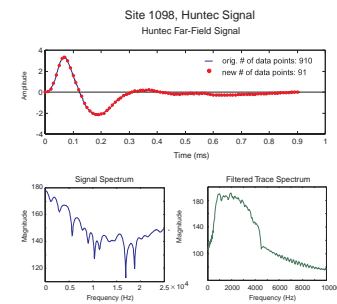
Seismic Units

Site 1099 was drilled to a depth of 107.5 mbsf in Palmer Deep Basin III (Kirby, 1993; Rebescu et al., 1998). Two main seismic units can be differentiated in the air gun profile (Fig. F50).

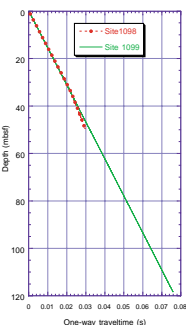
F43. Synthetic seismograms and acoustic properties of Site 1099 using three different source signals, p. 71.



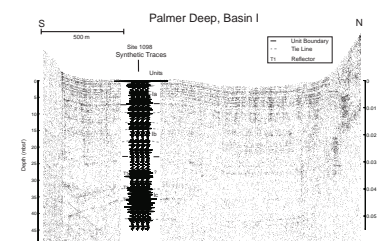
F44. Characteristics of the Huntec deep-tow boomer signal and a filtered synthetic trace, p. 72.



F45. Time-depth relationships at Sites 1098 and 1099, p. 73.



F46. Deep-tow boomer profile across Site 1098, p. 74.



Seismic Unit I (0–76 mbsf) is acoustically semitransparent (Fig. F50). A high-amplitude reflector, previously referred to as the MBR (Kirby, 1993; Rebesco et al., 1998), divides Unit I in two. Thickness of Unit I is uniform in the center of the basin and reduces toward the edges of the basin. High-resolution DTB profiles penetrate the upper 34 m of seismic Unit I to the MBR (Fig. F47). Acoustic character above the MBR in this high-resolution profile allows us to differentiate seven acoustic packages characterized by low-amplitude reflectors at the top and parallel higher amplitude reflectors at the bottom. In Figure F47, we assign letters from *a* through *g* to the base of acoustic packages at 4.5, 8, 10, 12, 14, 19, and 21 mbsf, respectively. The synthetic seismogram at this site shows the correlation between high-amplitude reflections and the base of the acoustic packages (Fig. F47). The deepest strong reflector in the DTB profiles and a high-amplitude reflection in the synthetic seismogram are found at 34 mbsf and correspond to the MBR (also named *h* in Fig. F47). The MBR in the air gun seismic profile is a horizontal reflector that can be traced across the basin. In the middle of the basin, the MBR has lower amplitude and an irregular surface. Toward the sides of the basin, it grades to a higher amplitude reflector that onlaps a more acoustically transparent and chaotic package of reflectors. The MBR in the DTB profiles is a reflector that parallels the irregularities of the sea bottom.

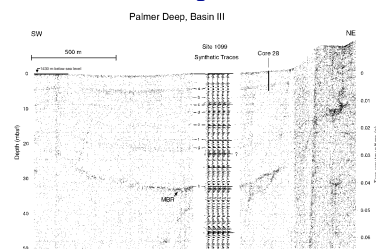
Seismic Unit II (76–107.5 mbsf) in the air gun profiles is characterized by horizontally stratified high-amplitude and continuous reflectors (Fig. F50). Reflectors in the upper part of this unit are flat-lying in the center of the basin, “climb” up at its eastern edge, and terminate abruptly in the western part of the basin. Below, reflectors exhibit typical onlap fill geometry either against the acoustic basement or against a package of irregular and chaotic reflectors. Thickness of seismic Unit II varies across the basin because of irregularities in the acoustic basement.

Interpretation

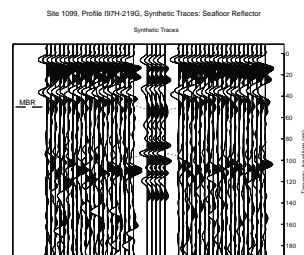
Seismic Unit I above the MBR (the top 34 mbsf) is dominantly massive and laminated muddy diatom ooze. The higher amplitude reflectors (i.e., Reflectors *a* through *g*) at the base of the seven acoustic packages identified in the DTB seismic profiles correspond to seven thin interbedded turbidites in the upper 23 m of the core. Reflectors *a*, *e*, and *f* coincide with the base of Units Ia, Ib, and Ic, respectively, of Rebesco et al. (1998). The MBR, apparent in both air gun and DTB profiles at 34 mbsf, corresponds to a layer of coarse sand and pebbles interpreted as a clast-poor diamict layer with a diatom clayey silt matrix (see “[Lithostratigraphy](#),” p. 3). The acoustically semitransparent unit below the MBR corresponds roughly to a thick interval of massive, diatom clayey silt and muddy diatom ooze (Fig. F11). High-amplitude stratified reflectors of seismic Unit II correspond to alternations of massive, bioturbated, muddy diatom ooze, laminated mud-bearing diatom ooze, and very fine-grained graded turbidites (see “[Lithostratigraphy](#),” p. 3).

The overall onlapping fill character of the seismic units drilled in the Palmer Deep basins suggests that the style of sedimentation was dominated by hemipelagic drape and by infilling of the basins with sediment gravity flows, probably from a local source. An intrabasinal source for sediments is suggested by the irregular reflector packages on the sides of the basin (i.e., the western side in Fig. F50). The “climbing” reflectors of

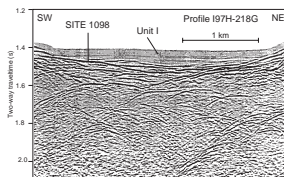
F47. Deep-tow boomer profile across Site 1099, [p. 75](#).



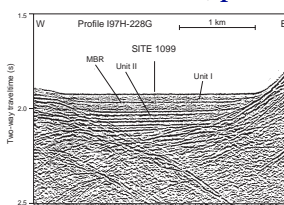
F48. Synthetic seismogram and GI gun reflection seismic profile I97H-219G of Basin III, [p. 76](#).



F49. GI gun seismic profile I97H-218G across Site 1098, [p. 77](#).



F50. Air gun seismic profile I97H-228G across Site 1099, [p. 78](#).



Unit I and the uppermost reflectors of Unit II at the edge of the basin may be interpreted as suggesting neotectonic activity in the basin.

REFERENCES

- Baker, P.A., and Kastner, M., 1981. Constraints on the formation of sedimentary dolomite. *Science*, 213:215–216.
- Froelich, P.N., Klinkhammer, G.P., Bender, M.L., Luedtke, N.A., Heath, G.R., Cullen, D., Dauphin, P., Hammond, D., Hartman, B., and Maynard, V., 1979. Early oxidation of organic matter in pelagic sediments of the eastern equatorial Atlantic: suboxic diagenesis. *Geochim. Cosmochim. Acta*, 43:1075–1090.
- Ishman, S.E., and Domack, E.W., 1994. Oceanographic controls on benthic foraminifers from the Bellingshausen margin of the Antarctic Peninsula. *Mar. Micropaleontology*, 24:119–155.
- Jahnke, R.A., Emerson, S.R., Roe, K.K., and Burnett, W.C., 1983. The present day formation of apatite in Mexican continental margin sediments. *Geochim. Cosmochim. Acta*, 47:259–266.
- Kastner, M., Keene, J.B., and Gieskes, J.M., 1977. Diagenesis of siliceous oozes, I. Chemical controls on the rate of opal-A to opal-CT transformation—an experimental study. *Geochim. Cosmochim. Acta*, 41:1041–1059.
- Kirby, M.E., 1993. High-resolution seismic stratigraphy and sedimentology of Holocene glacial marine deposits in the Palmer Deep, Bellingshausen Sea, Antarctica [B.A. thesis]. Hamilton College, Clinton, NY.
- Kirby, M.E., Domack, E.W., Ishman, S.E., and McClenen, C.E., 1998. Magnetic stratigraphy and sedimentology of Holocene glacial marine deposits in the Palmer Deep, Bellingshausen Sea, Antarctica. *Mar. Geol.*, 152:247–259.
- Leventer, A., Domack, E.W., Ishman, E., Brachfeld, S., McClenen, C.E., and Manley, P., 1996. Productivity cycles of 200–300 years in the Antarctic Peninsula region: understanding linkages among the sun, atmosphere, oceans, sea ice, and biota. *Geol. Soc. Am. Bull.*, 108:1626–1644.
- Osterman, L.E., and Kellogg, T.B., 1979. Recent benthic foraminifer distributions from the Ross Sea, Antarctica: relation to ecologic and oceanographic conditions. *J. Foraminiferal Res.*, 9:250–269.
- Paillard, D., Labeyrie, L., and Yiou, P., 1996. Macintosh program performs time-series analysis. *Eos*, 77:379.
- Pudsey, C.J., Barker, P.F., and Larter, R.D., 1994. Ice sheet retreat from the Antarctic Peninsula shelf. *Cont. Shelf Res.*, 14:1647–1675.
- Rebesco, M., Camerlenghi, A., DeSantis, L., Domack, E.W., and Kirby, M.E., 1998. Seismic stratigraphy of Palmer Deep: a fault bounded Late Quaternary sediment trap on the inner continental shelf, Antarctic Peninsula Pacific Margin. *Mar. Geol.*, 151:89–110.
- Rebesco, M., Camerlenghi, A., and Zanolla, C., in press. Bathymetry and morphogenesis of the continental margin west of the Antarctic Peninsula. *Terra Antarct.*
- Schuffert, J.D., Jahnke, R.A., Kastner, M., Leather, J., Sturz., A., and Wing, M.R., 1994. Rates of formation of modern phosphorite off western Mexico. *Geochim. Cosmochim. Acta*, 58:5001–5010.
- Wetzel, A., 1984. Bioturbation in deep-sea fine-grained sediments: influence of sediment texture, turbidite frequency and rates of environmental change. In Stow, D.A.V., and Piper D.J.W. (Eds.), *Fine-Grained Sediments: Deep Water Processes and Facies*. Geol. Soc. Spec. Publ. London, 24:595–608.

Figure F1. Location of Palmer Deep (bathymetry from Rebesco et al., *in press*). Note that the low resolution of this bathymetry does not show the three sub-basins that comprise Palmer Deep. See Figure F2, p. 29, for detailed bathymetry.

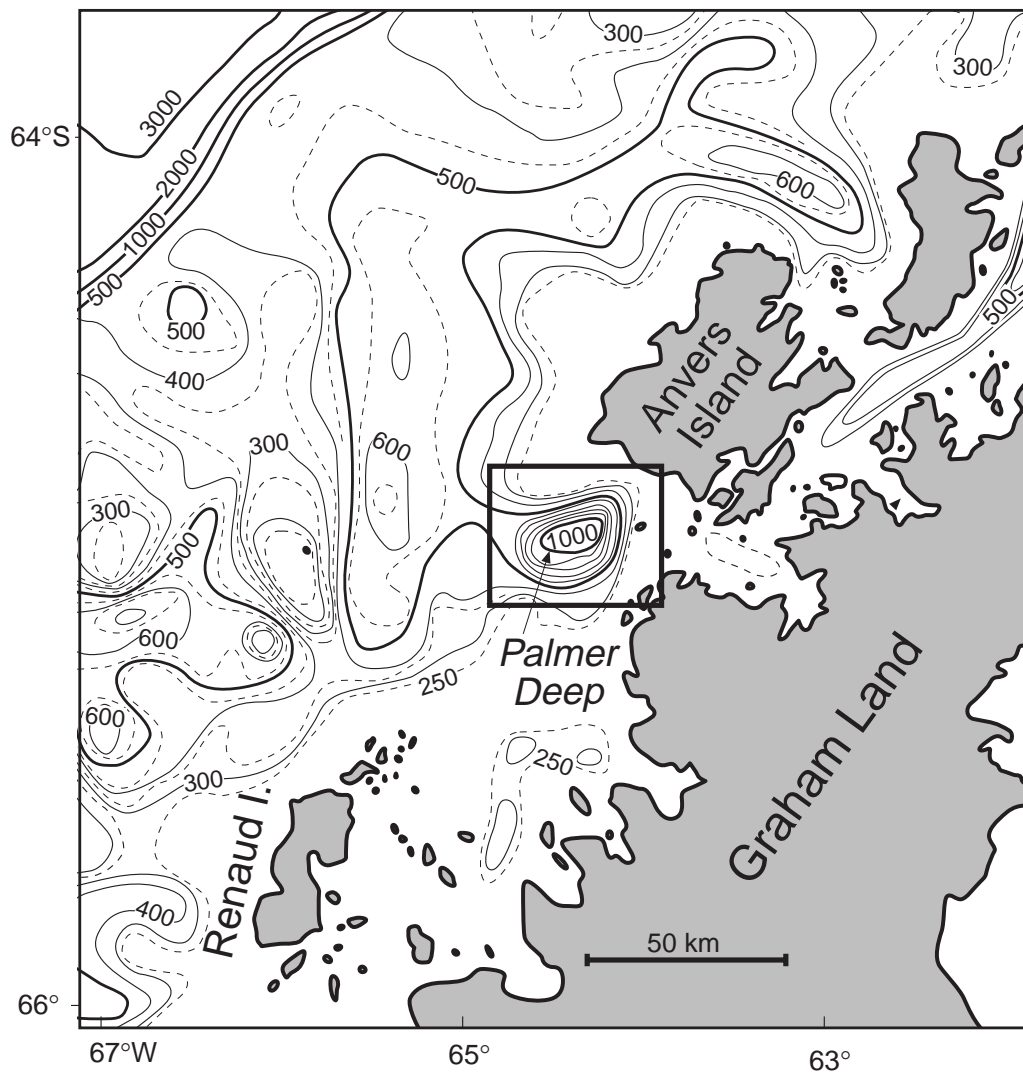


Figure F2. Bathymetry and location of site-survey seismic reflection profiles on Palmer Deep (revised from Kirby, 1993). Location of the 3.5-kHz sub-bottom profile obtained by the *JOIDES Resolution* (*JR*) is indicated by the thickest bold line.

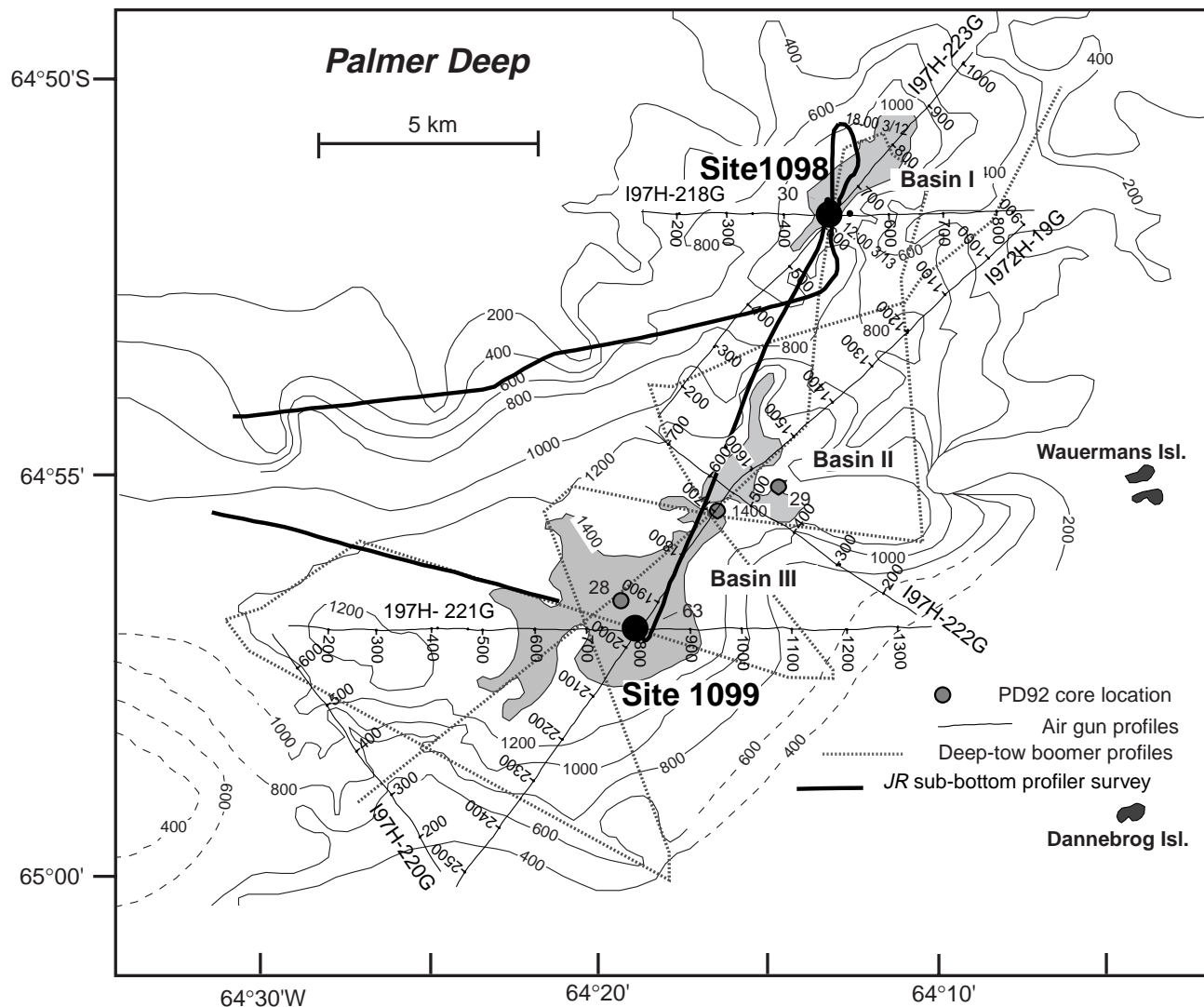


Figure F3. East-west air gun single-channel seismic reflection profile crossing Basin I over Site 1098 (see location in Fig. F2, p. 29). Acoustic energy is diffracted by the steep slopes of the basin sides.

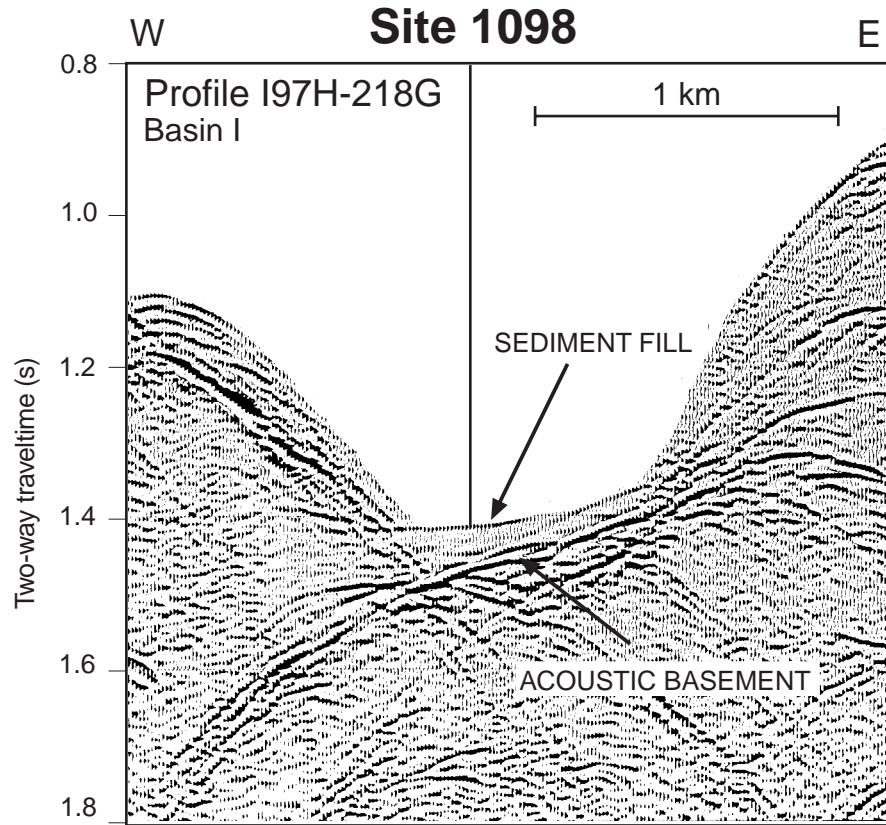


Figure F4. A. The 3.5-kHz sub-bottom profile collected at ~5 kt across Site 1098, in Palmer Deep Basin I (see location in Fig. F2, p. 29). The poor quality of the record was probably a result of the noise produced by other ships (*Polar Duke* and *Laurence M. Gould*) nearby and of the diffraction of acoustic energy by icebergs and steep basin sides. B. Detail of sub-bottom record on site collected at very low speed (~2 kt) during ship positioning.

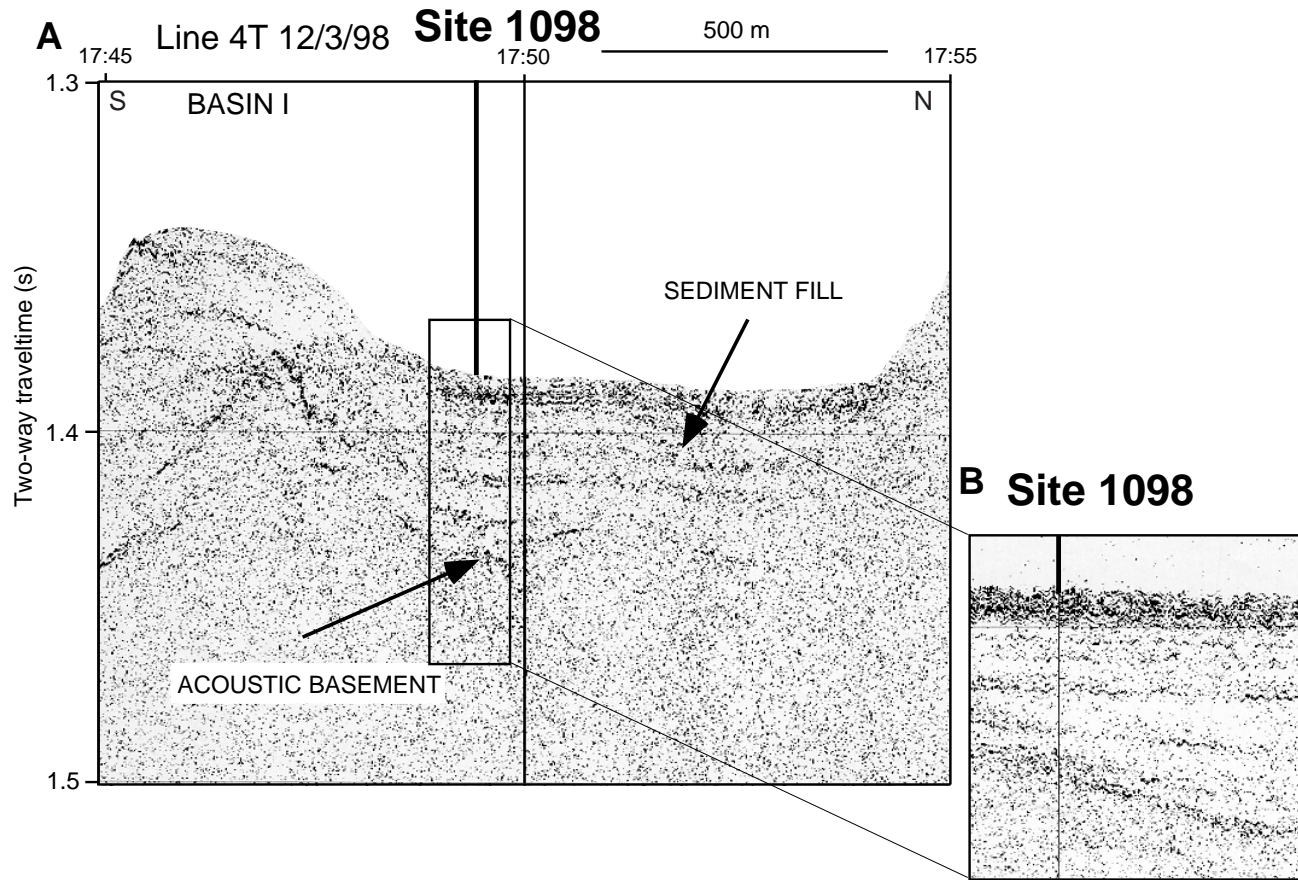


Figure F5. East-west air gun single-channel seismic reflection profile (A) and line drawing (B) crossing Basin III over Site 1099. F = a postulated normal fault that gives the structure of the basin a half-graben character (Rebesco et al., 1998).

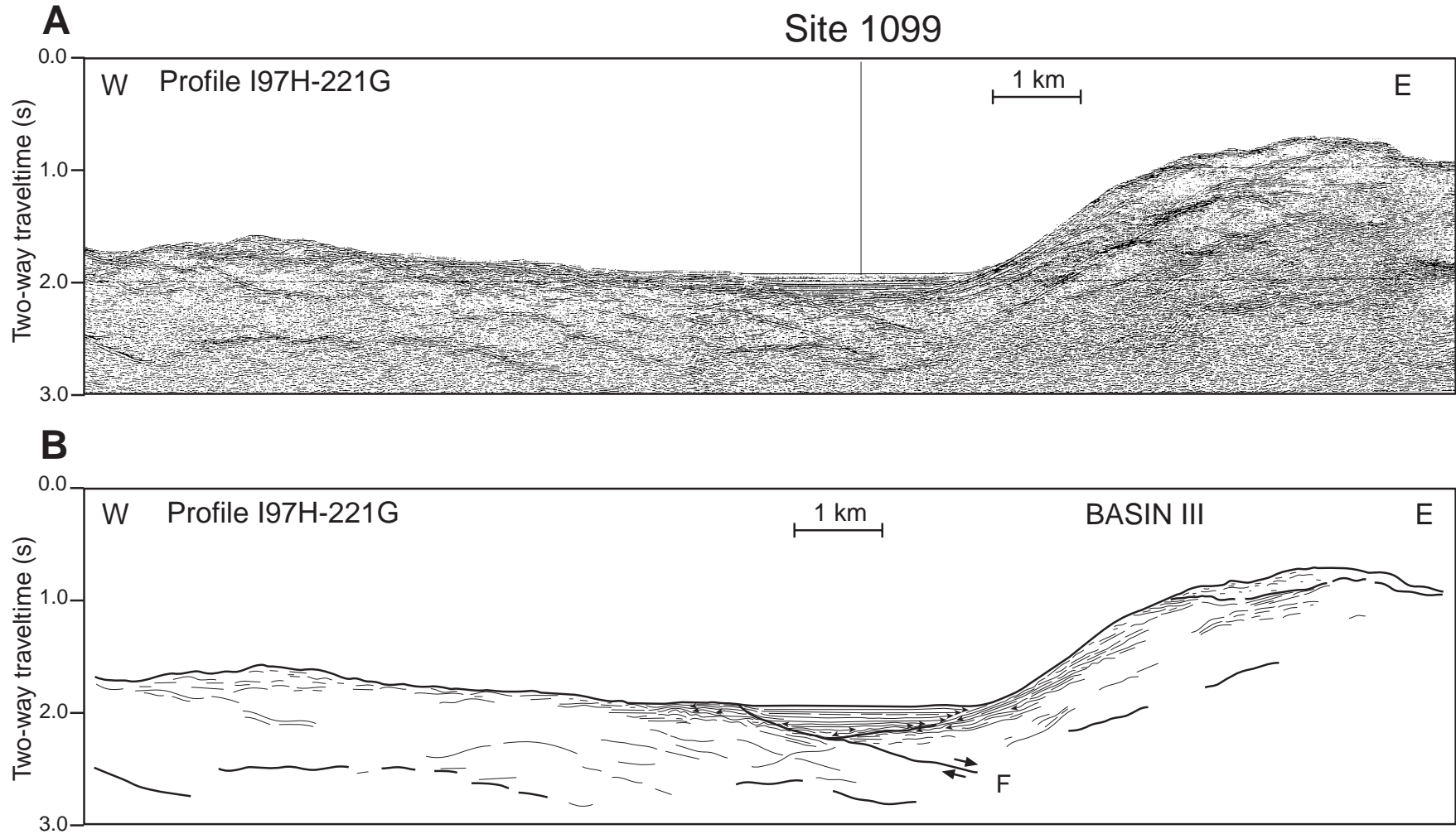


Figure F6. The 3.5-kHz sub-bottom profile collected at 5 kt across Site 1099, in Palmer Deep Basin III (see location in Fig. F2, p. 29) during site approach.

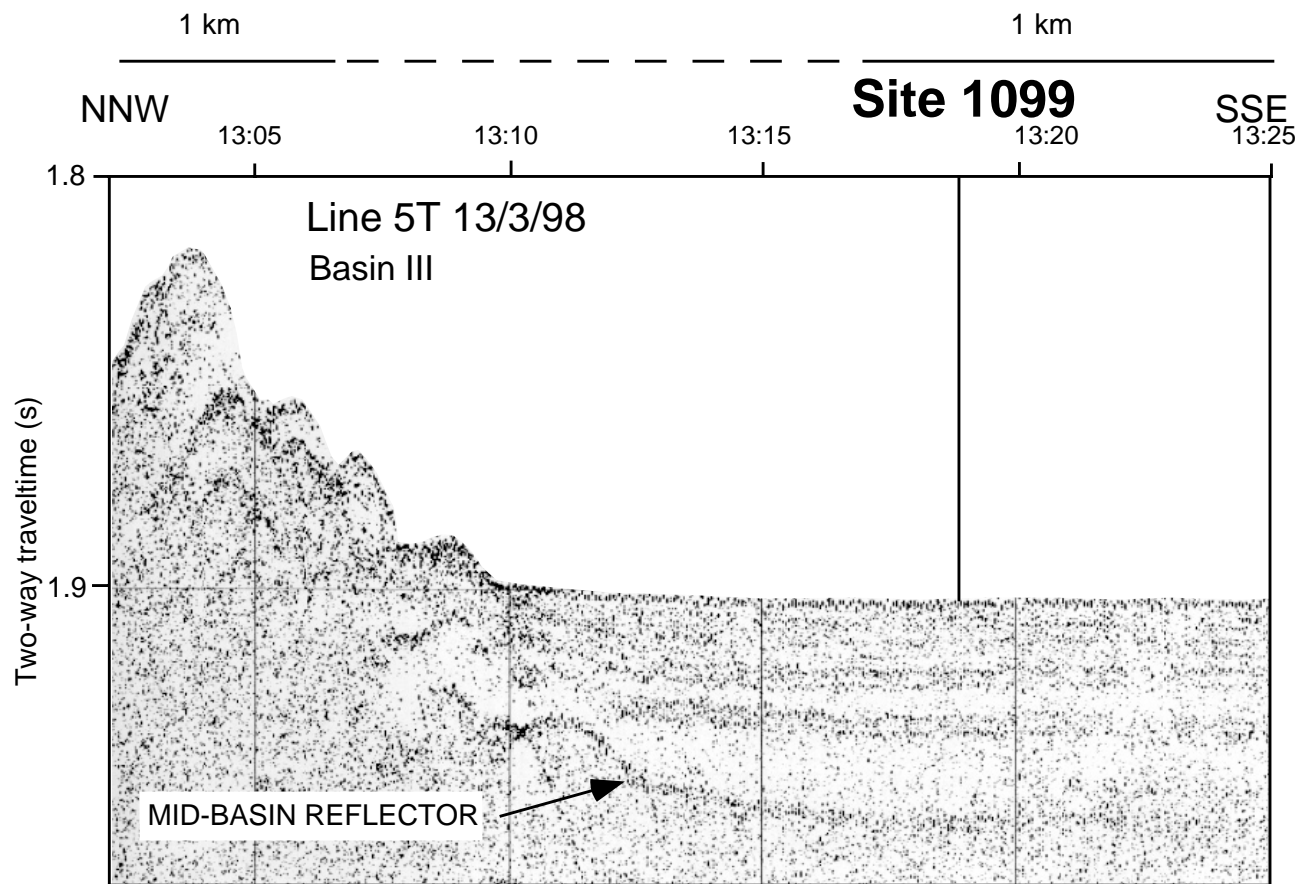


Figure F7. Lithostratigraphic column for Site 1098. Summarized lithology and percent biogenic component for Holes 1098A, 1098B, and 1098C. Magnetic susceptibility data are from Hole 1098B. Laminated oozes occur in packets 0.1–2.2 m thick. They dominate the sequence from 9 to 23 mbsf and below 40 mbsf. Massive, bioturbated ooze occurs in units 0.1–1.9 m thick. In the upper 6.5 m, laminated sediments have low values of magnetic susceptibility. Each turbidite base has high magnetic susceptibility. T.D. = total depth of each hole.

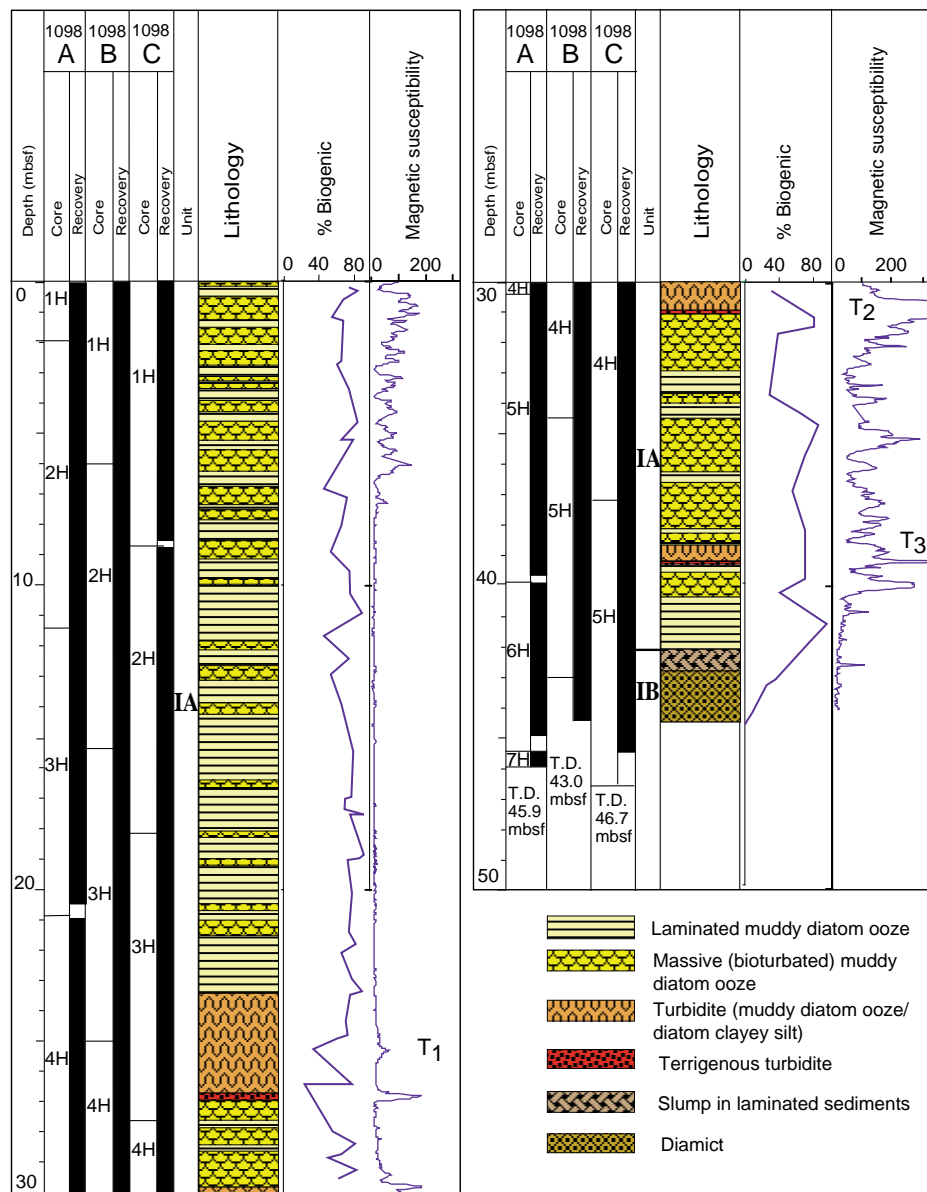


Figure F8. Sand:silt:clay ratio, percent biogenic and terrigenous, pebble occurrence, and chromaticity parameter a^* for Site 1098. In the first three columns, data points are joined by straight lines.

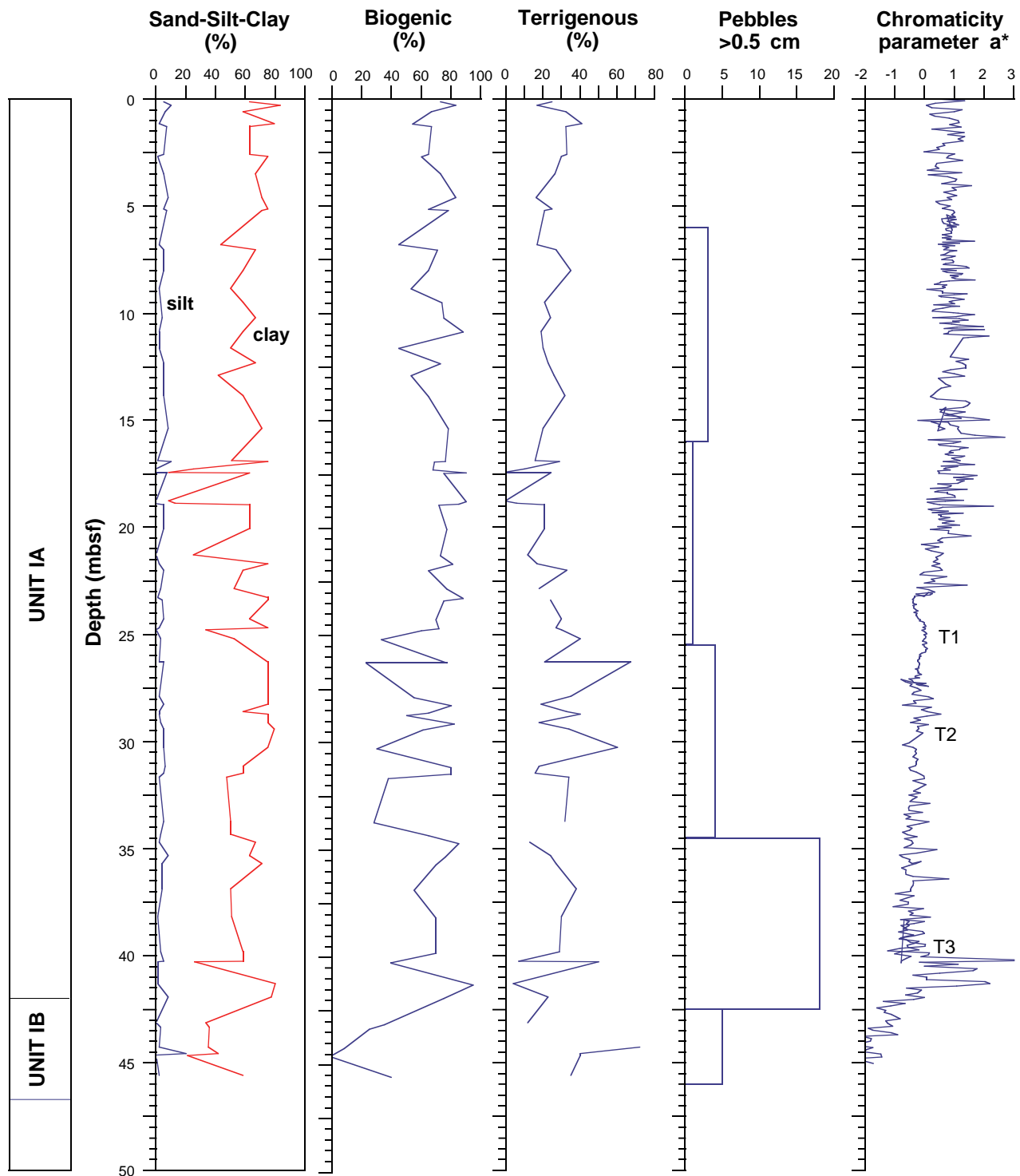


Figure F9. Laminated diatom ooze rich in *Corethon criophilum* (pale layers) or *Chaetoceros* spp. spores (dark layers; interval 178-1098B-1H-3, 69–93 cm).

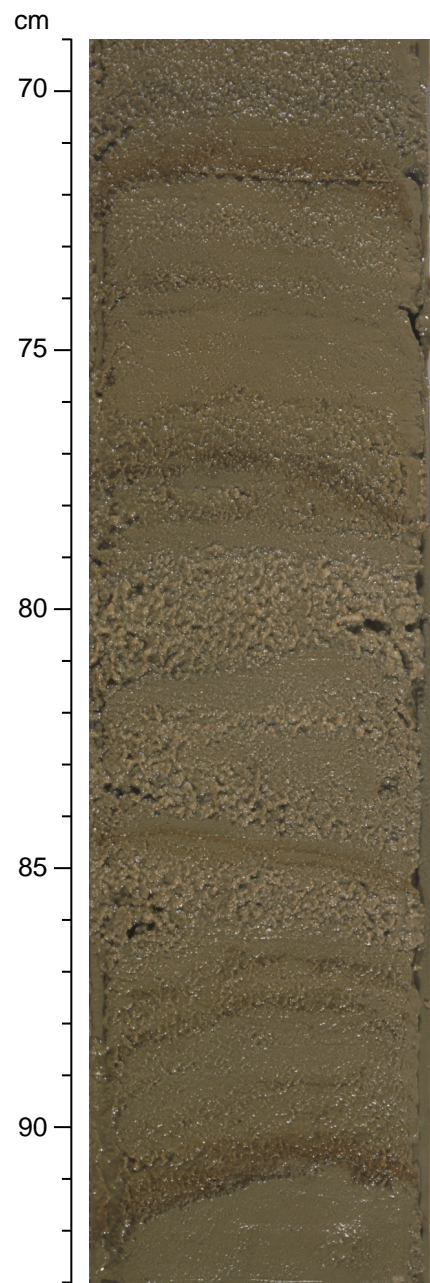


Figure F10. Deformation style in the lowest sediments recovered in Holes 1098A, 1098B, and 1098C. The base of turbidite T3 is used as a datum at the top of each column. The ship's offset between Holes 1098A, 1098B, and 1098C was 10 m to the north (i.e., toward the center of the basin).

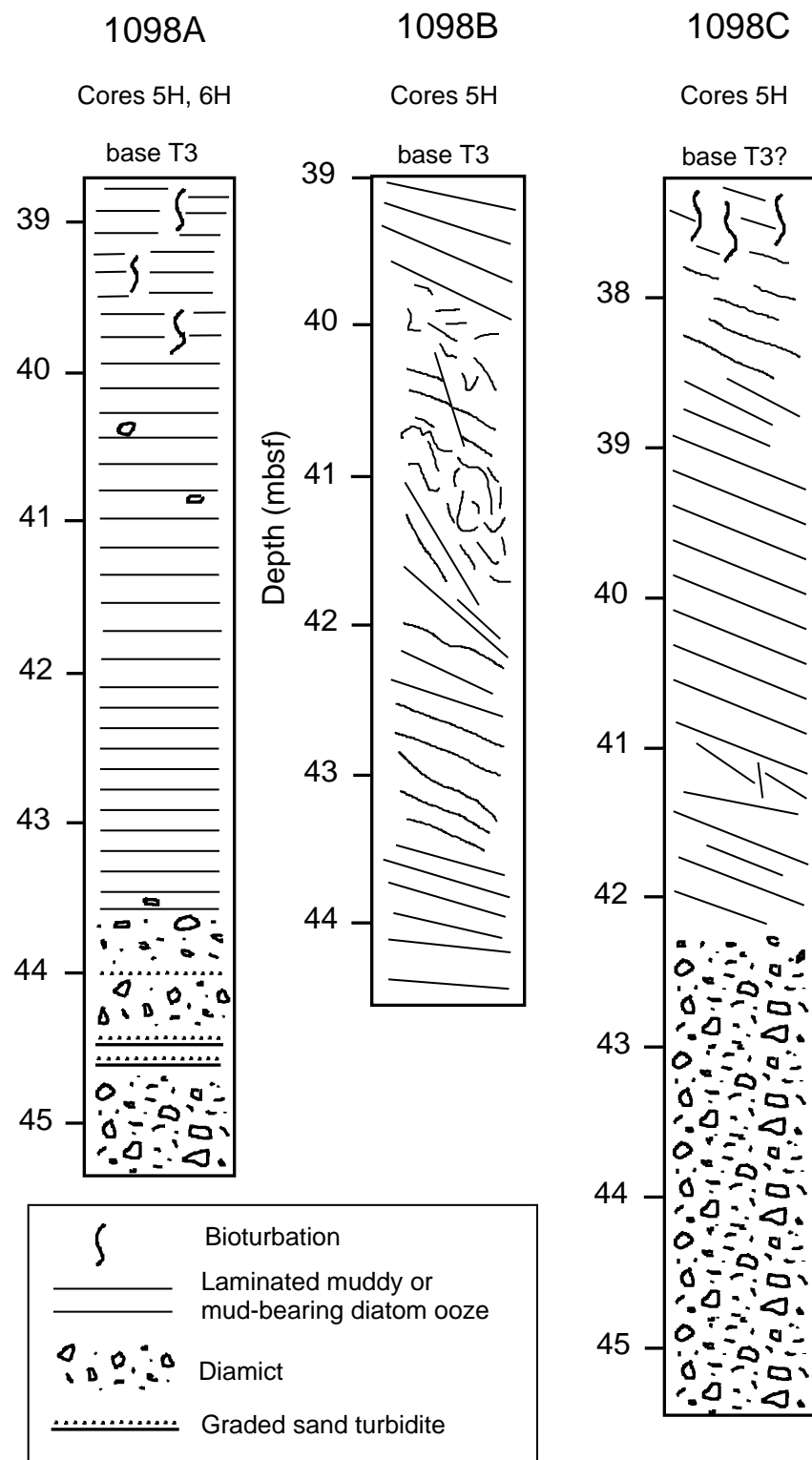


Figure F11. Lithostratigraphic column for Site 1099. Summarized lithology, percent biogenic component, and magnetic susceptibility data of Holes 1099A and 1099B. Laminated oozes occur in packets 0.1–2.2 m thick and dominate the sequence from 9 to 22 mbsf, between 35 to 40 mbsf, and below 87 mbsf. Massive, bioturbated ooze occurs in units 0.1–19 m thick. Each turbidite base has high magnetic susceptibility. T.D. = total depth of each hole.

Leg 178 Site 1099

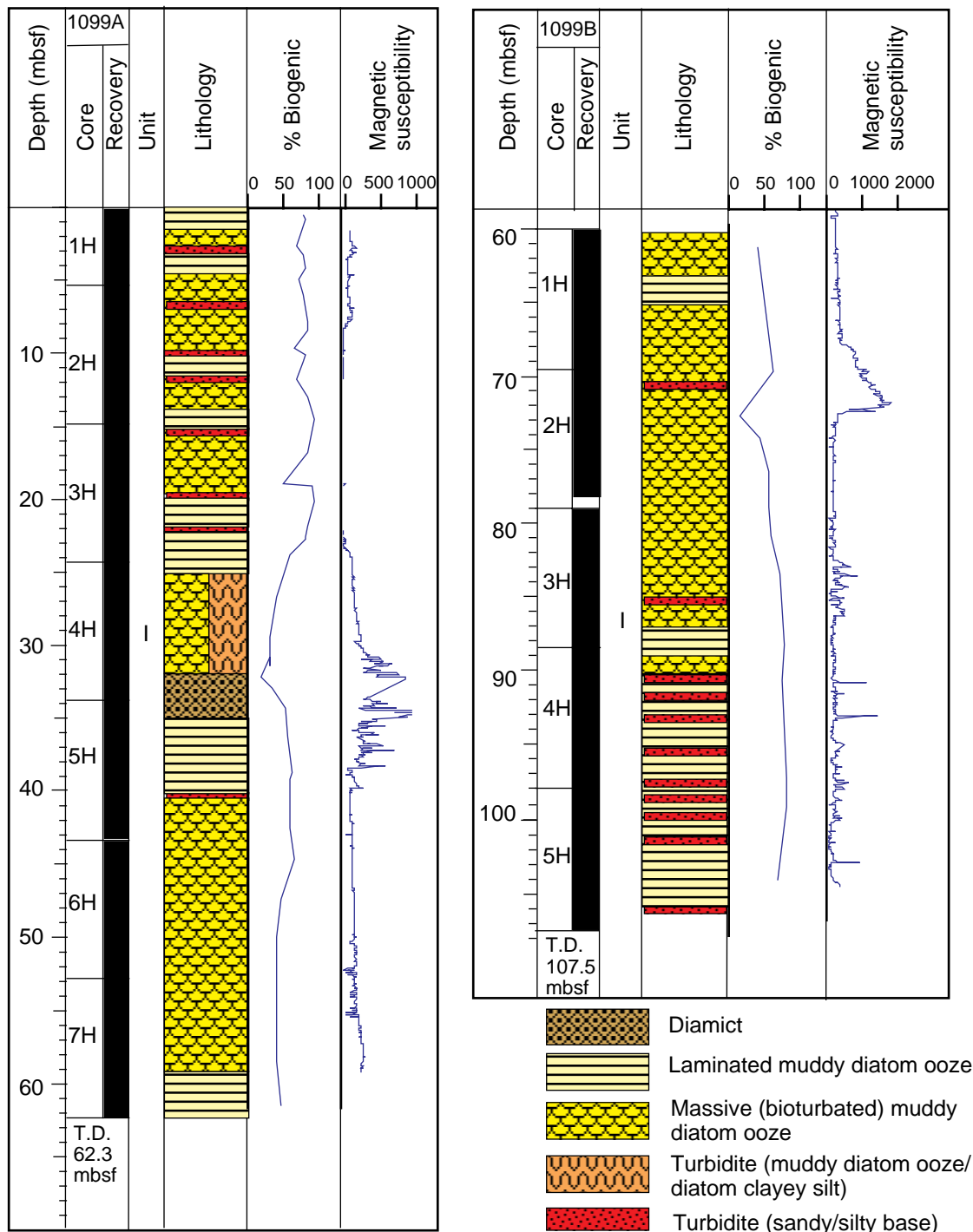


Figure F12. Sand:silt:clay ratio, percent biogenic and terrigenous, pebble occurrence, and chromaticity parameter a^* for Site 1099. In the first three columns, data points are joined by straight lines.

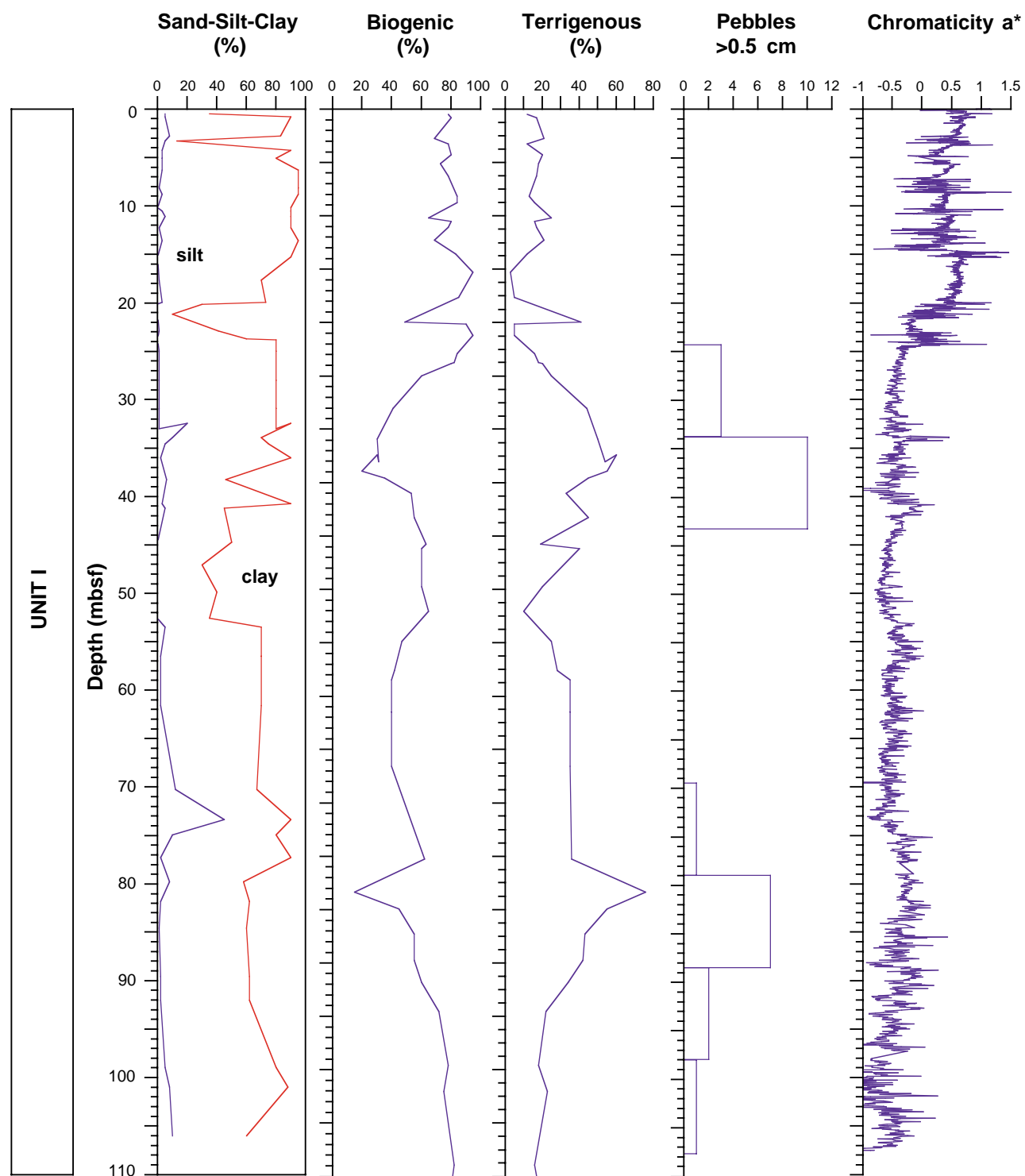


Figure F13. A. Massive mud-bearing diatom ooze (top part) with one lamina in interval 178-1099A-2H-3, 31–32 cm, of *Chaetoceros* spp. spores, and the top part of a turbidite in interval 178-1099A-2H-3, 7–42 cm. B. Laminated diatom ooze showing millimeter-scale laminae in the lower part of interval 178-1099B-5H-5, 15–17 cm, and at 178-1099B-5H-5, 10–12 cm, with subhorizontal *Phycosiphon* burrows. (Continued on next page.)

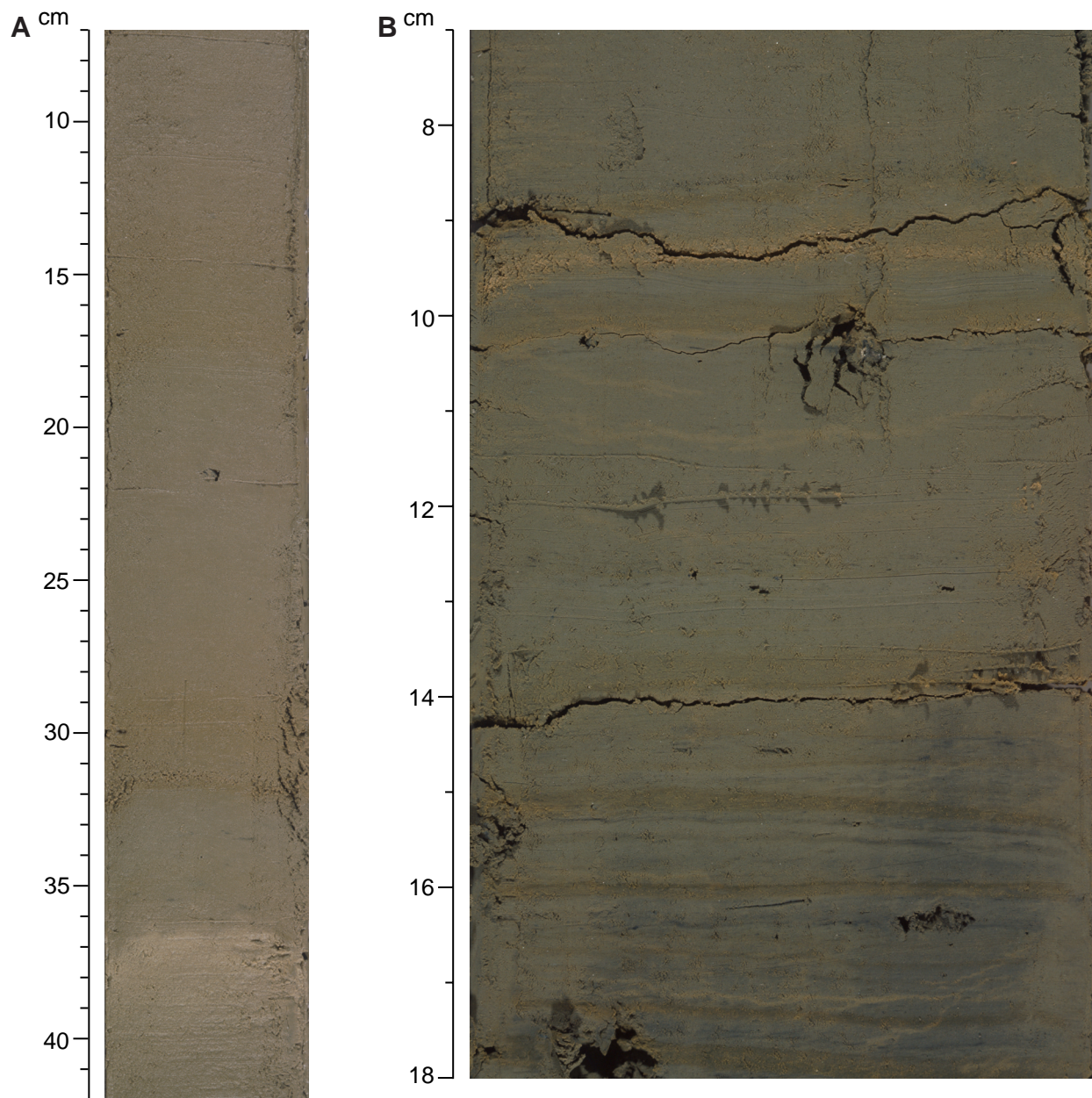


Figure F13 (continued). C. Diatom-bearing silty mud base of a turbidite, with shell fragments in interval 178-1099A-2H-3, 120–144 cm. The top 25 cm of the next section also has very coarse sand with mud rip-up clasts. Note horizontal gas expansion cracks. D. Turbidite bed with medium sand base grading to mud (interval 178-1099B-4H-5, 104–121 cm).

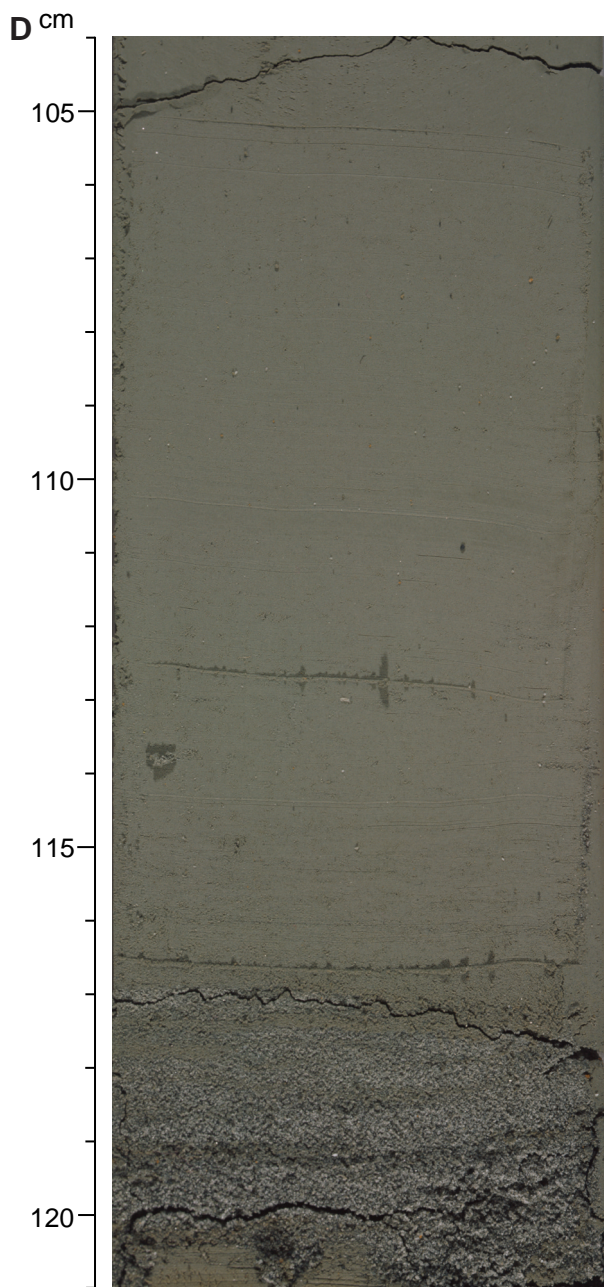
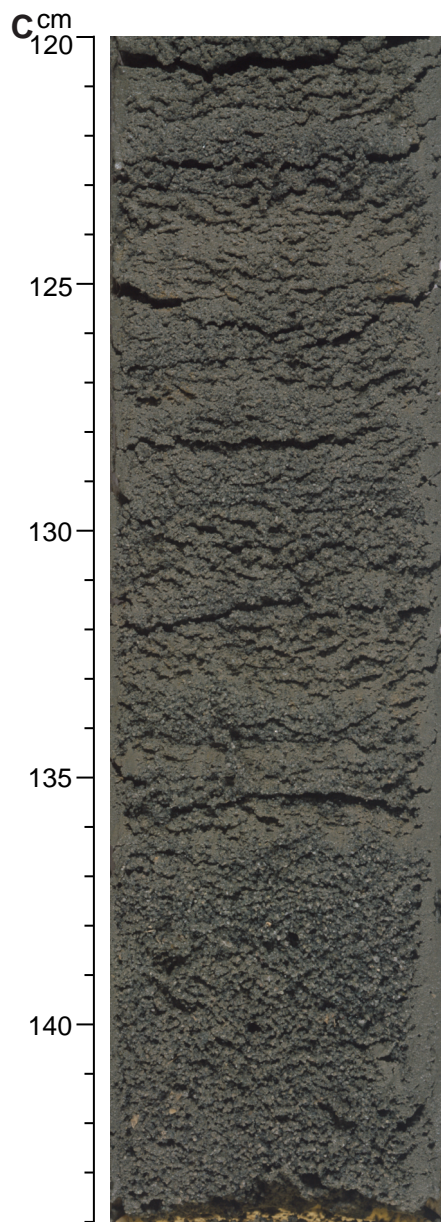


Figure F14. Preliminary results of relative diatom species abundance of *F. kerguelensis*, *Thalassiothrix* spp., *T. antarctica*, *E. antarctica*, *F. curta*, and *Chaetoceros* spp. spores in the major lithologies at Sites 1098 and 1099. Straight lines adjoin data points.

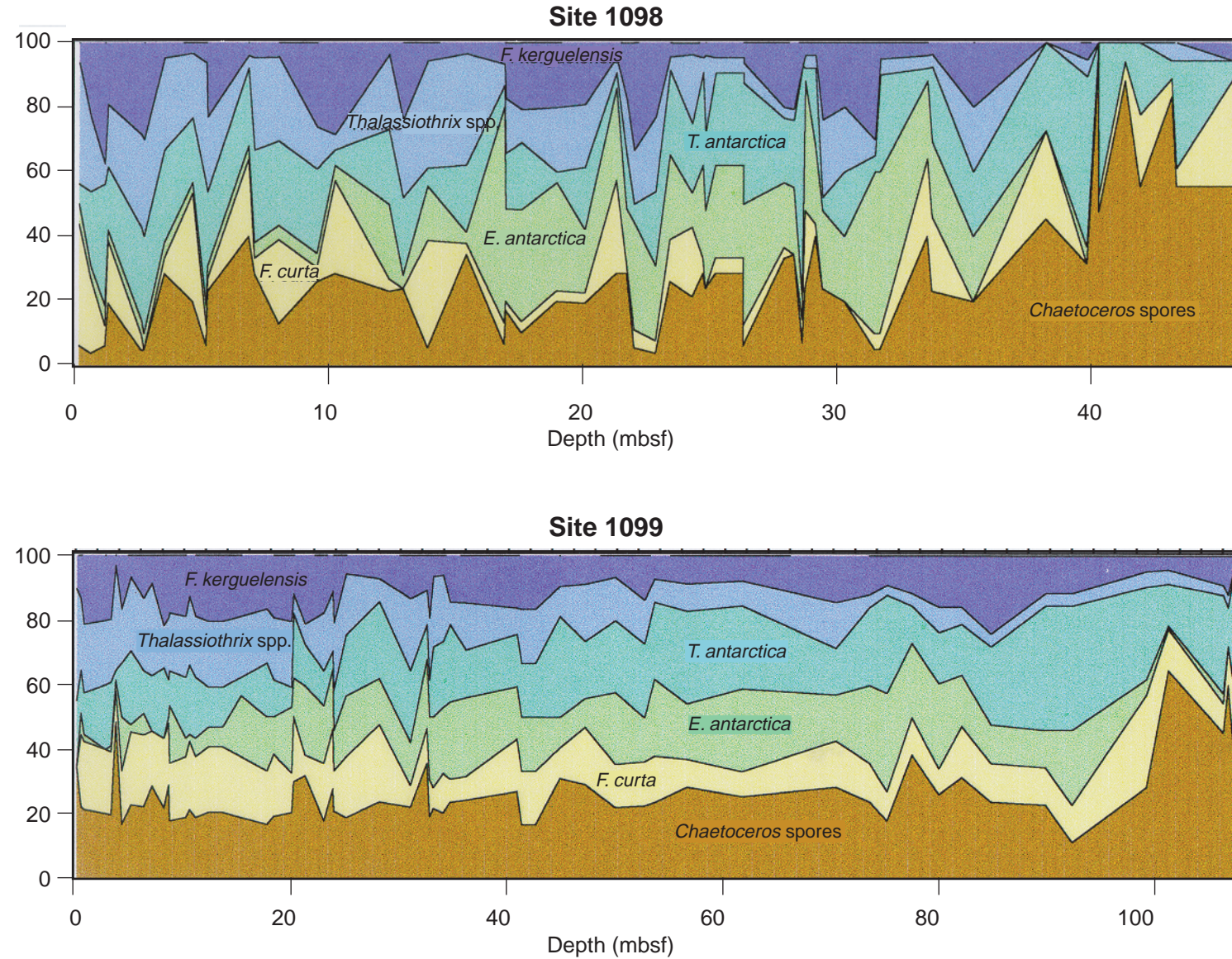


Figure F15. Results from core-catcher samples showing radiolarian abundance for Hole 1098C. Data from Holes 1099A and 1099B showing radiolarian abundance, foraminiferal assemblage zones, and depositional environments. A = abundant, C = common, F = few, B = barren.

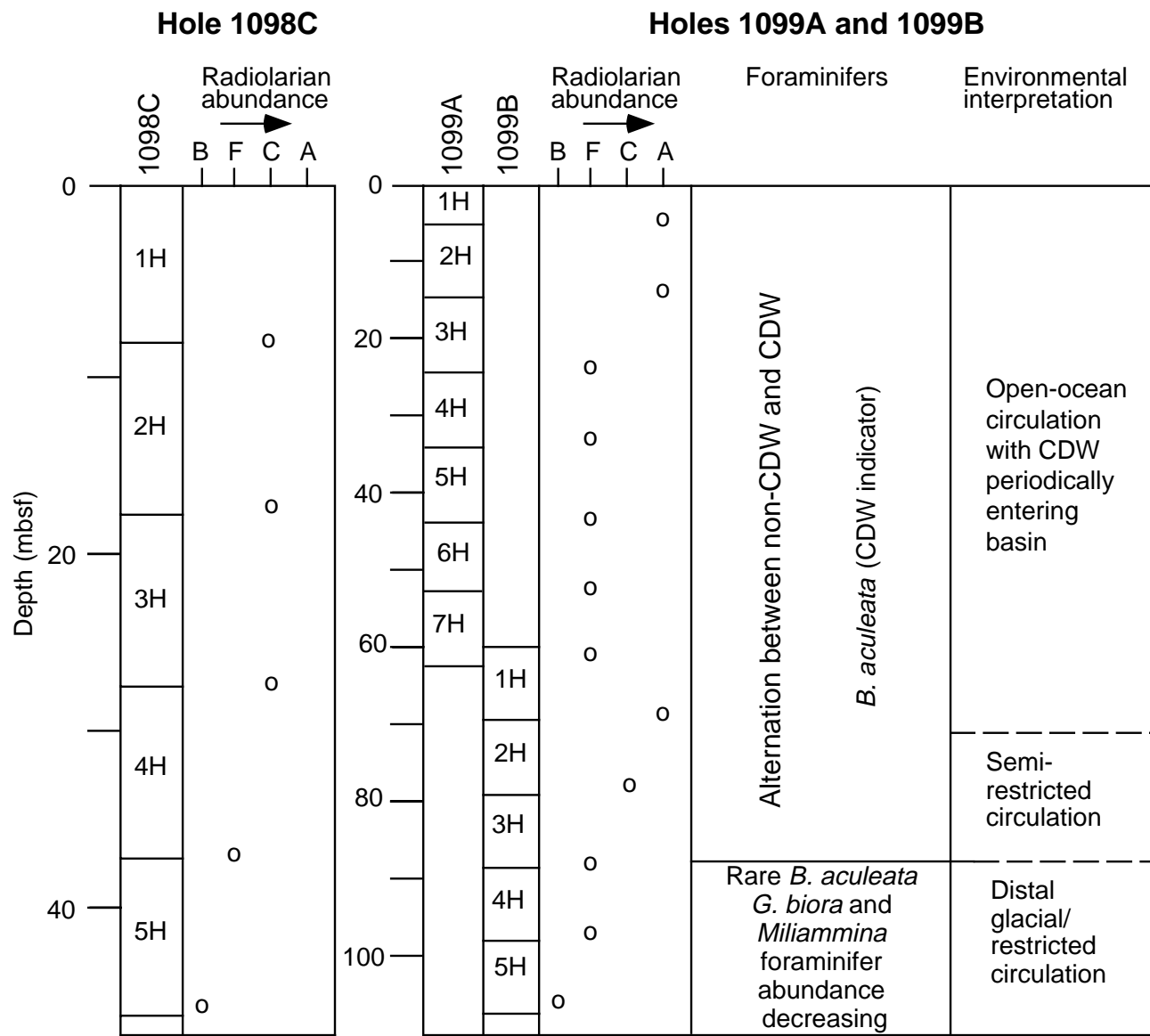


Figure F16. Magnetic inclination records from Basin I (Site 1098) vs. depth (mbsf).

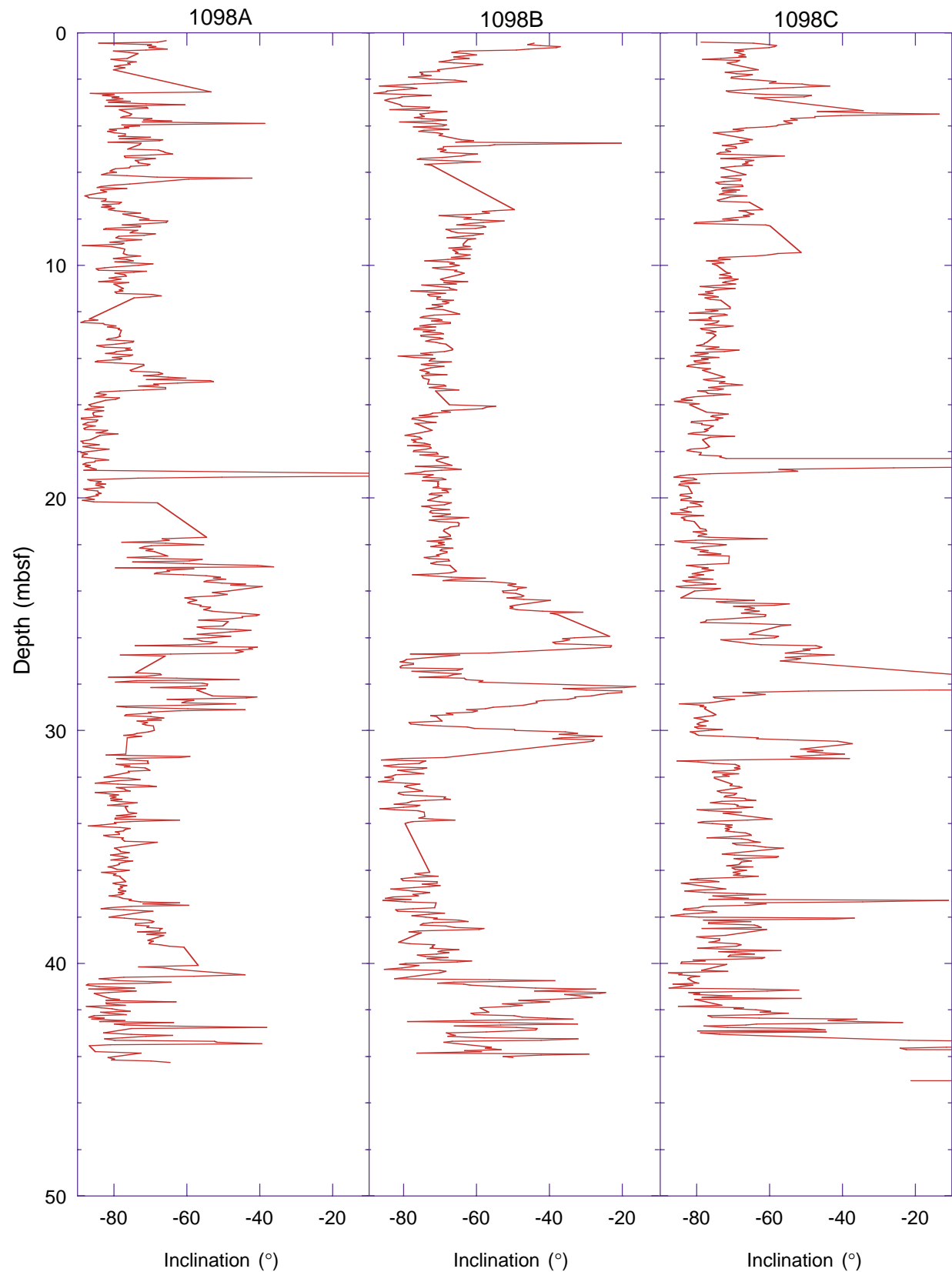


Figure F17. Intensity of remanence and magnetic susceptibility in Hole 1098C and Holes 1099A and 1099B vs. depth (mbsf).

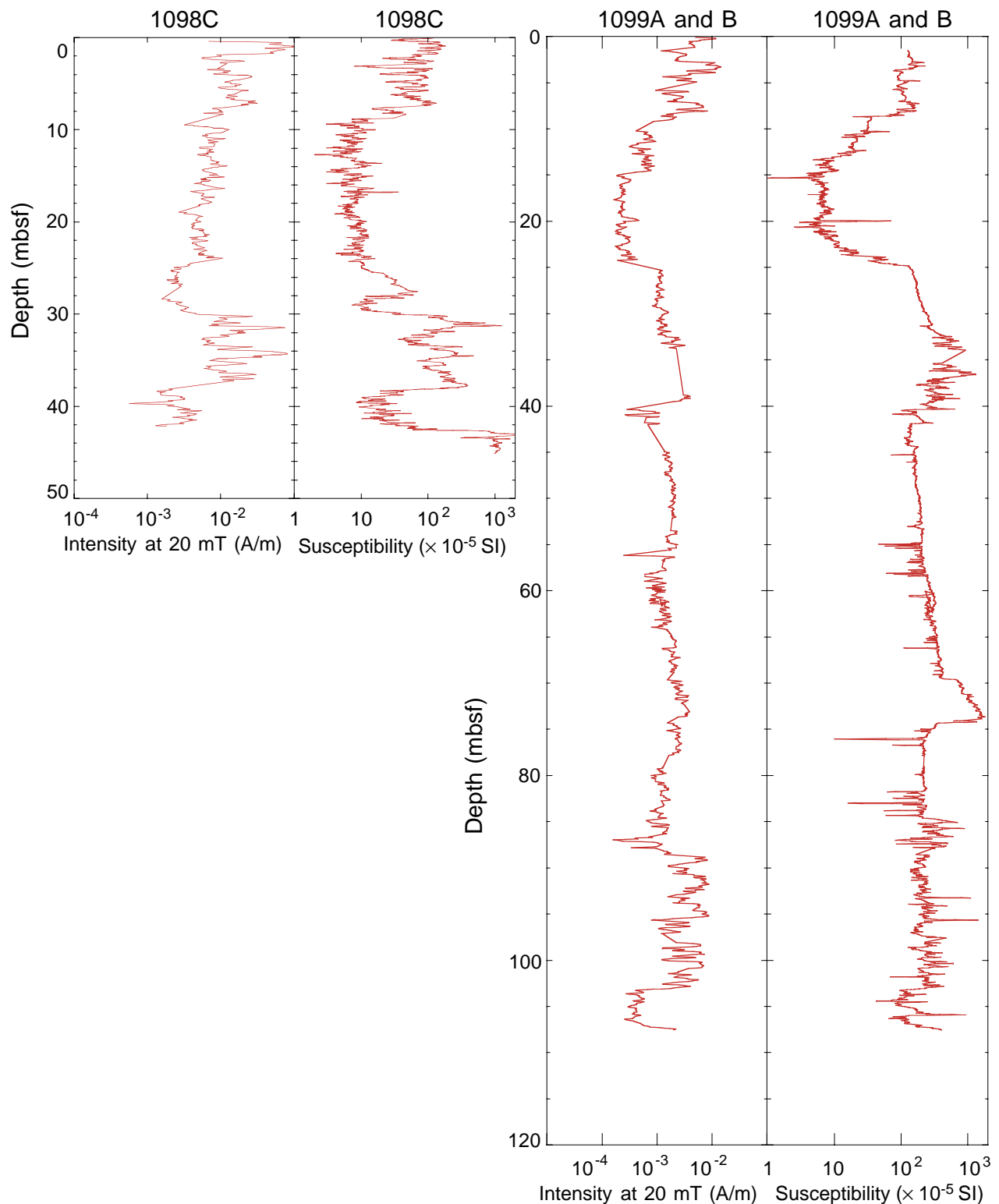


Figure F18. Comparison of inclinations and intensities of magnetization of split-core (line) and discrete sample (squares) measurements from Hole 1098C vs. depth (mbsf).

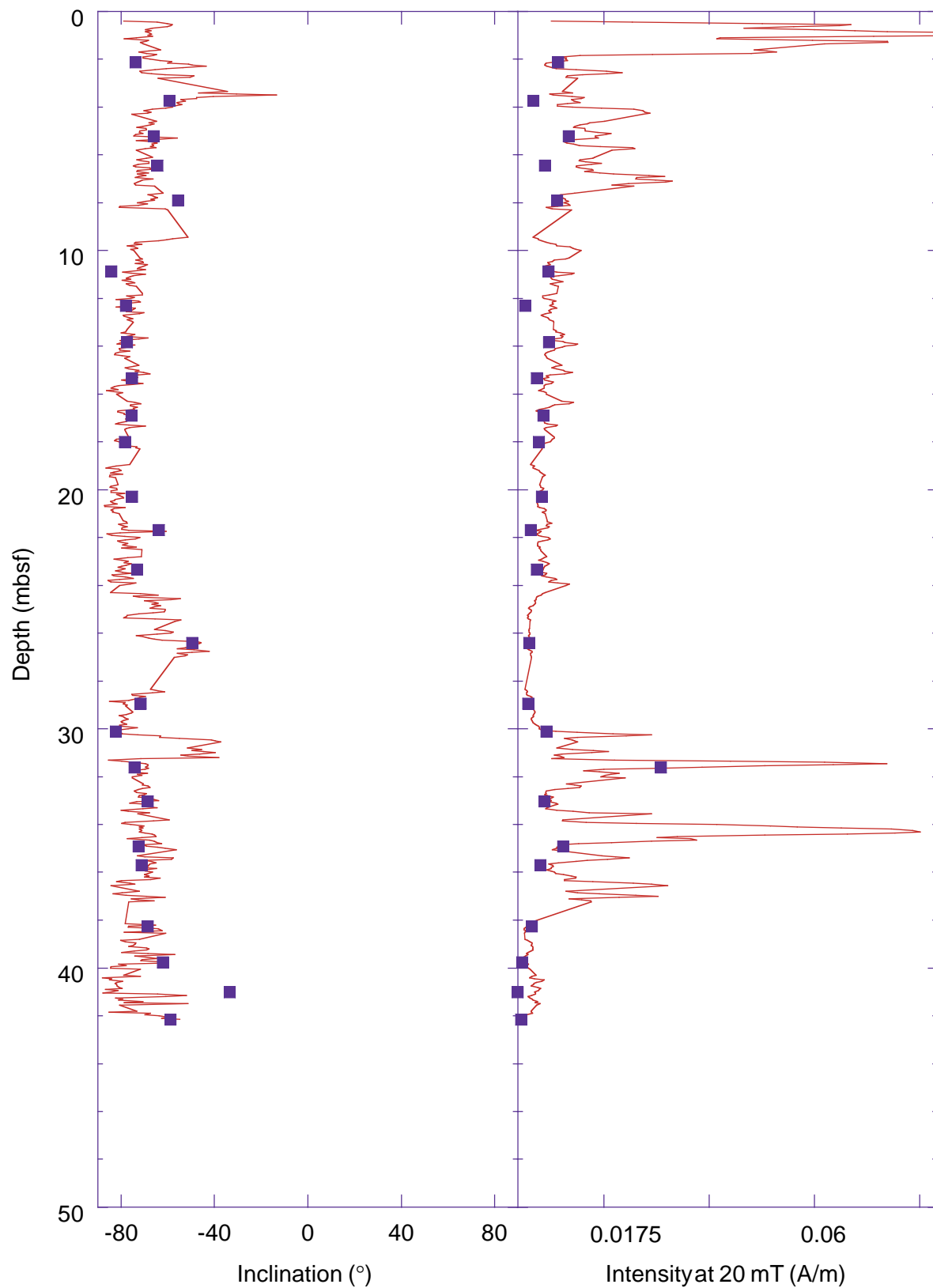


Figure F19. AF demagnetization of a typical discrete sample (178-1098C-1H-5, 44 cm). A. Orthogonal projection of the end-points of the remanence vector. Open and solid symbols represent the vertical and horizontal projections, respectively. The steeply inclined drill-string overprint was removed after AF demagnetization at 10 mT. B. Change in the intensity of remanence during AF demagnetization. C. Equal-area projection of the remanence vector during AF demagnetization.

Sample: 178-1098C-1H-5, 44.0 cm (6.44 mbsf)

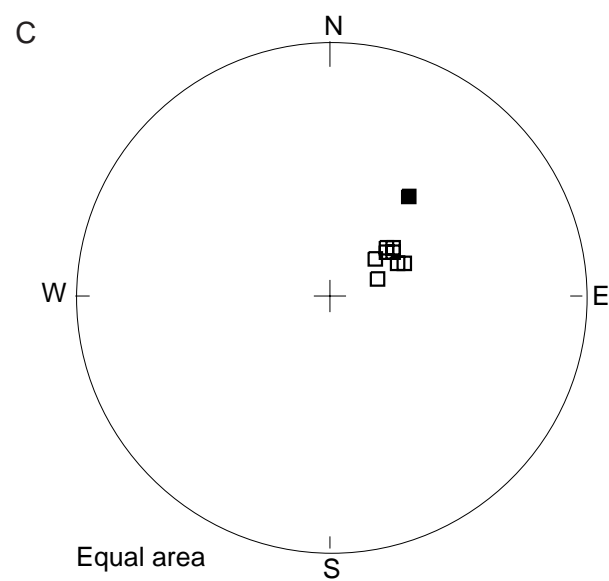
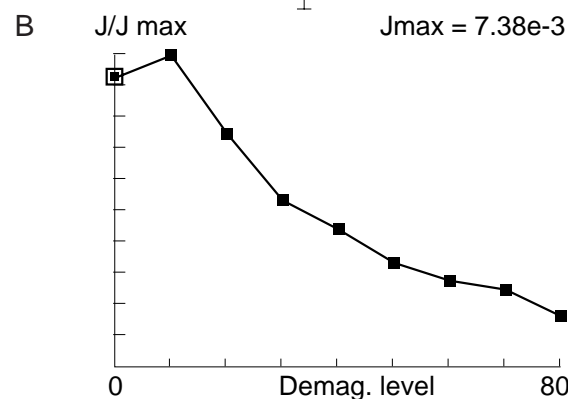
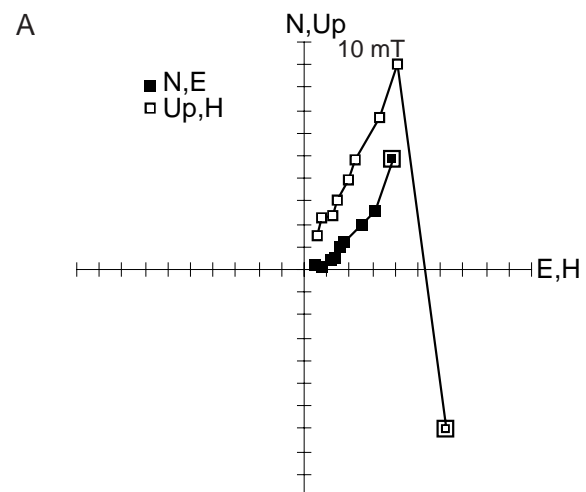


Figure F20. A. Intensity of remanence after AF demagnetization at 20 mT for split-core and discrete samples (squares) vs. depth (mbsf). B. Magnetic susceptibility at Hole 1098C vs. depth (mbsf). C. Maximum angular deviation angle for the discrete samples vs. depth (mbsf).

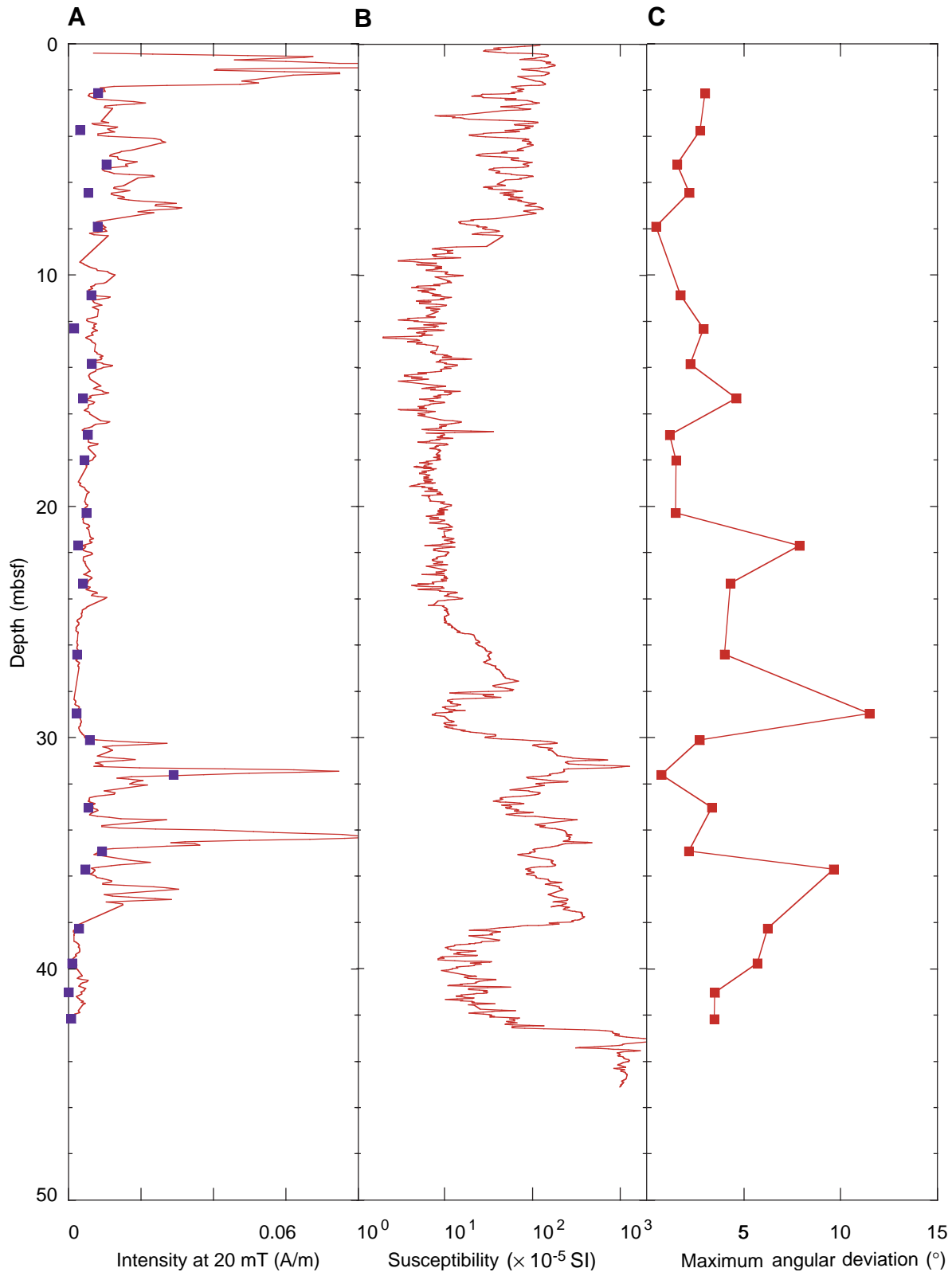


Figure F21. Relative paleointensity at Site 1098, obtained after normalization of the NRM at 20 mT by magnetic susceptibility.

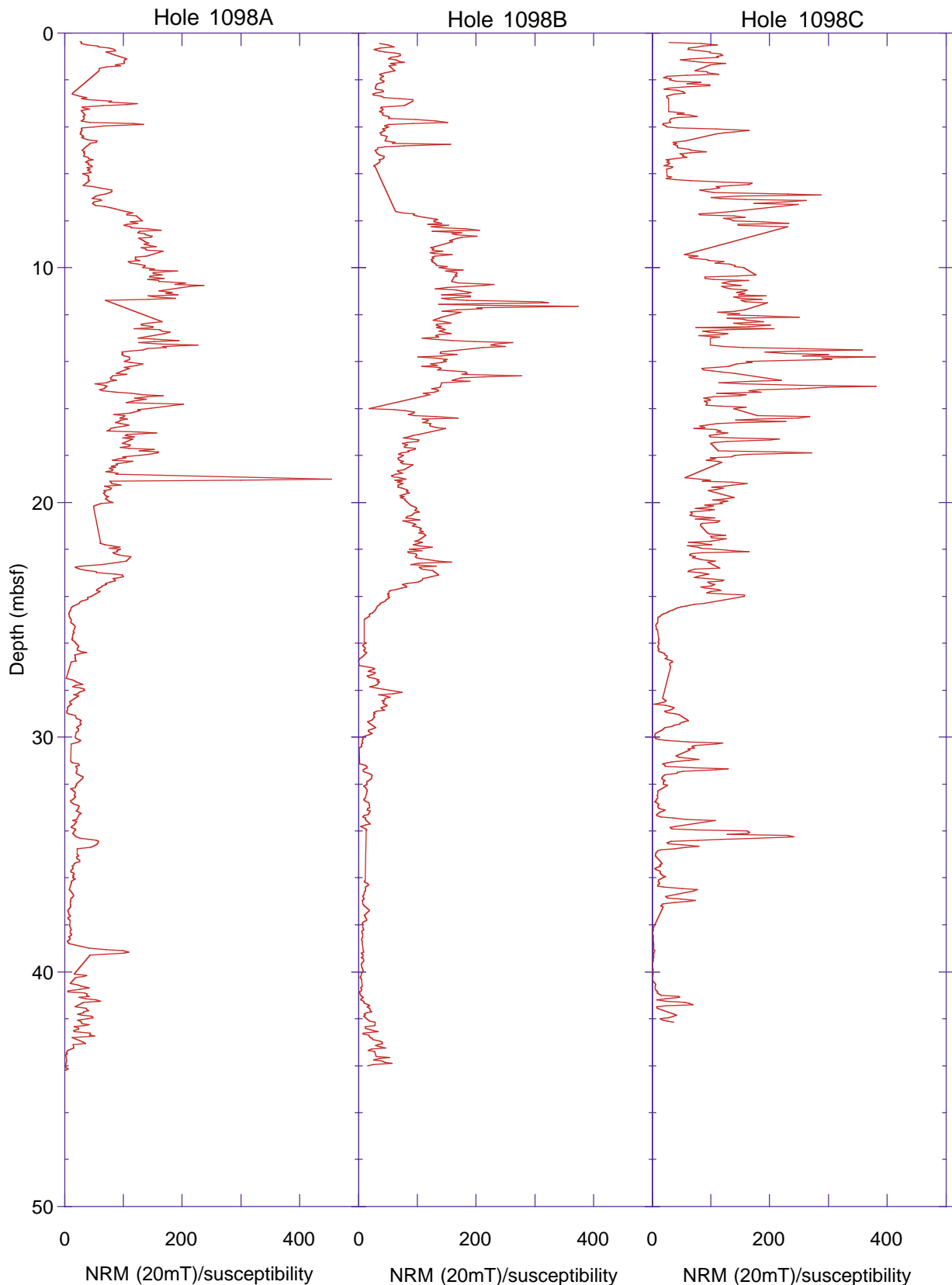


Figure F22. Inorganic carbon (wt%) and total organic carbon (wt%) from Hole 1098C.

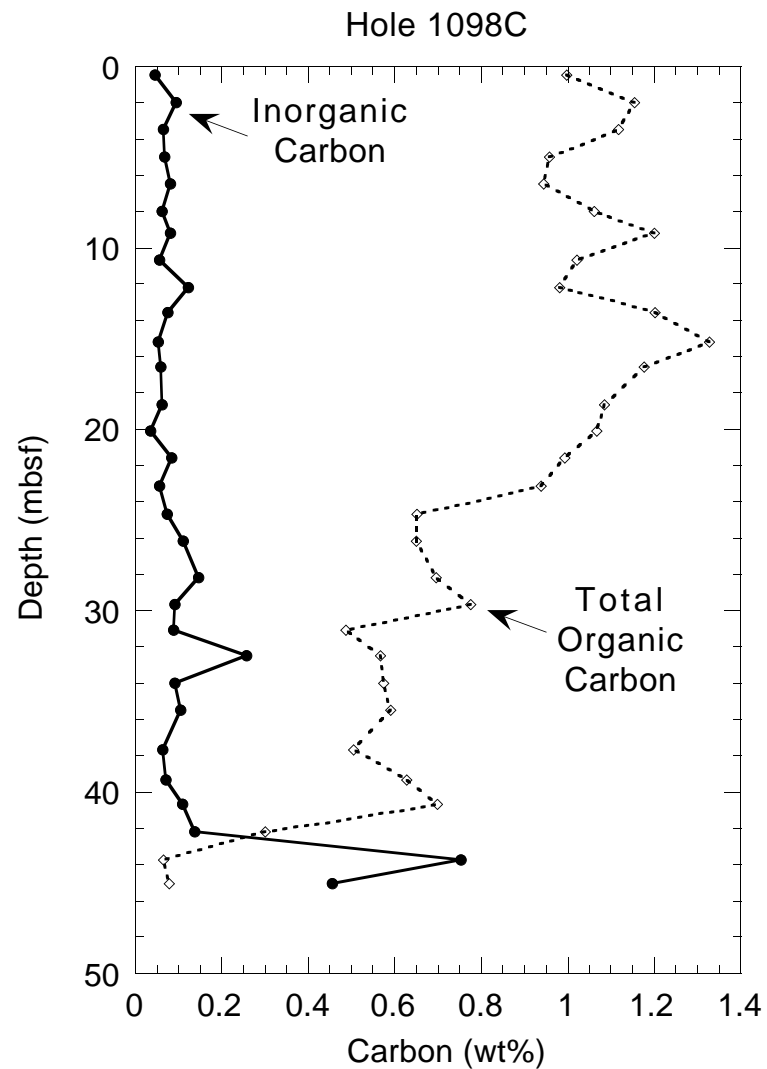


Figure F23. Inorganic carbon (wt%) and total organic carbon (wt%) from Site 1099.

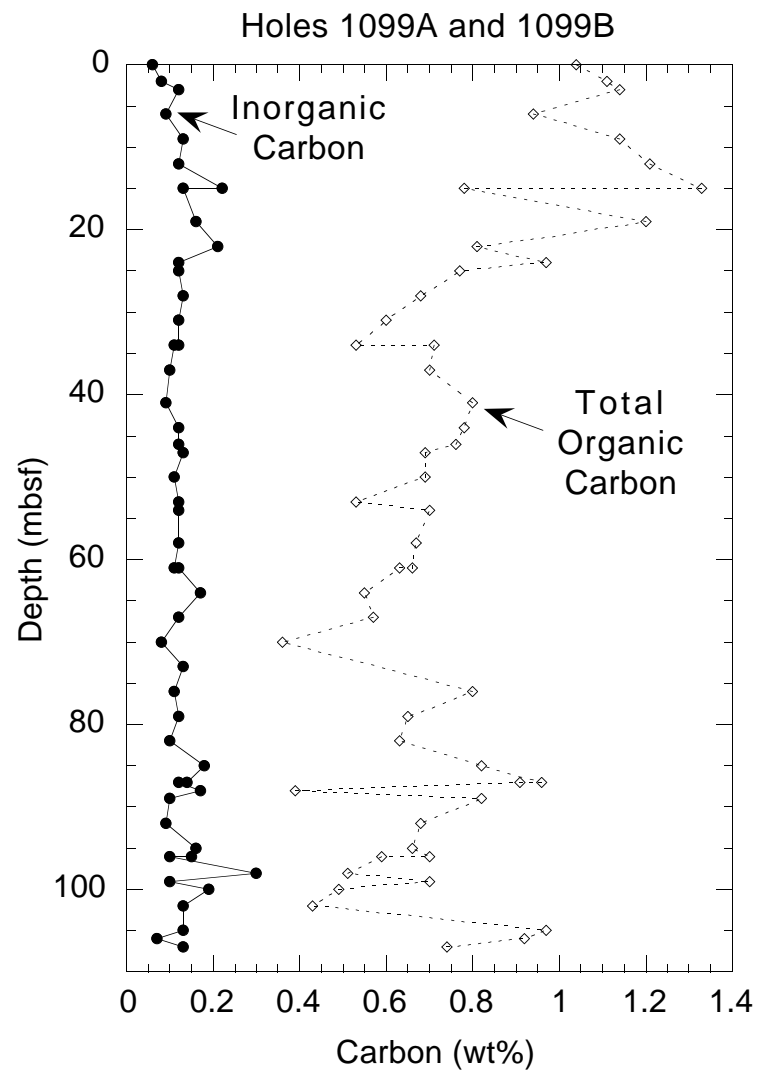


Figure F24. Profiles of interstitial water chemistry in Hole 1098C.

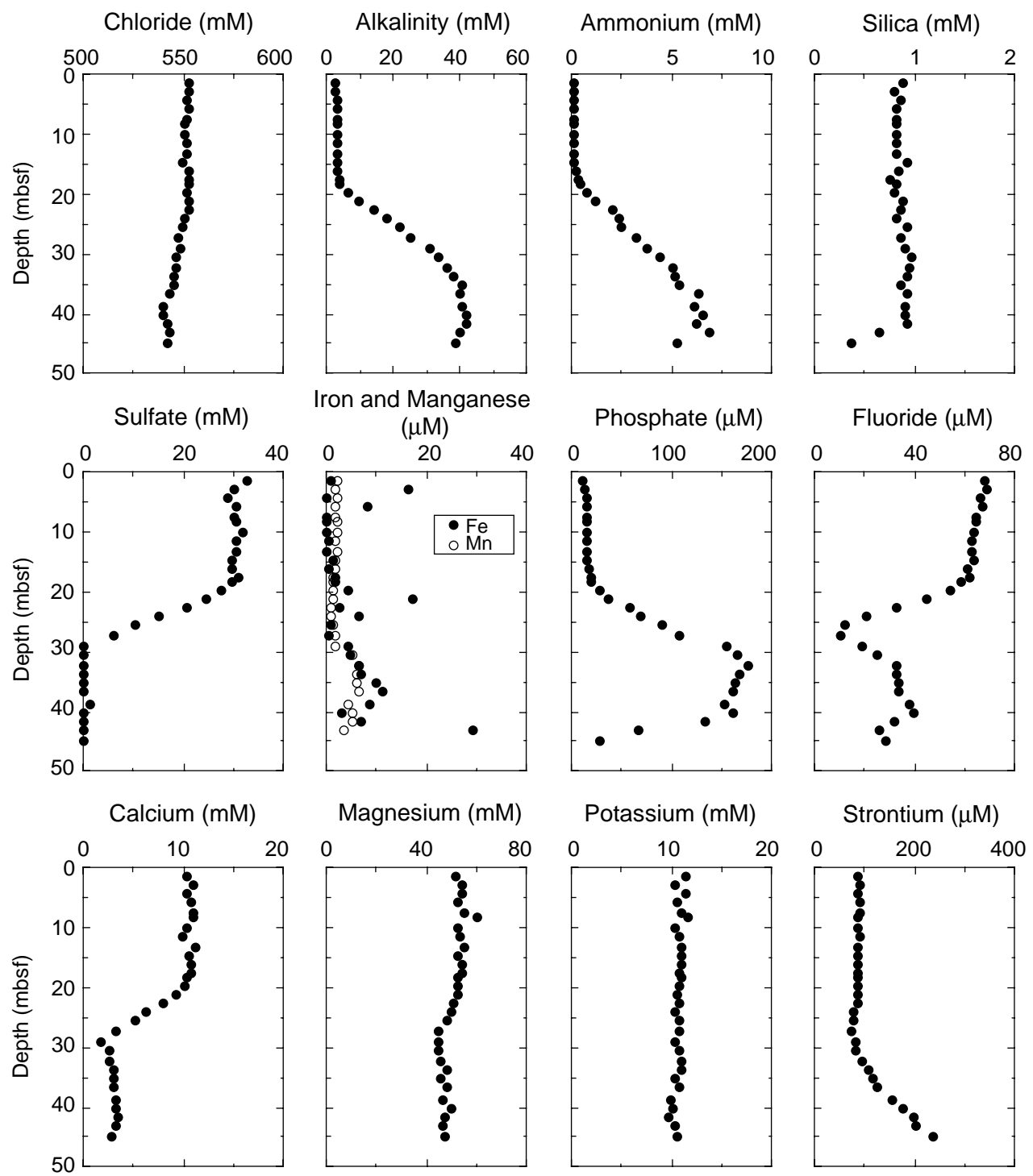


Figure F25. Profiles of interstitial water chemistry in Holes 1099A and 1099B.

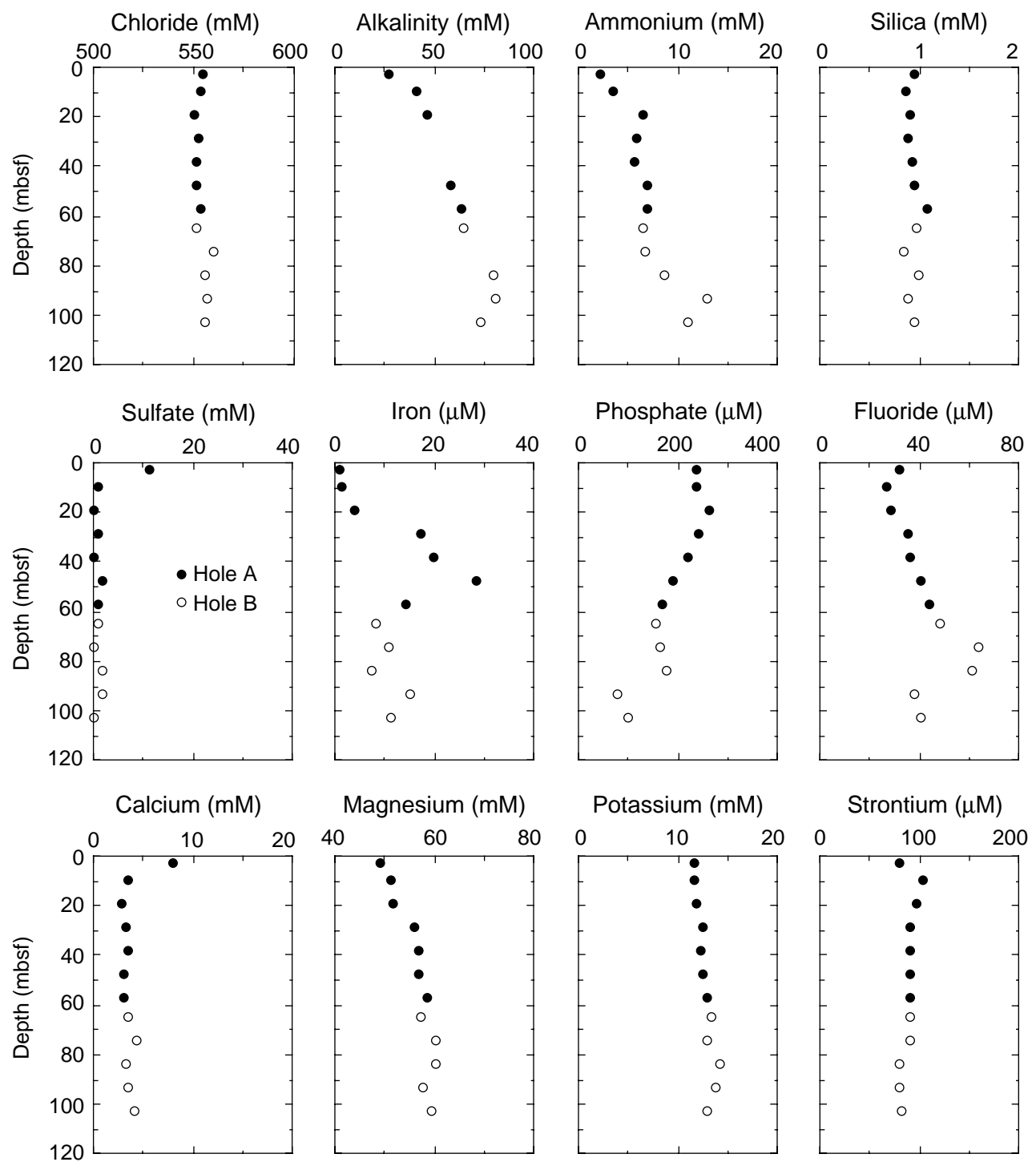


Figure F26. Raw data for (A) NGR, (B) GRAPE density, (C) magnetic susceptibility, and (D) *P*-wave velocity from Hole 1098C. GRAPE data were truncated at 1.2 g/cm³, magnetic susceptibility at 0 SI to remove equipment noise, and *P*-wave data on either side of 1500 and 1650 m/s to show the main signal more clearly.

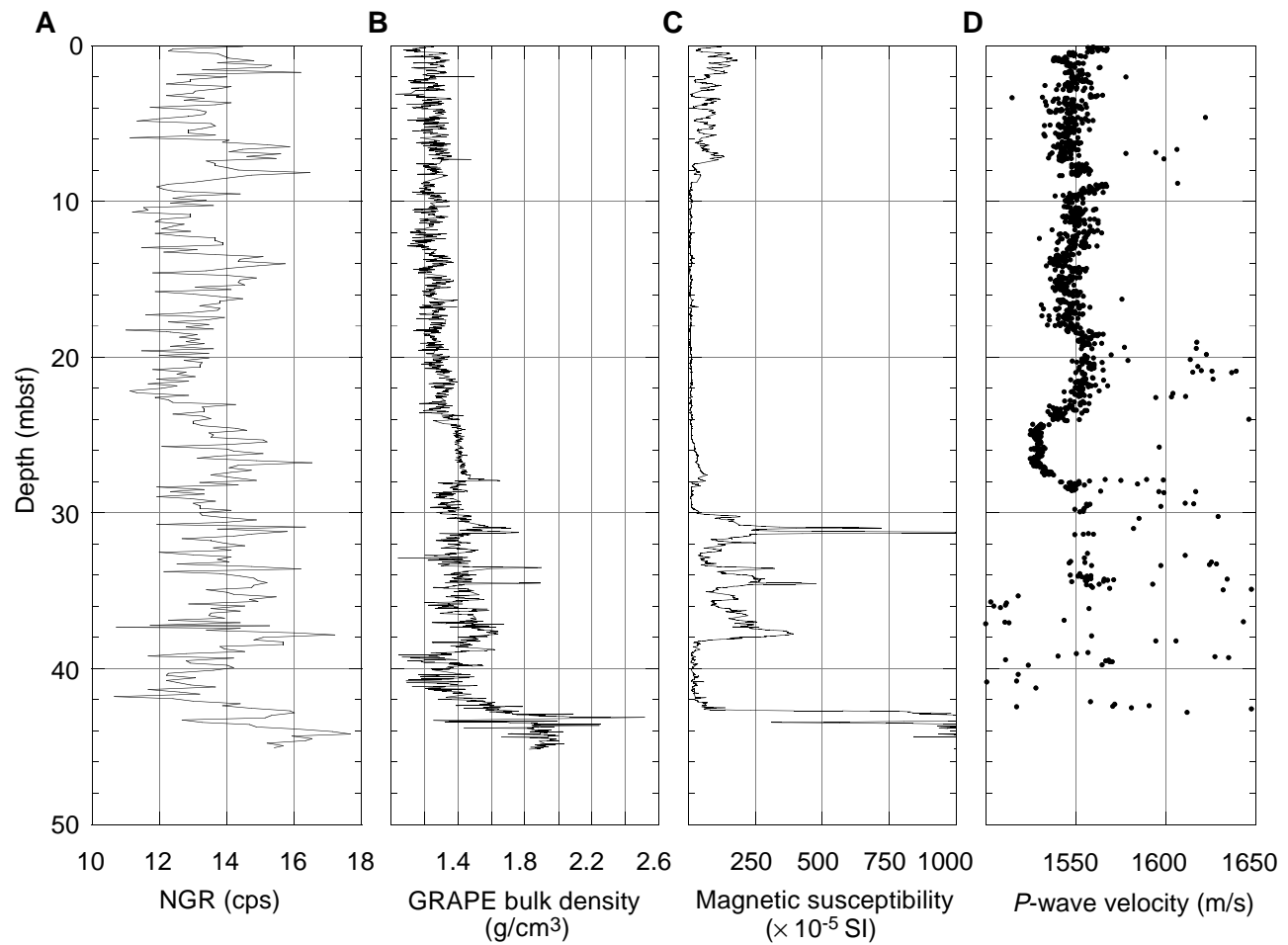


Figure F27. Amalgamated raw data for (A) NGR, (B) GRAPE density, and (C) magnetic susceptibility from Site 1099. GRAPE data were truncated at 1.2 g/cm³ and magnetic susceptibility data were truncated at 0 SI to remove equipment noise.

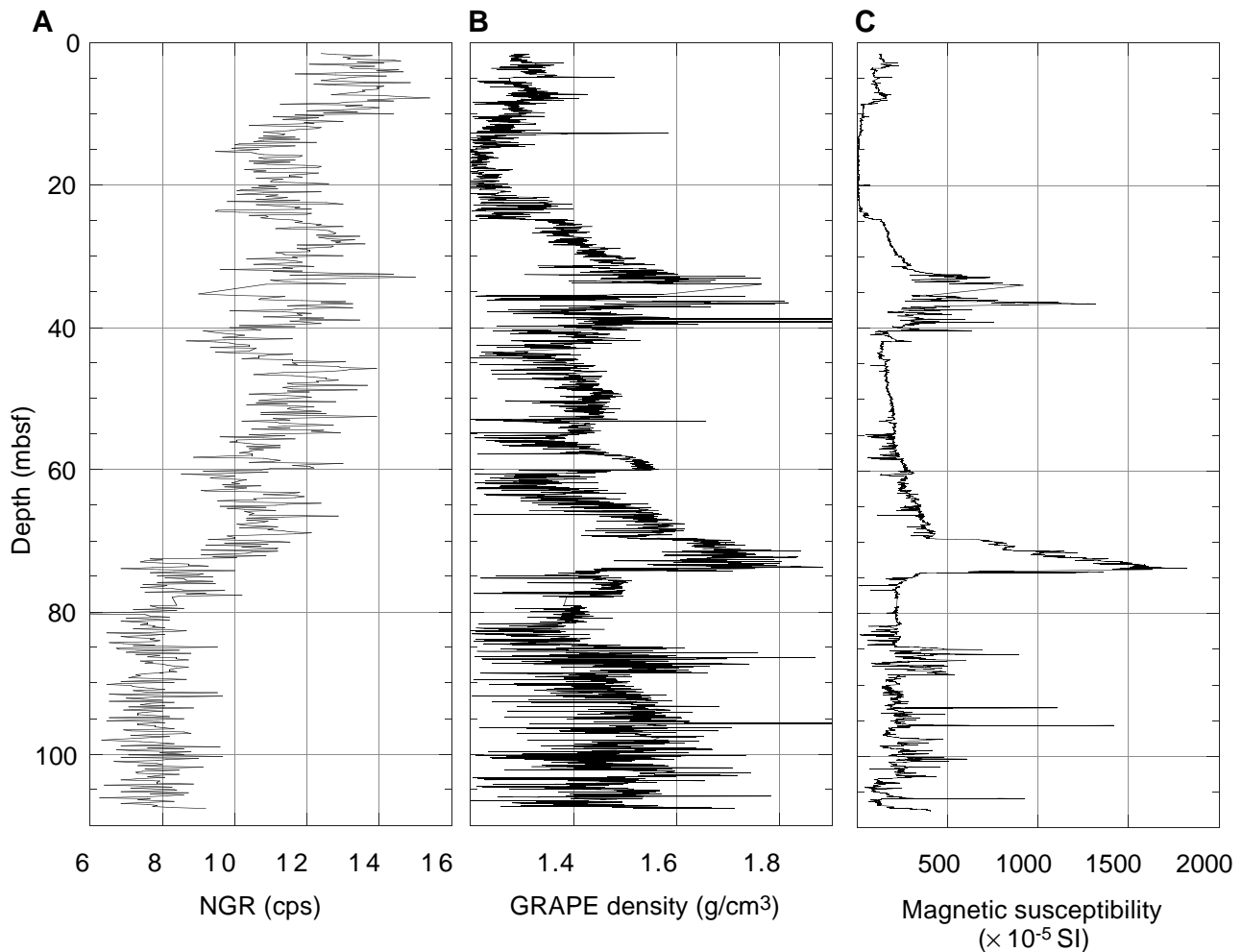


Figure F28. (A) GRAPE bulk density and (B) magnetic susceptibility vs. depth in the upper 8 mbsf for Hole 1098C.

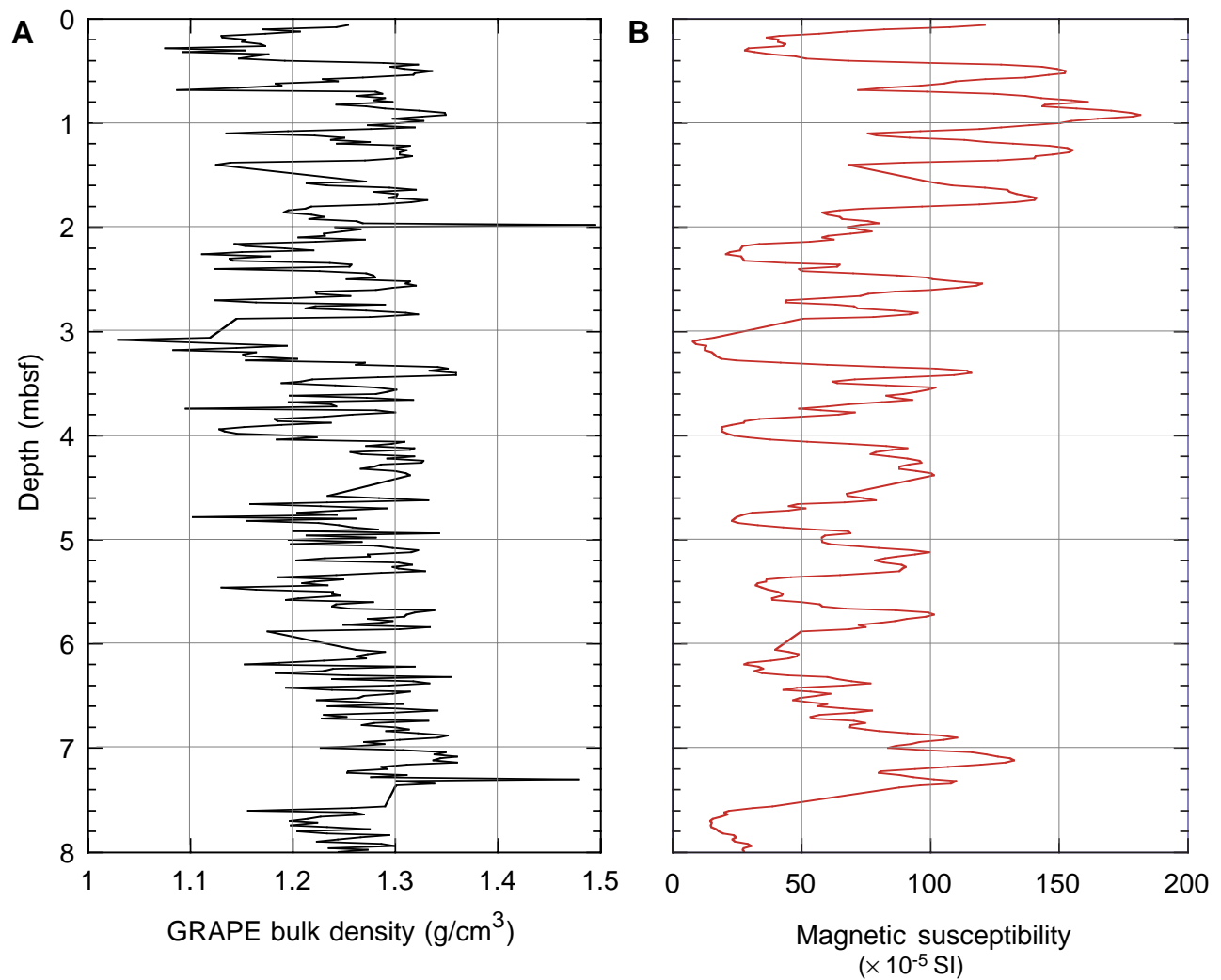


Figure F29. (A) MAD bulk density from index properties and raw GRAPE density, (B) porosity, and (C) grain density for Hole 1098C. MAD = moisture and density measurements.

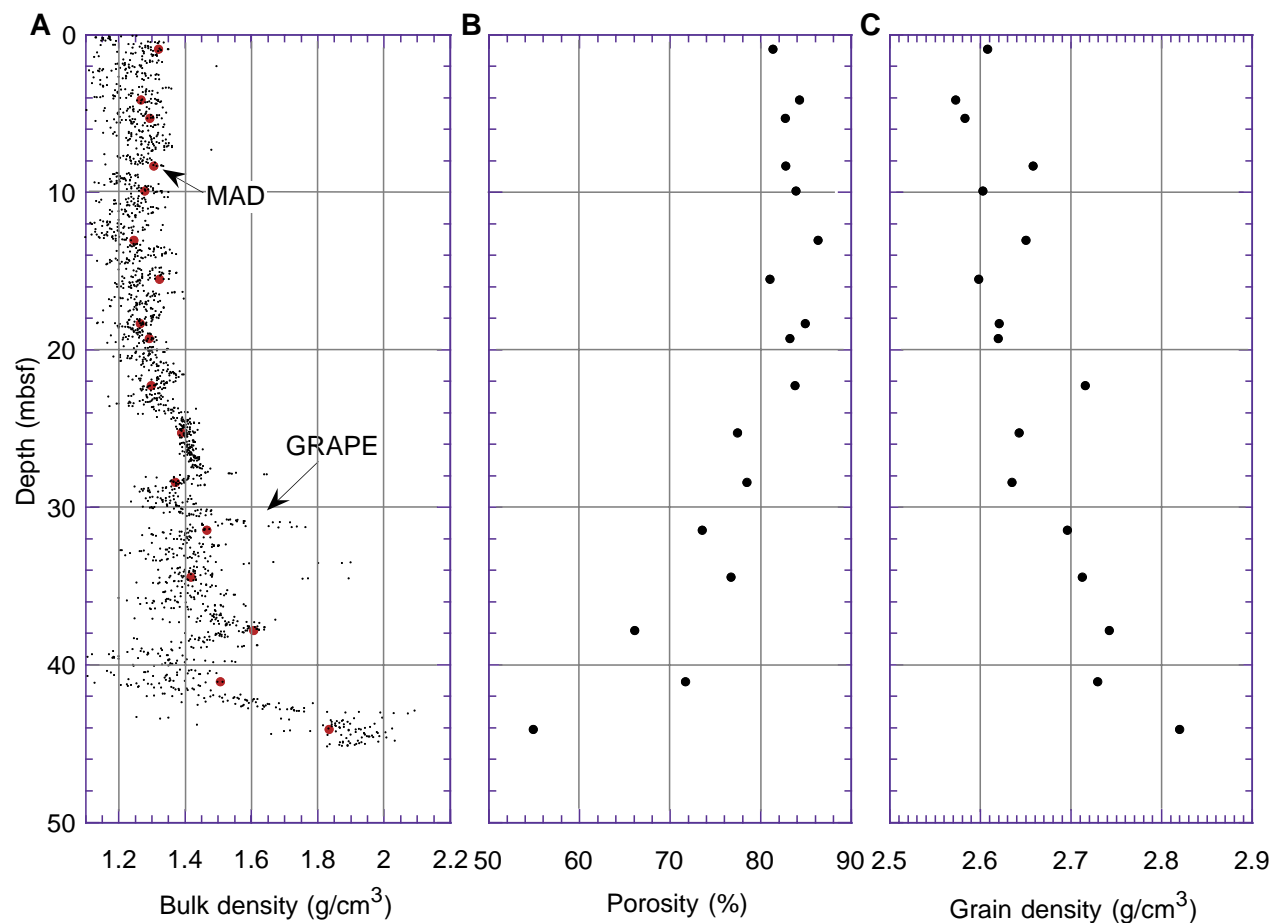


Figure F30. (A) MAD bulk density from index properties and raw GRAPE density, (B) porosity, and (C) grain density for Site 1099. MAD = moisture and density measurements.

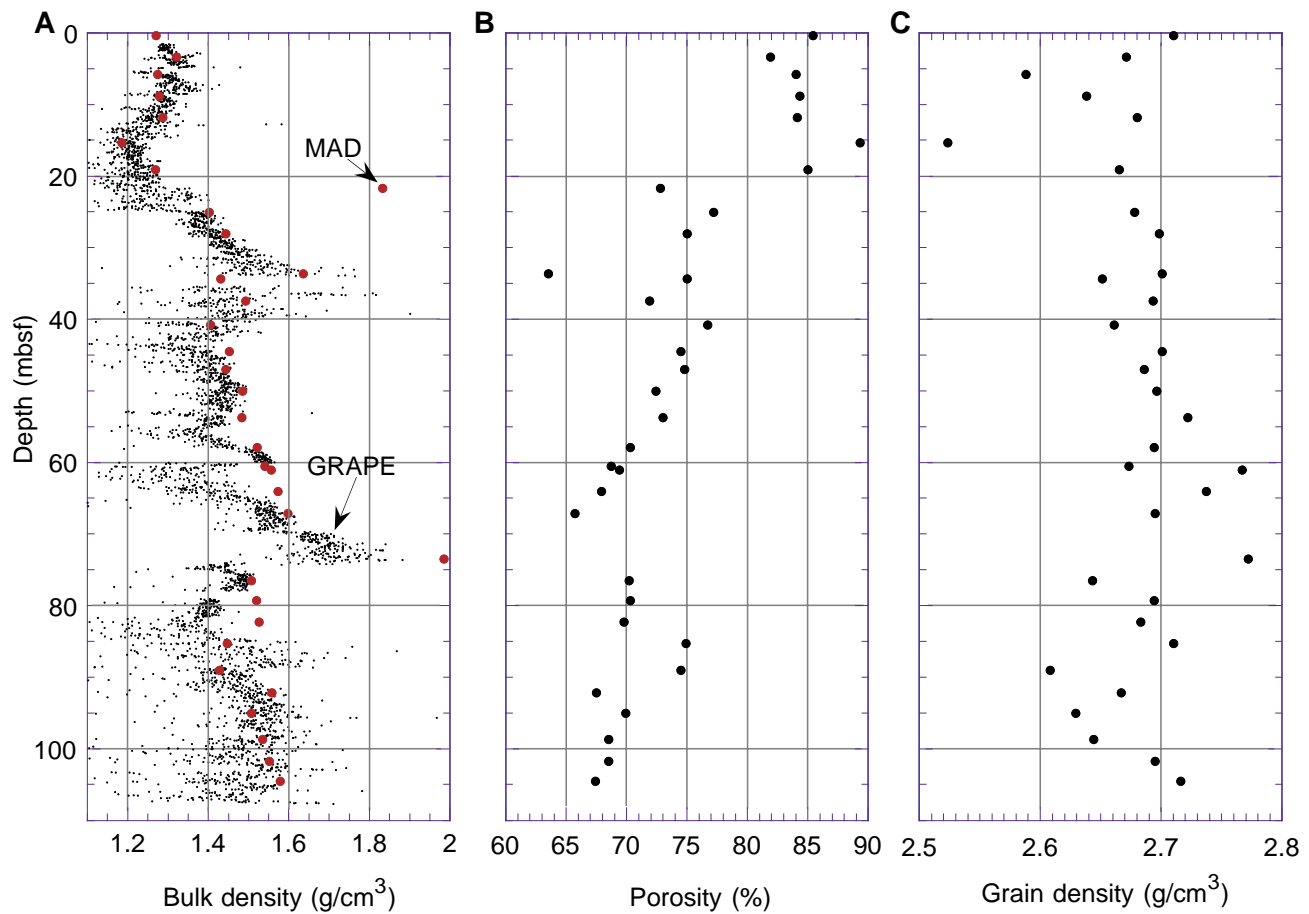


Figure F31. Raw PWS3 data from Sites (A) 1098 and (B) 1099.

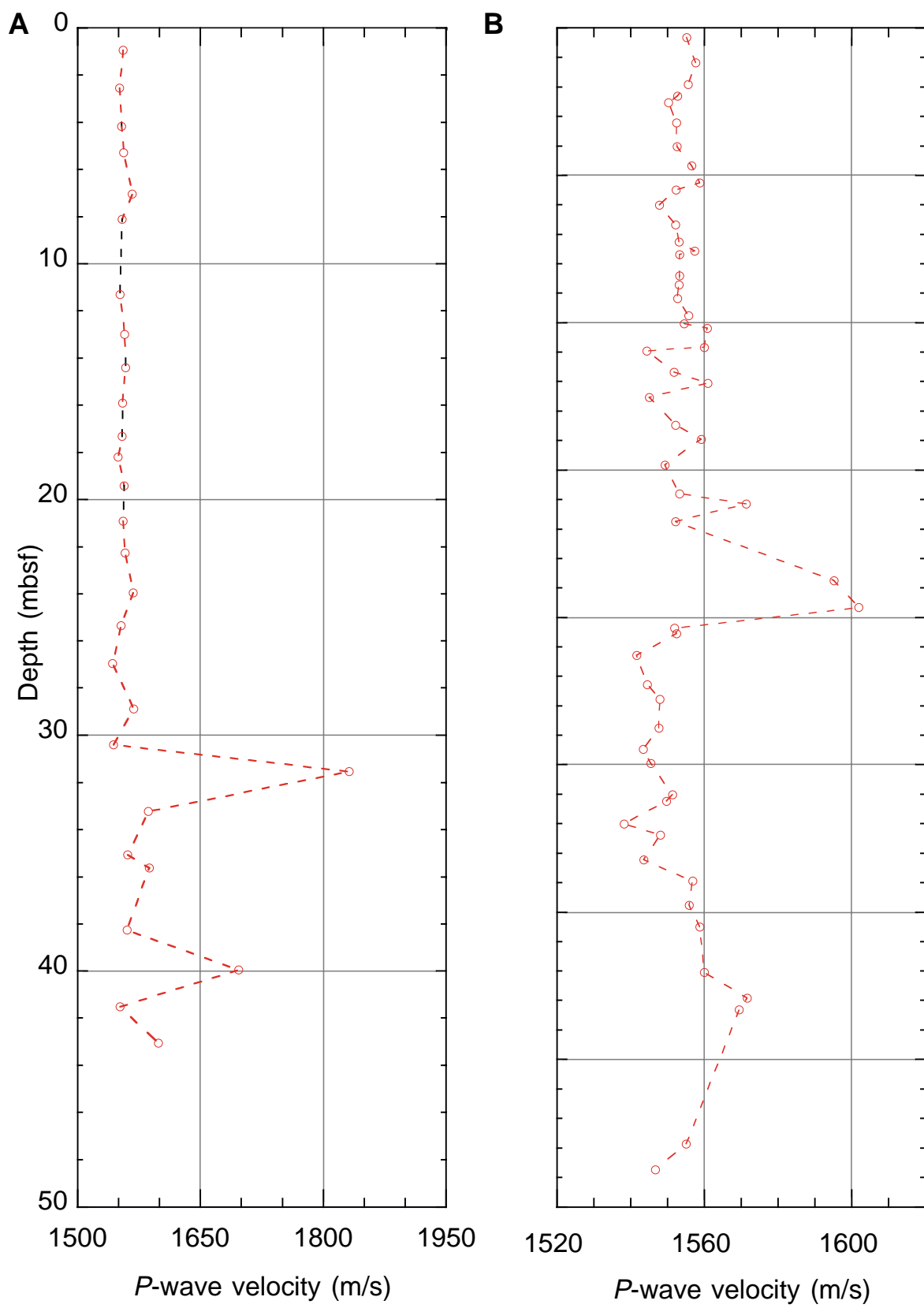


Figure F32. Thermal conductivity measurements at Site 1098.

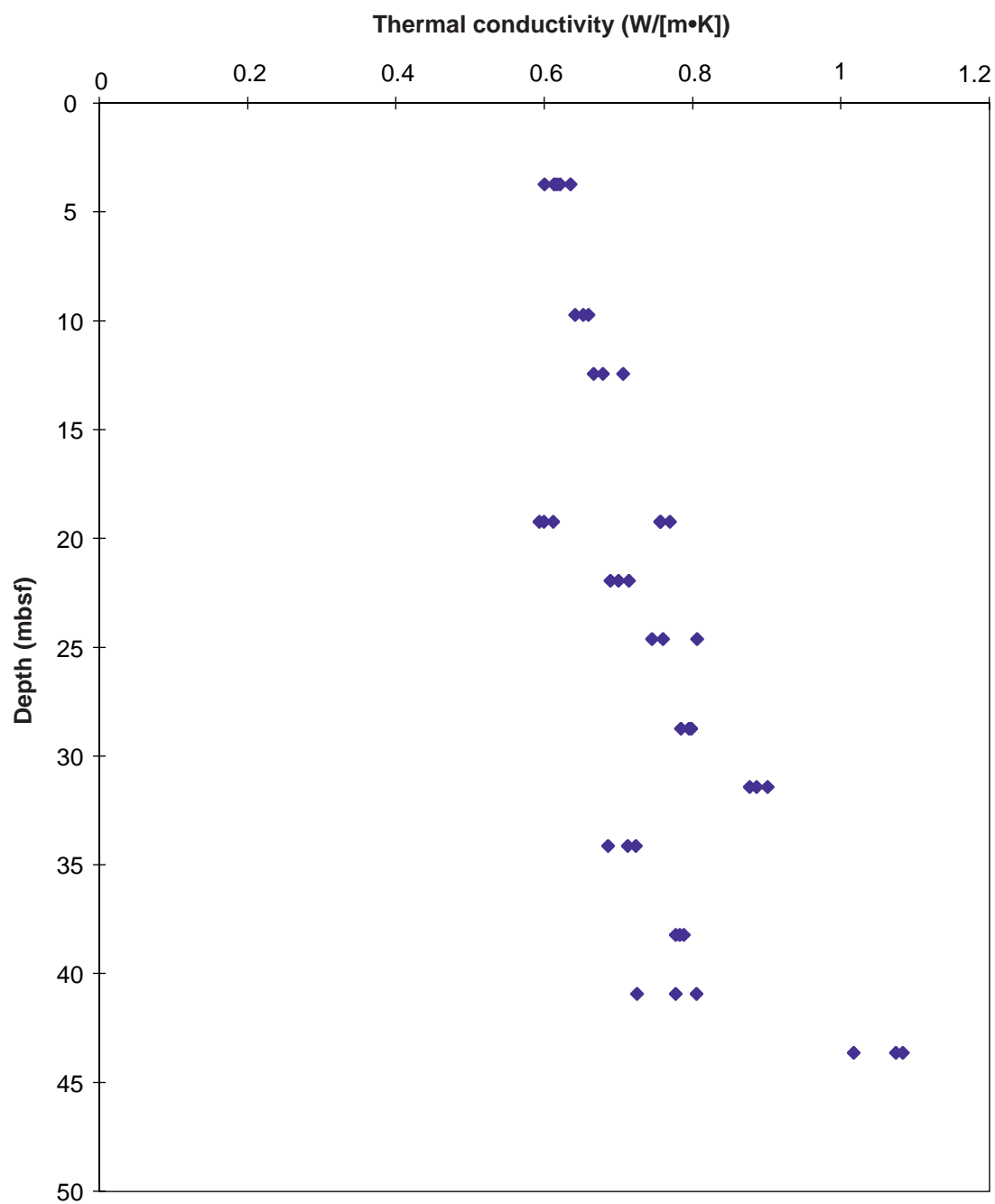


Figure F33. Thermal conductivity measurements at Site 1099.

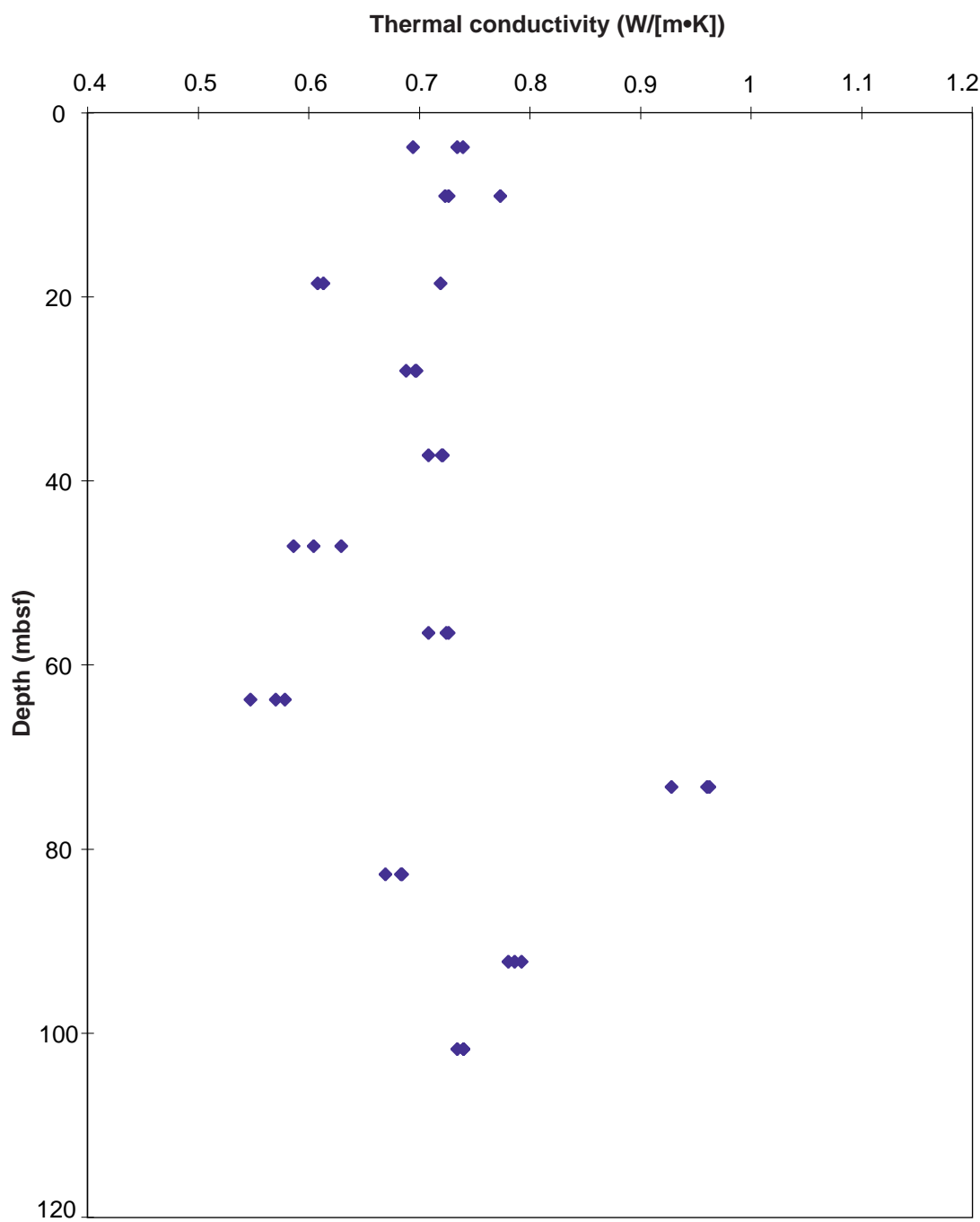


Figure F34. Color reflectance and GRAPE density data from Site 1098 on the mcd scale. Reflectance data are shown every fifth point. Lines for Holes 1098B (dotted) and 1098C (dashed) have been horizontally offset from the line for Hole 1098A (solid) for better display; therefore, values given on the horizontal scale are true values only for Hole 1098A.

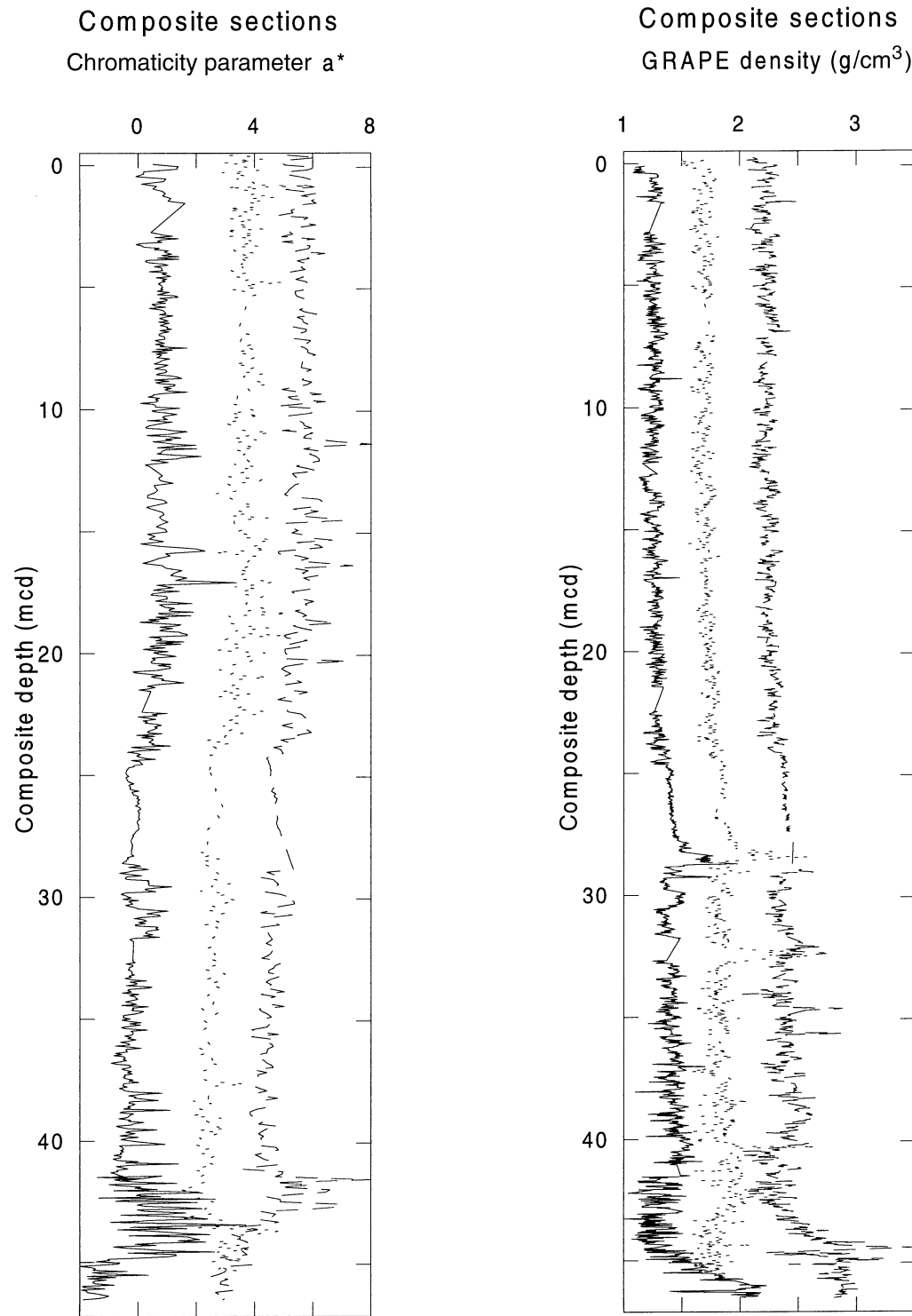


Figure F35. Magnetic susceptibility and GRAPE density data from Site 1099 on the mcd scale. Lines for Hole 1099B (dotted) have been horizontally offset from lines for Hole 1099A (solid) for better display; therefore, values given on the horizontal scale are true values only for Hole 1099A.

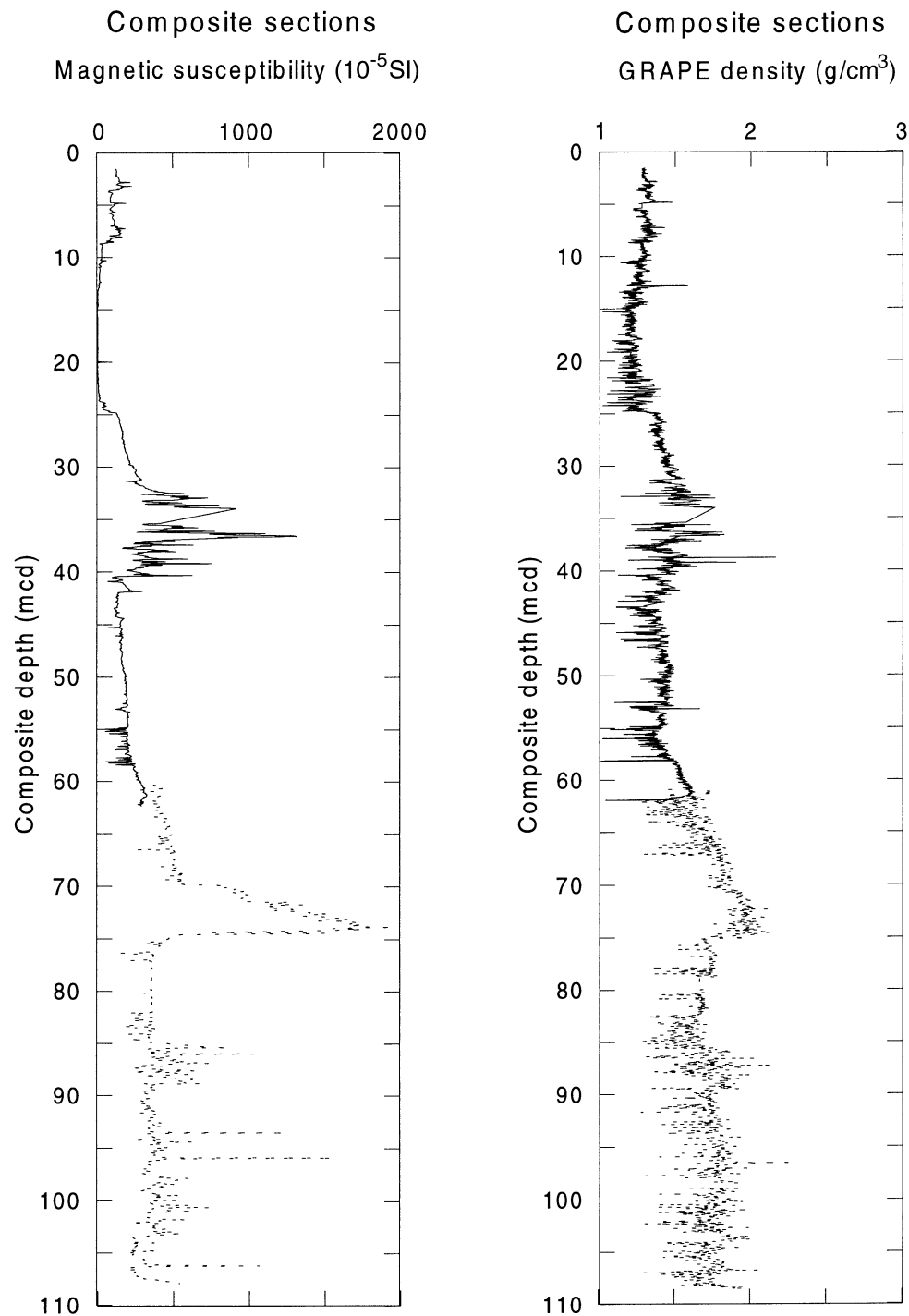


Figure F36. Magnetic susceptibility, color reflectance, GRAPE density, and natural gamma ray data with correlations (Site 1098). Composite depths are preliminary (see “[Composite Depths](#),” p. 23, in the “Explanatory Notes” chapter).

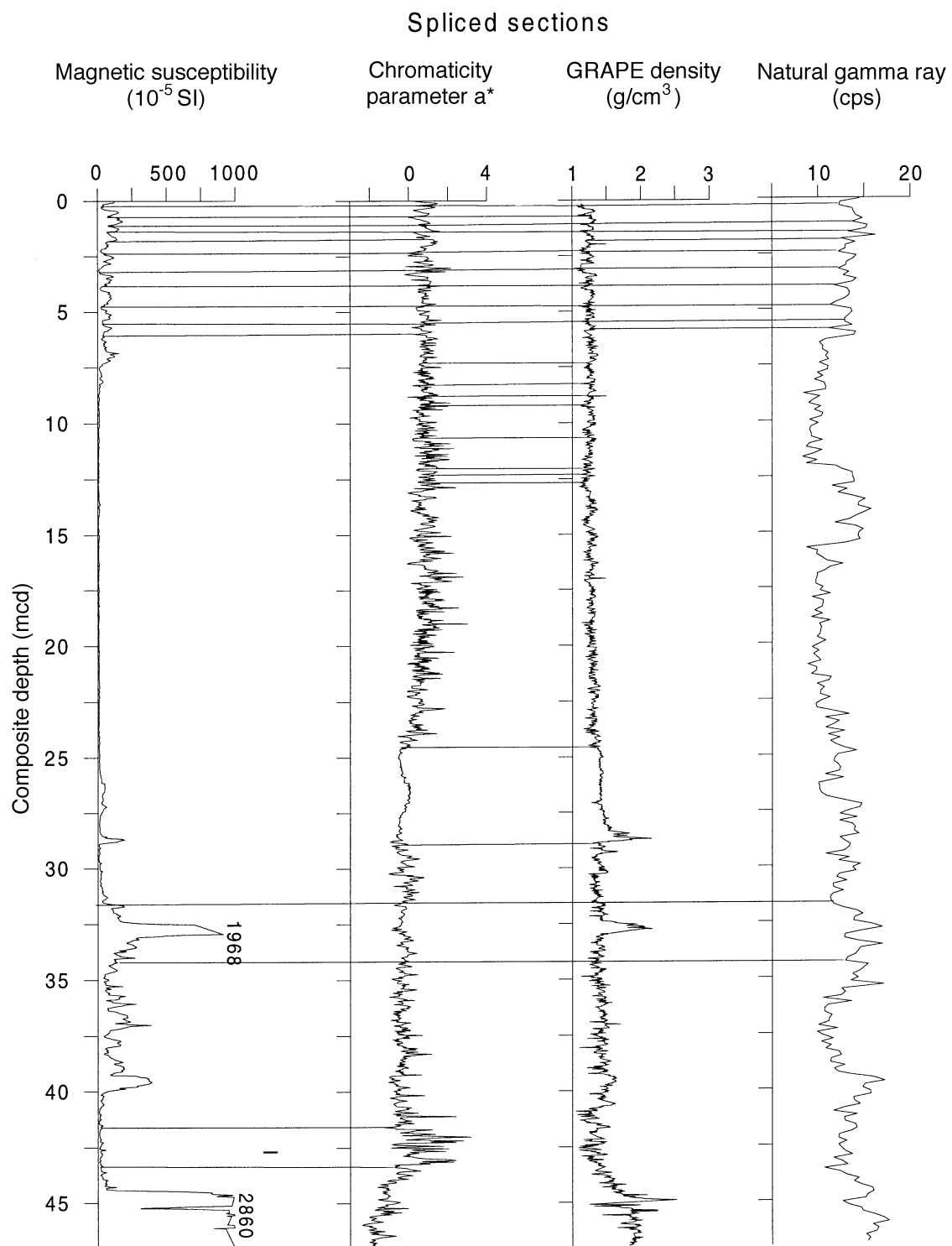


Figure F37. GRAPE density, magnetic susceptibility, color reflectance, and natural gamma ray data with correlations. D = direct correlation, I = inverse correlation (Site 1099). Composite depths are preliminary (see “[Composite Depths](#),” p. 23, in the “Explanatory Notes” chapter).

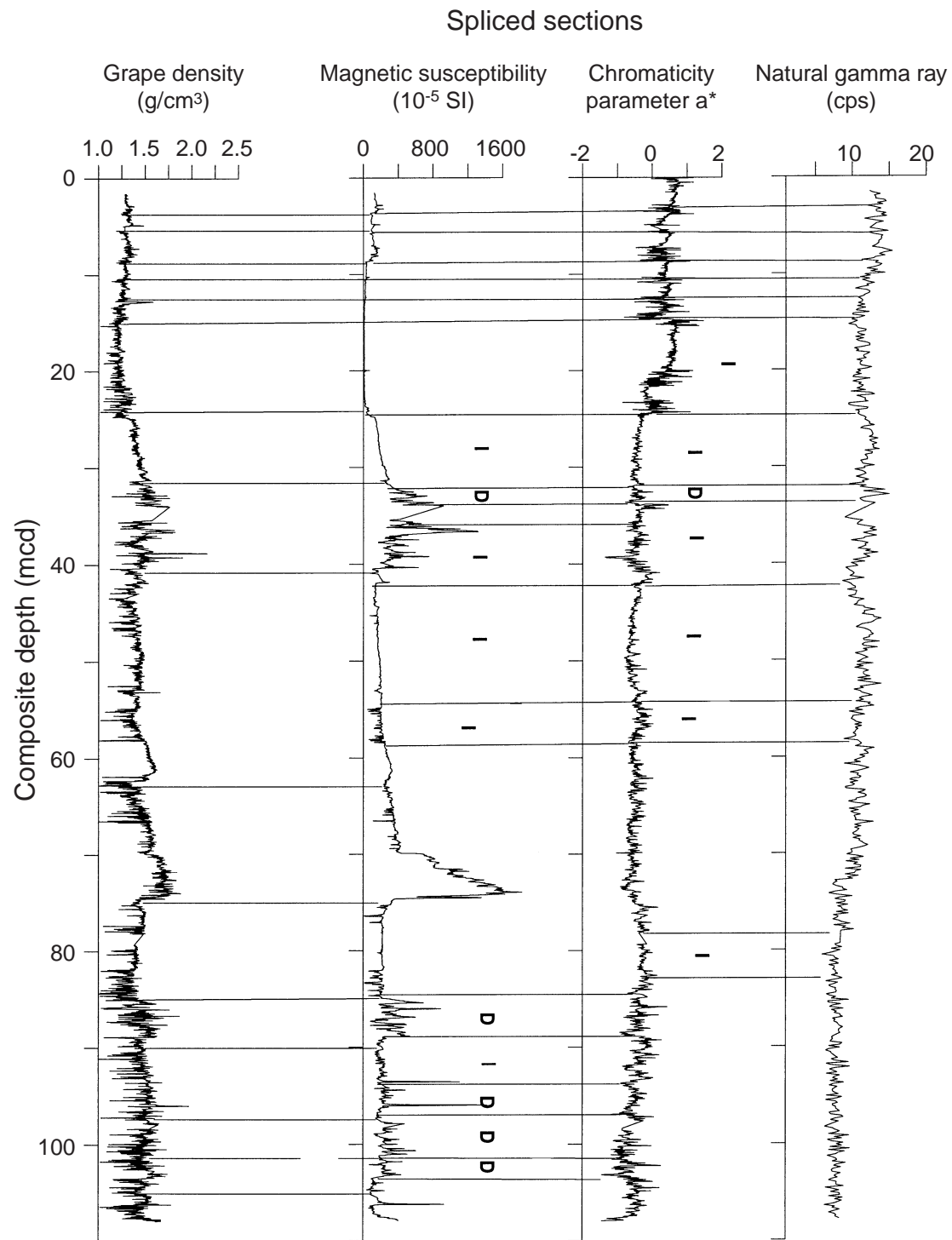


Figure F38. Depth offsets of Site 1098 mcd scale relative to mbsf depth. Crosses = Hole 1098A, circles = Hole 1098B, squares = Hole 1098C.

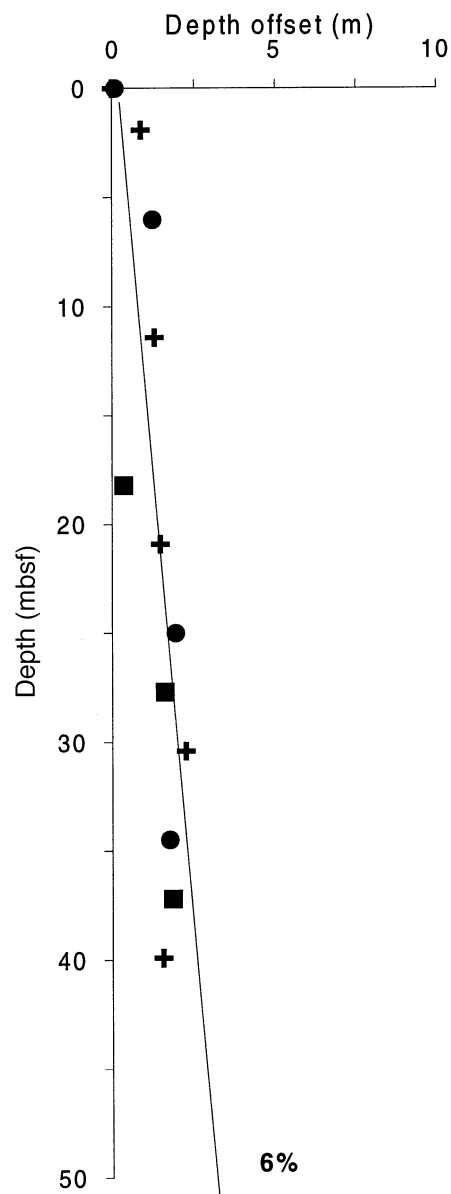


Figure F39. Depth offsets of Site 1099 mcd scale relative to mbsf depth. Circle = Hole 1099B.

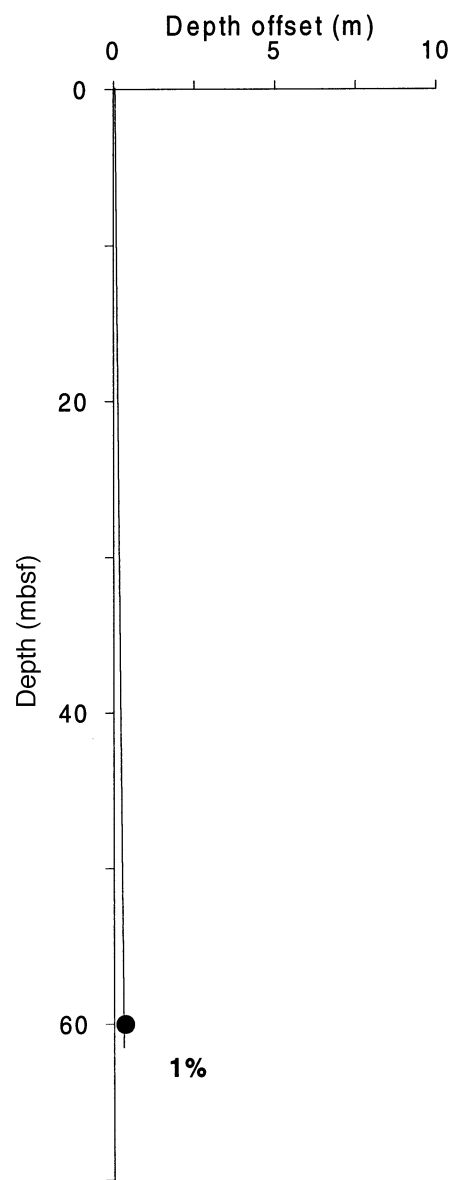


Figure F40. Two examples of spliced records for Site 1098. A. Color reflectance. B. GRAPE density data. Tie points used to form the splice are given in Table T31, p. 110.

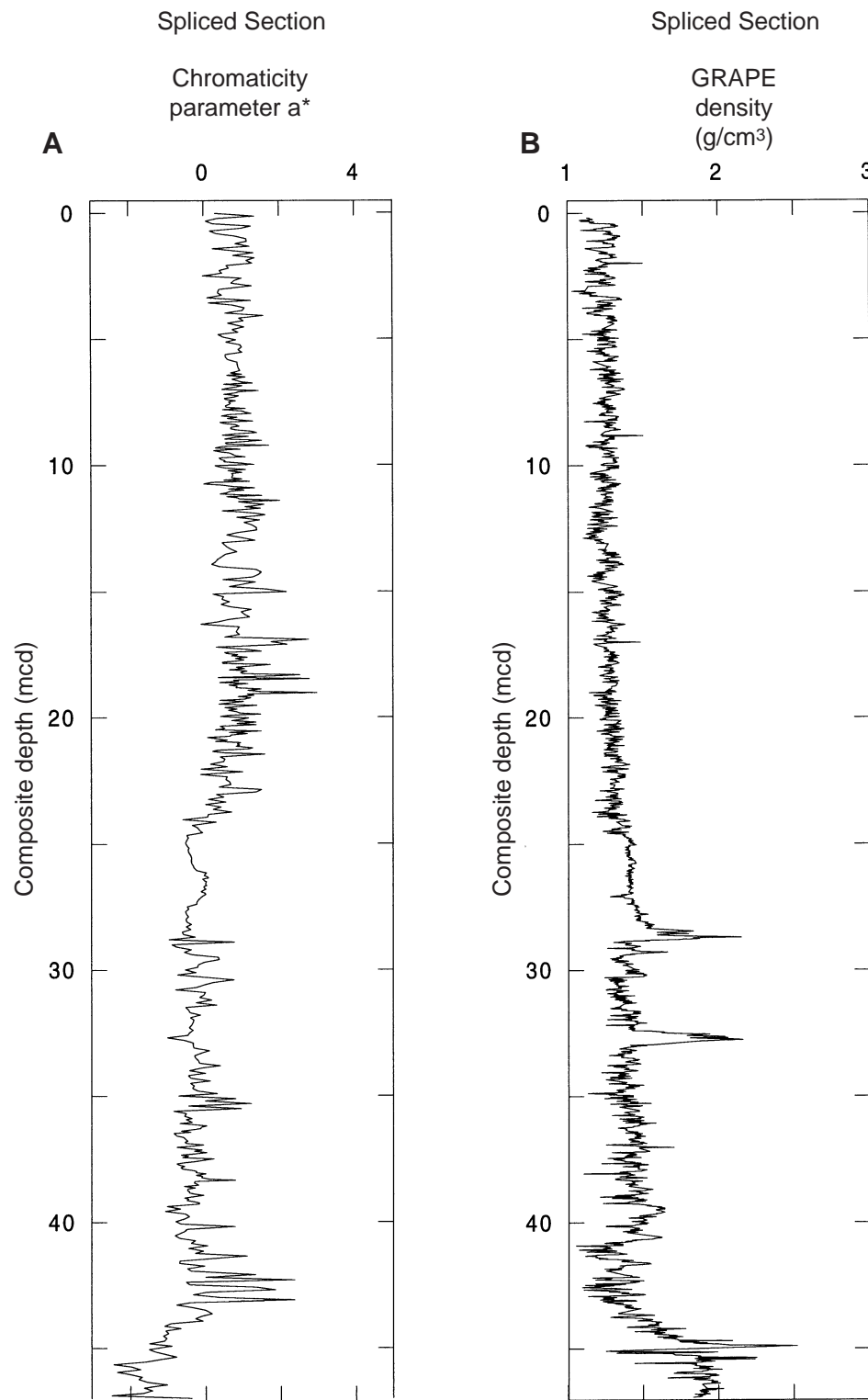


Figure F41. Two examples of spliced records for Site 1099. A. Magnetic susceptibility. B. Color reflectance data. Tie points used to form the splice are given in Table T31, p. 110.

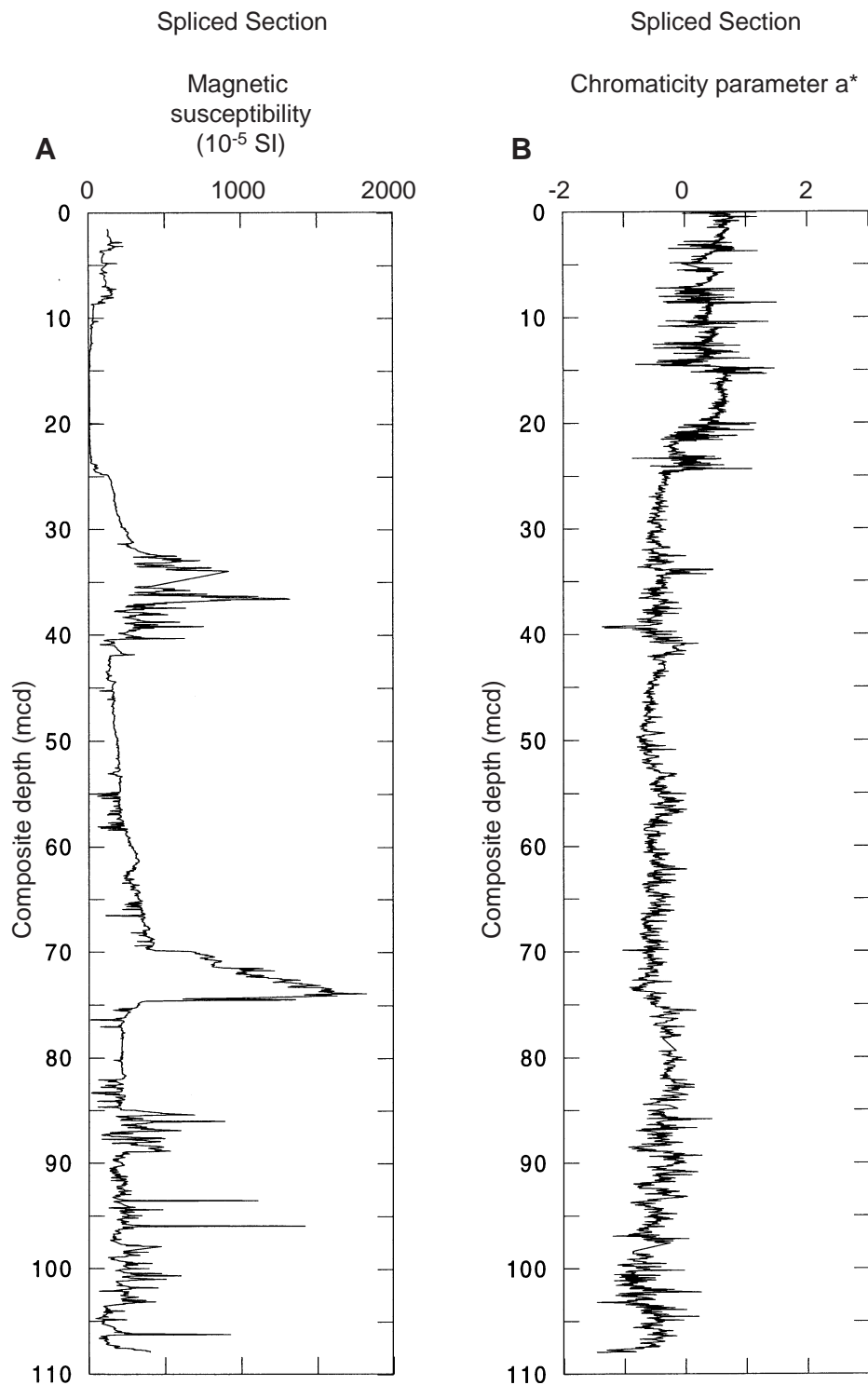


Figure F42. Synthetic seismogram and acoustic properties of Site 1098 using the Huntec deep-tow boomer signal.

Synthetic Seismogram, Site 1098 (MST Density, MST Velocity)

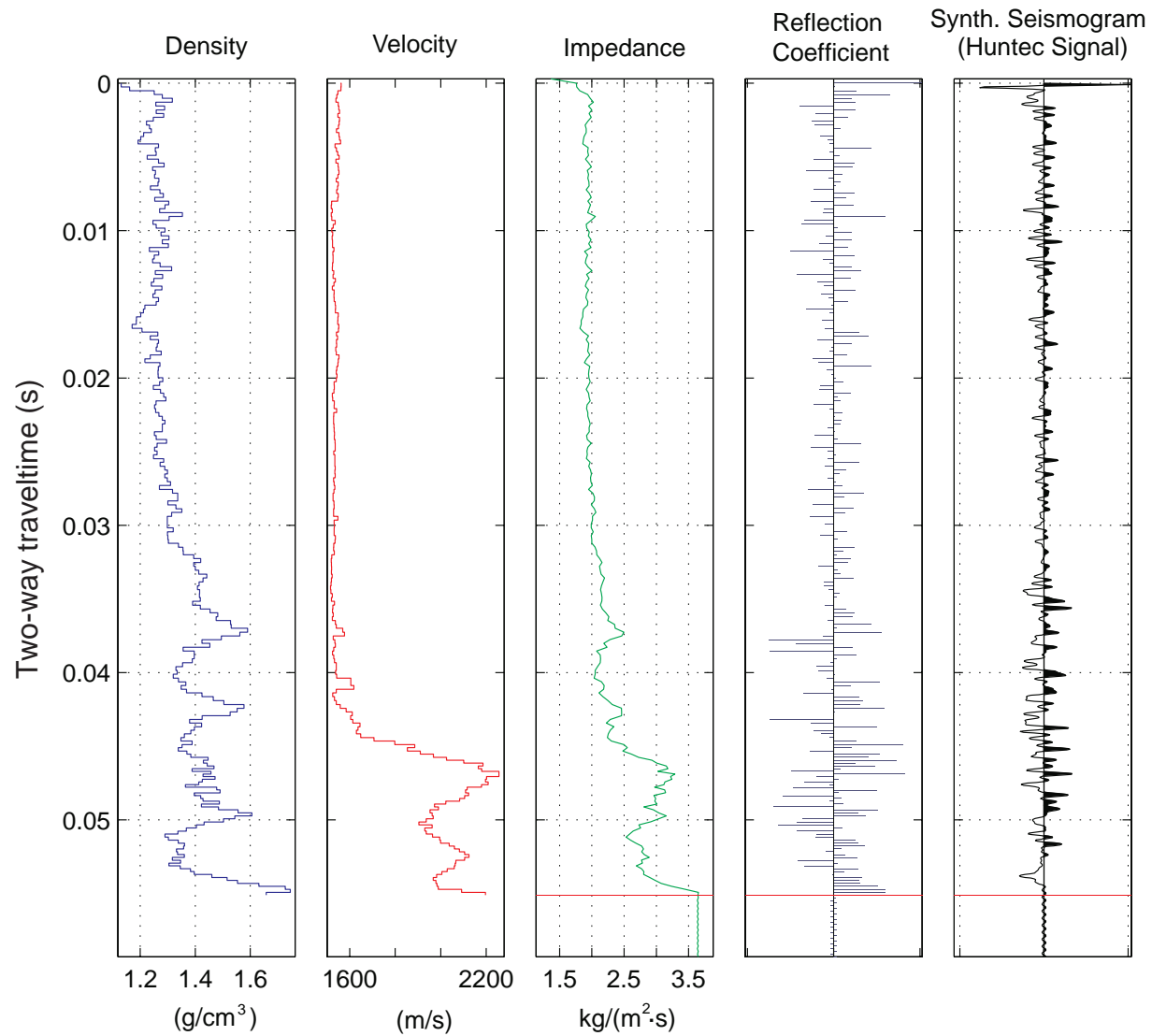


Figure F43. Synthetic seismograms and acoustic properties of Site 1099 using three different source signals.

Synthetic Seismograms, Site 1099 (MST Density, PWS3 Velocity)

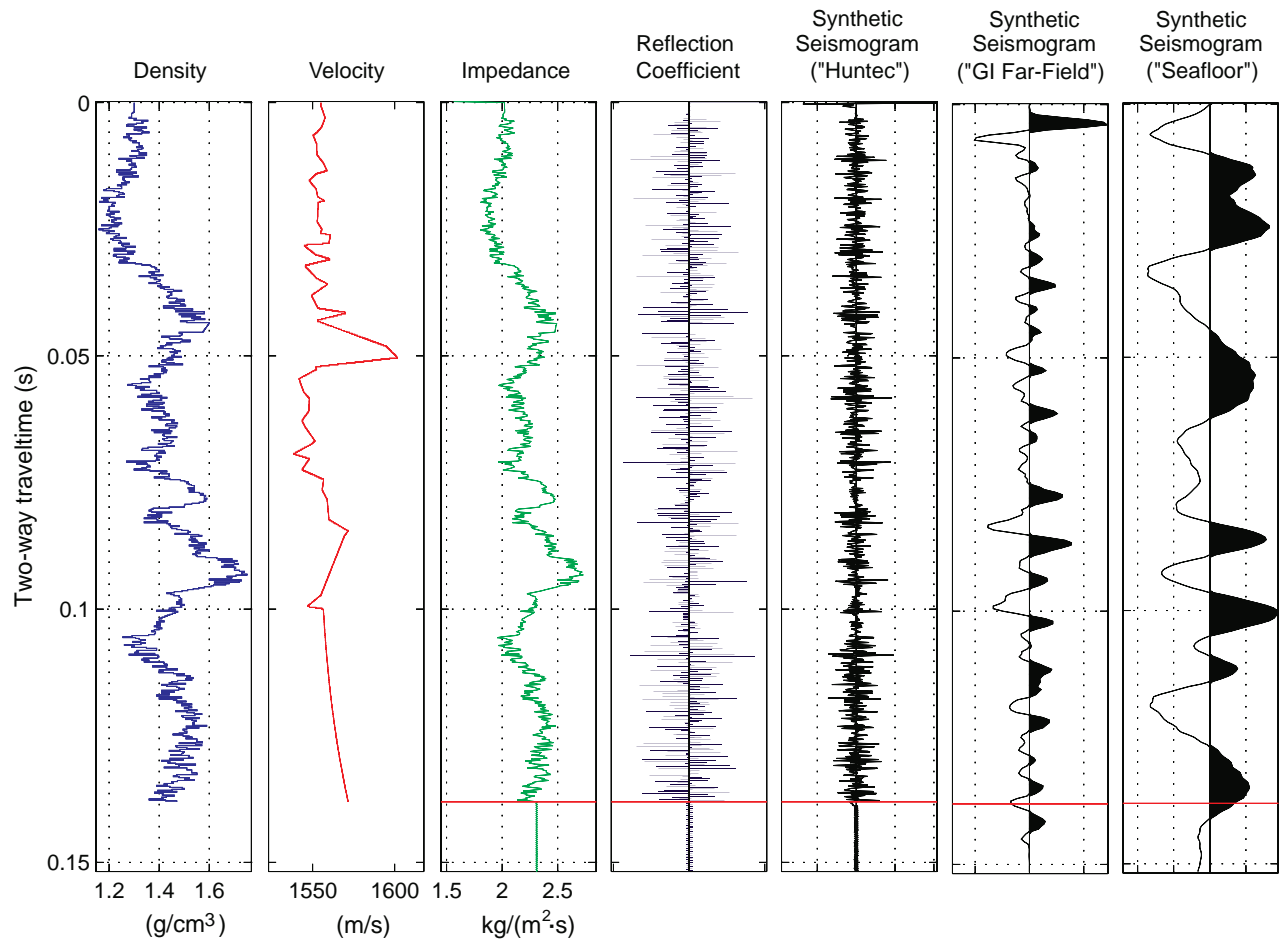
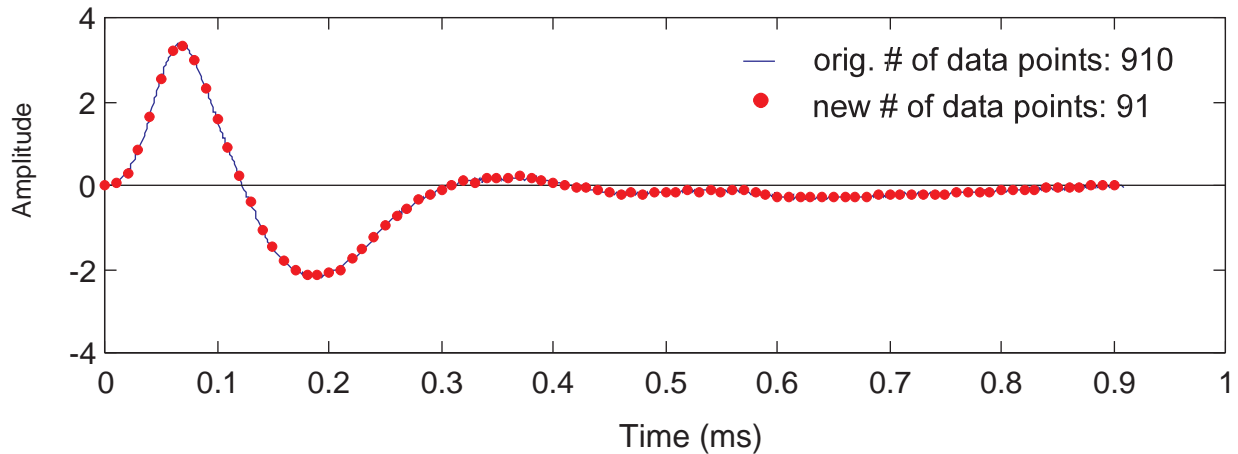


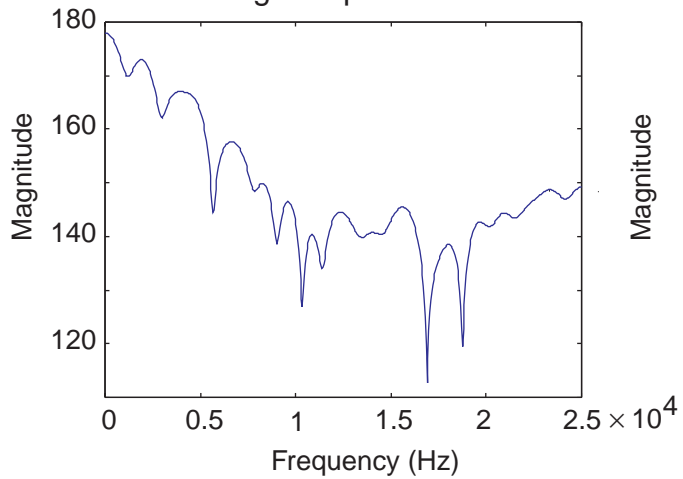
Figure F44. Characteristics of the Huntec deep-tow boomer signal and a filtered synthetic trace.

Site 1098, Huntec Signal

Huntec Far-Field Signal



Signal Spectrum



Filtered Trace Spectrum

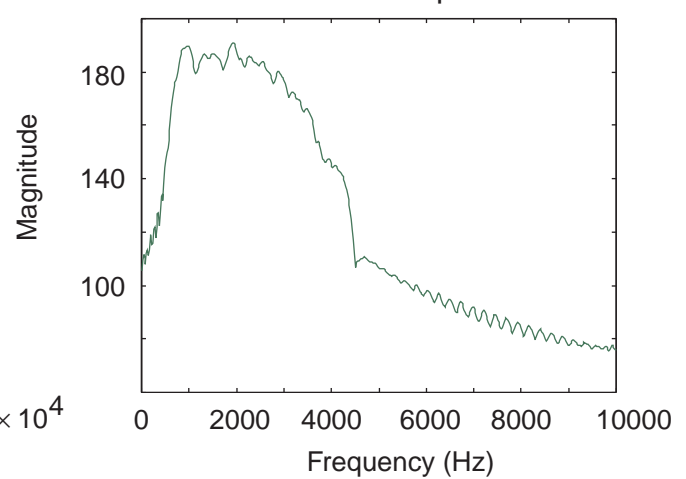


Figure F45. Time/depth relationships at Sites 1098 and 1099.

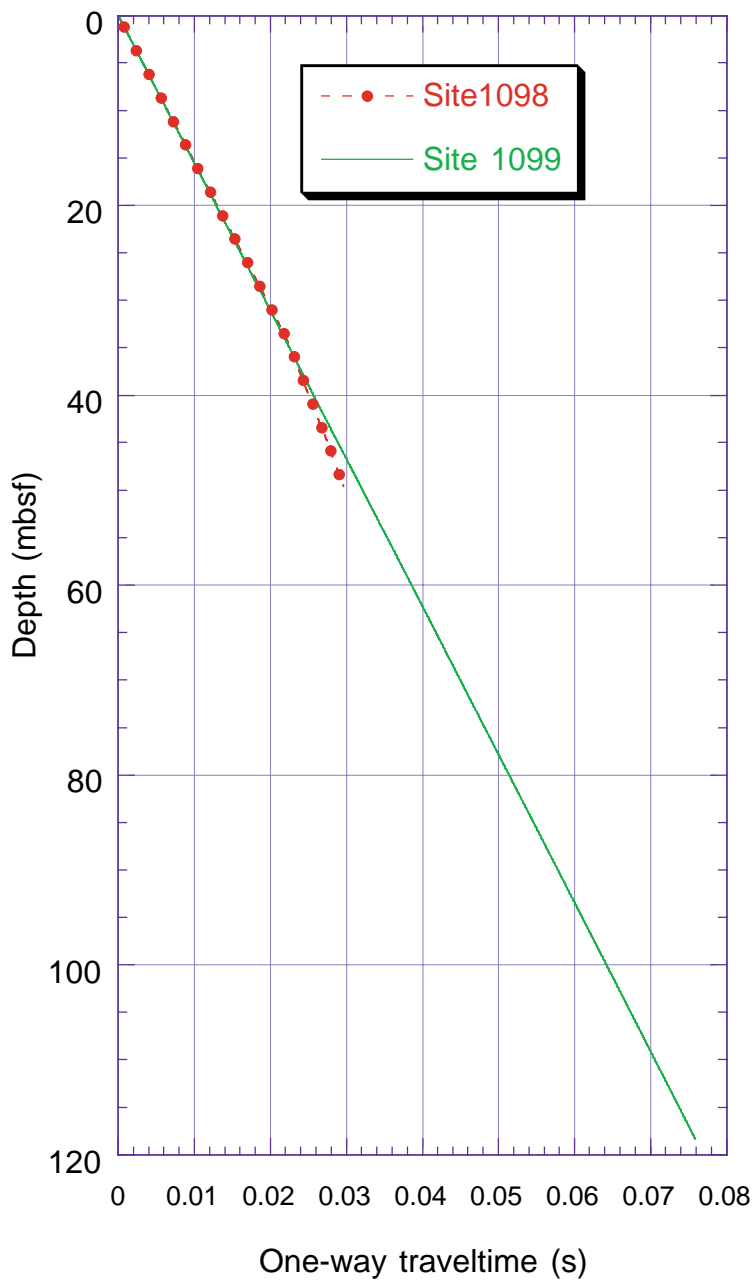


Figure F46. Deep-tow boomer profile across Site 1098. Comparison of seismic reflection data with synthetic seismogram is also shown as well as acoustic Subunits Ia, Ib, and Ic. Reflectors T1, T2, and T3 correspond to turbidite layers.

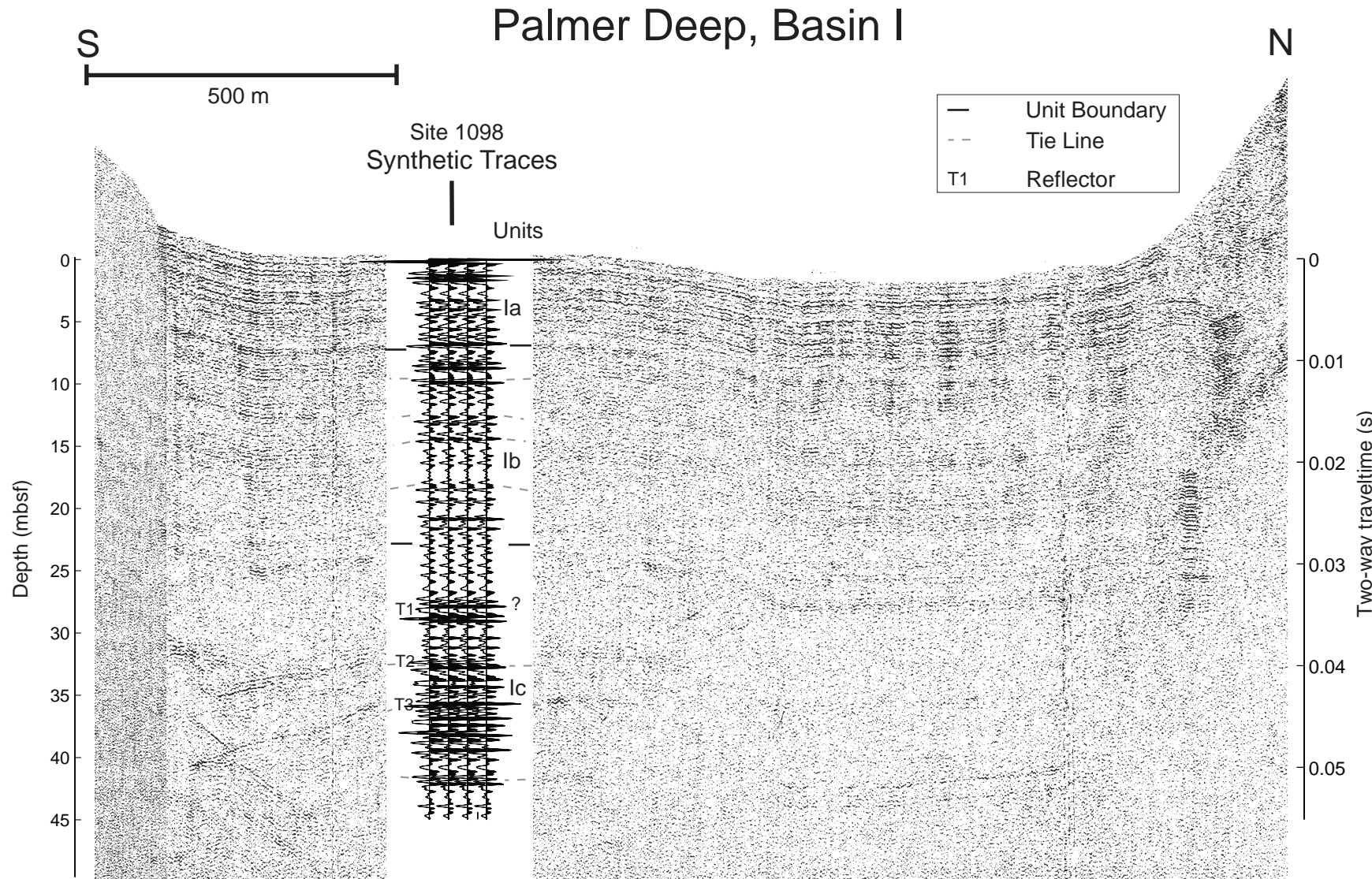


Figure F47. Deep-tow boomer profile across Site 1099. Comparison of seismic reflection data with synthetic seismogram is also shown. Letters *a* through *g* refer to acoustic packages discussed in the text. MBR = mid-basin reflector (*h*).

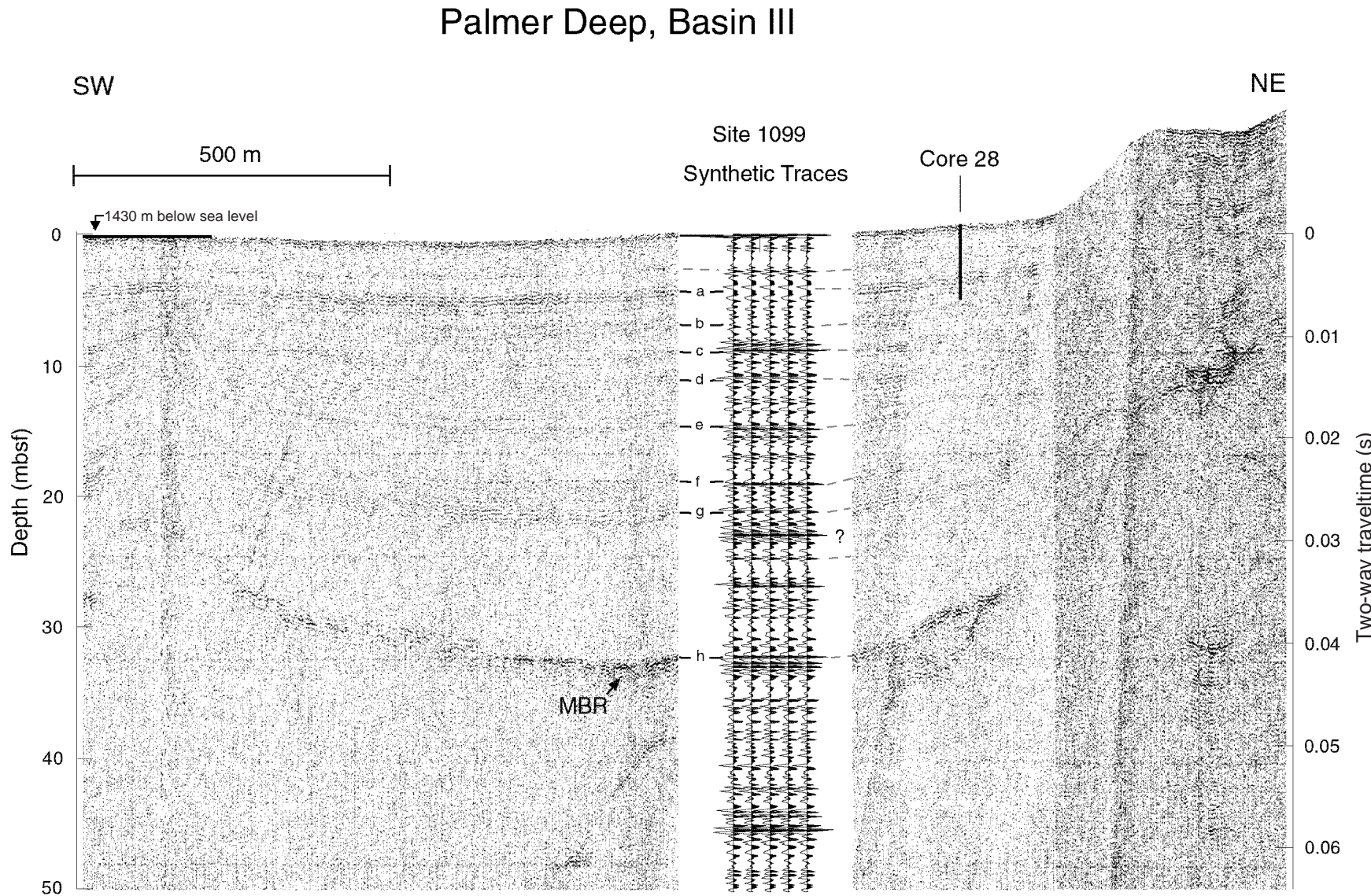


Figure F48. Synthetic seismogram and GI gun reflection seismic profile I97H-219G of Basin III. MBR = mid-basin reflector.

Site 1099, Profile I97H-219G, Synthetic Traces: Seafloor Reflector

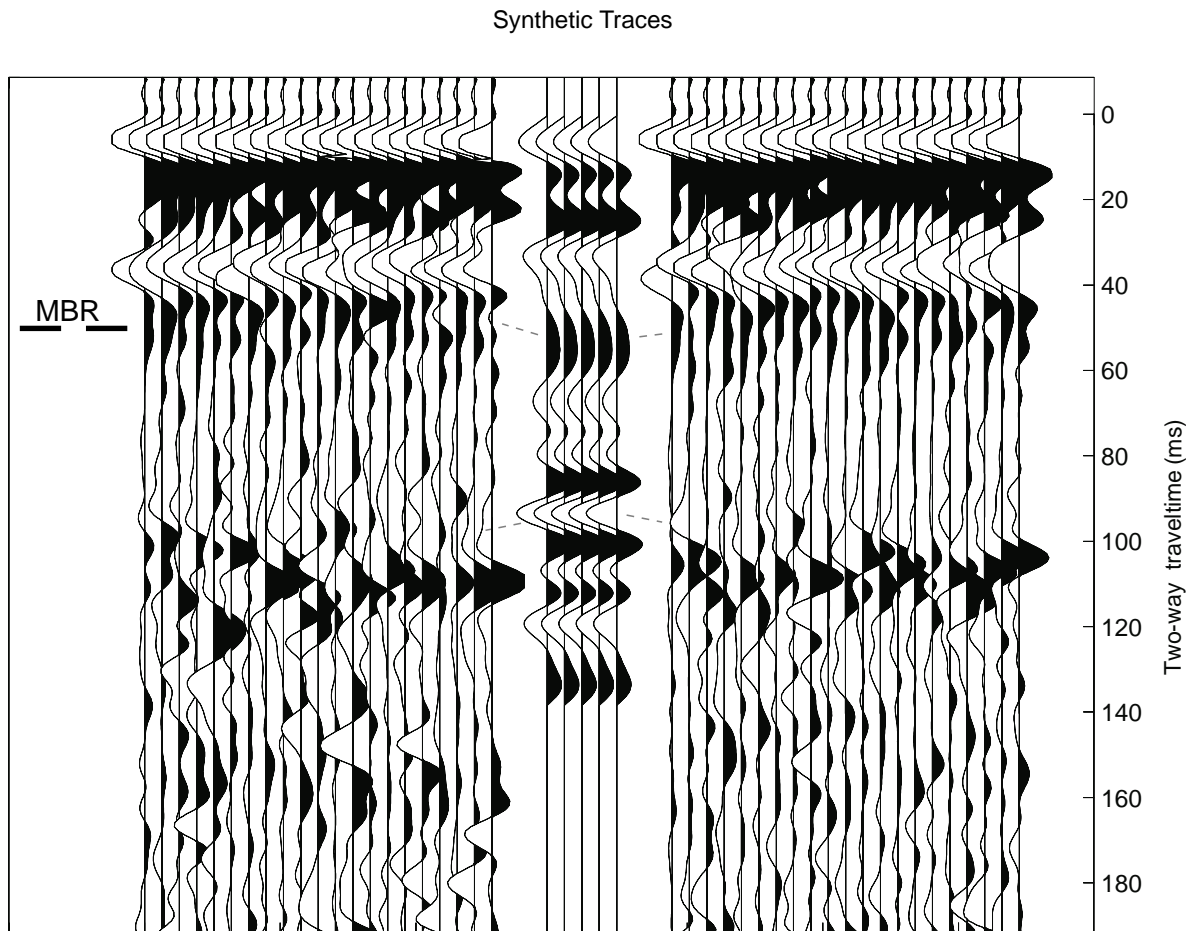


Figure F49. GI gun seismic profile I97H-218G across Palmer Deep Site 1098 (modified from Rebescu et al., 1998).

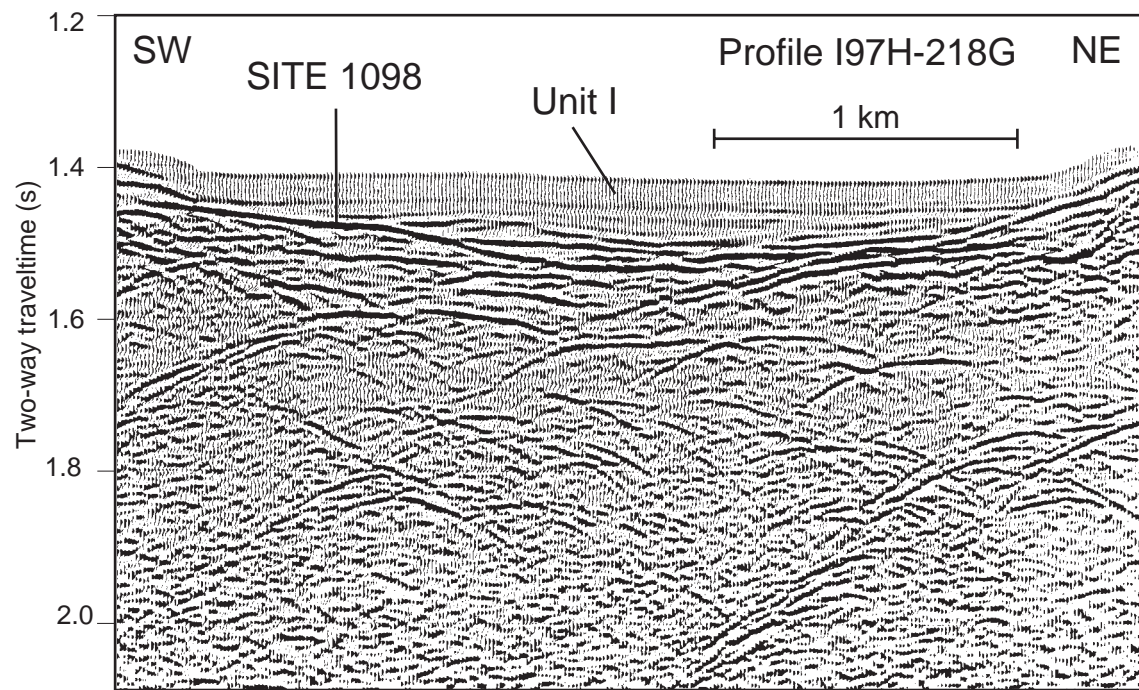
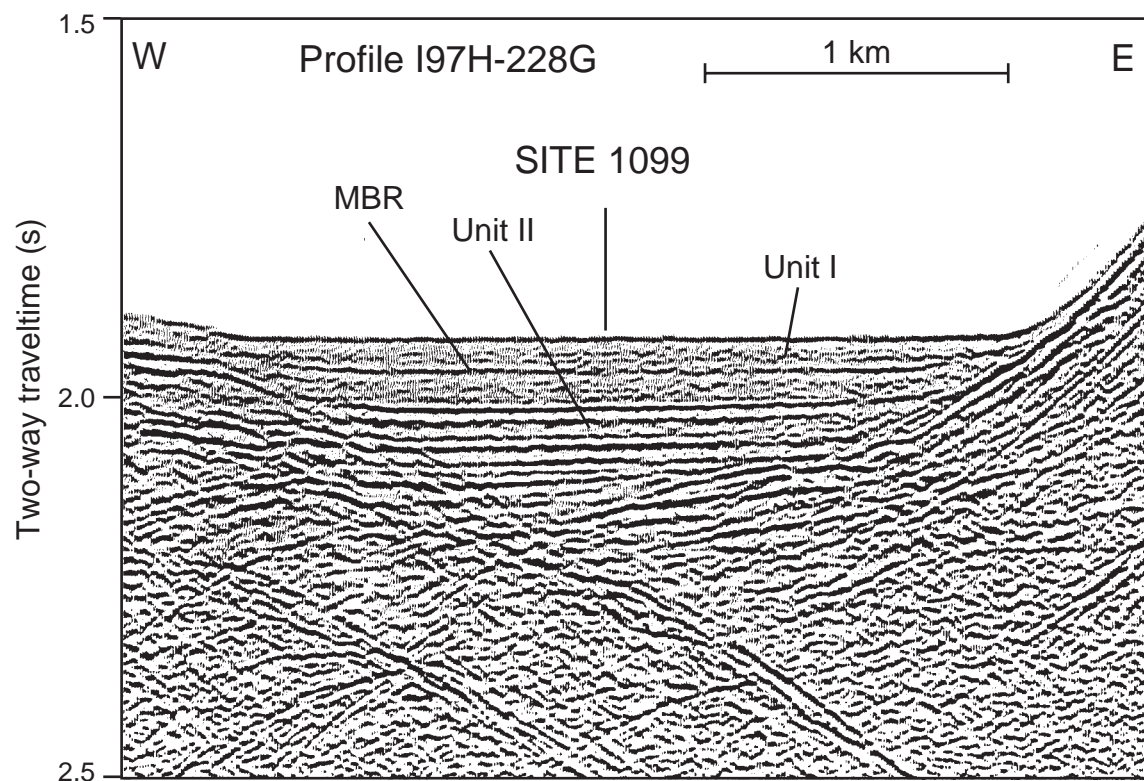


Figure F50. Air gun seismic profile I97H-228G across Palmer Deep Site 1099 (modified from Rebescu et al., 1998). MBR = mid-basin reflector.



SHIPBOARD SCIENTIFIC PARTY
CHAPTER 7, PALMER DEEP (SITES 1098 AND 1099)

79

Table T1. Coring summary for Sites 1098 and 1099.

Core	Date (March 1998)	Time (UTC)	Depth (mbsf)	Length cored (m)	Length recovered (m)	Recovery (%)
178-1098A-						
1H	12	1840	0.0-1.9	1.9	1.88	98.9
2H	12	1910	1.9-11.4	9.5	9.83	103.5
3H	12	1935	11.4-20.9	9.5	9.08	95.6
4H	12	1950	20.9-30.4	9.5	9.72	102.3
5H	12	2025	30.4-39.9	9.5	9.35	98.4
6H	12	2050	39.9-45.4	5.5	5.46	99.3
7H	12	2140	45.4-45.9	0.5	0.46	92.0
Coring totals:				45.9	45.78	99.7
178-1098B-						
1H	13	0010	0.0-6.0	6.0	5.96	99.3
2H	13	0035	6.0-15.5	9.5	9.75	102.6
3H	13	0130	15.5-25.0	9.5	9.88	104.0
4H	13	0230	25.0-34.5	9.5	9.09	95.7
5H	13	0325	34.5-43.0	8.5	9.98	117.4
Coring totals:				43.0	44.66	103.9
178-1098C-						
1H	13	0445	0.0-8.7	8.7	8.61	99.0
2H	13	0505	8.7-18.2	9.5	9.97	104.9
3H	13	0540	18.2-27.7	9.5	9.58	100.8
4H	13	0605	27.7-37.2	9.5	9.89	104.1
5H	13	0630	37.2-46.7	9.5	8.25	86.8
Coring totals:				46.7	46.30	99.1
178-1099A-						
1H	13	1500	0.0-5.3	5.3	5.28	99.6
2H	13	1535	5.3-14.8	9.5	9.81	103.3
3H	13	1605	14.8-24.3	9.5	9.78	102.9
4H	13	1635	24.3-33.8	9.5	9.86	103.8
5H	13	1715	33.8-43.3	9.5	9.38	98.7
6H	13	1750	43.3-52.8	9.5	9.80	103.2
7H	13	1845	52.8-62.3	9.5	9.83	103.5
Coring totals:				62.3	63.74	102.3
178-1099B-						
*****Drilled from 0 to 60.0 mbsf*****						
1H	13	2245	60.0-69.5	9.5	9.80	103.2
2H	13	2315	69.5-79.0	9.5	8.69	91.5
3H	13	2340	79.0-88.5	9.5	10.15	106.8
4H	14	0010	88.5-98.0	9.5	9.53	100.3
5H	14	0035	98.0-107.5	9.5	10.17	107.1
Coring totals:				47.5	48.34	101.8
Drilled:				60.0		
Total:				107.5		

Notes: UTC = Universal Time Coordinated. An expanded version of this coring summary table that includes lengths and depths of sections and comments on sampling is included in ASCII format in the [TABLES](#) directory.

Table T2. Summary of lithostratigraphic Unit I of Site 1098.

Subunit	Depth (mbsf)	Thickness (m)	Age	Lithology and characteristic features
IA	0.0-43.5 (Hole 1098A)	43.5 (Hole 1098A)	Holocene	Alternating massive olive-gray, brown, dark brown, dark gray muddy diatom oozes and laminated mud-bearing diatom oozes with diatom-bearing silty clays and clayey silts, slight to heavily bioturbated, some turbidite intervals
	0.0-43.0 (Hole 1098B)	43.0 (Hole 1098B)		
	0.0-42.2 (Hole 1098C)	42.2 (Hole 1098C)		
IB	43.5-45.9 (Hole 1098A)	2.4 (Hole 1098A)	Holocene	Coarse clastic material and pebbles
	42.2-46.7 (Hole 1098C)	4.5 (Hole 1098C)		

Table T3. Occurrence of pebbles >0.5 cm at Sites 1098 and 1099.

Core	Depth (mbsf)	Number of pebbles (ø >0.5cm)
178-1098A-		
1H	0.00	0
1H	5.99	0
2H	6.00	0
2H	6.01	3
2H	15.99	3
3H	16.00	0
3H	16.01	1
3H	25.49	1
4H	25.50	0
4H	25.51	4
4H	34.49	4
5H	34.50	0
5H	34.51	18
5H	42.49	18
6H	42.50	0
6H	42.51	5
6H	45.99	5
6H	46.00	0
178-1099A-		
4H	24.30	3
5H	33.80	10
178-1099B-		
2H	69.50	1
3H	79.00	7
4H	88.50	2
5H	98.00	1

Table T4. Summary of environmental indicator diatom species used at Sites 1098 and 1099.

Species	Description
<i>Fragilariopsis kerguelensis</i> and <i>Thalassiothrix</i> spp.	Open ocean; characteristic of Southern Ocean ooze belt
<i>Thalassiosira antarctica</i>	Associated with open-water primary productivity
<i>Eucampia antarctica</i>	Glacial conditions found in core tops near ice shelves in the Weddell Sea
<i>Fragilariopsis curta</i>	Sea-ice-dominated species in the ice-edge bloom
<i>Chaetoceros</i> spp. spores	This stressed spore form occurs during extreme stratification of the water column (nutrient-depleting phytoplankton blooms, followed by nitrogen deficiency)

Table T5. Split-core paleomagnetic measurements for Hole 1098A before demagnetization (NRM results).

Leg	Site	Hole	Core	Type	Section	Interval (cm)	Depth (mbsf)	Inclination (°)	Declination (°)	Intensity (A/m)	Demagnetization step (mT)	Run #
178	1098	A	1	H	1	10	0.1	-23.51	28.58	1.50E-01	0	10712
178	1098	A	1	H	1	15	0.15	-20.84	28.28	1.02E-01	0	10712
178	1098	A	1	H	1	20	0.2	-12.39	25.37	3.48E-02	0	10712
178	1098	A	1	H	1	25	0.25	13.47	18.13	1.28E-02	0	10712
178	1098	A	1	H	1	30	0.3	23.9	355.47	1.38E-02	0	10712
178	1098	A	1	H	1	35	0.35	17.32	354.46	1.42E-02	0	10712
178	1098	A	1	H	1	40	0.4	7.96	3.87	1.39E-02	0	10712
178	1098	A	1	H	1	45	0.45	-21.68	11.98	1.57E-02	0	10712
178	1098	A	1	H	1	50	0.5	-28.92	31.3	5.81E-02	0	10712
178	1098	A	1	H	1	55	0.55	-23.43	29.91	9.87E-02	0	10712
178	1098	A	1	H	1	60	0.6	-21.84	24.49	1.18E-01	0	10712
178	1098	A	1	H	1	65	0.65	-24.03	25.63	1.07E-01	0	10712
178	1098	A	1	H	1	70	0.7	-52.05	42.55	6.36E-02	0	10712
178	1098	A	1	H	1	75	0.75	-50.53	22.46	6.92E-02	0	10712
178	1098	A	1	H	1	80	0.8	-29.68	26.23	9.53E-02	0	10712
178	1098	A	1	H	1	85	0.85	-33.58	26.12	9.49E-02	0	10712
178	1098	A	1	H	1	90	0.9	-33.58	30.62	1.04E-01	0	10712
178	1098	A	1	H	2	10	1.1	-45.4	42.51	1.02E-01	0	10715
178	1098	A	1	H	2	15	1.15	-39.34	34.16	6.87E-02	0	10715
178	1098	A	1	H	2	20	1.2	-45.43	48.31	6.49E-02	0	10715
178	1098	A	1	H	2	25	1.25	-46.19	50.06	8.63E-02	0	10715
178	1098	A	1	H	2	30	1.3	-40.24	47.3	9.04E-02	0	10715
178	1098	A	1	H	2	35	1.35	-35	51.92	7.02E-02	0	10715
178	1098	A	1	H	2	40	1.4	-21.95	36.69	5.04E-02	0	10715
178	1098	A	1	H	2	45	1.45	25.67	22.79	7.67E-02	0	10715
178	1098	A	1	H	2	50	1.5	69.59	68.08	4.63E-02	0	10715
178	1098	A	1	H	2	55	1.55	-19.55	55.15	9.75E-03	0	10715
178	1098	A	1	H	2	60	1.6	-32.65	19.79	4.55E-02	0	10715
178	1098	A	2	H	1	10	2	-4.25	353.65	2.42E-02	0	10718
178	1098	A	2	H	1	15	2.05	4.24	12.69	1.41E-02	0	10718
178	1098	A	2	H	1	20	2.1	-16.98	19.86	1.50E-02	0	10718
178	1098	A	2	H	1	25	2.15	-19.25	351.92	3.66E-02	0	10718
178	1098	A	2	H	1	30	2.2	-13.46	352.21	5.20E-02	0	10718
178	1098	A	2	H	1	35	2.25	-8.34	354.05	4.83E-02	0	10718
178	1098	A	2	H	1	40	2.3	2.14	348.85	4.23E-02	0	10718
178	1098	A	2	H	1	45	2.35	17.39	335.18	2.98E-02	0	10718
178	1098	A	2	H	1	50	2.4	30.34	345.03	2.79E-02	0	10718
178	1098	A	2	H	1	55	2.45	50.83	346.81	2.72E-02	0	10718
178	1098	A	2	H	1	60	2.5	52.68	11.8	4.06E-02	0	10718
178	1098	A	2	H	1	65	2.55	61.22	347.77	3.62E-02	0	10718
178	1098	A	2	H	1	70	2.6	67.44	342.9	2.37E-02	0	10718
178	1098	A	2	H	1	75	2.65	56.29	2.08	2.74E-02	0	10718
178	1098	A	2	H	1	80	2.7	55.06	6.38	3.20E-02	0	10718
178	1098	A	2	H	1	85	2.75	66.79	15.07	3.15E-02	0	10718
178	1098	A	2	H	1	90	2.8	78.75	8.81	1.90E-02	0	10718
178	1098	A	2	H	1	95	2.85	46.13	358.99	2.21E-02	0	10718
178	1098	A	2	H	1	100	2.9	75.63	355.91	1.57E-02	0	10718
178	1098	A	2	H	1	105	2.95	61.68	90.44	4.73E-03	0	10718
178	1098	A	2	H	1	110	3	10.73	9.56	5.61E-03	0	10718
178	1098	A	2	H	1	115	3.05	12.77	125.71	3.48E-03	0	10718
178	1098	A	2	H	1	120	3.1	17.44	165.38	3.77E-03	0	10718
178	1098	A	2	H	1	125	3.15	12.97	355.31	1.50E-02	0	10718
178	1098	A	2	H	1	130	3.2	27.85	3.14	3.14E-02	0	10718
178	1098	A	2	H	1	135	3.25	57.6	11.72	2.38E-02	0	10718
178	1098	A	2	H	1	140	3.3	60.36	14.36	1.99E-02	0	10718
178	1098	A	2	H	2	10	3.5	43.18	15.41	3.03E-02	0	10721
178	1098	A	2	H	2	15	3.55	45.65	359.99	3.68E-02	0	10721
178	1098	A	2	H	2	20	3.6	59.94	345.44	3.21E-02	0	10721
178	1098	A	2	H	2	25	3.65	52.12	18.76	3.10E-02	0	10721
178	1098	A	2	H	2	30	3.7	60.95	26.39	2.91E-02	0	10721
178	1098	A	2	H	2	35	3.75	54.46	24.28	2.87E-02	0	10721
178	1098	A	2	H	2	40	3.8	73.26	302.46	1.81E-02	0	10721
178	1098	A	2	H	2	45	3.85	-35.4	312.51	1.41E-02	0	10721
178	1098	A	2	H	2	50	3.9	-1.41	34.6	2.49E-02	0	10721
178	1098	A	2	H	2	55	3.95	46.5	53.75	4.00E-03	0	10721

Note: Only a portion of this table appears here. The complete table is available in ASCII format in the [TABLES](#) directory.

Table T6. Split-core paleomagnetic measurements for Hole 1098A after 10-mT demagnetization.

Leg	Site	Hole	Core	Type	Section	Interval (cm)	Depth (mbsf)	Inclination (°)	Declination (°)	Intensity (A/m)	Demagnetization step (mT)	Run #
178	1098	A	1	H	1	10	0.1	-56.66	59.2	7.27E-02	10	10713
178	1098	A	1	H	1	15	0.15	-60.59	52.83	5.37E-02	10	10713
178	1098	A	1	H	1	20	0.2	-61.99	45.92	2.52E-02	10	10713
178	1098	A	1	H	1	25	0.25	-75.34	43.71	1.21E-02	10	10713
178	1098	A	1	H	1	30	0.3	-68.03	16.04	9.16E-03	10	10713
178	1098	A	1	H	1	35	0.35	-59.55	354.4	9.72E-03	10	10713
178	1098	A	1	H	1	40	0.4	-65.73	357.01	1.24E-02	10	10713
178	1098	A	1	H	1	45	0.45	-83.08	346.25	1.94E-02	10	10713
178	1098	A	1	H	1	50	0.5	-74.94	123.94	4.46E-02	10	10713
178	1098	A	1	H	1	55	0.55	-69.92	84.98	6.88E-02	10	10713
178	1098	A	1	H	1	60	0.6	-64.37	63.64	7.79E-02	10	10713
178	1098	A	1	H	1	65	0.65	-67.42	67.85	8.23E-02	10	10713
178	1098	A	1	H	1	70	0.7	-69.28	143.77	8.42E-02	10	10713
178	1098	A	1	H	1	75	0.75	-77.13	167.88	8.28E-02	10	10713
178	1098	A	1	H	1	80	0.8	-75.65	61.11	7.64E-02	10	10713
178	1098	A	1	H	1	85	0.85	-73.96	82.63	8.39E-02	10	10713
178	1098	A	1	H	1	90	0.9	-72.27	93.46	9.40E-02	10	10713
178	1098	A	1	H	2	10	1.1	-75.59	91.03	1.29E-01	10	10716
178	1098	A	1	H	2	15	1.15	-78.05	49.71	9.44E-02	10	10716
178	1098	A	1	H	2	20	1.2	-77.7	102.98	9.00E-02	10	10716
178	1098	A	1	H	2	25	1.25	-74.12	110.84	1.20E-01	10	10716
178	1098	A	1	H	2	30	1.3	-75.3	89.76	1.23E-01	10	10716
178	1098	A	1	H	2	35	1.35	-74.43	97.22	1.06E-01	10	10716
178	1098	A	1	H	2	40	1.4	-76.49	68.55	8.08E-02	10	10716
178	1098	A	1	H	2	45	1.45	-74.63	47.72	6.41E-02	10	10716
178	1098	A	1	H	2	50	1.5	-73.75	68.05	5.40E-02	10	10716
178	1098	A	1	H	2	55	1.55	-78.34	97.08	4.52E-02	10	10716
178	1098	A	1	H	2	60	1.6	-77.13	62.11	4.73E-02	10	10716
178	1098	A	2	H	1	10	2	-39.96	359.9	1.18E-02	10	10719
178	1098	A	2	H	1	15	2.05	-77.63	323.31	8.11E-03	10	10719
178	1098	A	2	H	1	20	2.1	-69.25	28.31	1.07E-02	10	10719
178	1098	A	2	H	1	25	2.15	-38.36	354.05	1.89E-02	10	10719
178	1098	A	2	H	1	30	2.2	-26.79	1.84	2.20E-02	10	10719
178	1098	A	2	H	1	35	2.25	-23.28	3.81	2.19E-02	10	10719
178	1098	A	2	H	1	40	2.3	-17.73	350.88	1.87E-02	10	10719
178	1098	A	2	H	1	45	2.35	-24.39	344.75	1.15E-02	10	10719
178	1098	A	2	H	1	50	2.4	-32.35	354.18	9.62E-03	10	10719
178	1098	A	2	H	1	55	2.45	-28.67	358.33	6.33E-03	10	10719
178	1098	A	2	H	1	60	2.5	-39.77	21.67	7.09E-03	10	10719
178	1098	A	2	H	1	65	2.55	-44.54	12.87	9.14E-03	10	10719
178	1098	A	2	H	1	70	2.6	-85.65	316.64	8.60E-03	10	10719
178	1098	A	2	H	1	75	2.65	-83.31	136.58	1.34E-02	10	10719
178	1098	A	2	H	1	80	2.7	-82.5	69.37	1.64E-02	10	10719
178	1098	A	2	H	1	85	2.75	-75.12	36.94	1.58E-02	10	10719
178	1098	A	2	H	1	90	2.8	-79.77	62.7	1.28E-02	10	10719
178	1098	A	2	H	1	95	2.85	-75	41.49	1.34E-02	10	10719
178	1098	A	2	H	1	100	2.9	-79.48	18.24	1.09E-02	10	10719
178	1098	A	2	H	1	105	2.95	-75.5	146.17	1.03E-02	10	10719
178	1098	A	2	H	1	110	3	-81.1	58.87	9.86E-03	10	10719
178	1098	A	2	H	1	115	3.05	-68.97	152.16	8.23E-03	10	10719
178	1098	A	2	H	1	120	3.1	-58.41	162.3	9.11E-03	10	10719
178	1098	A	2	H	1	125	3.15	-77.59	15.55	1.10E-02	10	10719
178	1098	A	2	H	1	130	3.2	-65.26	8.61	1.75E-02	10	10719
178	1098	A	2	H	1	135	3.25	-67.58	25.75	1.65E-02	10	10719
178	1098	A	2	H	1	140	3.3	-76.98	76.33	1.31E-02	10	10719
178	1098	A	2	H	2	10	3.5	-72.62	50.62	1.93E-02	10	10722
178	1098	A	2	H	2	15	3.55	-72.39	39.77	2.23E-02	10	10722
178	1098	A	2	H	2	20	3.6	-74.82	55.45	2.11E-02	10	10722
178	1098	A	2	H	2	25	3.65	-76.3	47.88	1.93E-02	10	10722
178	1098	A	2	H	2	30	3.7	-70.31	57.26	1.75E-02	10	10722
178	1098	A	2	H	2	35	3.75	-71.19	72.43	1.69E-02	10	10722
178	1098	A	2	H	2	40	3.8	-70.31	229.76	1.85E-02	10	10722
178	1098	A	2	H	2	45	3.85	-73.1	295.56	3.10E-02	10	10722
178	1098	A	2	H	2	50	3.9	-40.25	41.04	2.66E-02	10	10722
178	1098	A	2	H	2	55	3.95	-79.44	121.05	1.06E-02	10	10722

Note: Only a portion of this table appears here. The complete table is available in ASCII format in the [TABLES](#) directory.

Table T7. Split-core paleomagnetic measurements for Hole 1098A after 20-mT demagnetization.

Leg	Site	Hole	Core	Type	Section	Interval (cm)	Depth (mbsf)	Inclination (°)	Declination (°)	Intensity (A/m)	Demagnetization step (mT)	Run #
178	1098	A	1	H	1	10	0.1	-66.5	81	4.49E-02	20	10714
178	1098	A	1	H	1	15	0.15	-73.45	72.23	3.36E-02	20	10714
178	1098	A	1	H	1	20	0.2	-72.85	53.71	1.66E-02	20	10714
178	1098	A	1	H	1	25	0.25	-82.9	55.76	8.40E-03	20	10714
178	1098	A	1	H	1	30	0.3	-77.37	9.36	6.10E-03	20	10714
178	1098	A	1	H	1	35	0.35	-65.66	346.29	6.28E-03	20	10714
178	1098	A	1	H	1	40	0.4	-68	349.74	8.15E-03	20	10714
178	1098	A	1	H	1	45	0.45	-84.1	299.4	1.28E-02	20	10714
178	1098	A	1	H	1	50	0.5	-69.72	154.54	3.07E-02	20	10714
178	1098	A	1	H	1	55	0.55	-70.68	117.88	4.67E-02	20	10714
178	1098	A	1	H	1	60	0.6	-68.38	90.33	5.19E-02	20	10714
178	1098	A	1	H	1	65	0.65	-70.34	95.57	5.62E-02	20	10714
178	1098	A	1	H	1	70	0.7	-65.38	155.18	6.04E-02	20	10714
178	1098	A	1	H	1	75	0.75	-71.14	174.38	5.98E-02	20	10714
178	1098	A	1	H	1	80	0.8	-80.09	94.62	5.34E-02	20	10714
178	1098	A	1	H	1	85	0.85	-75.69	111.01	6.04E-02	20	10714
178	1098	A	1	H	1	90	0.9	-73.37	115.31	6.82E-02	20	10714
178	1098	A	1	H	2	10	1.1	-76.28	107.51	9.04E-02	20	10717
178	1098	A	1	H	2	15	1.15	-80.83	58.28	6.56E-02	20	10717
178	1098	A	1	H	2	20	1.2	-78.45	117.44	6.28E-02	20	10717
178	1098	A	1	H	2	25	1.25	-73.85	120.48	8.52E-02	20	10717
178	1098	A	1	H	2	30	1.3	-76.15	99.32	8.66E-02	20	10717
178	1098	A	1	H	2	35	1.35	-75.44	106.85	7.43E-02	20	10717
178	1098	A	1	H	2	40	1.4	-78.13	78.8	5.64E-02	20	10717
178	1098	A	1	H	2	45	1.45	-79.79	67.32	4.56E-02	20	10717
178	1098	A	1	H	2	50	1.5	-77	81.84	3.90E-02	20	10717
178	1098	A	1	H	2	55	1.55	-78.55	116.93	3.16E-02	20	10717
178	1098	A	1	H	2	60	1.6	-80.13	90.97	3.25E-02	20	10717
178	1098	A	2	H	1	10	2	-46.91	0.5	6.30E-03	20	10720
178	1098	A	2	H	1	15	2.05	-78.47	290.92	4.80E-03	20	10720
178	1098	A	2	H	1	20	2.1	-77.09	37.48	5.97E-03	20	10720
178	1098	A	2	H	1	25	2.15	-44.99	356.2	9.64E-03	20	10720
178	1098	A	2	H	1	30	2.2	-32.82	5.87	1.06E-02	20	10720
178	1098	A	2	H	1	35	2.25	-27.95	8.04	1.08E-02	20	10720
178	1098	A	2	H	1	40	2.3	-22.07	354.23	9.08E-03	20	10720
178	1098	A	2	H	1	45	2.35	-23.81	342.63	6.47E-03	20	10720
178	1098	A	2	H	1	50	2.4	-24.93	345.3	5.26E-03	20	10720
178	1098	A	2	H	1	55	2.45	-34.94	0.46	2.90E-03	20	10720
178	1098	A	2	H	1	60	2.5	-48.91	34.12	4.16E-03	20	10720
178	1098	A	2	H	1	65	2.55	-53.28	16.91	5.70E-03	20	10720
178	1098	A	2	H	1	70	2.6	-86.41	201.29	6.05E-03	20	10720
178	1098	A	2	H	1	75	2.65	-79.98	151.22	9.62E-03	20	10720
178	1098	A	2	H	1	80	2.7	-83.05	98	1.17E-02	20	10720
178	1098	A	2	H	1	85	2.75	-78.6	45	1.14E-02	20	10720
178	1098	A	2	H	1	90	2.8	-80.54	75.25	9.35E-03	20	10720
178	1098	A	2	H	1	95	2.85	-77.49	57.55	9.78E-03	20	10720
178	1098	A	2	H	1	100	2.9	-81.94	42.22	8.08E-03	20	10720
178	1098	A	2	H	1	105	2.95	-75.43	148.73	7.53E-03	20	10720
178	1098	A	2	H	1	110	3	-81.47	72.31	7.21E-03	20	10720
178	1098	A	2	H	1	115	3.05	-71.16	153.72	5.95E-03	20	10720
178	1098	A	2	H	1	120	3.1	-60.5	162.78	6.47E-03	20	10720
178	1098	A	2	H	1	125	3.15	-82.39	39.17	7.85E-03	20	10720
178	1098	A	2	H	1	130	3.2	-70.96	12.83	1.25E-02	20	10720
178	1098	A	2	H	1	135	3.25	-70.62	28.81	1.22E-02	20	10720
178	1098	A	2	H	1	140	3.3	-78.49	86.23	9.72E-03	20	10720
178	1098	A	2	H	2	10	3.5	-75.12	61.01	1.33E-02	20	10723
178	1098	A	2	H	2	15	3.55	-75.65	48.9	1.54E-02	20	10723
178	1098	A	2	H	2	20	3.6	-77.41	65.07	1.46E-02	20	10723
178	1098	A	2	H	2	25	3.65	-78.08	60.81	1.34E-02	20	10723
178	1098	A	2	H	2	30	3.7	-69.57	67.71	1.24E-02	20	10723
178	1098	A	2	H	2	35	3.75	-71.76	81.12	1.20E-02	20	10723
178	1098	A	2	H	2	40	3.8	-64.2	226.54	1.42E-02	20	10723
178	1098	A	2	H	2	45	3.85	-72.03	291.21	2.42E-02	20	10723
178	1098	A	2	H	2	50	3.9	-38.55	41.93	2.08E-02	20	10723
178	1098	A	2	H	2	55	3.95	-77.79	132.67	7.60E-03	20	10723

Note: Only a portion of this table appears here. The complete table is available in ASCII format in the [TABLES](#) directory.

Table T8. Split-core paleomagnetic measurements for Hole 1098A after processing the results from the 20-mT demagnetization step by removing measurements from drilling-disturbed intervals and measurements made within 10 cm of the ends of each core section.

Leg	Site	Hole	Core	Type	Section	Interval (cm)	Depth (mbst)	Inclination (°)	Declination (°)	Intensity (A/m)	Demagnetization step (mT)	Run #
178	1098	A	1	H	1	35	0.35	-65.66	346.29	6.28E-03	20	10714
178	1098	A	1	H	1	40	0.4	-68	349.74	8.15E-03	20	10714
178	1098	A	1	H	1	45	0.45	-84.1	299.4	1.28E-02	20	10714
178	1098	A	1	H	1	50	0.5	-69.72	154.54	3.07E-02	20	10714
178	1098	A	1	H	1	55	0.55	-70.68	117.88	4.67E-02	20	10714
178	1098	A	1	H	1	60	0.6	-68.38	90.33	5.19E-02	20	10714
178	1098	A	1	H	1	65	0.65	-70.34	95.57	5.62E-02	20	10714
178	1098	A	1	H	1	70	0.7	-65.38	155.18	6.04E-02	20	10714
178	1098	A	1	H	1	75	0.75	-71.14	174.38	5.98E-02	20	10714
178	1098	A	1	H	1	80	0.8	-80.09	94.62	5.34E-02	20	10714
178	1098	A	1	H	1	85	0.85	-75.69	111.01	6.04E-02	20	10714
178	1098	A	1	H	1	90	0.9	-73.37	115.31	6.82E-02	20	10714
178	1098	A	1	H	2	10	1.1	-76.28	107.51	9.04E-02	20	10717
178	1098	A	1	H	2	15	1.15	-80.83	58.28	6.56E-02	20	10717
178	1098	A	1	H	2	20	1.2	-78.45	117.44	6.28E-02	20	10717
178	1098	A	1	H	2	25	1.25	-73.85	120.48	8.52E-02	20	10717
178	1098	A	1	H	2	30	1.3	-76.15	99.32	8.66E-02	20	10717
178	1098	A	1	H	2	35	1.35	-75.44	106.85	7.43E-02	20	10717
178	1098	A	1	H	2	40	1.4	-78.13	78.8	5.64E-02	20	10717
178	1098	A	1	H	2	45	1.45	-79.79	67.32	4.56E-02	20	10717
178	1098	A	1	H	2	50	1.5	-77	81.84	3.90E-02	20	10717
178	1098	A	1	H	2	55	1.55	-78.55	116.93	3.16E-02	20	10717
178	1098	A	1	H	2	60	1.6	-80.13	90.97	3.25E-02	20	10717
178	1098	A	2	H	1	65	2.55	-53.28	16.91	5.70E-03	20	10720
178	1098	A	2	H	1	70	2.6	-86.41	201.29	6.05E-03	20	10720
178	1098	A	2	H	1	75	2.65	-79.98	151.22	9.62E-03	20	10720
178	1098	A	2	H	1	80	2.7	-83.05	98	1.17E-02	20	10720
178	1098	A	2	H	1	85	2.75	-78.6	45	1.14E-02	20	10720
178	1098	A	2	H	1	90	2.8	-80.54	75.25	9.35E-03	20	10720
178	1098	A	2	H	1	95	2.85	-77.49	57.55	9.78E-03	20	10720
178	1098	A	2	H	1	100	2.9	-81.94	42.22	8.08E-03	20	10720
178	1098	A	2	H	1	105	2.95	-75.43	148.73	7.53E-03	20	10720
178	1098	A	2	H	1	110	3	-81.47	72.31	7.21E-03	20	10720
178	1098	A	2	H	1	115	3.05	-71.16	153.72	5.95E-03	20	10720
178	1098	A	2	H	1	120	3.1	-60.5	162.78	6.47E-03	20	10720
178	1098	A	2	H	1	125	3.15	-82.39	39.17	7.85E-03	20	10720
178	1098	A	2	H	1	130	3.2	-70.96	12.83	1.25E-02	20	10720
178	1098	A	2	H	1	135	3.25	-70.62	28.81	1.22E-02	20	10720
178	1098	A	2	H	1	140	3.3	-78.49	86.23	9.72E-03	20	10720
178	1098	A	2	H	2	10	3.5	-75.12	61.01	1.33E-02	20	10723
178	1098	A	2	H	2	15	3.55	-75.65	48.9	1.54E-02	20	10723
178	1098	A	2	H	2	20	3.6	-77.41	65.07	1.46E-02	20	10723
178	1098	A	2	H	2	25	3.65	-78.08	60.81	1.34E-02	20	10723
178	1098	A	2	H	2	30	3.7	-69.57	67.71	1.24E-02	20	10723
178	1098	A	2	H	2	35	3.75	-71.76	81.12	1.20E-02	20	10723
178	1098	A	2	H	2	40	3.8	-64.2	226.54	1.42E-02	20	10723
178	1098	A	2	H	2	45	3.85	-72.03	291.21	2.42E-02	20	10723
178	1098	A	2	H	2	50	3.9	-38.55	41.93	2.08E-02	20	10723
178	1098	A	2	H	2	55	3.95	-77.79	132.67	7.60E-03	20	10723
178	1098	A	2	H	2	60	4	-72.87	154.93	7.28E-03	20	10723
178	1098	A	2	H	2	65	4.05	-77.17	75.24	9.41E-03	20	10723
178	1098	A	2	H	2	70	4.1	-75.92	26.02	1.10E-02	20	10723
178	1098	A	2	H	2	75	4.15	-81.11	25.74	1.05E-02	20	10723
178	1098	A	2	H	2	80	4.2	-79.28	26.09	1.05E-02	20	10723
178	1098	A	2	H	2	85	4.25	-81.65	37.51	1.15E-02	20	10723
178	1098	A	2	H	2	90	4.3	-79.77	48.59	1.36E-02	20	10723
178	1098	A	2	H	2	95	4.35	-76.87	27.02	1.31E-02	20	10723
178	1098	A	2	H	2	100	4.4	-76.83	104.38	1.12E-02	20	10723
178	1098	A	2	H	2	105	4.45	-78.73	80.61	1.25E-02	20	10723
178	1098	A	2	H	2	110	4.5	-70	19.24	1.26E-02	20	10723
178	1098	A	2	H	2	115	4.55	-78.38	74.04	8.67E-03	20	10723
178	1098	A	2	H	2	120	4.6	-66.59	155.62	8.47E-03	20	10723
178	1098	A	2	H	2	125	4.65	-67.5	156.21	9.81E-03	20	10723

Note: Only a portion of this table appears here. The complete table is available in ASCII format in the [TABLES](#) directory.

Table T9. Split-core paleomagnetic measurements for Hole 1098B before demagnetization (NRM results).

Leg	Site	Hole	Core	Type	Section	Interval (cm)	Depth (mbsf)	Inclination (°)	Declination (°)	Intensity (A/m)	Demagnetization step (mT)	Run #
178	1098	B	1	H	1	10	0.1	-1.79	21.14	8.57E-02	0	10808
178	1098	B	1	H	1	15	0.15	10.5	23.2	2.59E-02	0	10808
178	1098	B	1	H	1	20	0.2	31.35	15.63	1.27E-02	0	10808
178	1098	B	1	H	1	25	0.25	32.73	19.64	1.43E-02	0	10808
178	1098	B	1	H	1	30	0.3	67.01	41.28	8.53E-03	0	10808
178	1098	B	1	H	1	35	0.35	53.95	9.59	7.94E-03	0	10808
178	1098	B	1	H	1	40	0.4	-2.22	5.69	3.74E-02	0	10808
178	1098	B	1	H	1	45	0.45	-6.1	16.43	1.08E-01	0	10808
178	1098	B	1	H	1	50	0.5	-6.04	24.12	1.26E-01	0	10808
178	1098	B	1	H	1	55	0.55	-4.93	28.97	1.31E-01	0	10808
178	1098	B	1	H	1	60	0.6	2.46	31.88	1.15E-01	0	10808
178	1098	B	1	H	1	65	0.65	9.23	22.69	7.92E-02	0	10808
178	1098	B	1	H	1	70	0.7	9.56	14.36	8.09E-02	0	10808
178	1098	B	1	H	1	75	0.75	0.79	19.83	9.67E-02	0	10808
178	1098	B	1	H	1	80	0.8	-8.72	20.93	1.03E-01	0	10808
178	1098	B	1	H	1	85	0.85	-17	32.27	9.47E-02	0	10808
178	1098	B	1	H	1	90	0.9	-22.15	40.13	9.45E-02	0	10808
178	1098	B	1	H	1	95	0.95	-17.21	35.72	1.14E-01	0	10808
178	1098	B	1	H	1	100	1	-13.21	23.52	8.76E-02	0	10808
178	1098	B	1	H	1	105	1.05	-17.92	19.93	9.33E-02	0	10808
178	1098	B	1	H	1	110	1.1	-18.34	24.5	1.10E-01	0	10808
178	1098	B	1	H	1	115	1.15	-19.44	26.21	1.04E-01	0	10808
178	1098	B	1	H	1	120	1.2	-18.92	25.93	8.74E-02	0	10808
178	1098	B	1	H	1	125	1.25	-18.73	25.32	4.64E-02	0	10808
178	1098	B	1	H	1	130	1.3	-16.34	31.62	6.67E-02	0	10808
178	1098	B	1	H	1	135	1.35	-5.91	24.42	9.76E-02	0	10808
178	1098	B	1	H	1	140	1.4	5.24	19.08	5.75E-02	0	10808
178	1098	B	1	H	2	10	1.6	-7.48	16.42	8.17E-02	0	10811
178	1098	B	1	H	2	15	1.65	2.64	14.57	5.51E-02	0	10811
178	1098	B	1	H	2	20	1.7	27.36	33.24	2.15E-02	0	10811
178	1098	B	1	H	2	25	1.75	24.87	55.87	1.72E-02	0	10811
178	1098	B	1	H	2	30	1.8	18.49	16.77	3.04E-02	0	10811
178	1098	B	1	H	2	35	1.85	21	17.92	2.88E-02	0	10811
178	1098	B	1	H	2	40	1.9	24.31	28.72	2.47E-02	0	10811
178	1098	B	1	H	2	45	1.95	31.18	25.65	2.59E-02	0	10811
178	1098	B	1	H	2	50	2	44.99	32.26	2.09E-02	0	10811
178	1098	B	1	H	2	55	2.05	43.64	74.15	1.15E-02	0	10811
178	1098	B	1	H	2	60	2.1	35.53	84.33	9.57E-03	0	10811
178	1098	B	1	H	2	65	2.15	26.56	48.31	1.12E-02	0	10811
178	1098	B	1	H	2	70	2.2	45.9	27.31	1.48E-02	0	10811
178	1098	B	1	H	2	75	2.25	27.47	17.38	1.40E-02	0	10811
178	1098	B	1	H	2	80	2.3	20.66	7.49	3.66E-02	0	10811
178	1098	B	1	H	2	85	2.35	27.52	11.2	4.60E-02	0	10811
178	1098	B	1	H	2	90	2.4	40.84	24.14	3.49E-02	0	10811
178	1098	B	1	H	2	95	2.45	59.15	45.21	1.46E-02	0	10811
178	1098	B	1	H	2	100	2.5	59.19	20.37	6.80E-03	0	10811
178	1098	B	1	H	2	105	2.55	24.83	9.4	1.66E-02	0	10811
178	1098	B	1	H	2	110	2.6	32.22	2.52	3.17E-02	0	10811
178	1098	B	1	H	2	115	2.65	37.65	14.01	3.86E-02	0	10811
178	1098	B	1	H	2	120	2.7	52.04	44.67	2.83E-02	0	10811
178	1098	B	1	H	2	125	2.75	62.66	24.55	1.43E-02	0	10811
178	1098	B	1	H	2	130	2.8	68.74	303.87	6.10E-03	0	10811
178	1098	B	1	H	2	135	2.85	16.57	46.26	2.29E-03	0	10811
178	1098	B	1	H	2	140	2.9	2.71	19.89	3.43E-03	0	10811
178	1098	B	1	H	3	10	3.1	16.3	25.02	1.30E-02	0	10814
178	1098	B	1	H	3	15	3.15	29.46	23.36	3.70E-02	0	10814
178	1098	B	1	H	3	20	3.2	42.4	26.39	5.09E-02	0	10814
178	1098	B	1	H	3	25	3.25	66.81	29.77	3.73E-02	0	10814
178	1098	B	1	H	3	30	3.3	73.98	4.83	2.30E-02	0	10814
178	1098	B	1	H	3	35	3.35	44.03	26.97	3.30E-02	0	10814
178	1098	B	1	H	3	40	3.4	39.38	31.49	3.89E-02	0	10814
178	1098	B	1	H	3	45	3.45	38.16	22.14	3.52E-02	0	10814
178	1098	B	1	H	3	50	3.5	45.04	18.98	3.26E-02	0	10814
178	1098	B	1	H	3	55	3.55	55.09	27.28	1.94E-02	0	10814
178	1098	B	1	H	3	60	3.6	32.3	37.35	1.60E-02	0	10814

Note: Only a portion of this table appears here. The complete table is available in ASCII format in the [TABLES](#) directory.

Table T10. Split-core paleomagnetic measurements for Hole 1098B after 10-mT demagnetization.

Leg	Site	Hole	Core	Type	Section	Interval (cm)	Depth (mbsf)	Inclination (°)	Declination (°)	Intensity (A/m)	Demagnetization step (mT)	Run #
178	1098	B	1	H	1	10	0.1	-24.47	42.33	3.74E-02	10	10809
178	1098	B	1	H	1	15	0.15	-36.74	43.57	1.27E-02	10	10809
178	1098	B	1	H	1	20	0.2	-41.5	32.77	5.85E-03	10	10809
178	1098	B	1	H	1	25	0.25	-33.93	34.42	5.00E-03	10	10809
178	1098	B	1	H	1	30	0.3	-52.03	58	2.68E-03	10	10809
178	1098	B	1	H	1	35	0.35	-54.84	348.72	4.34E-03	10	10809
178	1098	B	1	H	1	40	0.4	-47.52	18.35	1.94E-02	10	10809
178	1098	B	1	H	1	45	0.45	-40.99	39.78	5.35E-02	10	10809
178	1098	B	1	H	1	50	0.5	-42.44	46.19	7.14E-02	10	10809
178	1098	B	1	H	1	55	0.55	-39.21	49.68	7.95E-02	10	10809
178	1098	B	1	H	1	60	0.6	-33.38	47.47	7.06E-02	10	10809
178	1098	B	1	H	1	65	0.65	-33.31	39.97	4.12E-02	10	10809
178	1098	B	1	H	1	70	0.7	-37.63	28.18	3.20E-02	10	10809
178	1098	B	1	H	1	75	0.75	-44.43	46.57	4.81E-02	10	10809
178	1098	B	1	H	1	80	0.8	-59.85	51.68	6.75E-02	10	10809
178	1098	B	1	H	1	85	0.85	-63.26	60.01	8.70E-02	10	10809
178	1098	B	1	H	1	90	0.9	-59.98	65.81	9.37E-02	10	10809
178	1098	B	1	H	1	95	0.95	-56.65	53.42	9.10E-02	10	10809
178	1098	B	1	H	1	100	1	-58.97	37.82	6.98E-02	10	10809
178	1098	B	1	H	1	105	1.05	-61.14	39.51	6.97E-02	10	10809
178	1098	B	1	H	1	110	1.1	-58.4	46.94	8.27E-02	10	10809
178	1098	B	1	H	1	115	1.15	-62.16	45.92	8.60E-02	10	10809
178	1098	B	1	H	1	120	1.2	-63.64	38.34	8.13E-02	10	10809
178	1098	B	1	H	1	125	1.25	-67.23	28.62	5.80E-02	10	10809
178	1098	B	1	H	1	130	1.3	-64	62.96	6.03E-02	10	10809
178	1098	B	1	H	1	135	1.35	-53.32	37.02	7.27E-02	10	10809
178	1098	B	1	H	1	140	1.4	-54.91	26.56	4.57E-02	10	10809
178	1098	B	1	H	2	10	1.6	-66.83	34.01	7.43E-02	10	10812
178	1098	B	1	H	2	15	1.65	-66.96	19.43	6.08E-02	10	10812
178	1098	B	1	H	2	20	1.7	-73.43	17.91	3.64E-02	10	10812
178	1098	B	1	H	2	25	1.75	-75.65	112.35	2.85E-02	10	10812
178	1098	B	1	H	2	30	1.8	-75.77	77.8	3.48E-02	10	10812
178	1098	B	1	H	2	35	1.85	-70.99	39.87	3.36E-02	10	10812
178	1098	B	1	H	2	40	1.9	-78.23	67.5	2.98E-02	10	10812
178	1098	B	1	H	2	45	1.95	-74.79	70.16	2.75E-02	10	10812
178	1098	B	1	H	2	50	2	-71.76	53.21	2.14E-02	10	10812
178	1098	B	1	H	2	55	2.05	-66.97	95.07	1.56E-02	10	10812
178	1098	B	1	H	2	60	2.1	-64.14	125.26	1.48E-02	10	10812
178	1098	B	1	H	2	65	2.15	-71.78	126.62	1.65E-02	10	10812
178	1098	B	1	H	2	70	2.2	-77.57	84.01	1.84E-02	10	10812
178	1098	B	1	H	2	75	2.25	-83.76	128.24	2.23E-02	10	10812
178	1098	B	1	H	2	80	2.3	-83.07	13.37	3.00E-02	10	10812
178	1098	B	1	H	2	85	2.35	-74.82	24.46	3.40E-02	10	10812
178	1098	B	1	H	2	90	2.4	-75.77	58.51	3.04E-02	10	10812
178	1098	B	1	H	2	95	2.45	-81.74	107.88	2.56E-02	10	10812
178	1098	B	1	H	2	100	2.5	-86.7	94.29	2.04E-02	10	10812
178	1098	B	1	H	2	105	2.55	-84.2	11.54	1.90E-02	10	10812
178	1098	B	1	H	2	110	2.6	-83.68	338.14	2.15E-02	10	10812
178	1098	B	1	H	2	115	2.65	-76.82	30.76	2.60E-02	10	10812
178	1098	B	1	H	2	120	2.7	-71.85	62.3	2.44E-02	10	10812
178	1098	B	1	H	2	125	2.75	-81.22	91.38	1.95E-02	10	10812
178	1098	B	1	H	2	130	2.8	-81.85	244.47	1.55E-02	10	10812
178	1098	B	1	H	2	135	2.85	-84.68	110.06	1.19E-02	10	10812
178	1098	B	1	H	2	140	2.9	-84.98	58.91	8.88E-03	10	10812
178	1098	B	1	H	3	10	3.1	-81.5	97.05	2.08E-02	10	10815
178	1098	B	1	H	3	15	3.15	-79.08	59.71	3.34E-02	10	10815
178	1098	B	1	H	3	20	3.2	-70.59	47.26	3.84E-02	10	10815
178	1098	B	1	H	3	25	3.25	-71.31	33.43	2.84E-02	10	10815
178	1098	B	1	H	3	30	3.3	-83.4	60.03	1.99E-02	10	10815
178	1098	B	1	H	3	35	3.35	-72.79	77.85	2.61E-02	10	10815
178	1098	B	1	H	3	40	3.4	-66.2	49.99	3.21E-02	10	10815
178	1098	B	1	H	3	45	3.45	-70.68	37.48	3.03E-02	10	10815
178	1098	B	1	H	3	50	3.5	-72.79	25.61	2.84E-02	10	10815
178	1098	B	1	H	3	55	3.55	-73.24	36.96	2.34E-02	10	10815
178	1098	B	1	H	3	60	3.6	-74.32	83.05	2.28E-02	10	10815

Note: Only a portion of this table appears here. The complete table is available in ASCII format in the [TABLES](#) directory.

Table T11. Split-core paleomagnetic measurements for Hole 1098B after 20-mT demagnetization.

Leg	Site	Hole	Core	Type	Section	Interval (cm)	Depth (mbsf)	Inclination (°)	Declination (°)	Intensity (A/m)	Demagnetization step (mT)	Run #
178	1098	B	1	H	1	10	0.1	-20.96	56.65	1.93E-02	20	10810
178	1098	B	1	H	1	15	0.15	-31.13	61.24	6.10E-03	20	10810
178	1098	B	1	H	1	20	0.2	-33.75	43.15	2.68E-03	20	10810
178	1098	B	1	H	1	25	0.25	-27.18	46.59	2.51E-03	20	10810
178	1098	B	1	H	1	30	0.3	-24.48	58.79	1.47E-03	20	10810
178	1098	B	1	H	1	35	0.35	-40.8	345.9	1.84E-03	20	10810
178	1098	B	1	H	1	40	0.4	-49.95	29.96	1.04E-02	20	10810
178	1098	B	1	H	1	45	0.45	-44.17	53.54	3.12E-02	20	10810
178	1098	B	1	H	1	50	0.5	-45.84	56.58	4.43E-02	20	10810
178	1098	B	1	H	1	55	0.55	-42.32	57.43	5.06E-02	20	10810
178	1098	B	1	H	1	60	0.6	-37.05	53.69	4.54E-02	20	10810
178	1098	B	1	H	1	65	0.65	-38.01	47.34	2.50E-02	20	10810
178	1098	B	1	H	1	70	0.7	-45.66	38.05	1.80E-02	20	10810
178	1098	B	1	H	1	75	0.75	-49	59.96	3.07E-02	20	10810
178	1098	B	1	H	1	80	0.8	-64.53	68.15	4.63E-02	20	10810
178	1098	B	1	H	1	85	0.85	-66.7	70.57	6.21E-02	20	10810
178	1098	B	1	H	1	90	0.9	-62.81	73.76	6.62E-02	20	10810
178	1098	B	1	H	1	95	0.95	-59.99	60.94	6.20E-02	20	10810
178	1098	B	1	H	1	100	1	-63.46	44.59	4.58E-02	20	10810
178	1098	B	1	H	1	105	1.05	-66.13	49.72	4.48E-02	20	10810
178	1098	B	1	H	1	110	1.1	-62.01	57.91	5.36E-02	20	10810
178	1098	B	1	H	1	115	1.15	-66	55.15	5.57E-02	20	10810
178	1098	B	1	H	1	120	1.2	-67.39	43.81	5.26E-02	20	10810
178	1098	B	1	H	1	125	1.25	-70.22	30.71	3.74E-02	20	10810
178	1098	B	1	H	1	130	1.3	-66.1	74.83	3.86E-02	20	10810
178	1098	B	1	H	1	135	1.35	-58.25	43.32	4.53E-02	20	10810
178	1098	B	1	H	1	140	1.4	-59.88	30.07	2.81E-02	20	10810
178	1098	B	1	H	2	10	1.6	-70.58	46.4	4.75E-02	20	10813
178	1098	B	1	H	2	15	1.65	-70.13	24.01	3.95E-02	20	10813
178	1098	B	1	H	2	20	1.7	-75.48	20.21	2.37E-02	20	10813
178	1098	B	1	H	2	25	1.75	-74.7	118.03	1.88E-02	20	10813
178	1098	B	1	H	2	30	1.8	-75.14	89.02	2.31E-02	20	10813
178	1098	B	1	H	2	35	1.85	-72.41	49.97	2.19E-02	20	10813
178	1098	B	1	H	2	40	1.9	-78.57	82.36	1.96E-02	20	10813
178	1098	B	1	H	2	45	1.95	-74.68	83.29	1.82E-02	20	10813
178	1098	B	1	H	2	50	2	-72.67	63.86	1.43E-02	20	10813
178	1098	B	1	H	2	55	2.05	-65.94	101.71	1.05E-02	20	10813
178	1098	B	1	H	2	60	2.1	-62.69	127.6	1.02E-02	20	10813
178	1098	B	1	H	2	65	2.15	-70.69	128.24	1.12E-02	20	10813
178	1098	B	1	H	2	70	2.2	-76.92	92.1	1.22E-02	20	10813
178	1098	B	1	H	2	75	2.25	-81.63	137.51	1.45E-02	20	10813
178	1098	B	1	H	2	80	2.3	-86.61	50.13	1.92E-02	20	10813
178	1098	B	1	H	2	85	2.35	-77.9	42	2.17E-02	20	10813
178	1098	B	1	H	2	90	2.4	-76.33	80.62	1.96E-02	20	10813
178	1098	B	1	H	2	95	2.45	-79.81	122.52	1.66E-02	20	10813
178	1098	B	1	H	2	100	2.5	-84.36	104.79	1.31E-02	20	10813
178	1098	B	1	H	2	105	2.55	-84.75	27.79	1.17E-02	20	10813
178	1098	B	1	H	2	110	2.6	-88.08	299.99	1.33E-02	20	10813
178	1098	B	1	H	2	115	2.65	-79.83	50.85	1.68E-02	20	10813
178	1098	B	1	H	2	120	2.7	-72.38	71.64	1.64E-02	20	10813
178	1098	B	1	H	2	125	2.75	-80.38	102.74	1.34E-02	20	10813
178	1098	B	1	H	2	130	2.8	-81.13	236.18	1.08E-02	20	10813
178	1098	B	1	H	2	135	2.85	-83.67	120.37	8.52E-03	20	10813
178	1098	B	1	H	2	140	2.9	-85.1	73.21	6.35E-03	20	10813
178	1098	B	1	H	3	10	3.1	-80.88	104.53	1.47E-02	20	10816
178	1098	B	1	H	3	15	3.15	-80.37	68.98	2.34E-02	20	10816
178	1098	B	1	H	3	20	3.2	-72.81	51.63	2.68E-02	20	10816
178	1098	B	1	H	3	25	3.25	-73.24	36.02	2.00E-02	20	10816
178	1098	B	1	H	3	30	3.3	-83.75	72.44	1.39E-02	20	10816
178	1098	B	1	H	3	35	3.35	-73.42	85.46	1.80E-02	20	10816
178	1098	B	1	H	3	40	3.4	-68.01	55.07	2.19E-02	20	10816
178	1098	B	1	H	3	45	3.45	-73.05	42.33	2.07E-02	20	10816
178	1098	B	1	H	3	50	3.5	-75.47	29.08	1.97E-02	20	10816
178	1098	B	1	H	3	55	3.55	-74.94	42.5	1.65E-02	20	10816
178	1098	B	1	H	3	60	3.6	-74.29	90.55	1.63E-02	20	10816

Note: Only a portion of this table appears here. The complete table is available in ASCII format in the [TABLES](#) directory.

Table T12. Split-core paleomagnetic measurements for Hole 1098B after processing the results from the 20-mT demagnetization step by removing measurements from drilling-disturbed intervals and measurements made within 10 cm of the ends of each core section.

Leg	Site	Hole	Core	Type	Section	Interval (cm)	Depth (mbst)	Inclination (°)	Declination (°)	Intensity (A/m)	Demagnetization step (mT)	Run #
178	1098	B	1	H	1	45	0.45	-44.17	53.54	3.12E-02	20	10810
178	1098	B	1	H	1	50	0.5	-45.84	56.58	4.43E-02	20	10810
178	1098	B	1	H	1	55	0.55	-42.32	57.43	5.06E-02	20	10810
178	1098	B	1	H	1	60	0.6	-37.05	53.69	4.54E-02	20	10810
178	1098	B	1	H	1	65	0.65	-38.01	47.34	2.50E-02	20	10810
178	1098	B	1	H	1	70	0.7	-45.66	38.05	1.80E-02	20	10810
178	1098	B	1	H	1	75	0.75	-49	59.96	3.07E-02	20	10810
178	1098	B	1	H	1	80	0.8	-64.53	68.15	4.63E-02	20	10810
178	1098	B	1	H	1	85	0.85	-66.7	70.57	6.21E-02	20	10810
178	1098	B	1	H	1	90	0.9	-62.81	73.76	6.62E-02	20	10810
178	1098	B	1	H	1	95	0.95	-59.99	60.94	6.20E-02	20	10810
178	1098	B	1	H	1	100	1	-63.46	44.59	4.58E-02	20	10810
178	1098	B	1	H	1	105	1.05	-66.13	49.72	4.48E-02	20	10810
178	1098	B	1	H	1	110	1.1	-62.01	57.91	5.36E-02	20	10810
178	1098	B	1	H	1	115	1.15	-66	55.15	5.57E-02	20	10810
178	1098	B	1	H	1	120	1.2	-67.39	43.81	5.26E-02	20	10810
178	1098	B	1	H	1	125	1.25	-70.22	30.71	3.74E-02	20	10810
178	1098	B	1	H	1	130	1.3	-66.1	74.83	3.86E-02	20	10810
178	1098	B	1	H	1	135	1.35	-58.25	43.32	4.53E-02	20	10810
178	1098	B	1	H	1	140	1.4	-59.88	30.07	2.81E-02	20	10810
178	1098	B	1	H	2	10	1.6	-70.58	46.4	4.75E-02	20	10813
178	1098	B	1	H	2	15	1.65	-70.13	24.01	3.95E-02	20	10813
178	1098	B	1	H	2	20	1.7	-75.48	20.21	2.37E-02	20	10813
178	1098	B	1	H	2	25	1.75	-74.7	118.03	1.88E-02	20	10813
178	1098	B	1	H	2	30	1.8	-75.14	89.02	2.31E-02	20	10813
178	1098	B	1	H	2	35	1.85	-72.41	49.97	2.19E-02	20	10813
178	1098	B	1	H	2	40	1.9	-78.57	82.36	1.96E-02	20	10813
178	1098	B	1	H	2	45	1.95	-74.68	83.29	1.82E-02	20	10813
178	1098	B	1	H	2	50	2	-72.67	63.86	1.43E-02	20	10813
178	1098	B	1	H	2	55	2.05	-65.94	101.71	1.05E-02	20	10813
178	1098	B	1	H	2	60	2.1	-62.69	127.6	1.02E-02	20	10813
178	1098	B	1	H	2	65	2.15	-70.69	128.24	1.12E-02	20	10813
178	1098	B	1	H	2	70	2.2	-76.92	92.1	1.23E-02	20	10813
178	1098	B	1	H	2	75	2.25	-81.63	137.51	1.45E-02	20	10813
178	1098	B	1	H	2	80	2.3	-86.61	50.13	1.92E-02	20	10813
178	1098	B	1	H	2	85	2.35	-77.9	42	2.17E-02	20	10813
178	1098	B	1	H	2	90	2.4	-76.33	80.62	1.96E-02	20	10813
178	1098	B	1	H	2	95	2.45	-79.81	122.52	1.66E-02	20	10813
178	1098	B	1	H	2	100	2.5	-84.36	104.79	1.31E-02	20	10813
178	1098	B	1	H	2	105	2.55	-84.75	27.79	1.17E-02	20	10813
178	1098	B	1	H	2	110	2.6	-88.08	299.99	1.33E-02	20	10813
178	1098	B	1	H	2	115	2.65	-79.83	50.85	1.68E-02	20	10813
178	1098	B	1	H	2	120	2.7	-72.38	71.64	1.64E-02	20	10813
178	1098	B	1	H	2	125	2.75	-80.38	102.74	1.34E-02	20	10813
178	1098	B	1	H	2	130	2.8	-81.13	236.18	1.08E-02	20	10813
178	1098	B	1	H	2	135	2.85	-83.67	120.37	8.52E-03	20	10813
178	1098	B	1	H	2	140	2.9	-85.1	73.21	6.35E-03	20	10813
178	1098	B	1	H	3	10	3.1	-80.88	104.53	1.47E-02	20	10816
178	1098	B	1	H	3	15	3.15	-80.37	68.98	2.34E-02	20	10816
178	1098	B	1	H	3	20	3.2	-72.81	51.63	2.68E-02	20	10816
178	1098	B	1	H	3	25	3.25	-73.24	36.02	2.00E-02	20	10816
178	1098	B	1	H	3	30	3.3	-83.75	72.44	1.39E-02	20	10816
178	1098	B	1	H	3	35	3.35	-73.42	85.46	1.80E-02	20	10816
178	1098	B	1	H	3	40	3.4	-68.01	55.07	2.19E-02	20	10816
178	1098	B	1	H	3	45	3.45	-73.05	42.33	2.07E-02	20	10816
178	1098	B	1	H	3	50	3.5	-75.47	29.08	1.97E-02	20	10816
178	1098	B	1	H	3	55	3.55	-74.94	42.5	1.65E-02	20	10816
178	1098	B	1	H	3	60	3.6	-74.29	90.55	1.63E-02	20	10816
178	1098	B	1	H	3	65	3.65	-76.91	87.71	1.58E-02	20	10816
178	1098	B	1	H	3	70	3.7	-74.97	73.59	1.40E-02	20	10816
178	1098	B	1	H	3	75	3.75	-68.22	20.26	1.23E-02	20	10816
178	1098	B	1	H	3	80	3.8	-71.93	10.29	9.01E-03	20	10816
178	1098	B	1	H	3	85	3.85	-80.98	44.42	8.14E-03	20	10816

Note: Only a portion of this table appears here. The complete table is available in ASCII format in the [TABLES](#) directory.

Table T13. Split-core paleomagnetic measurements for Hole 1098C before demagnetization (NRM results).

Leg	Site	Hole	Core	Type	Section	Interval (cm)	Depth (mbsf)	Inclination (°)	Declination (°)	Intensity (A/m)	Demagnetization step (mT)	Run #
178	1098	C	1	H	1	10	0.1	4.85	26.04	4.32E-02	0	10904
178	1098	C	1	H	1	15	0.15	17.41	29.26	2.89E-02	0	10904
178	1098	C	1	H	1	20	0.2	44.93	20.8	1.69E-02	0	10904
178	1098	C	1	H	1	25	0.25	56.36	17.86	1.92E-02	0	10904
178	1098	C	1	H	1	30	0.3	73.02	7.17	1.62E-02	0	10904
178	1098	C	1	H	1	35	0.35	78.69	15.27	1.29E-02	0	10904
178	1098	C	1	H	1	40	0.4	58.3	8.87	1.56E-02	0	10904
178	1098	C	1	H	1	45	0.45	7.65	10.56	5.57E-02	0	10904
178	1098	C	1	H	1	50	0.5	2.93	2.21	8.73E-02	0	10904
178	1098	C	1	H	1	55	0.55	-4.54	345.9	8.84E-02	0	10904
178	1098	C	1	H	1	60	0.6	-8.43	337.91	8.30E-02	0	10904
178	1098	C	1	H	1	65	0.65	-10.92	341.88	7.03E-02	0	10904
178	1098	C	1	H	1	70	0.7	-14.21	343.67	5.08E-02	0	10904
178	1098	C	1	H	1	75	0.75	-17.32	347.66	7.12E-02	0	10904
178	1098	C	1	H	1	80	0.8	-13.4	348.68	8.79E-02	0	10904
178	1098	C	1	H	1	85	0.85	-16.46	347.02	9.11E-02	0	10904
178	1098	C	1	H	1	90	0.9	-21.61	338.09	1.03E-01	0	10904
178	1098	C	1	H	1	95	0.95	-25.02	330.92	1.00E-01	0	10904
178	1098	C	1	H	1	100	1	-25.92	335.17	8.98E-02	0	10904
178	1098	C	1	H	1	105	1.05	-14.57	331.91	7.10E-02	0	10904
178	1098	C	1	H	1	110	1.1	10.21	325.61	2.84E-02	0	10904
178	1098	C	1	H	1	115	1.15	-5.61	347.39	3.96E-02	0	10904
178	1098	C	1	H	1	120	1.2	-7.22	347.13	8.75E-02	0	10904
178	1098	C	1	H	1	125	1.25	-8.58	346.79	9.38E-02	0	10904
178	1098	C	1	H	1	130	1.3	-8.48	343.32	7.14E-02	0	10904
178	1098	C	1	H	1	135	1.35	1.06	332.58	5.56E-02	0	10904
178	1098	C	1	H	2	10	1.6	1.22	327.08	6.38E-02	0	10907
178	1098	C	1	H	2	15	1.65	5.18	329.2	6.38E-02	0	10907
178	1098	C	1	H	2	20	1.7	12	336.38	5.50E-02	0	10907
178	1098	C	1	H	2	25	1.75	22.2	334.74	5.49E-02	0	10907
178	1098	C	1	H	2	30	1.8	49.65	317.47	4.02E-02	0	10907
178	1098	C	1	H	2	35	1.85	65.7	318.71	2.84E-02	0	10907
178	1098	C	1	H	2	40	1.9	57.32	340.06	3.17E-02	0	10907
178	1098	C	1	H	2	45	1.95	57.96	345.08	3.86E-02	0	10907
178	1098	C	1	H	2	50	2	64.54	339.83	3.81E-02	0	10907
178	1098	C	1	H	2	55	2.05	58.52	340.14	3.82E-02	0	10907
178	1098	C	1	H	2	60	2.1	57.24	349.06	3.43E-02	0	10907
178	1098	C	1	H	2	65	2.15	70.73	338.06	2.65E-02	0	10907
178	1098	C	1	H	2	70	2.2	64.76	301.52	1.68E-02	0	10907
178	1098	C	1	H	2	75	2.25	57.46	315.01	1.46E-02	0	10907
178	1098	C	1	H	2	80	2.3	51.81	324.89	1.82E-02	0	10907
178	1098	C	1	H	2	85	2.35	50.69	340.99	2.96E-02	0	10907
178	1098	C	1	H	2	90	2.4	66.85	329.67	3.08E-02	0	10907
178	1098	C	1	H	2	95	2.45	56.63	330.84	3.58E-02	0	10907
178	1098	C	1	H	2	100	2.5	52.29	333.31	4.55E-02	0	10907
178	1098	C	1	H	2	105	2.55	53.43	333.35	5.08E-02	0	10907
178	1098	C	1	H	2	110	2.6	60.83	327.63	4.68E-02	0	10907
178	1098	C	1	H	2	115	2.65	63.69	326.93	3.86E-02	0	10907
178	1098	C	1	H	2	120	2.7	60.61	322.98	3.20E-02	0	10907
178	1098	C	1	H	2	125	2.75	50.82	340.19	3.78E-02	0	10907
178	1098	C	1	H	2	130	2.8	51.53	346.22	4.63E-02	0	10907
178	1098	C	1	H	3	10	3.1	71.73	327.12	1.60E-02	0	10910
178	1098	C	1	H	3	15	3.15	58.47	322.66	2.16E-02	0	10910
178	1098	C	1	H	3	20	3.2	60.33	301.8	2.80E-02	0	10910
178	1098	C	1	H	3	25	3.25	68.1	305.91	3.18E-02	0	10910
178	1098	C	1	H	3	30	3.3	72.81	334.71	4.05E-02	0	10910
178	1098	C	1	H	3	35	3.35	65.33	332.02	5.62E-02	0	10910
178	1098	C	1	H	3	40	3.4	68.74	311.01	6.59E-02	0	10910
178	1098	C	1	H	3	45	3.45	79.23	274.32	5.67E-02	0	10910
178	1098	C	1	H	3	50	3.5	74.01	345.52	5.01E-02	0	10910
178	1098	C	1	H	3	55	3.55	55.65	336.37	6.06E-02	0	10910
178	1098	C	1	H	3	60	3.6	59.95	320.73	5.26E-02	0	10910
178	1098	C	1	H	3	65	3.65	64.65	319.23	4.91E-02	0	10910
178	1098	C	1	H	3	70	3.7	72.59	278.13	3.96E-02	0	10910
178	1098	C	1	H	3	75	3.75	68.82	291.9	2.98E-02	0	10910

Note: Only a portion of this table appears here. The complete table is available in ASCII format in the [TABLES](#) directory.

Table T14. Split-core paleomagnetic measurements for Hole 1098C after 10-mT demagnetization.

Leg	Site	Hole	Core	Type	Section	Interval (cm)	Depth (mbsf)	Inclination (°)	Declination (°)	Intensity (A/m)	Demagnetization step (mT)	Run #
178	1098	C	1	H	1	10	0.1	-54.68	43.21	1.37E-02	10	10905
178	1098	C	1	H	1	15	0.15	-41.88	36.98	9.93E-03	10	10905
178	1098	C	1	H	1	20	0.2	-46.54	41.83	4.90E-03	10	10905
178	1098	C	1	H	1	25	0.25	-51.8	77.19	3.65E-03	10	10905
178	1098	C	1	H	1	30	0.3	-78.29	314.86	3.73E-03	10	10905
178	1098	C	1	H	1	35	0.35	-71.79	14.86	3.82E-03	10	10905
178	1098	C	1	H	1	40	0.4	-77.64	65.27	9.66E-03	10	10905
178	1098	C	1	H	1	45	0.45	-67.7	316.74	3.01E-02	10	10905
178	1098	C	1	H	1	50	0.5	-61.78	312.76	6.27E-02	10	10905
178	1098	C	1	H	1	55	0.55	-57.73	313.99	8.74E-02	10	10905
178	1098	C	1	H	1	60	0.6	-57.06	316.08	8.67E-02	10	10905
178	1098	C	1	H	1	65	0.65	-58.09	328.17	7.58E-02	10	10905
178	1098	C	1	H	1	70	0.7	-64.74	319.24	6.21E-02	10	10905
178	1098	C	1	H	1	75	0.75	-68.96	308.44	8.00E-02	10	10905
178	1098	C	1	H	1	80	0.8	-65.5	319.93	9.13E-02	10	10905
178	1098	C	1	H	1	85	0.85	-67.63	314.69	9.97E-02	10	10905
178	1098	C	1	H	1	90	0.9	-66.45	308.37	1.23E-01	10	10905
178	1098	C	1	H	1	95	0.95	-65.64	306.2	1.35E-01	10	10905
178	1098	C	1	H	1	100	1	-67.35	307.42	1.25E-01	10	10905
178	1098	C	1	H	1	105	1.05	-65.04	305.76	9.74E-02	10	10905
178	1098	C	1	H	1	110	1.1	-72.07	307.68	5.59E-02	10	10905
178	1098	C	1	H	1	115	1.15	-76.56	301.48	5.66E-02	10	10905
178	1098	C	1	H	1	120	1.2	-65.61	309.91	8.43E-02	10	10905
178	1098	C	1	H	1	125	1.25	-67.39	309.77	1.03E-01	10	10905
178	1098	C	1	H	1	130	1.3	-70.74	304.26	1.01E-01	10	10905
178	1098	C	1	H	1	135	1.35	-69	300.32	8.38E-02	10	10905
178	1098	C	1	H	2	10	1.6	-60.66	300.65	6.90E-02	10	10908
178	1098	C	1	H	2	15	1.65	-64.91	300.74	7.24E-02	10	10908
178	1098	C	1	H	2	20	1.7	-70.07	300.63	7.33E-02	10	10908
178	1098	C	1	H	2	25	1.75	-66.58	317.46	6.56E-02	10	10908
178	1098	C	1	H	2	30	1.8	-62.07	315.12	3.81E-02	10	10908
178	1098	C	1	H	2	35	1.85	-62.48	301.57	1.80E-02	10	10908
178	1098	C	1	H	2	40	1.9	-65.69	308.48	1.26E-02	10	10908
178	1098	C	1	H	2	45	1.95	-66.37	320.13	1.40E-02	10	10908
178	1098	C	1	H	2	50	2	-63.73	315.23	1.38E-02	10	10908
178	1098	C	1	H	2	55	2.05	-58.47	322.26	1.47E-02	10	10908
178	1098	C	1	H	2	60	2.1	-51.42	340.49	1.26E-02	10	10908
178	1098	C	1	H	2	65	2.15	-53.33	326.35	8.45E-03	10	10908
178	1098	C	1	H	2	70	2.2	-47.62	287.91	7.88E-03	10	10908
178	1098	C	1	H	2	75	2.25	-46.29	298.97	7.59E-03	10	10908
178	1098	C	1	H	2	80	2.3	-41.49	298.5	8.45E-03	10	10908
178	1098	C	1	H	2	85	2.35	-49.39	316.9	1.04E-02	10	10908
178	1098	C	1	H	2	90	2.4	-56.22	317.89	1.15E-02	10	10908
178	1098	C	1	H	2	95	2.45	-63.41	288.28	1.70E-02	10	10908
178	1098	C	1	H	2	100	2.5	-68.92	304	2.57E-02	10	10908
178	1098	C	1	H	2	105	2.55	-67.85	314.81	3.00E-02	10	10908
178	1098	C	1	H	2	110	2.6	-63.35	319.5	2.58E-02	10	10908
178	1098	C	1	H	2	115	2.65	-57.88	317.43	1.89E-02	10	10908
178	1098	C	1	H	2	120	2.7	-46.28	310.75	1.45E-02	10	10908
178	1098	C	1	H	2	125	2.75	-46.44	315.18	1.46E-02	10	10908
178	1098	C	1	H	2	130	2.8	-58.06	325.78	1.79E-02	10	10908
178	1098	C	1	H	3	10	3.1	61.07	298.38	6.15E-03	10	10911
178	1098	C	1	H	3	15	3.15	46.49	298.47	1.06E-02	10	10911
178	1098	C	1	H	3	20	3.2	44.56	287.57	1.49E-02	10	10911
178	1098	C	1	H	3	25	3.25	53.12	288.04	1.44E-02	10	10911
178	1098	C	1	H	3	30	3.3	45.14	249.16	9.21E-03	10	10911
178	1098	C	1	H	3	35	3.35	-32.53	252.62	1.23E-02	10	10911
178	1098	C	1	H	3	40	3.4	-44.44	280.76	1.54E-02	10	10911
178	1098	C	1	H	3	45	3.45	-26.46	282.09	9.16E-03	10	10911
178	1098	C	1	H	3	50	3.5	-11.98	249.9	1.02E-02	10	10911
178	1098	C	1	H	3	55	3.55	-40.12	270.79	1.55E-02	10	10911
178	1098	C	1	H	3	60	3.6	-45.63	294.96	1.93E-02	10	10911
178	1098	C	1	H	3	65	3.65	-46.18	283.37	1.80E-02	10	10911
178	1098	C	1	H	3	70	3.7	-53.62	264.71	1.48E-02	10	10911
178	1098	C	1	H	3	75	3.75	-52.31	246.35	1.56E-02	10	10911

Note: Only a portion of this table appears here. The complete table is available in ASCII format in the [TABLES](#) directory.

Table T15. Split-core paleomagnetic measurements for Hole 1098C after 20-mT demagnetization.

Leg	Site	Hole	Core	Type	Section	Interval (cm)	Depth (mbsf)	Inclination (°)	Declination (°)	Intensity (A/m)	Demagnetization step (mT)	Run #
178	1098	C	1	H	1	10	0.1	-80.55	5.16	7.22E-03	20	10906
178	1098	C	1	H	1	15	0.15	-58.67	22.63	4.79E-03	20	10906
178	1098	C	1	H	1	20	0.2	-65.56	41.39	2.49E-03	20	10906
178	1098	C	1	H	1	25	0.25	-68.44	115.19	2.16E-03	20	10906
178	1098	C	1	H	1	30	0.3	-71.23	272.94	2.76E-03	20	10906
178	1098	C	1	H	1	35	0.35	-73.31	37.89	2.67E-03	20	10906
178	1098	C	1	H	1	40	0.4	-78.82	100.22	6.95E-03	20	10906
178	1098	C	1	H	1	45	0.45	-64.48	279.38	2.33E-02	20	10906
178	1098	C	1	H	1	50	0.5	-60.22	291.61	4.96E-02	20	10906
178	1098	C	1	H	1	55	0.55	-58.08	303.85	6.74E-02	20	10906
178	1098	C	1	H	1	60	0.6	-58.62	309.63	6.51E-02	20	10906
178	1098	C	1	H	1	65	0.65	-60.21	324.32	5.59E-02	20	10906
178	1098	C	1	H	1	70	0.7	-66.39	313.9	4.58E-02	20	10906
178	1098	C	1	H	1	75	0.75	-69.63	298.78	6.01E-02	20	10906
178	1098	C	1	H	1	80	0.8	-67.2	311.18	6.82E-02	20	10906
178	1098	C	1	H	1	85	0.85	-69.6	305.46	7.47E-02	20	10906
178	1098	C	1	H	1	90	0.9	-68.11	301.63	9.30E-02	20	10906
178	1098	C	1	H	1	95	0.95	-66.79	302.14	1.02E-01	20	10906
178	1098	C	1	H	1	100	1	-68.37	302.34	9.40E-02	20	10906
178	1098	C	1	H	1	105	1.05	-66.44	301.58	7.20E-02	20	10906
178	1098	C	1	H	1	110	1.1	-73.39	304.68	4.10E-02	20	10906
178	1098	C	1	H	1	115	1.15	-78.49	287.05	4.03E-02	20	10906
178	1098	C	1	H	1	120	1.2	-68.24	297.41	5.97E-02	20	10906
178	1098	C	1	H	1	125	1.25	-69.21	298.14	7.48E-02	20	10906
178	1098	C	1	H	1	130	1.3	-71.68	294.12	7.49E-02	20	10906
178	1098	C	1	H	1	135	1.35	-70.33	293.57	6.21E-02	20	10906
178	1098	C	1	H	2	10	1.6	-63.11	295.3	4.79E-02	20	10909
178	1098	C	1	H	2	15	1.65	-67.91	294.23	5.05E-02	20	10909
178	1098	C	1	H	2	20	1.7	-72.24	289.78	5.25E-02	20	10909
178	1098	C	1	H	2	25	1.75	-69.11	311.22	4.73E-02	20	10909
178	1098	C	1	H	2	30	1.8	-64.72	313.37	2.73E-02	20	10909
178	1098	C	1	H	2	35	1.85	-66.22	298.64	1.27E-02	20	10909
178	1098	C	1	H	2	40	1.9	-70.45	297.03	8.88E-03	20	10909
178	1098	C	1	H	2	45	1.95	-70.55	306.02	9.91E-03	20	10909
178	1098	C	1	H	2	50	2	-67.53	302.72	9.75E-03	20	10909
178	1098	C	1	H	2	55	2.05	-63.15	311.02	1.01E-02	20	10909
178	1098	C	1	H	2	60	2.1	-58.23	332.26	8.44E-03	20	10909
178	1098	C	1	H	2	65	2.15	-60.05	318.13	5.91E-03	20	10909
178	1098	C	1	H	2	70	2.2	-51.09	281.67	5.70E-03	20	10909
178	1098	C	1	H	2	75	2.25	-49.28	294.77	5.52E-03	20	10909
178	1098	C	1	H	2	80	2.3	-43.57	294.53	5.98E-03	20	10909
178	1098	C	1	H	2	85	2.35	-53.57	311.41	7.10E-03	20	10909
178	1098	C	1	H	2	90	2.4	-60.55	310.87	7.94E-03	20	10909
178	1098	C	1	H	2	95	2.45	-65.35	276.89	1.19E-02	20	10909
178	1098	C	1	H	2	100	2.5	-71.92	292.73	1.81E-02	20	10909
178	1098	C	1	H	2	105	2.55	-71.13	305.63	2.12E-02	20	10909
178	1098	C	1	H	2	110	2.6	-66.84	313.87	1.82E-02	20	10909
178	1098	C	1	H	2	115	2.65	-61.05	313.13	1.33E-02	20	10909
178	1098	C	1	H	2	120	2.7	-48.59	307.57	1.01E-02	20	10909
178	1098	C	1	H	2	125	2.75	-50.49	309.07	9.84E-03	20	10909
178	1098	C	1	H	2	130	2.8	-64.03	315.9	1.22E-02	20	10909
178	1098	C	1	H	3	10	3.1	61.31	288.93	4.43E-03	20	10912
178	1098	C	1	H	3	15	3.15	46.2	293.92	7.49E-03	20	10912
178	1098	C	1	H	3	20	3.2	43.67	284.47	1.05E-02	20	10912
178	1098	C	1	H	3	25	3.25	52.62	283.46	1.00E-02	20	10912
178	1098	C	1	H	3	30	3.3	41.09	240.37	6.50E-03	20	10912
178	1098	C	1	H	3	35	3.35	-34.31	246.08	9.17E-03	20	10912
178	1098	C	1	H	3	40	3.4	-46.84	273.09	1.12E-02	20	10912
178	1098	C	1	H	3	45	3.45	-30.55	275.55	6.61E-03	20	10912
178	1098	C	1	H	3	50	3.5	-13.48	244.56	7.26E-03	20	10912
178	1098	C	1	H	3	55	3.55	-40.46	262.55	1.11E-02	20	10912
178	1098	C	1	H	3	60	3.6	-47.57	286.13	1.35E-02	20	10912
178	1098	C	1	H	3	65	3.65	-47.56	274.73	1.29E-02	20	10912
178	1098	C	1	H	3	70	3.7	-54.22	258.56	1.09E-02	20	10912
178	1098	C	1	H	3	75	3.75	-52.49	240.37	1.15E-02	20	10912

Note: Only a portion of this table appears here. The complete table is available in ASCII format in the [TABLES](#) directory.

Table T16. Split-core paleomagnetic measurements for Hole 1098C after processing the results from the 20-mT demagnetization step by removing measurements from drilling-disturbed intervals and measurements made within 10 cm of the ends of each core section.

Leg	Site	Hole	Core	Type	Section	Interval (cm)	Depth (mbst)	Inclination (°)	Declination (°)	Intensity (A/m)	Demagnetization step (mT)	Run #
178	1098	C	1	H	1	40	0.4	-78.82	100.22	6.95E-03	20	10906
178	1098	C	1	H	1	45	0.45	-64.48	279.38	2.33E-02	20	10906
178	1098	C	1	H	1	50	0.5	-60.22	291.61	4.96E-02	20	10906
178	1098	C	1	H	1	55	0.55	-58.08	303.85	6.75E-02	20	10906
178	1098	C	1	H	1	60	0.6	-58.62	309.63	6.51E-02	20	10906
178	1098	C	1	H	1	65	0.65	-60.21	324.32	5.59E-02	20	10906
178	1098	C	1	H	1	70	0.7	-66.39	313.9	4.58E-02	20	10906
178	1098	C	1	H	1	75	0.75	-69.63	298.78	6.01E-02	20	10906
178	1098	C	1	H	1	80	0.8	-67.2	311.18	6.82E-02	20	10906
178	1098	C	1	H	1	85	0.85	-69.6	305.46	7.47E-02	20	10906
178	1098	C	1	H	1	90	0.9	-68.11	301.63	9.30E-02	20	10906
178	1098	C	1	H	1	95	0.95	-66.79	302.14	1.02E-01	20	10906
178	1098	C	1	H	1	100	1	-68.37	302.34	9.40E-02	20	10906
178	1098	C	1	H	1	105	1.05	-66.44	301.58	7.20E-02	20	10906
178	1098	C	1	H	1	110	1.1	-73.39	304.68	4.10E-02	20	10906
178	1098	C	1	H	1	115	1.15	-78.49	287.05	4.03E-02	20	10906
178	1098	C	1	H	1	120	1.2	-68.24	297.41	5.97E-02	20	10906
178	1098	C	1	H	1	125	1.25	-69.21	298.14	7.48E-02	20	10906
178	1098	C	1	H	1	130	1.3	-71.68	294.12	7.49E-02	20	10906
178	1098	C	1	H	1	135	1.35	-70.33	293.57	6.21E-02	20	10906
178	1098	C	1	H	2	10	1.6	-63.11	295.3	4.79E-02	20	10909
178	1098	C	1	H	2	15	1.65	-67.91	294.23	5.05E-02	20	10909
178	1098	C	1	H	2	20	1.7	-72.24	289.78	5.25E-02	20	10909
178	1098	C	1	H	2	25	1.75	-69.11	311.22	4.73E-02	20	10909
178	1098	C	1	H	2	30	1.8	-64.72	313.37	2.73E-02	20	10909
178	1098	C	1	H	2	35	1.85	-66.22	298.64	1.27E-02	20	10909
178	1098	C	1	H	2	40	1.9	-70.45	297.03	8.88E-03	20	10909
178	1098	C	1	H	2	45	1.95	-70.55	306.02	9.91E-03	20	10909
178	1098	C	1	H	2	50	2	-67.53	302.72	9.75E-03	20	10909
178	1098	C	1	H	2	55	2.05	-63.15	311.02	1.01E-02	20	10909
178	1098	C	1	H	2	60	2.1	-58.23	332.26	8.44E-03	20	10909
178	1098	C	1	H	2	65	2.15	-60.05	318.13	5.91E-03	20	10909
178	1098	C	1	H	2	70	2.2	-51.09	281.67	5.70E-03	20	10909
178	1098	C	1	H	2	75	2.25	-49.28	294.77	5.52E-03	20	10909
178	1098	C	1	H	2	80	2.3	-43.57	294.53	5.98E-03	20	10909
178	1098	C	1	H	2	85	2.35	-53.57	311.41	7.11E-03	20	10909
178	1098	C	1	H	2	90	2.4	-60.55	310.87	7.94E-03	20	10909
178	1098	C	1	H	2	95	2.45	-65.35	276.89	1.19E-02	20	10909
178	1098	C	1	H	2	100	2.5	-71.92	292.73	1.81E-02	20	10909
178	1098	C	1	H	2	105	2.55	-71.13	305.63	2.12E-02	20	10909
178	1098	C	1	H	2	110	2.6	-66.84	313.87	1.82E-02	20	10909
178	1098	C	1	H	2	115	2.65	-61.05	313.13	1.33E-02	20	10909
178	1098	C	1	H	2	120	2.7	-48.59	307.57	1.01E-02	20	10909
178	1098	C	1	H	2	125	2.75	-50.49	309.07	9.84E-03	20	10909
178	1098	C	1	H	2	130	2.8	-64.03	315.9	1.22E-02	20	10909
178	1098	C	1	H	3	35	3.35	-34.31	246.08	9.17E-03	20	10912
178	1098	C	1	H	3	40	3.4	-46.84	273.09	1.12E-02	20	10912
178	1098	C	1	H	3	45	3.45	-30.55	275.55	6.61E-03	20	10912
178	1098	C	1	H	3	50	3.5	-13.48	244.56	7.26E-03	20	10912
178	1098	C	1	H	3	55	3.55	-40.46	262.55	1.11E-02	20	10912
178	1098	C	1	H	3	60	3.6	-47.57	286.13	1.35E-02	20	10912
178	1098	C	1	H	3	65	3.65	-47.56	274.73	1.29E-02	20	10912
178	1098	C	1	H	3	70	3.7	-54.22	258.56	1.09E-02	20	10912
178	1098	C	1	H	3	75	3.75	-52.49	240.37	1.15E-02	20	10912
178	1098	C	1	H	3	80	3.8	-56.1	254.23	1.27E-02	20	10912
178	1098	C	1	H	3	85	3.85	-55.36	271.09	1.01E-02	20	10912
178	1098	C	1	H	3	90	3.9	-53.77	259.84	8.11E-03	20	10912
178	1098	C	1	H	3	95	3.95	-57.53	245.22	8.15E-03	20	10912
178	1098	C	1	H	3	100	4	-58.12	246.89	1.12E-02	20	10912
178	1098	C	1	H	3	105	4.05	-60.76	232.21	1.71E-02	20	10912
178	1098	C	1	H	3	110	4.1	-66.39	229.51	2.35E-02	20	10912
178	1098	C	1	H	3	115	4.15	-70.06	248.47	2.54E-02	20	10912
178	1098	C	1	H	3	120	4.2	-67.21	246.83	2.58E-02	20	10912

Note: Only a portion of this table appears here. The complete table is available in ASCII format in the [TABLES](#) directory.

Table T17. Split-core paleomagnetic measurements for Hole 1099A before demagnetization (NRM results).

Leg	Site	Hole	Core	Type	Section	Interval (cm)	Depth (mbsf)	Inclination (°)	Declination (°)	Intensity (A/m)	Demagnetization step (mT)	Run #
178	1099	A	1	H	1	10	0.1	-13.33	22.62	1.08E-01	0	11000
178	1099	A	1	H	1	15	0.15	-24.66	10.13	1.36E-01	0	11000
178	1099	A	1	H	1	20	0.2	-27.64	4.22	1.77E-01	0	11000
178	1099	A	1	H	1	25	0.25	-25.65	11.75	1.94E-01	0	11000
178	1099	A	1	H	1	30	0.3	-23.05	19.14	1.59E-01	0	11000
178	1099	A	1	H	1	35	0.35	-16.79	4.95	9.39E-02	0	11000
178	1099	A	1	H	1	40	0.4	-7.17	343.18	7.48E-02	0	11000
178	1099	A	1	H	1	45	0.45	-11.45	351.84	7.75E-02	0	11000
178	1099	A	1	H	1	50	0.5	-20.66	14.99	7.37E-02	0	11000
178	1099	A	1	H	1	55	0.55	-11.55	4.48	5.46E-02	0	11000
178	1099	A	1	H	1	60	0.6	-0.52	0.91	5.88E-02	0	11000
178	1099	A	1	H	1	65	0.65	3.97	1.28	6.35E-02	0	11000
178	1099	A	1	H	1	70	0.7	9.64	2.61	7.31E-02	0	11000
178	1099	A	1	H	1	75	0.75	13.05	8.65	7.59E-02	0	11000
178	1099	A	1	H	1	80	0.8	11.92	3.27	8.73E-02	0	11000
178	1099	A	1	H	1	85	0.85	11.26	1.74	9.06E-02	0	11000
178	1099	A	1	H	1	90	0.9	10.75	1.51	8.85E-02	0	11000
178	1099	A	1	H	1	95	0.95	9.89	355.15	8.57E-02	0	11000
178	1099	A	1	H	1	100	1	9.88	350.64	8.61E-02	0	11000
178	1099	A	1	H	1	105	1.05	11.12	348.81	8.87E-02	0	11000
178	1099	A	1	H	1	110	1.1	12.77	344.99	8.43E-02	0	11000
178	1099	A	1	H	1	115	1.15	13.01	339.9	8.99E-02	0	11000
178	1099	A	1	H	1	120	1.2	15.89	331.28	1.12E-01	0	11000
178	1099	A	1	H	1	125	1.25	22.59	326.17	1.34E-01	0	11000
178	1099	A	1	H	1	130	1.3	30.24	338.08	1.28E-01	0	11000
178	1099	A	1	H	1	135	1.35	32.4	353.65	1.27E-01	0	11000
178	1099	A	1	H	1	140	1.4	31.75	2.92	1.27E-01	0	11000
178	1099	A	1	H	2	10	1.6	51.55	12.85	7.92E-02	0	11003
178	1099	A	1	H	2	15	1.65	54.41	29.08	7.45E-02	0	11003
178	1099	A	1	H	2	20	1.7	48.75	27.11	8.71E-02	0	11003
178	1099	A	1	H	2	25	1.75	51.98	38.63	8.58E-02	0	11003
178	1099	A	1	H	2	30	1.8	52.37	53.18	6.72E-02	0	11003
178	1099	A	1	H	2	35	1.85	40.83	35.44	6.26E-02	0	11003
178	1099	A	1	H	2	40	1.9	36.83	29.5	5.88E-02	0	11003
178	1099	A	1	H	2	45	1.95	40.86	27.58	4.62E-02	0	11003
178	1099	A	1	H	2	50	2	47.6	40.84	3.92E-02	0	11003
178	1099	A	1	H	2	55	2.05	48.78	40.35	4.20E-02	0	11003
178	1099	A	1	H	2	60	2.1	52.96	45.22	4.49E-02	0	11003
178	1099	A	1	H	2	65	2.15	56.71	39.69	4.91E-02	0	11003
178	1099	A	1	H	2	70	2.2	55.88	33.33	5.21E-02	0	11003
178	1099	A	1	H	2	75	2.25	56.04	34.32	5.85E-02	0	11003
178	1099	A	1	H	2	80	2.3	63.41	30.46	5.95E-02	0	11003
178	1099	A	1	H	2	85	2.35	65.36	27.91	6.09E-02	0	11003
178	1099	A	1	H	2	90	2.4	61.8	36.35	6.24E-02	0	11003
178	1099	A	1	H	2	95	2.45	67.64	33.5	6.11E-02	0	11003
178	1099	A	1	H	2	100	2.5	62	22.64	6.35E-02	0	11003
178	1099	A	1	H	2	105	2.55	49.86	27.26	8.04E-02	0	11003
178	1099	A	1	H	2	110	2.6	58.85	48.59	8.05E-02	0	11003
178	1099	A	1	H	2	115	2.65	65.99	65.57	7.33E-02	0	11003
178	1099	A	1	H	2	120	2.7	62.23	55.24	6.89E-02	0	11003
178	1099	A	1	H	2	125	2.75	50.98	62.33	6.55E-02	0	11003
178	1099	A	1	H	2	130	2.8	29.04	89	5.54E-02	0	11003
178	1099	A	1	H	2	135	2.85	-25.36	111.74	6.29E-02	0	11003
178	1099	A	1	H	3	10	3.1	8.53	107.26	4.79E-02	0	11006
178	1099	A	1	H	3	15	3.15	-21.88	78.77	8.55E-02	0	11006
178	1099	A	1	H	3	20	3.2	3.34	60.67	9.16E-02	0	11006
178	1099	A	1	H	3	25	3.25	-38.41	138.32	6.68E-02	0	11006
178	1099	A	1	H	3	30	3.3	-53.54	109.4	9.96E-02	0	11006
178	1099	A	1	H	3	35	3.35	-58.42	108.85	9.15E-02	0	11006
178	1099	A	1	H	3	40	3.4	-60.44	110.09	8.44E-02	0	11006
178	1099	A	1	H	3	45	3.45	-56.97	88.16	8.41E-02	0	11006
178	1099	A	1	H	3	50	3.5	-59.26	103.05	9.04E-02	0	11006
178	1099	A	1	H	3	55	3.55	-62.59	107.28	8.40E-02	0	11006
178	1099	A	1	H	3	60	3.6	-64.63	89.65	6.27E-02	0	11006
178	1099	A	1	H	3	65	3.65	-41.97	64	2.56E-02	0	11006

Note: Only a portion of this table appears here. The complete table is available in ASCII format in the [TABLES](#) directory.

Table T18. Split-core paleomagnetic measurements for Hole 1099A after 10-mT demagnetization.

Leg	Site	Hole	Core	Type	Section	Interval (cm)	Depth (mbsf)	Inclination (°)	Declination (°)	Intensity (A/m)	Demagnetization step (mT)	Run #
178	1099	A	1	H	1	10	0.1	-47.08	25.4	7.26E-02	10	11001
178	1099	A	1	H	1	15	0.15	-60.18	3.37	1.17E-01	10	11001
178	1099	A	1	H	1	20	0.2	-58.5	355.79	1.58E-01	10	11001
178	1099	A	1	H	1	25	0.25	-55.97	8.75	1.62E-01	10	11001
178	1099	A	1	H	1	30	0.3	-55.31	18.55	1.38E-01	10	11001
178	1099	A	1	H	1	35	0.35	-56.24	354.04	9.91E-02	10	11001
178	1099	A	1	H	1	40	0.4	-54.08	326.95	8.10E-02	10	11001
178	1099	A	1	H	1	45	0.45	-56.76	336.56	8.21E-02	10	11001
178	1099	A	1	H	1	50	0.5	-54.53	8.89	7.20E-02	10	11001
178	1099	A	1	H	1	55	0.55	-63.09	353.9	5.09E-02	10	11001
178	1099	A	1	H	1	60	0.6	-59.42	344.98	5.72E-02	10	11001
178	1099	A	1	H	1	65	0.65	-56.04	341.82	5.96E-02	10	11001
178	1099	A	1	H	1	70	0.7	-48.54	351.73	5.81E-02	10	11001
178	1099	A	1	H	1	75	0.75	-44.49	2.27	5.47E-02	10	11001
178	1099	A	1	H	1	80	0.8	-37.69	356.79	6.07E-02	10	11001
178	1099	A	1	H	1	85	0.85	-36.89	357.45	6.37E-02	10	11001
178	1099	A	1	H	1	90	0.9	-38.79	356.45	6.51E-02	10	11001
178	1099	A	1	H	1	95	0.95	-40.72	345.62	6.64E-02	10	11001
178	1099	A	1	H	1	100	1	-40.09	338.99	6.76E-02	10	11001
178	1099	A	1	H	1	105	1.05	-38.74	337.42	6.83E-02	10	11001
178	1099	A	1	H	1	110	1.1	-41.08	332.5	6.61E-02	10	11001
178	1099	A	1	H	1	115	1.15	-39.11	328.03	7.12E-02	10	11001
178	1099	A	1	H	1	120	1.2	-26.52	320.47	8.45E-02	10	11001
178	1099	A	1	H	1	125	1.25	-12.46	315.8	9.37E-02	10	11001
178	1099	A	1	H	1	130	1.3	-6.32	326.6	7.50E-02	10	11001
178	1099	A	1	H	1	135	1.35	-3.98	344.47	6.45E-02	10	11001
178	1099	A	1	H	1	140	1.4	-3.08	354.49	6.41E-02	10	11001
178	1099	A	1	H	2	10	1.6	-27.56	42.06	2.02E-02	10	11004
178	1099	A	1	H	2	15	1.65	-33.26	70.76	2.40E-02	10	11004
178	1099	A	1	H	2	20	1.7	-23.21	53.7	3.03E-02	10	11004
178	1099	A	1	H	2	25	1.75	-23.39	71.71	3.31E-02	10	11004
178	1099	A	1	H	2	30	1.8	-40.21	94.51	3.76E-02	10	11004
178	1099	A	1	H	2	35	1.85	-52.41	68.43	4.29E-02	10	11004
178	1099	A	1	H	2	40	1.9	-58.73	58.89	4.60E-02	10	11004
178	1099	A	1	H	2	45	1.95	-70.04	64.33	4.59E-02	10	11004
178	1099	A	1	H	2	50	2	-70.97	95.15	4.61E-02	10	11004
178	1099	A	1	H	2	55	2.05	-69.36	90.82	4.50E-02	10	11004
178	1099	A	1	H	2	60	2.1	-65.31	93.03	4.33E-02	10	11004
178	1099	A	1	H	2	65	2.15	-64.01	88.98	3.77E-02	10	11004
178	1099	A	1	H	2	70	2.2	-64.43	80.79	3.49E-02	10	11004
178	1099	A	1	H	2	75	2.25	-58.49	76.55	3.45E-02	10	11004
178	1099	A	1	H	2	80	2.3	-63.17	81.09	3.17E-02	10	11004
178	1099	A	1	H	2	85	2.35	-62.82	77.66	3.04E-02	10	11004
178	1099	A	1	H	2	90	2.4	-54.83	79.49	3.21E-02	10	11004
178	1099	A	1	H	2	95	2.45	-57.67	91.43	2.95E-02	10	11004
178	1099	A	1	H	2	100	2.5	-65.09	64.84	2.92E-02	10	11004
178	1099	A	1	H	2	105	2.55	-41.88	42.42	3.55E-02	10	11004
178	1099	A	1	H	2	110	2.6	-37.87	77.79	2.86E-02	10	11004
178	1099	A	1	H	2	115	2.65	-43.47	110.92	2.90E-02	10	11004
178	1099	A	1	H	2	120	2.7	-49.78	88.11	3.40E-02	10	11004
178	1099	A	1	H	2	125	2.75	-48.1	87.34	4.71E-02	10	11004
178	1099	A	1	H	2	130	2.8	-53.62	124.67	8.46E-02	10	11004
178	1099	A	1	H	2	135	2.85	-62.65	140.75	1.46E-01	10	11004
178	1099	A	1	H	3	10	3.1	-60.87	127.41	1.01E-01	10	11007
178	1099	A	1	H	3	15	3.15	-65.7	135.28	1.55E-01	10	11007
178	1099	A	1	H	3	20	3.2	-69.98	127.52	1.62E-01	10	11007
178	1099	A	1	H	3	25	3.25	-71.67	131.32	1.75E-01	10	11007
178	1099	A	1	H	3	30	3.3	-72.7	130.21	1.88E-01	10	11007
178	1099	A	1	H	3	35	3.35	-73.57	137.94	1.77E-01	10	11007
178	1099	A	1	H	3	40	3.4	-75.03	137.73	1.65E-01	10	11007
178	1099	A	1	H	3	45	3.45	-75.14	120.11	1.51E-01	10	11007
178	1099	A	1	H	3	50	3.5	-73.1	136.4	1.62E-01	10	11007
178	1099	A	1	H	3	55	3.55	-76.1	137.09	1.57E-01	10	11007
178	1099	A	1	H	3	60	3.6	-79.29	115.34	1.21E-01	10	11007
178	1099	A	1	H	3	65	3.65	-79.84	90.17	7.37E-02	10	11007

Note: Only a portion of this table appears here. The complete table is available in ASCII format in the [TABLES](#) directory.

Table T19. Split-core paleomagnetic measurements for Hole 1099A after 20-mT demagnetization.

Leg	Site	Hole	Core	Type	Section	Interval (cm)	Depth (mbsf)	Inclination (°)	Declination (°)	Intensity (A/m)	Demagnetization step (mT)	Run #
178	1099	A	1	H	1	10	0.1	-53.94	21.38	5.03E-02	20	11002
178	1099	A	1	H	1	15	0.15	-64.27	355.2	8.49E-02	20	11002
178	1099	A	1	H	1	20	0.2	-61.97	348.49	1.16E-01	20	11002
178	1099	A	1	H	1	25	0.25	-60.83	4.35	1.17E-01	20	11002
178	1099	A	1	H	1	30	0.3	-60.09	15.74	9.95E-02	20	11002
178	1099	A	1	H	1	35	0.35	-59.53	350.67	7.37E-02	20	11002
178	1099	A	1	H	1	40	0.4	-57.32	321.84	6.01E-02	20	11002
178	1099	A	1	H	1	45	0.45	-60.9	329.02	6.09E-02	20	11002
178	1099	A	1	H	1	50	0.5	-59.94	4.54	5.33E-02	20	11002
178	1099	A	1	H	1	55	0.55	-68.52	344.12	3.85E-02	20	11002
178	1099	A	1	H	1	60	0.6	-64.83	335.09	4.25E-02	20	11002
178	1099	A	1	H	1	65	0.65	-61.34	331.89	4.39E-02	20	11002
178	1099	A	1	H	1	70	0.7	-55.68	344.29	4.15E-02	20	11002
178	1099	A	1	H	1	75	0.75	-52.82	357.13	3.84E-02	20	11002
178	1099	A	1	H	1	80	0.8	-45.06	352.7	4.15E-02	20	11002
178	1099	A	1	H	1	85	0.85	-43.95	354.29	4.32E-02	20	11002
178	1099	A	1	H	1	90	0.9	-45.4	352.97	4.47E-02	20	11002
178	1099	A	1	H	1	95	0.95	-46.48	340.86	4.63E-02	20	11002
178	1099	A	1	H	1	100	1	-45.21	334.16	4.73E-02	20	11002
178	1099	A	1	H	1	105	1.05	-43.83	332.73	4.77E-02	20	11002
178	1099	A	1	H	1	110	1.1	-46.37	327.3	4.64E-02	20	11002
178	1099	A	1	H	1	115	1.15	-44.17	323.83	4.98E-02	20	11002
178	1099	A	1	H	1	120	1.2	-30.46	317.21	5.84E-02	20	11002
178	1099	A	1	H	1	125	1.25	-15.53	312.9	6.40E-02	20	11002
178	1099	A	1	H	1	130	1.3	-9.88	322.76	4.96E-02	20	11002
178	1099	A	1	H	1	135	1.35	-8.12	340.77	4.07E-02	20	11002
178	1099	A	1	H	1	140	1.4	-7.16	350.89	3.99E-02	20	11002
178	1099	A	1	H	2	10	1.6	-43.95	75.3	1.20E-02	20	11005
178	1099	A	1	H	2	15	1.65	-40.34	97.25	1.72E-02	20	11005
178	1099	A	1	H	2	20	1.7	-33.47	72.34	1.92E-02	20	11005
178	1099	A	1	H	2	25	1.75	-31.05	87.29	2.28E-02	20	11005
178	1099	A	1	H	2	30	1.8	-43.2	107.42	2.81E-02	20	11005
178	1099	A	1	H	2	35	1.85	-57.13	83.72	3.04E-02	20	11005
178	1099	A	1	H	2	40	1.9	-64.16	75.41	3.27E-02	20	11005
178	1099	A	1	H	2	45	1.95	-73.07	88.57	3.37E-02	20	11005
178	1099	A	1	H	2	50	2	-69.79	115.99	3.49E-02	20	11005
178	1099	A	1	H	2	55	2.05	-68.69	111.02	3.42E-02	20	11005
178	1099	A	1	H	2	60	2.1	-65.07	108.96	3.31E-02	20	11005
178	1099	A	1	H	2	65	2.15	-63.99	107.01	2.90E-02	20	11005
178	1099	A	1	H	2	70	2.2	-65.21	100.93	2.67E-02	20	11005
178	1099	A	1	H	2	75	2.25	-60.96	91.77	2.60E-02	20	11005
178	1099	A	1	H	2	80	2.3	-64.64	97.19	2.45E-02	20	11005
178	1099	A	1	H	2	85	2.35	-64.44	94.4	2.33E-02	20	11005
178	1099	A	1	H	2	90	2.4	-57.13	94.92	2.41E-02	20	11005
178	1099	A	1	H	2	95	2.45	-57.66	109.28	2.29E-02	20	11005
178	1099	A	1	H	2	100	2.5	-67.78	91.32	2.22E-02	20	11005
178	1099	A	1	H	2	105	2.55	-50.3	53.51	2.46E-02	20	11005
178	1099	A	1	H	2	110	2.6	-44.14	91.44	2.13E-02	20	11005
178	1099	A	1	H	2	115	2.65	-46.33	120.38	2.28E-02	20	11005
178	1099	A	1	H	2	120	2.7	-52.84	96.34	2.58E-02	20	11005
178	1099	A	1	H	2	125	2.75	-50.99	92.97	3.50E-02	20	11005
178	1099	A	1	H	2	130	2.8	-53.86	129.88	6.49E-02	20	11005
178	1099	A	1	H	2	135	2.85	-62.17	144.8	1.13E-01	20	11005
178	1099	A	1	H	3	10	3.1	-62.68	133.72	7.73E-02	20	11008
178	1099	A	1	H	3	15	3.15	-65.94	140.32	1.20E-01	20	11008
178	1099	A	1	H	3	20	3.2	-69.94	135.92	1.27E-01	20	11008
178	1099	A	1	H	3	25	3.25	-71.87	135.72	1.36E-01	20	11008
178	1099	A	1	H	3	30	3.3	-72.93	134.06	1.45E-01	20	11008
178	1099	A	1	H	3	35	3.35	-73.64	141.19	1.37E-01	20	11008
178	1099	A	1	H	3	40	3.4	-75.26	141.65	1.25E-01	20	11008
178	1099	A	1	H	3	45	3.45	-75.46	125.89	1.13E-01	20	11008
178	1099	A	1	H	3	50	3.5	-73.05	141.47	1.21E-01	20	11008
178	1099	A	1	H	3	55	3.55	-76.12	140.73	1.17E-01	20	11008
178	1099	A	1	H	3	60	3.6	-79.43	119.65	8.98E-02	20	11008
178	1099	A	1	H	3	65	3.65	-80.56	95.33	5.41E-02	20	11008

Note: Only a portion of this table appears here. The complete table is available in ASCII format in the [TABLES](#) directory.

Table T20. Split-core paleomagnetic measurements for Hole 1099A after processing the results from the 20-mT demagnetization step by removing measurements from drilling-disturbed intervals and measurements made within 10 cm of the ends of each core section.

Leg	Site	Hole	Core	Type	Section	Interval (cm)	Depth (mbst)	Inclination (°)	Declination (°)	Intensity (A/m)	Demagnetization step (mT)	Run #
178	1099	A	1	H	1	10	0.1	-53.94	21.38	5.03E-02	20	11002
178	1099	A	1	H	1	15	0.15	-64.27	355.2	8.49E-02	20	11002
178	1099	A	1	H	1	20	0.2	-61.97	348.49	1.16E-01	20	11002
178	1099	A	1	H	1	25	0.25	-60.83	4.35	1.17E-01	20	11002
178	1099	A	1	H	1	30	0.3	-60.09	15.74	9.95E-02	20	11002
178	1099	A	1	H	1	35	0.35	-59.53	350.67	7.37E-02	20	11002
178	1099	A	1	H	1	40	0.4	-57.32	321.84	6.01E-02	20	11002
178	1099	A	1	H	1	45	0.45	-60.9	329.02	6.09E-02	20	11002
178	1099	A	1	H	1	50	0.5	-59.94	4.54	5.33E-02	20	11002
178	1099	A	1	H	1	55	0.55	-68.52	344.12	3.85E-02	20	11002
178	1099	A	1	H	1	60	0.6	-64.83	335.09	4.26E-02	20	11002
178	1099	A	1	H	1	65	0.65	-61.34	331.89	4.39E-02	20	11002
178	1099	A	1	H	1	70	0.7	-55.68	344.29	4.15E-02	20	11002
178	1099	A	1	H	1	75	0.75	-52.82	357.13	3.84E-02	20	11002
178	1099	A	1	H	1	80	0.8	-45.06	352.7	4.15E-02	20	11002
178	1099	A	1	H	1	85	0.85	-43.95	354.29	4.32E-02	20	11002
178	1099	A	1	H	1	90	0.9	-45.4	352.97	4.47E-02	20	11002
178	1099	A	1	H	1	95	0.95	-46.48	340.86	4.63E-02	20	11002
178	1099	A	1	H	1	100	1	-45.21	334.16	4.73E-02	20	11002
178	1099	A	1	H	1	105	1.05	-43.83	332.73	4.77E-02	20	11002
178	1099	A	1	H	1	110	1.1	-46.37	327.3	4.64E-02	20	11002
178	1099	A	1	H	1	115	1.15	-44.17	323.83	4.98E-02	20	11002
178	1099	A	1	H	2	10	1.6	-43.95	75.3	1.20E-02	20	11005
178	1099	A	1	H	2	15	1.65	-40.34	97.25	1.72E-02	20	11005
178	1099	A	1	H	2	20	1.7	-33.47	72.34	1.93E-02	20	11005
178	1099	A	1	H	2	25	1.75	-31.05	87.29	2.28E-02	20	11005
178	1099	A	1	H	2	30	1.8	-43.2	107.42	2.81E-02	20	11005
178	1099	A	1	H	2	35	1.85	-57.13	83.72	3.04E-02	20	11005
178	1099	A	1	H	2	40	1.9	-64.16	75.41	3.28E-02	20	11005
178	1099	A	1	H	2	45	1.95	-73.07	88.57	3.37E-02	20	11005
178	1099	A	1	H	2	50	2	-69.79	115.99	3.49E-02	20	11005
178	1099	A	1	H	2	55	2.05	-68.69	111.02	3.42E-02	20	11005
178	1099	A	1	H	2	60	2.1	-65.07	108.96	3.31E-02	20	11005
178	1099	A	1	H	2	65	2.15	-63.99	107.01	2.90E-02	20	11005
178	1099	A	1	H	2	70	2.2	-65.21	100.93	2.67E-02	20	11005
178	1099	A	1	H	2	75	2.25	-60.96	91.77	2.60E-02	20	11005
178	1099	A	1	H	2	80	2.3	-64.64	97.19	2.45E-02	20	11005
178	1099	A	1	H	2	85	2.35	-64.44	94.4	2.33E-02	20	11005
178	1099	A	1	H	2	90	2.4	-57.13	94.92	2.41E-02	20	11005
178	1099	A	1	H	2	95	2.45	-57.66	109.28	2.29E-02	20	11005
178	1099	A	1	H	2	100	2.5	-67.78	91.32	2.22E-02	20	11005
178	1099	A	1	H	2	105	2.55	-50.3	53.51	2.46E-02	20	11005
178	1099	A	1	H	2	110	2.6	-44.14	91.44	2.13E-02	20	11005
178	1099	A	1	H	2	115	2.65	-46.33	120.38	2.28E-02	20	11005
178	1099	A	1	H	2	120	2.7	-52.84	96.34	2.58E-02	20	11005
178	1099	A	1	H	2	125	2.75	-50.99	92.97	3.50E-02	20	11005
178	1099	A	1	H	2	130	2.8	-53.86	129.88	6.49E-02	20	11005
178	1099	A	1	H	2	135	2.85	-62.17	144.8	1.13E-01	20	11005
178	1099	A	1	H	3	10	3.1	-62.68	133.72	7.73E-02	20	11008
178	1099	A	1	H	3	15	3.15	-65.94	140.32	1.20E-01	20	11008
178	1099	A	1	H	3	20	3.2	-69.94	135.92	1.27E-01	20	11008
178	1099	A	1	H	3	25	3.25	-71.87	135.72	1.36E-01	20	11008
178	1099	A	1	H	3	30	3.3	-72.93	134.06	1.45E-01	20	11008
178	1099	A	1	H	3	35	3.35	-73.64	141.19	1.37E-01	20	11008
178	1099	A	1	H	3	40	3.4	-75.26	141.65	1.25E-01	20	11008
178	1099	A	1	H	3	45	3.45	-75.46	125.89	1.13E-01	20	11008
178	1099	A	1	H	3	50	3.5	-73.05	141.47	1.21E-01	20	11008
178	1099	A	1	H	3	55	3.55	-76.12	140.73	1.17E-01	20	11008
178	1099	A	1	H	3	60	3.6	-79.43	119.65	8.98E-02	20	11008
178	1099	A	1	H	3	65	3.65	-80.56	95.33	5.41E-02	20	11008
178	1099	A	1	H	3	70	3.7	-76.96	113.3	3.69E-02	20	11008
178	1099	A	1	H	3	75	3.75	-78.81	113.66	3.47E-02	20	11008
178	1099	A	1	H	3	80	3.8	-72.68	140.3	5.51E-02	20	11008

Note: Only a portion of this table appears here. The complete table is available in ASCII format in the [TABLES](#) directory.

Table T21. Split-core paleomagnetic measurements for Hole 1099B before demagnetization (NRM results).

Leg	Site	Hole	Core	Type	Section	Interval (cm)	Depth (mbsf)	Inclination (°)	Declination (°)	Intensity (A/m)	Demagnetization step (mT)	Run #
178	1099	B	1	H	1	10	60.1	50.46	6.5	1.36E-01	0	11132
178	1099	B	1	H	1	15	60.15	63.97	16.41	1.41E-01	0	11132
178	1099	B	1	H	1	20	60.2	71.37	50.68	1.89E-01	0	11132
178	1099	B	1	H	1	25	60.25	71.44	59.85	2.32E-01	0	11132
178	1099	B	1	H	1	30	60.3	75.89	56.43	2.46E-01	0	11132
178	1099	B	1	H	1	35	60.35	79.59	74.82	2.34E-01	0	11132
178	1099	B	1	H	1	40	60.4	71.7	74.92	2.03E-01	0	11132
178	1099	B	1	H	1	45	60.45	74.84	57.92	1.57E-01	0	11132
178	1099	B	1	H	1	50	60.5	74.01	347.91	7.49E-02	0	11132
178	1099	B	1	H	1	55	60.55	-0.53	357.15	7.09E-02	0	11132
178	1099	B	1	H	1	60	60.6	-4.15	4.2	1.47E-01	0	11132
178	1099	B	1	H	1	65	60.65	26.79	18.24	1.53E-01	0	11132
178	1099	B	1	H	1	70	60.7	65.1	40.75	1.86E-01	0	11132
178	1099	B	1	H	1	75	60.75	73.44	35.19	2.11E-01	0	11132
178	1099	B	1	H	1	80	60.8	75.19	15.43	2.13E-01	0	11132
178	1099	B	1	H	1	85	60.85	77.74	355.59	2.02E-01	0	11132
178	1099	B	1	H	1	90	60.9	78.15	21.03	1.89E-01	0	11132
178	1099	B	1	H	1	95	60.95	72.82	26.33	1.84E-01	0	11132
178	1099	B	1	H	1	100	61	74.39	26.25	1.84E-01	0	11132
178	1099	B	1	H	1	105	61.05	76.32	24.94	1.81E-01	0	11132
178	1099	B	1	H	1	110	61.1	75.15	10.89	1.79E-01	0	11132
178	1099	B	1	H	1	115	61.15	73.19	19.47	1.74E-01	0	11132
178	1099	B	1	H	1	120	61.2	68.85	25.1	1.70E-01	0	11132
178	1099	B	1	H	1	125	61.25	69.24	21.58	1.68E-01	0	11132
178	1099	B	1	H	1	130	61.3	72.51	15.81	1.68E-01	0	11132
178	1099	B	1	H	1	135	61.35	73.22	22.14	1.72E-01	0	11132
178	1099	B	1	H	1	140	61.4	68.56	21.94	1.75E-01	0	11132
178	1099	B	1	H	2	10	61.6	66.69	20.34	1.64E-01	0	11135
178	1099	B	1	H	2	15	61.65	65.39	10.95	1.65E-01	0	11135
178	1099	B	1	H	2	20	61.7	67.52	20	1.66E-01	0	11135
178	1099	B	1	H	2	25	61.75	67.51	21.47	1.64E-01	0	11135
178	1099	B	1	H	2	30	61.8	62.95	4.36	1.77E-01	0	11135
178	1099	B	1	H	2	35	61.85	66.24	1.41	1.86E-01	0	11135
178	1099	B	1	H	2	40	61.9	65.38	13.01	1.78E-01	0	11135
178	1099	B	1	H	2	45	61.95	66.62	13.74	1.77E-01	0	11135
178	1099	B	1	H	2	50	62	66.01	14.08	1.85E-01	0	11135
178	1099	B	1	H	2	55	62.05	65.19	18.35	1.95E-01	0	11135
178	1099	B	1	H	2	60	62.1	66.96	24.03	1.99E-01	0	11135
178	1099	B	1	H	2	65	62.15	70.35	27.89	1.99E-01	0	11135
178	1099	B	1	H	2	70	62.2	70.79	24.22	1.96E-01	0	11135
178	1099	B	1	H	2	75	62.25	71.24	23.16	1.95E-01	0	11135
178	1099	B	1	H	2	80	62.3	71.46	26.82	1.97E-01	0	11135
178	1099	B	1	H	2	85	62.35	68.55	11.42	1.97E-01	0	11135
178	1099	B	1	H	2	90	62.4	69.88	20.61	1.88E-01	0	11135
178	1099	B	1	H	2	95	62.45	69.68	28.41	1.82E-01	0	11135
178	1099	B	1	H	2	100	62.5	74.64	31.37	1.87E-01	0	11135
178	1099	B	1	H	2	105	62.55	74.83	26.8	1.80E-01	0	11135
178	1099	B	1	H	2	110	62.6	72.25	4.08	1.78E-01	0	11135
178	1099	B	1	H	2	115	62.65	72.97	20.03	1.74E-01	0	11135
178	1099	B	1	H	2	120	62.7	74.08	27.91	1.77E-01	0	11135
178	1099	B	1	H	2	125	62.75	78.71	27.51	1.88E-01	0	11135
178	1099	B	1	H	2	130	62.8	82.84	69.07	1.98E-01	0	11135
178	1099	B	1	H	2	135	62.85	76.92	46.28	1.77E-01	0	11135
178	1099	B	1	H	2	140	62.9	70.11	24.47	1.92E-01	0	11135
178	1099	B	1	H	3	10	63.1	71.95	72.06	1.53E-01	0	11138
178	1099	B	1	H	3	15	63.15	61.82	38.06	1.36E-01	0	11138
178	1099	B	1	H	3	20	63.2	63.09	18.52	1.82E-01	0	11138
178	1099	B	1	H	3	25	63.25	69.55	17.5	1.88E-01	0	11138
178	1099	B	1	H	3	30	63.3	68.77	23.68	2.00E-01	0	11138
178	1099	B	1	H	3	35	63.35	73.12	25.65	1.95E-01	0	11138
178	1099	B	1	H	3	40	63.4	73.92	23.8	1.81E-01	0	11138
178	1099	B	1	H	3	45	63.45	73.85	21.94	1.78E-01	0	11138
178	1099	B	1	H	3	50	63.5	76.77	0.45	1.82E-01	0	11138
178	1099	B	1	H	3	55	63.55	72.18	2.46	1.88E-01	0	11138
178	1099	B	1	H	3	60	63.6	68.9	15.37	1.98E-01	0	11138

Note: Only a portion of this table appears here. The complete table is available in ASCII format in the [TABLES](#) directory.

Table T22. Split-core paleomagnetic measurements for Hole 1099B after 10-mT demagnetization.

Leg	Site	Hole	Core	Type	Section	Interval (cm)	Depth (mbsf)	Inclination (°)	Declination (°)	Intensity (A/m)	Demagnetization step (mT)	Run #
178	1099	B	1	H	1	10	60.1	-6.42	14.08	4.12E-02	10	11133
178	1099	B	1	H	1	15	60.15	4.46	57.5	2.94E-02	10	11133
178	1099	B	1	H	1	20	60.2	22.72	94.22	3.83E-02	10	11133
178	1099	B	1	H	1	25	60.25	31.58	99.26	4.28E-02	10	11133
178	1099	B	1	H	1	30	60.3	39.04	95.44	4.13E-02	10	11133
178	1099	B	1	H	1	35	60.35	40.42	105.31	3.54E-02	10	11133
178	1099	B	1	H	1	40	60.4	23.66	102.75	3.19E-02	10	11133
178	1099	B	1	H	1	45	60.45	9.52	95.38	2.11E-02	10	11133
178	1099	B	1	H	1	50	60.5	-28.57	31.89	1.91E-02	10	11133
178	1099	B	1	H	1	55	60.55	-16.12	13.15	6.32E-02	10	11133
178	1099	B	1	H	1	60	60.6	-7.62	14.28	9.02E-02	10	11133
178	1099	B	1	H	1	65	60.65	12.16	29.75	5.44E-02	10	11133
178	1099	B	1	H	1	70	60.7	50.55	75.25	3.45E-02	10	11133
178	1099	B	1	H	1	75	60.75	61	75.37	2.55E-02	10	11133
178	1099	B	1	H	1	80	60.8	41.48	52.66	1.49E-02	10	11133
178	1099	B	1	H	1	85	60.85	5.17	37.98	1.21E-02	10	11133
178	1099	B	1	H	1	90	60.9	-20.49	49.75	1.15E-02	10	11133
178	1099	B	1	H	1	95	60.95	-35.4	47.92	1.43E-02	10	11133
178	1099	B	1	H	1	100	61	-31.93	72.98	1.50E-02	10	11133
178	1099	B	1	H	1	105	61.05	-35.85	84.23	1.71E-02	10	11133
178	1099	B	1	H	1	110	61.1	-47.91	60.59	1.64E-02	10	11133
178	1099	B	1	H	1	115	61.15	-41.83	57.1	1.94E-02	10	11133
178	1099	B	1	H	1	120	61.2	-36.9	59.2	2.13E-02	10	11133
178	1099	B	1	H	1	125	61.25	-38.18	61.51	1.79E-02	10	11133
178	1099	B	1	H	1	130	61.3	-53.6	60.65	1.32E-02	10	11133
178	1099	B	1	H	1	135	61.35	-52.13	78.37	1.35E-02	10	11133
178	1099	B	1	H	1	140	61.4	-42.55	74.34	1.71E-02	10	11133
178	1099	B	1	H	2	10	61.6	-63.04	42.22	1.67E-02	10	11136
178	1099	B	1	H	2	15	61.65	-60.64	61.66	1.62E-02	10	11136
178	1099	B	1	H	2	20	61.7	-63.12	45.14	1.75E-02	10	11136
178	1099	B	1	H	2	25	61.75	-70.45	23.89	1.84E-02	10	11136
178	1099	B	1	H	2	30	61.8	-59.46	21.34	2.09E-02	10	11136
178	1099	B	1	H	2	35	61.85	-56.73	15.86	2.19E-02	10	11136
178	1099	B	1	H	2	40	61.9	-64.43	31.48	1.76E-02	10	11136
178	1099	B	1	H	2	45	61.95	-63.13	63.9	1.33E-02	10	11136
178	1099	B	1	H	2	50	62	-59.87	76.15	1.32E-02	10	11136
178	1099	B	1	H	2	55	62.05	-52.56	67.55	1.50E-02	10	11136
178	1099	B	1	H	2	60	62.1	-46.71	63.57	1.75E-02	10	11136
178	1099	B	1	H	2	65	62.15	-44.5	53.33	1.88E-02	10	11136
178	1099	B	1	H	2	70	62.2	-48.92	31.19	1.52E-02	10	11136
178	1099	B	1	H	2	75	62.25	-45.93	15.29	1.41E-02	10	11136
178	1099	B	1	H	2	80	62.3	-36.9	32.73	1.56E-02	10	11136
178	1099	B	1	H	2	85	62.35	-43.63	38.99	1.49E-02	10	11136
178	1099	B	1	H	2	90	62.4	-44.2	40.65	1.58E-02	10	11136
178	1099	B	1	H	2	95	62.45	-40.55	52.24	1.64E-02	10	11136
178	1099	B	1	H	2	100	62.5	-44.72	95.49	1.93E-02	10	11136
178	1099	B	1	H	2	105	62.55	-47.74	101.21	2.03E-02	10	11136
178	1099	B	1	H	2	110	62.6	-73.86	46.22	1.53E-02	10	11136
178	1099	B	1	H	2	115	62.65	-64.53	69.6	1.47E-02	10	11136
178	1099	B	1	H	2	120	62.7	-54.71	72.77	1.40E-02	10	11136
178	1099	B	1	H	2	125	62.75	-46.4	70.2	1.77E-02	10	11136
178	1099	B	1	H	2	130	62.8	-42.59	72.67	2.14E-02	10	11136
178	1099	B	1	H	2	135	62.85	-42.64	91.35	1.87E-02	10	11136
178	1099	B	1	H	2	140	62.9	-33.13	103.4	2.04E-02	10	11136
178	1099	B	1	H	3	10	63.1	-9.37	63.31	1.61E-02	10	11139
178	1099	B	1	H	3	15	63.15	-22.57	51.43	1.17E-02	10	11139
178	1099	B	1	H	3	20	63.2	-24.27	56.22	1.80E-02	10	11139
178	1099	B	1	H	3	25	63.25	-40.21	76.8	1.88E-02	10	11139
178	1099	B	1	H	3	30	63.3	-54.97	65.67	1.96E-02	10	11139
178	1099	B	1	H	3	35	63.35	-53.16	46.71	2.07E-02	10	11139
178	1099	B	1	H	3	40	63.4	-56.03	52.52	1.72E-02	10	11139
178	1099	B	1	H	3	45	63.45	-68.74	76.22	1.25E-02	10	11139
178	1099	B	1	H	3	50	63.5	-50.96	235.12	1.05E-02	10	11139
178	1099	B	1	H	3	55	63.55	-74.56	317.63	1.20E-02	10	11139
178	1099	B	1	H	3	60	63.6	-33.05	32.45	1.84E-02	10	11139

Note: Only a portion of this table appears here. The complete table is available in ASCII format in the [TABLES](#) directory.

Table T23. Split-core paleomagnetic measurements for Hole 1099B after 20-mT demagnetization.

Leg	Site	Hole	Core	Type	Section	Interval (cm)	Depth (mbsf)	Inclination (°)	Declination (°)	Intensity (A/m)	Demagnetization step (mT)	Run #
178	1099	B	1	H	1	10	60.1	-7.97	12.38	2.71E-02	20	11134
178	1099	B	1	H	1	15	60.15	2.63	61.4	1.83E-02	20	11134
178	1099	B	1	H	1	20	60.2	19.48	98.73	2.59E-02	20	11134
178	1099	B	1	H	1	25	60.25	27.93	101.91	2.90E-02	20	11134
178	1099	B	1	H	1	30	60.3	35.58	97.6	2.78E-02	20	11134
178	1099	B	1	H	1	35	60.35	37.32	107.24	2.36E-02	20	11134
178	1099	B	1	H	1	40	60.4	21.01	104.82	2.12E-02	20	11134
178	1099	B	1	H	1	45	60.45	6.63	96.42	1.37E-02	20	11134
178	1099	B	1	H	1	50	60.5	-30.72	30.04	1.11E-02	20	11134
178	1099	B	1	H	1	55	60.55	-16.04	11.89	3.24E-02	20	11134
178	1099	B	1	H	1	60	60.6	-7.16	13.54	4.29E-02	20	11134
178	1099	B	1	H	1	65	60.65	15.02	32.65	2.96E-02	20	11134
178	1099	B	1	H	1	70	60.7	50.52	75.06	2.23E-02	20	11134
178	1099	B	1	H	1	75	60.75	61.7	79.17	1.52E-02	20	11134
178	1099	B	1	H	1	80	60.8	31.79	60.42	7.45E-03	20	11134
178	1099	B	1	H	1	85	60.85	-19.3	39.43	8.02E-03	20	11134
178	1099	B	1	H	1	90	60.9	-44.81	55.01	8.89E-03	20	11134
178	1099	B	1	H	1	95	60.95	-55.84	54.26	1.13E-02	20	11134
178	1099	B	1	H	1	100	61	-50.27	83.46	1.22E-02	20	11134
178	1099	B	1	H	1	105	61.05	-50.31	93.15	1.41E-02	20	11134
178	1099	B	1	H	1	110	61.1	-61.73	70.65	1.39E-02	20	11134
178	1099	B	1	H	1	115	61.15	-55.19	66.6	1.55E-02	20	11134
178	1099	B	1	H	1	120	61.2	-49.96	66.97	1.64E-02	20	11134
178	1099	B	1	H	1	125	61.25	-52.8	69.52	1.43E-02	20	11134
178	1099	B	1	H	1	130	61.3	-69.14	81.28	1.19E-02	20	11134
178	1099	B	1	H	1	135	61.35	-65.67	101.82	1.24E-02	20	11134
178	1099	B	1	H	1	140	61.4	-57.34	92.22	1.43E-02	20	11134
178	1099	B	1	H	2	10	61.6	-76.75	67.08	1.36E-02	20	11137
178	1099	B	1	H	2	15	61.65	-70.07	92.06	1.34E-02	20	11137
178	1099	B	1	H	2	20	61.7	-74.82	68.83	1.44E-02	20	11137
178	1099	B	1	H	2	25	61.75	-82.83	34.45	1.52E-02	20	11137
178	1099	B	1	H	2	30	61.8	-73.12	31.89	1.61E-02	20	11137
178	1099	B	1	H	2	35	61.85	-70.77	24.12	1.68E-02	20	11137
178	1099	B	1	H	2	40	61.9	-77.74	55.38	1.43E-02	20	11137
178	1099	B	1	H	2	45	61.95	-71.72	102.58	1.17E-02	20	11137
178	1099	B	1	H	2	50	62	-66.52	114.61	1.17E-02	20	11137
178	1099	B	1	H	2	55	62.05	-62.97	99.24	1.27E-02	20	11137
178	1099	B	1	H	2	60	62.1	-60.04	84.56	1.41E-02	20	11137
178	1099	B	1	H	2	65	62.15	-59.02	67.31	1.47E-02	20	11137
178	1099	B	1	H	2	70	62.2	-67.43	39.35	1.23E-02	20	11137
178	1099	B	1	H	2	75	62.25	-66.94	14.92	1.12E-02	20	11137
178	1099	B	1	H	2	80	62.3	-56.67	39.19	1.18E-02	20	11137
178	1099	B	1	H	2	85	62.35	-62.17	56.42	1.18E-02	20	11137
178	1099	B	1	H	2	90	62.4	-60.68	55.91	1.26E-02	20	11137
178	1099	B	1	H	2	95	62.45	-55.05	65.31	1.30E-02	20	11137
178	1099	B	1	H	2	100	62.5	-52.34	110.48	1.64E-02	20	11137
178	1099	B	1	H	2	105	62.55	-53.64	115.54	1.75E-02	20	11137
178	1099	B	1	H	2	110	62.6	-79.46	98.53	1.40E-02	20	11137
178	1099	B	1	H	2	115	62.65	-70.5	97.27	1.34E-02	20	11137
178	1099	B	1	H	2	120	62.7	-65.27	94.47	1.26E-02	20	11137
178	1099	B	1	H	2	125	62.75	-57.67	82.56	1.51E-02	20	11137
178	1099	B	1	H	2	130	62.8	-52.57	80.2	1.80E-02	20	11137
178	1099	B	1	H	2	135	62.85	-52.65	102.03	1.56E-02	20	11137
178	1099	B	1	H	2	140	62.9	-41.17	118.55	1.73E-02	20	11137
178	1099	B	1	H	3	10	63.1	-27.44	71.99	1.20E-02	20	11140
178	1099	B	1	H	3	15	63.15	-43.49	65.09	9.05E-03	20	11140
178	1099	B	1	H	3	20	63.2	-40.8	72.42	1.43E-02	20	11140
178	1099	B	1	H	3	25	63.25	-50.97	93.64	1.71E-02	20	11140
178	1099	B	1	H	3	30	63.3	-65.17	87.06	1.79E-02	20	11140
178	1099	B	1	H	3	35	63.35	-65.7	62.17	1.83E-02	20	11140
178	1099	B	1	H	3	40	63.4	-67.57	72.01	1.61E-02	20	11140
178	1099	B	1	H	3	45	63.45	-74.11	122.75	1.36E-02	20	11140
178	1099	B	1	H	3	50	63.5	-58.42	203.5	1.31E-02	20	11140
178	1099	B	1	H	3	55	63.55	-85.13	201.88	1.32E-02	20	11140
178	1099	B	1	H	3	60	63.6	-53.03	42.91	1.49E-02	20	11140

Note: Only a portion of this table appears here. The complete table is available in ASCII format in the [TABLES](#) directory.

Table T24. Split-core paleomagnetic measurements for Hole 1099B after processing the results from the 20-mT demagnetization step by removing measurements from drilling-disturbed intervals and measurements made within 10 cm of the ends of each core section.

Leg	Site	Hole	Core	Type	Section	Interval (cm)	Depth (mbst)	Inclination (°)	Declination (°)	Intensity (A/m)	Demagnetization step (mT)	Run #
178	1099	B	1	H	1	95	60.95	-55.84	54.26	1.13E-02	20	11134
178	1099	B	1	H	1	100	61	-50.27	83.46	1.22E-02	20	11134
178	1099	B	1	H	1	105	61.05	-50.31	93.15	1.41E-02	20	11134
178	1099	B	1	H	1	110	61.1	-61.73	70.65	1.39E-02	20	11134
178	1099	B	1	H	1	115	61.15	-55.19	66.6	1.55E-02	20	11134
178	1099	B	1	H	1	120	61.2	-49.96	66.97	1.64E-02	20	11134
178	1099	B	1	H	1	125	61.25	-52.8	69.52	1.43E-02	20	11134
178	1099	B	1	H	1	130	61.3	-69.14	81.28	1.19E-02	20	11134
178	1099	B	1	H	1	135	61.35	-65.67	101.82	1.24E-02	20	11134
178	1099	B	1	H	1	140	61.4	-57.34	92.22	1.43E-02	20	11134
178	1099	B	1	H	2	10	61.6	-76.75	67.08	1.36E-02	20	11137
178	1099	B	1	H	2	15	61.65	-70.07	92.06	1.34E-02	20	11137
178	1099	B	1	H	2	20	61.7	-74.82	68.83	1.44E-02	20	11137
178	1099	B	1	H	2	25	61.75	-82.83	34.45	1.52E-02	20	11137
178	1099	B	1	H	2	30	61.8	-73.12	31.89	1.61E-02	20	11137
178	1099	B	1	H	2	35	61.85	-70.77	24.12	1.68E-02	20	11137
178	1099	B	1	H	2	40	61.9	-77.74	55.38	1.43E-02	20	11137
178	1099	B	1	H	2	45	61.95	-71.72	102.58	1.17E-02	20	11137
178	1099	B	1	H	2	50	62	-66.52	114.61	1.17E-02	20	11137
178	1099	B	1	H	2	55	62.05	-62.97	99.24	1.27E-02	20	11137
178	1099	B	1	H	2	60	62.1	-60.04	84.56	1.41E-02	20	11137
178	1099	B	1	H	2	65	62.15	-59.02	67.31	1.48E-02	20	11137
178	1099	B	1	H	2	70	62.2	-67.43	39.35	1.23E-02	20	11137
178	1099	B	1	H	2	75	62.25	-66.94	14.92	1.12E-02	20	11137
178	1099	B	1	H	2	80	62.3	-56.67	39.19	1.18E-02	20	11137
178	1099	B	1	H	2	85	62.35	-62.17	56.42	1.18E-02	20	11137
178	1099	B	1	H	2	90	62.4	-60.68	55.91	1.26E-02	20	11137
178	1099	B	1	H	2	95	62.45	-55.05	65.31	1.30E-02	20	11137
178	1099	B	1	H	2	100	62.5	-52.34	110.48	1.65E-02	20	11137
178	1099	B	1	H	2	105	62.55	-53.64	115.54	1.75E-02	20	11137
178	1099	B	1	H	2	110	62.6	-79.46	98.53	1.40E-02	20	11137
178	1099	B	1	H	2	115	62.65	-70.5	97.27	1.34E-02	20	11137
178	1099	B	1	H	2	120	62.7	-65.27	94.47	1.26E-02	20	11137
178	1099	B	1	H	2	125	62.75	-57.67	82.56	1.51E-02	20	11137
178	1099	B	1	H	2	130	62.8	-52.57	80.2	1.80E-02	20	11137
178	1099	B	1	H	2	135	62.85	-52.65	102.03	1.56E-02	20	11137
178	1099	B	1	H	2	140	62.9	-41.17	118.55	1.73E-02	20	11137
178	1099	B	1	H	3	10	63.1	-27.44	71.99	1.20E-02	20	11140
178	1099	B	1	H	3	15	63.15	-43.49	65.09	9.05E-03	20	11140
178	1099	B	1	H	3	20	63.2	-40.8	72.42	1.43E-02	20	11140
178	1099	B	1	H	3	25	63.25	-50.97	93.64	1.71E-02	20	11140
178	1099	B	1	H	3	30	63.3	-65.17	87.06	1.79E-02	20	11140
178	1099	B	1	H	3	35	63.35	-65.7	62.17	1.83E-02	20	11140
178	1099	B	1	H	3	40	63.4	-67.57	72.01	1.61E-02	20	11140
178	1099	B	1	H	3	45	63.45	-74.11	122.75	1.36E-02	20	11140
178	1099	B	1	H	3	50	63.5	-58.42	203.5	1.31E-02	20	11140
178	1099	B	1	H	3	55	63.55	-85.13	201.88	1.32E-02	20	11140
178	1099	B	1	H	3	60	63.6	-53.03	42.91	1.49E-02	20	11140
178	1099	B	1	H	3	65	63.65	-46.2	19.52	1.53E-02	20	11140
178	1099	B	1	H	3	70	63.7	-53.02	347.78	1.23E-02	20	11140
178	1099	B	1	H	3	75	63.75	-59.27	245.6	1.14E-02	20	11140
178	1099	B	1	H	3	80	63.8	-79.22	321.68	1.08E-02	20	11140
178	1099	B	1	H	3	85	63.85	-47.75	15.23	1.29E-02	20	11140
178	1099	B	1	H	3	90	63.9	-46.14	23.54	1.03E-02	20	11140
178	1099	B	1	H	3	95	63.95	-72.55	76.15	7.90E-03	20	11140
178	1099	B	1	H	3	100	64	-73.8	136.05	1.05E-02	20	11140
178	1099	B	1	H	3	105	64.05	-83.63	351.84	1.13E-02	20	11140
178	1099	B	1	H	3	110	64.1	-72.94	316.7	1.25E-02	20	11140
178	1099	B	1	H	3	115	64.15	-72.39	305.84	1.38E-02	20	11140
178	1099	B	1	H	3	120	64.2	-76.2	348.07	1.54E-02	20	11140
178	1099	B	1	H	3	125	64.25	-82.09	3.52	1.58E-02	20	11140
178	1099	B	1	H	3	130	64.3	-85.68	96.52	1.53E-02	20	11140
178	1099	B	1	H	3	135	64.35	-79.71	58.27	1.59E-02	20	11140

Note: Only a portion of this table appears here. The complete table is available in ASCII format in the [TABLES](#) directory.

Table T25. Discrete sample NRM and AF demagnetization results for Hole 1098C.

Leg	Site	Hole	Core	Type	Section	Interval (cm)	Depth (mbsf)	Inclination (°)	Declination (°)	Intensity (A/m)	Mx (A·m)	My (A·m)	Mz (A·m)	Demagnetization step (mT)
178	1098	C	1	H	2	63	2.13	54.12	20.14	1.57E-02	6.89E-08	2.53E-08	1.02E-07	0
178	1098	C	1	H	2	63	2.13	-72.32	11.98	1.14E-02	2.71E-08	5.75E-09	-8.69E-08	10
178	1098	C	1	H	2	63	2.13	-73.79	19.59	8.23E-03	1.73E-08	6.16E-09	-6.32E-08	20
178	1098	C	1	H	2	63	2.13	-78.54	23.17	5.62E-03	8.22E-09	3.52E-09	-4.41E-08	30
178	1098	C	1	H	2	63	2.13	-77.98	26.14	4.15E-03	6.21E-09	3.05E-09	-3.25E-08	40
178	1098	C	1	H	2	63	2.13	-76.45	49.24	3.00E-03	3.67E-09	4.25E-09	-2.33E-08	50
178	1098	C	1	H	2	63	2.13	-69.34	37.29	2.02E-03	4.53E-09	3.45E-09	-1.51E-08	60
178	1098	C	1	H	2	63	2.13	-75.04	74.57	1.80E-03	9.90E-10	3.59E-09	-1.39E-08	70
178	1098	C	1	H	2	63	2.13	-68.7	57.78	1.53E-03	2.36E-09	3.75E-09	-1.14E-08	80
178	1098	C	1	H	3	75	3.75	46	23.42	7.15E-03	3.64E-08	1.58E-08	4.11E-08	0
178	1098	C	1	H	3	75	3.75	-56.25	26.19	4.44E-03	1.77E-08	8.71E-09	-2.95E-08	10
178	1098	C	1	H	3	75	3.75	-59.26	29.37	3.22E-03	1.15E-08	6.45E-09	-2.21E-08	20
178	1098	C	1	H	3	75	3.75	-60.63	25.22	2.41E-03	8.56E-09	4.03E-09	-1.68E-08	30
178	1098	C	1	H	3	75	3.75	-57.65	34.84	1.96E-03	6.90E-09	4.80E-09	-1.33E-08	40
178	1098	C	1	H	3	75	3.75	-54.96	31.59	1.31E-03	5.12E-09	3.15E-09	-8.57E-09	50
178	1098	C	1	H	3	75	3.75	-48.9	29.17	1.19E-03	5.45E-09	3.04E-09	-7.16E-09	60
178	1098	C	1	H	3	75	3.75	-68.91	26.88	8.72E-04	2.24E-09	1.14E-09	-6.51E-09	70
178	1098	C	1	H	3	75	3.75	-66.53	42	6.73E-04	1.59E-09	1.43E-09	-4.94E-09	80
178	1098	C	1	H	4	71	5.21	48.85	22.85	1.36E-02	6.59E-08	2.78E-08	8.18E-08	0
178	1098	C	1	H	4	71	5.21	-64.05	14.69	1.44E-02	4.88E-08	1.28E-08	-1.04E-07	10
178	1098	C	1	H	4	71	5.21	-66.06	19.55	1.04E-02	3.17E-08	1.13E-08	-7.58E-08	20
178	1098	C	1	H	4	71	5.21	-67.9	19.74	7.48E-03	2.12E-08	7.60E-09	-5.54E-08	30
178	1098	C	1	H	4	71	5.21	-67.24	20.29	5.40E-03	1.57E-08	5.79E-09	-3.98E-08	40
178	1098	C	1	H	4	71	5.21	-65.36	14.8	3.90E-03	1.26E-08	3.33E-09	-2.84E-08	50
178	1098	C	1	H	4	71	5.21	-61.59	26.06	2.73E-03	9.33E-09	4.56E-09	-1.92E-08	60
178	1098	C	1	H	4	71	5.21	-67.09	20.41	2.20E-03	6.41E-09	2.39E-09	-1.62E-08	70
178	1098	C	1	H	4	71	5.21	-72.81	11.11	2.17E-03	5.03E-09	9.87E-10	-1.66E-08	80
178	1098	C	1	H	5	44	6.44	48.45	38.07	6.87E-03	2.87E-08	2.25E-08	4.11E-08	0
178	1098	C	1	H	5	44	6.44	-66.05	49.31	7.38E-03	1.56E-08	1.82E-08	-5.40E-08	10
178	1098	C	1	H	5	44	6.44	-64.6	50.89	5.54E-03	1.20E-08	1.48E-08	-4.00E-08	20
178	1098	C	1	H	5	44	6.44	-66.91	52.12	3.97E-03	7.65E-09	9.83E-09	-2.92E-08	30
178	1098	C	1	H	5	44	6.44	-65.62	54.29	3.28E-03	6.32E-09	8.79E-09	-2.39E-08	40
178	1098	C	1	H	5	44	6.44	-66.1	63.75	2.50E-03	3.58E-09	7.26E-09	-1.83E-08	50
178	1098	C	1	H	5	44	6.44	-63.71	65.7	2.03E-03	2.97E-09	6.57E-09	-1.46E-08	60
178	1098	C	1	H	5	44	6.44	-74.02	69.61	1.84E-03	1.42E-09	3.81E-09	-1.42E-08	70
178	1098	C	1	H	5	44	6.44	-71.28	50.32	1.23E-03	2.02E-09	2.43E-09	-9.33E-09	80
178	1098	C	1	H	6	41	7.91	8.39	16.36	7.72E-03	5.86E-08	1.72E-08	9.00E-09	0
178	1098	C	1	H	6	41	7.91	-54.21	15.88	1.05E-02	4.73E-08	1.34E-08	-6.82E-08	10
178	1098	C	1	H	6	41	7.91	-55.55	19.85	8.02E-03	3.41E-08	1.23E-08	-5.29E-08	20
178	1098	C	1	H	6	41	7.91	-55.68	20.42	5.98E-03	2.53E-08	9.41E-09	-3.95E-08	30
178	1098	C	1	H	6	41	7.91	-55.49	19.76	5.07E-03	2.16E-08	7.77E-09	-3.34E-08	40
178	1098	C	1	H	6	41	7.91	-55.68	29.11	4.06E-03	1.60E-08	8.90E-09	-2.68E-08	50
178	1098	C	1	H	6	41	7.91	-51.13	29.11	3.24E-03	1.42E-08	7.91E-09	-2.02E-08	60
178	1098	C	1	H	6	41	7.91	-57.14	21.26	2.84E-03	1.15E-08	4.47E-09	-1.91E-08	70
178	1098	C	1	H	6	41	7.91	-58.21	22.04	2.54E-03	9.94E-09	4.02E-09	-1.73E-08	80
178	1098	C	2	H	2	67	10.87	-89.62	74.39	5.57E-03	7.90E-11	2.83E-10	-4.46E-08	0
178	1098	C	2	H	2	67	10.87	-84.47	135.04	7.94E-03	-4.33E-09	4.32E-09	-6.32E-08	10
178	1098	C	2	H	2	67	10.87	-84.3	146.28	6.27E-03	-4.15E-09	2.77E-09	-4.99E-08	20
178	1098	C	2	H	2	67	10.87	-85.66	148.07	4.61E-03	-2.37E-09	1.48E-09	-3.68E-08	30
178	1098	C	2	H	2	67	10.87	-81.66	162.19	3.63E-03	-4.01E-09	1.29E-09	-2.87E-08	40
178	1098	C	2	H	2	67	10.87	-81.45	138.64	2.84E-03	-2.53E-09	2.23E-09	-2.25E-08	50
178	1098	C	2	H	2	67	10.87	-81.73	153.07	2.33E-03	-2.39E-09	1.22E-09	-1.85E-08	60
178	1098	C	2	H	2	67	10.87	-79.85	138.7	1.61E-03	-1.70E-09	1.49E-09	-1.27E-08	70
178	1098	C	2	H	2	67	10.87	-80.65	173.19	1.59E-03	-2.05E-09	2.45E-10	-1.25E-08	80
178	1098	C	2	H	3	62	12.32	-69.63	8.97	1.75E-03	4.80E-09	7.58E-10	-1.31E-08	0
178	1098	C	2	H	3	62	12.32	-77.16	18.01	2.02E-03	3.41E-09	1.11E-09	-1.57E-08	10
178	1098	C	2	H	3	62	12.32	-78	21.45	1.57E-03	2.43E-09	9.53E-10	-1.23E-08	20
178	1098	C	2	H	3	62	12.32	-76.63	36.69	9.90E-04	1.47E-09	1.09E-09	-7.71E-09	30
178	1098	C	2	H	3	62	12.32	-77.69	348.76	5.26E-04	8.80E-10	-1.75E-10	-4.11E-09	40
178	1098	C	2	H	3	62	12.32	-86.33	319.56	3.62E-04	1.41E-10	-1.20E-10	-2.89E-09	50
178	1098	C	2	H	3	62	12.32	-75.3	34.44	2.54E-04	4.25E-10	2.91E-10	-1.96E-09	60
178	1098	C	2	H	3	62	12.32	40.97	196.19	4.02E-05	-2.33E-10	-6.77E-11	2.11E-10	70
178	1098	C	2	H	3	62	12.32	-67.03	263.13	1.43E-04	-5.32E-11	-4.42E-10	-1.05E-09	80
178	1098	C	2	H	4	64	13.84	-78.21	201.84	6.04E-03	-9.16E-09	-3.67E-09	-4.73E-08	0
178	1098	C	2	H	4	64	13.84	-78.39	180.03	8.30E-03	-1.34E-08	-7.27E-12	-6.50E-08	10
178	1098	C	2	H	4	64	13.84	-77.55	172.94	6.41E-03	-1.10E-08	1.36E-09	-5.01E-08	20

Note: Only a portion of this table appears here. The complete table is available in ASCII format in the **TABLES** directory.

Table T26. Results from the principal component analysis of discrete paleomagnetic samples.

Leg	Hole	Core	Section	Interval (cm)	Depth (mbsf)	Inclination (°)	Declination (°)	MAD	Length	Devang	Steps	Low	High	Option
178	1098C	1H	2	63	2.13	-78.2	357.2	2.98	4.15E-02	8.46	4	30	80	FRE
178	1098C	1H	3	75	3.75	-56.7	26.9	2.73	2.56E-02	5	4	20	80	FRE
178	1098C	1H	4	71	5.21	-65	20.3	1.53	8.25E-02	2.27	4	20	80	FRE
178	1098C	1H	5	44	6.44	-63	51	2.18	4.32E-02	3.1	4	20	80	FRE
178	1098C	1H	6	41	7.91	-54.4	19.1	0.44	5.48E-02	1.95	4	20	80	FRE
178	1098C	2H	2	67	10.87	-85.5	139.8	1.71	4.69E-02	2.9	4	20	80	FRE
178	1098C	2H	3	62	12.32	-77	23.5	2.89	1.45E-02	3.33	4	20	80	FRE
178	1098C	2H	4	64	13.84	-84	178	2.23	3.54E-02	11.74	4	30	80	FRE
178	1098C	2H	5	64	15.34	-74.7	143.9	4.59	3.15E-02	0.9	4	20	80	FRE
178	1098C	2H	6	71	16.91	-76.8	164.6	1.16	4.34E-02	2.98	4	20	80	FRE
178	1098C	2H	7	31	18.01	-83.9	132.3	1.49	2.38E-02	4.22	4	30	80	FRE
178	1098C	3H	2	58	20.28	-74.8	29.3	1.46	4.13E-02	2.23	4	20	80	FRE
178	1098C	3H	3	50	21.7	-76.2	343.2	7.87	1.82E-02	17.3	4	30	80	FRE
178	1098C	3H	4	63	23.33	-76.7	9.8	4.3	1.75E-02	11.31	4	40	80	FRE
178	1098C	3H	6	71	26.41	-53.1	336.8	4	2.03E-02	5.38	4	20	80	FRE
178	1098C	4H	1	125	28.95	-57.7	258.4	11.49	1.10E-02	17.32	4	30	70	FRE
178	1098C	4H	2	91	30.11	-85.2	242.2	2.69	5.74E-02	6.59	4	20	80	FRE
178	1098C	4H	3	91	31.61	-76	222.2	0.73	2.81E-01	4.85	4	20	80	FRE
178	1098C	4H	4	82	33.02	-76.5	252.1	3.33	3.78E-02	14.03	4	30	80	FRE
178	1098C	4H	5	121	34.91	-71.5	246	2.15	7.06E-02	2.41	4	20	80	FRE
178	1098C	4H	6	49	35.69	4.5	267.9	9.64	8.52E-03	46.3	4	50	80	FRE
178	1098C	5H	1	105	38.25	-2.4	271.9	6.21	8.09E-03	146.54	4	50	80	FRE
178	1098C	5H	2	106	39.76	-0.6	92.2	5.68	2.49E-03	8.74	4	50	80	FRE
178	1098C	5H	3	77	41.02	0.2	89.4	3.47	9.84E-04	3.32	4	50	80	FRE
178	1098C	5H	4	41	42.16	-4.9	261.7	3.45	1.50E-03	131.12	4	50	80	FRE

Notes: MAD = maximum angular deviation, Devang = deviation angle (degrees). This table also appears in ASCII format in the [TABLES](#) directory.

Table T27. Headspace methane concentrations at Sites 1098 and 1099.

Core, section, interval (cm)	Depth (mbsf)	Methane (ppm)
178-1098A-		
1H-2, 65-70	1.65	183
2H-4, 0-5	6.40	9
3H-4, 0-5	15.90	4
4H-4, 0-5	25.40	6
5H-4, 0-5	34.90	32,000
6H-4, 0-5	44.40	16,200
178-1099A-		
1H-3, 0-5	3.00	352
2H-4, 0-5	9.80	3,410
3H-4, 0-5	19.30	42,200
4H-4, 0-5	28.85	49,800
5H-4, 0-5	38.50	78,500
6H-4, 0-5	47.83	112,000
7H-4, 0-5	57.30	13,500
178-1099B-		
1H-4, 0-5	64.50	45,000
2H-4, 0-5	74.00	12,700
3H-4, 0-5	83.55	6,960
4H-4, 0-5	93.00	13,500
5H-4, 0-5	102.50	9,770

Table T28. Summary of inorganic carbon and elemental analyses for Holes 1098C, 1099A, and 1099B. (Continued on next page.)

Core, section, interval (cm)	Depth (mbsf)	IC (wt%)	CaCO ₃ (wt%)	TOC (wt%)	Carbon (wt%)	TN (wt%)	Sulfur (wt%)
178-1098C-							
1H-1, 50-51	0.50	0.05	0.39	1.00	1.04	0.10	0.24
1H-2, 50-51	2.00	0.09	0.79	1.15	1.25	0.11	0.47
1H-3, 50-51	3.50	0.06	0.54	1.12	1.18	0.12	0.70
1H-4, 50-51	5.00	0.07	0.56	0.96	1.02	0.09	0.71
1H-5, 50-51	6.50	0.08	0.68	0.94	1.03	0.10	0.81
1H-6, 50-51	8.00	0.06	0.52	1.06	1.12	0.10	0.75
2H-1, 50-51	9.20	0.08	0.67	1.20	1.28	0.12	0.98
2H-2, 50-51	10.70	0.06	0.47	1.02	1.08	0.10	1.08
2H-3, 50-51	12.20	0.12	1.02	0.98	1.10	0.10	1.00
2H-4, 40-41	13.60	0.08	0.63	1.20	1.28	0.09	0.91
2H-5, 50-51	15.20	0.05	0.44	1.33	1.38	0.13	0.97
2H-6, 40-41	16.60	0.06	0.50	1.18	1.24	0.13	0.88
3H-1, 48-49	18.68	0.06	0.52	1.08	1.15	0.11	1.08
3H-2, 43-44	20.13	0.04	0.30	1.07	1.10	0.09	0.85
3H-3, 40-41	21.60	0.08	0.71	0.99	1.08	0.09	0.87
3H-4, 44-45	23.14	0.06	0.47	0.94	0.99	0.10	0.84
3H-5, 50-51	24.70	0.07	0.62	0.65	0.73	0.06	0.77
3H-6, 50-51	26.20	0.11	0.93	0.65	0.76	0.07	0.68
4H-1, 49-50	28.19	0.15	1.22	0.70	0.84	0.07	0.62
4H-2, 49-51	29.69	0.09	0.77	0.78	0.87	0.09	0.83
4H-3, 40-41	31.10	0.09	0.74	0.49	0.58	0.04	0.42
4H-4, 30-31	32.50	0.26	2.14	0.57	0.82	0.06	0.76
4H-5, 30-31	34.00	0.09	0.76	0.57	0.67	0.06	0.15
4H-6, 30-31	35.50	0.10	0.87	0.59	0.69	0.07	0.26
5H-1, 50-51	37.70	0.06	0.53	0.51	0.57	0.05	0.00
5H-2, 64-65	39.34	0.07	0.59	0.63	0.70	0.07	1.03
5H-3, 44-45	40.69	0.11	0.90	0.70	0.81	0.07	1.08
5H-4, 47-48	42.22	0.14	1.14	0.30	0.44	0.05	0.99
5H-5, 50-51	43.75	0.75	6.28	0.06	0.82	0.01	0.00
5H-6, 30-31	45.05	0.46	3.80	0.08	0.53	0.01	0.00
178-1099A-							
1H-1, 40-41	0.40	0.06	0.54	1.04	1.10	0.08	0.23
1H-2, 40-41	1.90	0.08	0.68	1.11	1.19	0.10	0.21
1H-3, 40-41	3.40	0.12	1.02	1.14	1.26	0.10	0.11
2H-1, 50-51	5.80	0.09	0.76	0.94	1.03	0.09	0.32
2H-3, 50-51	8.80	0.13	1.10	1.14	1.27	0.12	0.67
2H-5, 50-51	11.80	0.12	1.01	1.21	1.34	0.11	0.76
2H-7, 50-51	14.80	0.22	1.80	1.33	1.54	0.12	0.49
3H-1, 54-55	15.34	0.13	1.05	0.78	0.90	0.07	0.07
3H-3, 133-134	19.13	0.16	1.37	1.20	1.37	0.13	0.78
3H-5, 96-97	21.76	0.21	1.74	0.81	1.02	0.09	0.70
3H-7, 37-38	24.17	0.12	1.01	0.97	1.09	0.10	0.27
4H-1, 70-71	25.00	0.12	1.01	0.77	0.89	0.07	0.33
4H-3, 70-71	28.05	0.13	1.10	0.68	0.81	0.07	0.30
4H-5, 66-67	31.01	0.12	1.03	0.60	0.72	0.02	0.25
4H-7, 30-31	33.65	0.12	0.97	0.53	0.64	0.05	0.18
5H-1, 51-52	34.31	0.11	0.93	0.71	0.82	0.05	0.31
5H-3, 50-51	37.40	0.10	0.80	0.70	0.80	0.06	0.28
5H-5, 76-77	40.78	0.09	0.76	0.80	0.89	0.07	0.08
6H-1, 119-120	44.49	0.12	1.01	0.78	0.91	0.07	0.31
6H-2, 70-71	45.53	0.12	0.96	0.76	0.88	0.07	0.27
6H-3, 70-71	47.03	0.13	1.07	0.69	0.82	0.07	0.30
6H-5, 65-66	49.99	0.11	0.93	0.69	0.80	0.07	0.33
6H-7, 36-37	52.70	0.12	1.02	0.52	0.65	0.05	0.32
7H-1, 97-98	53.77	0.12	0.97	0.70	0.81	0.06	0.28
7H-4, 59-60	57.89	0.12	0.98	0.67	0.79	0.04	0.17
7H-6, 29-30	60.59	0.11	0.91	0.66	0.77	0.10	0.32
178-1099B-							
1H-1, 111-112	61.11	0.12	0.97	0.63	0.74	0.10	0.34
1H-3, 111-112	64.11	0.17	1.46	0.55	0.73	0.10	0.36
1H-5, 111-112	67.11	0.12	0.96	0.57	0.68	0.08	0.34
2H-1, 40-41	69.90	0.08	0.70	0.36	0.44	0.06	0.31
2H-3, 40-41	72.90	0.13	1.11	*	*	*	*
2H-5, 40-41	75.90	0.11	0.94	0.80	0.91	0.12	0.28
3H-1, 30-31	79.30	0.12	0.98	0.65	0.77	0.12	0.31

Table T28 (continued).

Core, section, interval (cm)	Depth (mbsf)	IC (wt%)	CaCO ₃ (wt%)	TOC (wt%)	Carbon (wt%)	TN (wt%)	Sulfur (wt%)
3H-3, 30-31	82.35	0.10	0.83	0.63	0.73	0.11	0.27
3H-5, 30-31	85.35	0.18	1.51	0.82	1.00	0.12	0.39
3H-6, 44-45	86.99	0.14	1.14	0.96	1.09	0.16	0.55
3H-6, 60-61	87.15	0.12	0.99	0.91	1.03	0.14	0.68
3H-7, 30-31	88.35	0.17	1.38	0.39	0.55	0.08	0.53
4H-1, 53-54	89.03	0.10	0.86	0.82	0.92	0.13	0.34
4H-3, 60-61	92.10	0.09	0.76	0.68	0.77	0.11	0.36
4H-5, 50-51	95.00	0.16	1.31	0.66	0.82	0.12	0.33
4H-6, 33-34	96.14	0.15	1.24	0.70	0.85	0.11	0.53
4H-6, 58-59	96.39	0.10	0.81	0.59	0.68	0.11	0.31
4H-7, 20-21	97.51	0.30	2.50	0.51	0.81	0.11	0.16
5H-1, 70-71	98.70	0.10	0.87	0.70	0.81	0.12	0.62
5H-2, 50-51	100.00	0.19	1.60	0.49	0.68	0.11	0.36
5H-3, 55-56	101.55	0.13	1.12	0.43	0.56	0.11	0.11
5H-5, 70-71	104.70	0.13	1.07	0.97	1.10	0.15	0.52
5H-6, 50-51	106.00	0.07	0.62	0.92	0.99	0.14	0.56
5H-7, 21-22	107.21	0.13	1.10	0.74	0.87	0.14	0.51

Notes: IC = inorganic carbon, CaCO₃ = calcium carbonate, TOC = total organic carbon, TN = total nitrogen. * = values missing because of power failure.

Table T29. Results of interstitial water analyses for Holes 1098C, 1099A, and 1099B.

Core, section, interval (cm)	Depth (mbsf)	pH	Salinity	Cl ⁻ (mM)	Alkalinity (mM)	NH ₄ ⁺ (mM)	Si(OH) ₄ (mM)	SO ₄ ²⁻ (mM)	Mn ²⁺ (μM)	Fe ²⁺ (μM)	PO ₄ ³⁻ (μM)	F ⁻ (μM)	Ca ²⁺ (mM)	Mg ²⁺ (mM)	K ⁺ (mM)	Sr ²⁺ (μM)
178-1098C-																
1H-1, 145-150	1.45	7.8	35.0	552	2.70	0.08	0.88	32.4	2.3	0.8	10.6	67.7	10.3	51.5	11.3	87
1H-2, 145-150	2.95	7.7	35.0	553	2.88	0.09	0.79	30.2	1.8	16.5	13.8	68.7	10.8	54.3	10.3	88
1H-3, 145-150	4.45	7.8	34.2	551	3.03	0.10	0.85	28.8	2.3	0.0	14.3	66.1	10.2	54.2	11.3	87
1H-4, 145-150	5.95	7.8	35.0	552	3.08	0.11	0.81	30.4	1.8	8.4	15.5	66.9	10.6	52.2	10.6	88
1H-5, 145-150	7.45	7.7	34.5	551	3.07	0.11	0.82	29.9	1.8	0.0	15.6	64.3	11.0	54.7	10.9	88
1H-6, 91-96	8.41	7.7	34.5	550	3.02	0.12	0.82	30.6	2.3	0.1	14.3	64.5	10.9	59.9	11.6	87
2H-1, 145-150	10.15	7.8	35.0	550	3.19	0.13	0.81	31.5	2.3	0.0	15.3	63.2	10.3	52.3	10.3	85
2H-2, 145-150	11.65	7.8	35.0	551	3.16	0.14	0.81	30.5	1.8	0.5	15.6	62.8	9.9	53.3	10.7	88
2H-3, 145-150	13.15	7.7	35.0	551	3.07	0.16	0.82	30.5	2.3	0.0	15.7	62.5	11.2	55.0	10.9	87
2H-4, 145-150	14.65	7.8	35.0	549	3.12	0.15	0.92	29.6	1.8	1.2	15.6	63.5	10.5	52.5	11.0	84
2H-5, 145-150	16.15	7.8	35.0	552	3.31	0.19	0.84	29.4	1.8	0.4	17.1	61.1	10.8	54.2	10.9	85
2H-6, 145-150	17.65	7.8	35.0	553	3.64	0.27	0.75	30.9	1.4	1.7	18.7	62.0	10.7	54.2	10.7	87
2H-7, 73-78	18.43	7.8	35.0	552	4.11	0.38	0.81	29.6	1.4	1.8	20.1	58.5	10.3	52.2	10.9	87
3H-1, 145-150	19.65	7.9	34.5	551	6.13	0.71	0.79	27.3	1.4	4.2	28.2	53.6	10.1	52.1	10.8	85
3H-2, 145-150	21.15	8.0	35.0	552	9.67	1.15	0.87	24.3	1.4	16.9	35.4	44.5	9.3	52.1	10.5	85
3H-3, 145-150	22.65	8.0	34.0	553	14.2	2.06	0.87	20.5	0.9	2.6	57.6	32.2	7.9	50.8	10.7	85
3H-4, 145-150	24.15	8.0	34.0	550	18.1	2.36	0.82	15.0	0.9	6.3	68.2	20.9	6.2	49.7	10.3	79
3H-5, 145-150	25.65	8.0	33.0	549	21.9	2.42	0.91	10.2	1.4	1.0	90.0	11.8	5.1	47.6	10.8	76
3H-6, 145-150	27.15	8.0	33.0	547	24.9	3.23	0.86	5.9	1.8	0.4	108	10.2	3.3	44.3	10.8	72
4H-1, 145-150	29.15	8.0	33.0	548	31.1	3.79	0.89	0.0	1.8	4.2	154	19.2	1.7	45.0	10.2	82
4H-2, 145-150	30.65	8.0	33.5	546	33.5	4.40	0.95	0.0	5.2	4.7	165	25.0	2.5	44.5	10.8	82
4H-3, 145-150	32.15	8.0	33.0	546	36.0	5.01	0.94	0.0	6.5	6.4	176	32.6	2.5	45.3	10.9	95
4H-4, 145-150	33.65	8.0	—	545	38.0	5.18	0.91	0.0	6.1	6.9	168	32.8	3.1	48.0	10.9	105
4H-5, 145-150	35.15	8.0	—	545	40.4	5.34	0.87	0.1	6.1	9.8	164	33.4	3.1	45.7	10.2	114
4H-6, 145-150	36.65	8.0	33.0	543	40.1	6.31	0.92	0.0	6.3	11.0	161	33.8	3.0	48.3	10.8	123
5H-1, 145-150	38.65	8.0	34.0	540	40.7	6.08	0.90	1.1	4.3	8.6	152	37.3	3.2	46.7	9.8	154
5H-2, 145-150	40.15	7.9	34.0	540	41.5	6.52	0.90	0.0	5.2	3.0	161	39.5	3.3	49.7	10.0	174
5H-3, 145-150	41.70	8.0	35.0	542	42.1	6.19	0.93	0.0	5.2	7.0	133	32.1	3.5	46.9	9.6	196
5H-4, 145-150	43.20	8.0	35.0	543	40.0	6.90	0.64	0.0	3.4	29.1	67.3	26.0	3.2	46.1	10.3	202
5H-5, 145-150	44.70	8.0	—	542	38.4	5.25	0.36	0.0	—	—	28.5	28.7	2.8	47.0	10.5	237
178-1099A-																
1H-2, 147-150	2.97	8.0	34.5	554	26.8	2.09	0.95	11.1	5.2	1.0	235	31.6	7.9	48.9	11.5	80
2H-3, 147-150	9.77	8.1	34.0	553	40.7	3.39	0.86	0.8	1.1	1.2	236	26.3	3.3	51.2	11.6	102
3H-3, 147-150	19.27	8.0	34.0	550	46.4	6.33	0.90	0.0	0.7	3.7	261	28.2	2.7	51.6	11.8	96
4H-3, 147-150	28.82	8.0	34.0	552	—	5.69	0.88	0.7	6.8	17.0	242	34.9	3.2	56.0	12.4	91
5H-3, 147-150	38.37	8.0	35.0	551	—	5.67	0.92	0.0	5.9	19.8	219	35.8	3.4	56.9	12.2	90
6H-3, 147-150	47.80	8.0	35.0	551	57.5	6.76	0.94	1.7	4.5	28.4	187	40.2	2.9	56.7	12.4	90
7H-3, 147-150	57.27	8.0	35.0	553	63.2	6.77	1.07	0.8	3.6	14.1	169	44.0	3.1	58.5	12.9	88
178-1099B-																
1H-3, 147-150	64.47	8.0	35.5	551	64.3	6.44	0.97	0.9	3.2	8.3	155	48.2	3.3	57.2	13.3	90
2H-3, 147-150	73.97	—	36.0	560	—	6.60	0.83	0.0	6.3	10.9	163	63.4	4.3	60.1	12.9	90
3H-3, 147-150	83.52	8.0	36.0	555	79.8	8.65	0.98	1.5	2.5	7.2	176	61.2	3.3	60.3	14.1	79
4H-3, 147-150	92.97	7.9	36.5	556	80.7	12.75	0.87	1.5	2.5	14.8	78	37.3	3.5	57.6	13.7	78
5H-3, 147-150	102.47	7.9	36.0	555	73.1	10.84	0.95	0.0	2.9	11.2	101	40.4	4.0	59.4	12.9	80

Note: — = no analysis.

Table T30. Depth offsets of the Sites 1098 and 1099
 mcd scale relative to mbsf depth.

Core	Depth (mbsf)	Depth (mcd)	Offset (m)
178-1098A-			
1H	0.01	-0.05	-0.06
2H	1.91	2.75	0.84
3H	11.41	12.67	1.26
4H	20.91	22.35	1.44
5H	30.41	32.63	2.22
6H	39.91	41.43	1.52
178-1098B-			
1H	0.01	0.05	0.04
2H	6.01	7.21	1.2
3H	15.51	16.71	1.2
4H	25.01	26.91	1.9
5H	34.51	36.23	1.72
178-1098C-			
1H	0.01	0.01	0
2H	8.71	8.71	0
3H	18.21	18.51	0.3
4H	27.71	29.29	1.58
5H	37.21	39.03	1.82
178-1099A-			
1H	0.01	0.01	0
2H	5.31	5.31	0
3H	14.81	14.81	0
4H	24.32	24.32	0
5H	33.82	33.82	0
6H	43.32	43.32	0
7H	52.82	52.82	0
178-1099B-			
1H	60.02	60.34	0.32
2H	69.52	69.84	0.32
3H	79.02	79.34	0.32
4H	88.52	88.84	0.32
5H	98.07	98.39	0.32

Note: To shift from one scale to another, add the offset values to the
 mbsf depths. The depths are from the bottom of each section.

Table T31. Spliced cores for Holes 1098A, 1098B, 1098C, 1099A, and 1099B.

Hole, core, section, interval (cm)	Depth (mbsf)	Depth (mcd)		Hole, core, section, interval (cm)	Depth (mbsf)	Depth (mcd)
1098C-1H-5, 24	6.24	6.24	Tie	1098A-2H-3, 50	5.40	6.24
1098A-2H-7, 28	11.18	12.02	Tie	1098C-2H-3, 32	12.02	12.02
1098C-2H-5, 88	15.58	15.58	Tie	1098A-3H-2, 142	14.32	15.58
1098A-3H-6, 126	20.16	21.42	Tie	1098B-3H-4, 22	20.22	21.42
1098B-3H-7, 44	24.94	26.14	Tie	1098A-4H-3, 80	24.70	26.14
1098A-4H-4, 14	25.54	26.98	Tie	1098B-4H-1, 8	25.08	26.98
1098B-4H-7, 38	33.98	35.88	Tie	1098A-5H-3, 26	33.66	35.88
1098A-5H-5, 66	37.06	39.28	Tie	1098C-5H-1, 26	37.46	39.28
1098C-5H-6, 47	45.17	46.99				
1099A-1H-4, 46	4.96	4.96	Append	1099A-2H-1, 0	5.30	5.30
1099A-2H-7, 54	14.84	14.84	Append	1099A-3H-1, 0	14.80	14.80
1099A-3H-7, 50	24.30	24.30	Append	1099A-4H-1, 0	24.30	24.30
1099A-4H-7, 62	33.97	33.97	Append	1099A-5H-1, 0	33.80	33.80
1099A-5H-6, 144	43.01	43.01	Append	1099A-6H-1, 0	43.30	43.30
1099A-6H-7, 44	52.78	52.78	Append	1099A-7H-1, 0	52.80	52.80
1099A-7H-7, 50	62.30	62.30	Tie	1099B-1H-2, 48	61.98	62.30
1099B-1H-7, 44	69.44	69.76	Append	1099B-2H-1, 0	69.50	69.82
1099B-2H-6, 90	77.90	78.22	Append	1099B-3H-1, 0	79.00	79.32
1099B-3H-7, 54	88.59	88.91	Tie	1099B-4H-1, 8.5	88.59	88.91
1099B-4H-7, 28	97.59	97.91	Append	1099B-5H-1, 0	98.00	98.32
1099B-5H-7, 62	107.62	107.94				